The Dissertation Committee for Jonathan William Franzosa Certifies that this is the approved version of the following dissertation:

Evolution of the Brain in Theropoda (Dinosauria)

Committee:

Timothy Rowe, Supervisor

Christopher Bell

Matthew Colbert

James Sprinkle

Walter Wilczynski

Evolution of the Brain in Theropoda (Dinosauria)

by

Jonathan William Franzosa, B.S.

Dissertation

Presented to the Faculty of the Graduate School of

The University of Texas at Austin

in Partial Fulfillment

of the Requirements

for the Degree of

Doctor of Philosophy

The University of Texas at Austin

May, 2004

Dedication

To my loving wife Beth, whose tireless support and encouragement made the timely completion of this dissertation possible.

Acknowledgments

There are several people that I would like to thank for helping make the completion of this dissertation possible. First, I would like to thank my committee members for their thoughtful remarks and suggestions, which improved the quality of this dissertation. I would like to thank Dr. Wann Langston for access to the *Acrocanthosaurus atokensis* braincase and dataset, Dr. Sankar Chatterjee for access to the *Allosaurus fragilis, Anhanguera santanae,* and *Rhamphorhynchus muensteri* datasets, Dr.s Jim Clark and Mark Norell for access to the *Byronosaurus jaffei, Citipati osmolskae, Mongolodon junior,* and Zos Canyon troodontid datasets, Dr. Tim Rowe for access to the *Apteryx sp., Diplodocus hayi,* and *Saurosuchus galilei* datasets, Dr.s Scott Sampson and Larry Witmer for access to the *Majungatholus atopus* dataset, Mr. David Dufeau for access to the *Anas platyrhynchos, Chauna chavaria,* and *Crypturellus cinnamomeus* datasets, Mr. Jackson Dodd for access to the *Dinornis giganteus* dataset, Dr. John Foster for the loan of the *Ceratosaurus magnicornis* braincase, and Mr. Mark Robbins for the loan of the *Chauna chavaria* and *Crypturellus cinnamomeus* skulls. I would also like to thank Dr.s Richard Ketcham, Matthew Colbert, Jessie Maisano, and the rest of the High-Resolution X-ray Computed Tomography Facility staff for scanning and processing of the datasets. For permission to use figures, I thank the Ernst Mayr Library of the Museum of Comparative Zoology, Indiana University Press, Nuttall Ornithological Club, Peabody Museum, and Dr.s

Christopher Brochu, Emily Buchholtz, Peter Galton, and James Hopson. Many thanks to the vertebrate paleontology graduate students for their helpful conversations and input. Lastly, much love and thanks to my parents for their support and encouragement.

Evolution of the Brain in Theropoda (Dinosauria)

Publication No._____

Jonathan William Franzosa, Ph.D.

The University of Texas at Austin, 2004

Supervisor: Timothy B. Rowe

The description of natural and artificial endocasts has become routine since the work of Tilly Edinger. Most workers write little more than simple descriptions of isolated specimens because endocasts are rare, and scattered throughout the world. Harry Jerison took the next step and broadly compared endocasts in detail, using them for evolutionary studies of brain size and intelligence. In those studies, Jerison concluded that dinosaurs (excluding birds) had the brain size expected for "reptiles" of their size. However insightful, many equations and assumptions Jerison used are now questioned. The goals of this study are to continue the comparative work of Edinger and Jerison, and to employ more modern techniques and information than was available when Jerison's studies were conducted, to either verify or overturn his hypotheses.

Most of this study was completed using the Department's High Resolution X-ray Computed Tomographic (CT) Scanner, which allowed digital endocasts to

be made from intact braincases. This increased the number of taxa available for analyses to 18. These endocasts are described in detail, allowing 14 characters to be identified and scored. Several analyses are done, one using just the examined taxa and characters, and three in which the characters are added to existing data matrices. These analyses showed the 14 characters contain useful phylogenetic information, and one of the phylogenies had a polytomy resolved owing to the addition of the characters.

The endocast characters also show similarities in brain architecture between pterosaurs and birds, and indicate that an avian-style brain evolved gradually through the theropod lineage. The character transitions that show the gradual evolution in the cerebral hemispheres, optic lobes, floccular lobes, and other brain features in the sequence of studied endocasts form the basis for testing inferences about theropod biology, behavior, and intelligence. Trends concerning theropod sensory and prey catching ability are tested and supported, indicating that theropods became more dependent on sight, and less dependent on smell, over time, and developed better hand-eye coordination, agility, and balance for capturing smaller prey, whereas using Encephalization Quotients for intelligence determination is disputed. This hypothesis testing is one of the strengths of digital endocasts.

Table of Contents

List of Tables

List of Figures

Chapter 1: Introduction

PALEONEUROLOGY AND ENDOCASTS

Paleoneurology is the study of the brain and nervous system of fossil animals, in particular of fossil vertebrates. The goal of paleoneurological studies is to determine how the brain, and its associated nervous system, evolved in a particular group (Buchholtz and Seyfarth, 1999). Fossils generally lack soft tissue, so inquiries into this area are made by looking at the osteology of the braincase, and by looking at the cavities that, in life, held the brain and other associated soft tissues. Studies of the individual braincase bones in multiple taxa and specimens can reveal how the organization of foramina and sutures changed through time, but to elucidate changes occurring in the soft tissues of the brain, the entire endocranial cavity must be examined and studied.

The easiest way to study the endocranial cavity is with an endocast. Although an endocast can refer to a cast of any specified space, it will here be limited to the endocranial cavity. A natural endocast, as described by Hopson (1979:41), is a cast "in which the rock matrix filling the cranial cavity is exposed by removal of the surrounding skull bones so as to leave a stone cast of the endocranial cavity. Such a cast resembles, to a greater or lesser extent, the brain which in life lay within the cranial cavity."

Unfortunately, natural endocasts are rare, and often the skull must be disarticulated to obtain these and describe their features. Often this is unacceptable, especially if the skull is the only one known for a particular taxon.

In many instances, artificial endocasts can be prepared from molds of the endocranial cavities of specimens, or from the serial grinding of a skull and the reproduction of the outline of the endocranial cavity (Hopson, 1979). These methods increase the number of endocasts available for study, but the overall number is still very limited for particular groups, such as theropod dinosaurs.

Despite this scarcity of endocasts, several workers have dedicated themselves to the study of these objects. A brief overview given here provides a historical perspective on the development of the field.

PRIMARY ENDOCAST WORKERS

Othniel Charles Marsh (Figure 1)

One of the first people to describe a large variety of endocasts was Othniel Charles Marsh starting in the 1870s (Marsh, 1874; 1880a; 1880b; 1881; 1881-1882; 1884a; 1884b; 1886; 1889; 1890; 1891; 1895). While doing these descriptions, Marsh came up with a series of 'laws' that he felt held true for brain evolution. Those 'laws' were (List taken verbatim from Jerison, 1973:15)

1.) All Tertiary mammals had small brains.

2.) There was a gradual increase in the size of the brain during this period.

3.) This increase was confined mainly to the cerebral hemispheres, or higher portions of the brain.

4.) In some groups, the convolutions of the brain have gradually become more complex.

5.) In some, the cerebellum and the olfactory lobes have even diminished in size.

6.) There is some evidence that the same general law of brain growth holds good for Birds and Reptiles from the Cretaceous to the present time.

7.) The brain of a mammal belonging to a vigorous race, fitted for a long survival, is larger than the average brain, of that period, in the same group.

8.) The brain of a mammal of a declining race is smaller than the average of its co[n]temporaries of the same group.

Although these laws now are known to be false, they represent the earliest attempts at using endocasts to study the evolution of brains. Of more pertinence to this study, Marsh also wrote a monograph, and at least one other paper, on Odontornithes, which included *Hesperornis* and *Ichthyornis* (Marsh, 1880a; 1881-1882). In his monograph (1880a), Marsh illustrated and described the endocasts of both birds as being very reptilian in character, representing an intermediate stage of brain evolution between reptiles and extant birds. This claim was later proven false by Tilly Edinger (1951).

Johanna Gabriele Ottilie ('Tilly') Edinger (Figure 2)

The first person to study endocasts in great detail was Tilly Edinger, whose pioneering work basically founded modern paleoneurology in the 1920s. The fact that she studied neurology was not surprising, because her father was a pioneer in the field of comparative neurology. One of her earliest works dealing with endocasts came in her dissertation on *Nothosaurus*, in which she described

Figure 1. Othniel Charles Marsh.

Othniel Charles Marsh was one of the first people to study and describe a large variety of endocasts. One of his best-known works dealing with endocasts is his monograph on Odontornithes. Picture from web. URL: www.peabody.yale.edu/people/whoswho/MarshOC.html. Courtesy of the Peabody Museum, Yale University.

Figure 2. Johanna Gabriele Ottilie ('Tilly') Edinger.

Tilly Edinger is the founder of modern paleoneurology. She also studied a large variety of endocasts, and disputed the 'laws' of brain evolution that were laid out by Marsh. Picture from web. URL: www.wellesley.edu/Anniversary/edinger.html. From the collections of the Ernst Mayr Library of the Museum of Comparative Zoology, Harvard University.

its endocast; this description was later published separately (Edinger, 1921; Buchholtz and Seyfarth, 1999). After studying the endocasts of extinct bats (Edinger, 1926a), she also became one of the loudest critics of Marsh's 'laws' of brain evolution.

Tilly Edinger had spent her entire life and career in Germany until 1939, when she was forced to flee with the increase in power of Hitler's regime. She spent a short period of time in London, before coming to America and obtaining a position at Harvard with the help of Alfred Sherwood Romer (Buchholtz and Seyfarth, 1999). It is while she was here in the United States that two of her greatest contributions were completed. The first, *Evolution of the Horse Brain*, was completed in 1948. In this work, Edinger (1948) described the changes that occurred in a series of horse brains from *Eohippus* to modern day *Equus*. This monograph was one of the first attempts to study a series of brains along a phylogenetic lineage, and examine how the various parts of the brain changed from those seen in an ancestor millions of years earlier to the modern day brain of an extant species. It is this type of study that I am undertaking in this dissertation. The second, and maybe Edinger's most important, work, was finished and published after her death (Edinger, 1975). *Paleoneurology 1804-1966. An Annotated Bibliography*, was published posthumously. This work is a compendium of the literature on endocasts for all vertebrate animals from 1804-1966. Everything from agnathans to hominids can be found in this work. The main section of bibliographic information is alphabetical by author, with an appendix containing all references to hominid material. There is also a systematic

index, prepared mainly by Dr. Joan Echols, that is organized taxonomically, and lists the authors and years for works on each group.

In addition to those two works, Tilly Edinger wrote a large number of papers on the endocasts from a wide array of animals (Edinger, 1921; 1928; 1929; 1934; 1937; 1938; 1956; 1962), including a large volume of work on flying vertebrates (Edinger, 1925; 1926a; 1926b; 1927; 1941; 1951). The first of these was a paper on *Archaeopteryx* (Edinger, 1925), which was soon followed by another on *Archaeopteryx* (Edinger, 1926b) that provided a detailed description of what could be seen of the endocast of the British specimen. Edinger also studied the endocasts of some Tertiary bats in 1926, and from those studies came to refute Marsh's 'laws,' as mentioned above (Buchholtz and Seyfarth, 1999). Her next studies centered on pterosaurs. Edinger wrote one paper in 1927, followed by a later paper in 1941, in which a description of the brain of *Pterodactylus* was given. In 1941, Edinger also wrote a paper with C. Wiman on *Aepyornis* and *Mullerornis* (Wiman and Edinger, 1941). The more telling article on birds that Edinger wrote came in 1951, when she reevaluated the endocasts of *Hesperornis* and *Ichthyornis* that Marsh had described. In that paper, Edinger revealed that Marsh's descriptions were based almost completely on what he thought the brains would look like, and in fact, he had no endocast material whatsoever! Edinger described what material was present, and what could be attained from it, doing a great deal to try and dispel the myth of what Cretaceous bird brains were like that Marsh had created with his monograph on the Odontornithes (Marsh, 1880a). She showed that the brains of *Hesperornis* and *Ichthyornis* were similar to modern

birds in all respects, and that Marsh's claims that they were more reptilian-like than bird-like was completely unfounded (Edinger, 1951). This clarification is very important because *Hesperornis* and *Ichthyornis* occupy a position on the avian family tree that is very scarcely represented, and an incorrect accounting of material in these taxa could lead to a great deal of trouble for analyses such as those I perform as part of this dissertation.

Harry Jerison

Although Marsh and Edinger described many endocasts, they rarely did much else with them. Marsh attempted some generalizations with his 'laws,' but even those were based more on qualitative criteria than actual measurements. The first person to use endocasts as a source of quantitative data for inferring brain evolution was Harry Jerison, who was a professor at the University of California at Los Angeles.

Harry Jerison used quantitative data taken from endocasts in an effort to determine whether fossil taxa, such as non-avian theropods, had larger or smaller brains than expected for their particular body size, using extant taxa for comparison. The results of his study showed that non-avian theropods had a brain-body weight ratio consistent with "reptiles" (excluding birds), meaning that they did not have anomalously small brains for their size. The study also showed that "fish" and "reptiles" have smaller brains than mammals and birds of the same body size. Jerison believed this meant birds and mammals could process more

information, and were therefore more 'intelligent' than "lower" vertebrates (Jerison, 1969; 1973).

The 'intelligence' that Jerison refers to can be gauged by a measure of encephalization, or an "enlargement of the brain beyond that expected from the enlargement of the body" (Jerison, 1985:21). So the larger the brain is, the more information it can process, and the more intelligent the animal. Jerison set out to illustrate this by making quantitative measurements using endocasts. The method he used (described below) led him to believe that there is an "orderliness... [to] the evolution of encephalization" (Jerison, 1985:24). There are eight conclusions that he drew from this orderliness. Those are (All verbatim from Jerison, 1985:24-25):

> (i) A basal lower vertebrate grade of encephalization evolved in the earliest bony fish, amphibians and reptiles and has continued to the present as a steady-state or equilibrium maintained for at least 350 million years. Since about two-thirds of living vertebrate species are members of these three classes of vertebrates, this basal grade is the norm for vertebrates.
>
> (ii) There are variations in encephalization within the lower vertebrate groups, the most interesting being between herbivorous and carnivorous dinosaurs. The carnivores were apparently significantly more encephalized.
>
> (iii) The earliest fossil birds and mammals with known endocasts had evolved to a higher grade, representing at least three or four times as much brain as in lower vertebrate species of comparable body size. This progressive or 'anagenetic' evolution occurred at least 150 million years ago, and in the case of the mammals may have begun with their reptilian ancestors at least 50 million years earlier.
>
> (iv) Within the mammals there is a good fossil record of the brain, which is consistent with a picture of steady-states punctuated by rapid evolution to higher grades. However, many grades of encephalization are represented in living mammalian species, with some (opossum, hedgehog) at the same grade as the earliest of the mammals.

(v) Two unusual conclusions are evident in the history of encephalization in primates. First, primates have always been a brainy order, perhaps doing with their brains what many other species did by morphological specializations. Second, the evolution of encephalization in the primates followed rather than preceded or even accompanied other adaptations by primates to their niches.

(vi) The highest grade of encephalization is shared by humans and bottlenosed dolphins (*Tursiops truncatus*). The sapient grade was attained about 200 000 years ago, but cetaceans may have reached their highest grade 18 million years ago.

(vii) Encephalization in the hominids is a phenomenon of the past three to five million years, and its rapidity appears to have been unique in vertebrate evolution.

(viii) These results suggest two complementary conclusions. First, the long steady-states that occurred in most groups indicate that, on the whole, encephalization was not a major element in vertebrate evolution. A particular grade of encephalization tended to be maintained once it was achieved. On the other hand, its appearance in many different and distantly related groups is evidence of some Darwinian 'fitness' for encephalization.

Jerison's concept of the evolution of encephalization was based on some equations that he developed plotting body weight (in kg) against brain weight (in g) for modern day "fish", "reptiles" (minus birds), birds, and mammals. These data, on a log-log graph, were lumped into two general groups that were described using minimum convex polygons with no internal angles greater than 180 degrees. Birds and mammals were grouped together as "higher" vertebrates in one polygon, and the fish and reptiles together as "lower" vertebrates in another. Each of these polygons had a visually fitted slope of 2/3 (Figure 3). With these data, Jerison used Snell's allometry equation (1892) as an equation for calculating the

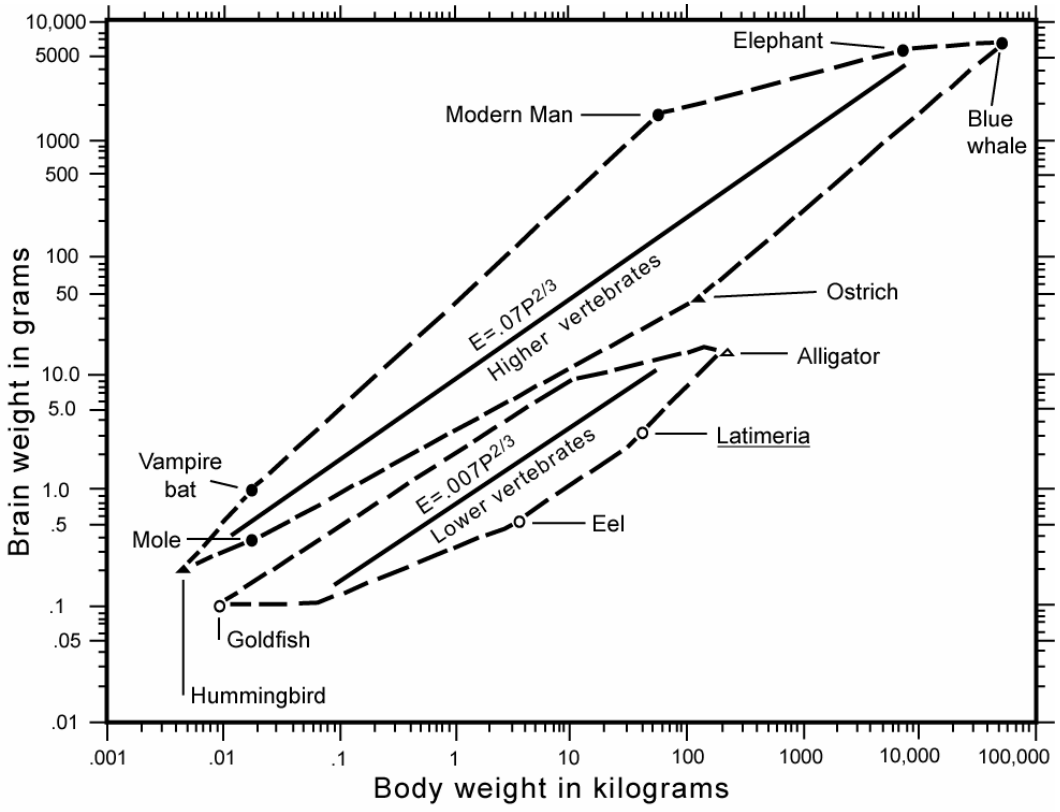

Figure 3. Chart showing the brain weight to body weight of several extant taxa.

Two groups are delineated using minimum convex polygons. The upper polygon contains mammals and birds, and the lower polygon contains "fish" and "reptiles." Redrawn based on Jerison (1969).

expected brain size of animals. The equation is: $E_e=kP^{\alpha}$, where: E_e=expected brain weight (in g), P=body weight (in g), α=2/3- the slope of the visually fitted line, and k is a constant equal to the value of E_e when P=1, or the y-intercept of the equation when in logarithmic form (Jerison, 1969; 1973; Hopson, 1980). For extinct animals such as non-avian theropods, P was determined by estimating their volume using scale models (Colbert, 1962), and then calculating their weight by multiplying the volume by the animal's specific gravity, or by using the circumference of the femur to calculate a weight (Anderson et al., 1985).

By using the data obtained from the above method, an encephalization quotient can be calculated. The encephalization quotient is $EQ=E_i/E_e$, where: E_i is the measured brain size, and E_e is the expected brain size (obtained from the previous equation) (Jerison, 1973). The measured brain size for non-avian theropods, E_i, was determined by using graphic double integration to estimate the volume of an endocast. Graphic double integration, as described by Jerison, is performed by placing

> a series of equidistant parallel measurements … through lateral and dorsal projections of the endocast. The averages of the two sets of measurements are treated as the lengths of the principal axes of an ellipse, and the endocast volume is approximated by the volume of the elliptical cylinder in which this ellipse is the cross section and the distance between Nerve XII and the anterior tip of the forebrain is the height (Jerison, 1969:582) (Figure 4).

Jerison argued that the error between this method of obtaining the volume, and the actual volume of the endocast, was always under 5%.

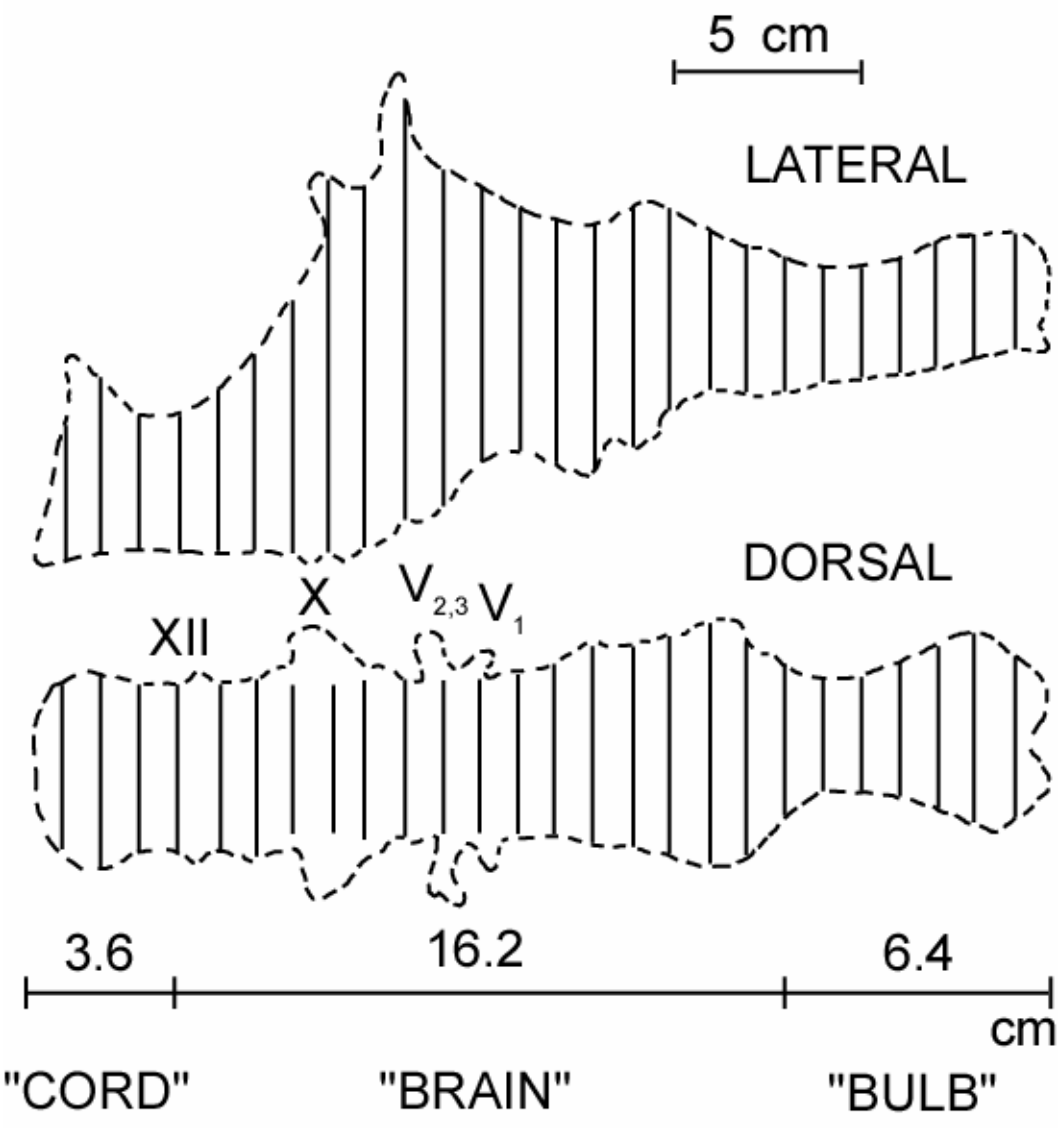

Figure 4. Graphic double integration.

Graphic double integration is the method Jerison used to determine an approximate volume for an endocast based solely on dorsal and lateral illustrations. The outline is that of the *Tyrannosaurus rex* endocast illustrated by Osborn (1912). Redrawn based on Jerison (1969).

Jerison made one final correction to his volume estimates based on an assumption that the brain of non-avian theropods only filled about 50% of the braincase. This was based on comparisons with extant reptiles like *Sphenodon* (Jerison, 1969), in which half of the endocranial space is occupied by venous sinuses, endolymphatic structures, and dura mater. There are also some areas seen in the endocast that may have been separated from the main cranial cavity by cartilaginous barriers during the animal's lifetime, and, after death, the loss of this cartilage may cause the size of the main cavity to appear larger than it was in reality (e.g., supraoccipital cartilage area; Hopson, 1979). A correction for brain size was not made for fossil sharks, pterosaurs, birds, or mammals because their brains almost completely filled the endocranial cavity (Jerison, 1973).

Once the measurements are corrected, they are placed into the equation. When the encephalization quotient is greater than 1.0, it means the brain is larger than expected for an average animal of the inspected animal's size and group. For example, humans, having an E_i of 1350g and a P of 70,000g, would have an EQ of 6.3. In other words, the human brain is about 6 times larger than expected for an 'average' mammal (Jerison, 1973). Similarly, EQs of less than 1.0 imply a smaller brain than expected for an average animal of its group. Hopson (1977) used EQ to determine relative agility and speeds between various groups of non-avian theropods, and also used it to argue against endothermy for most of them. When calculating EQ, Hopson modified Jerison's allometric scaling factor of 2/3 to account for Bauchot's (1978) claim that this scaling factor results in overly heavy brain weight estimates for very heavy animals, such as sauropods and

whales (Bauchot and Stephan, 1969). By making a correction that involved the hyperbolic tangent, values more consistent with what was expected based on the data were obtained (Bauchot, 1978), so Hopson used the corrected weights given by Bauchot (Hopson, 1980).

Although the above procedures and calculations seem sound, there are several assumptions that, if incorrect, can lead to erroneous results:

1.) The assumption that the brains of non-avian theropods only filled 50% of the cranial cavity, if incorrect, would invalidate all following measurements and hypotheses.

2.) The graphic double integration method, used to determine the overall size of the endocasts, is imprecise. Jerison himself stated that errors up to 5% had been found with this method (Jerison, 1969). Although this may not seem like much, when using the results to delineate minimum convex polygons with borders that are very close to each other, a deviation of 5% can be the difference between overlap and no overlap.

3.) The visually fitted line of 2/3 may also be incorrect, leading to errors in expected brain weight estimates. Bauchot recognized that this value of 2/3 may be wrong for heavier animals, but do his corrections correctly solve the deficiencies? Bauchot admits his curve begins to decrease when considering animals of a very high weight, like the largest sauropods, and may be invalid (Bauchot, 1978). The models used to estimate the weights of the dinosaurs must also be critically evaluated. Hypotheses about the biology and physiology of dinosaurs changed

dramatically over time, and many of the models used by Colbert are incorrect according to the best available modern data. Any errors in those models were greatly accentuated when the volumes were multiplied by the scaling factor of the model (Colbert, 1962).

4.) Sample size has to be taken into account as well. Owing to the limited number of natural and artificial endocasts, many taxa were left out of Jerison's study. Specimens that were too small, too fragile, or too valuable to risk damage through preparation, such as *Herrerasaurus*, were also unavailable. Because of this paucity of specimens, it is hard to observe any trends that may be visible when a larger number of specimens and taxa are available for study.

5.) The relative maturity of the specimens from which endocasts were derived is also problematic. It is likely that several of the specimens used by Jerison were not fully-grown, based on the observation that the majority of animals within any particular group die before reaching maturity (Malthus, 1798). Use of measurements from immature specimens would give incorrect results in the construction of the polygons. Their use could not be avoided though, because several of these groups may only have one good natural, or artificial, endocast.

Even with the problems mentioned above, Jerison's attempt to make quantitative measurements with endocasts was an important step leading toward new methods that are being used today.

Leonard Radinsky

Leonard Radinsky conducted a fair amount of endocast work with mammals (Radinsky, 1973; 1976; 1977; 1978; 1981), and derived an equation that he viewed as an improvement on Jerison's method of comparing brain weight to body weight to determine relative brain size. The measure he proposed compares endocranial volume to the area of the foramen magnum (Figure 5) (Radinsky, 1967). The equation is set up as follows: log y= log b + k log x, where: y= log endocranial volume, x= log foramen magnum area, b= y-intercept, and k= slope.

In his 1967 analysis, Radinsky asserted that the data vindicated the equation, and showed that that method could be used to compare modern mammals with fossil mammals. That equation is intriguing, but it has apparently not been tested or verified with recent bird taxa.

Radinsky (1978) also disputed Jerison's claim (Jerison, 1970; 1973) that carnivores had larger brains than contemporaneous ungulates since the Early Tertiary. In the initial study, Jerison stated that since their evolution in the Early Tertiary, carnivores had larger brains than ungulates, and that Paleogene carnivores and ungulates had larger brains than 'archaic' carnivores and ungulates, and this is why the Paleogene types survived to produce the modern lineages of carnivores and ungulates (Jerison, 1973; Romer, 1966). In Radinsky's (1978) paper, though, he showed that there were many errors made by Jerison, and there is no evidence that 1) carnivores had larger brains than ungulates, and 2) 'archaic'

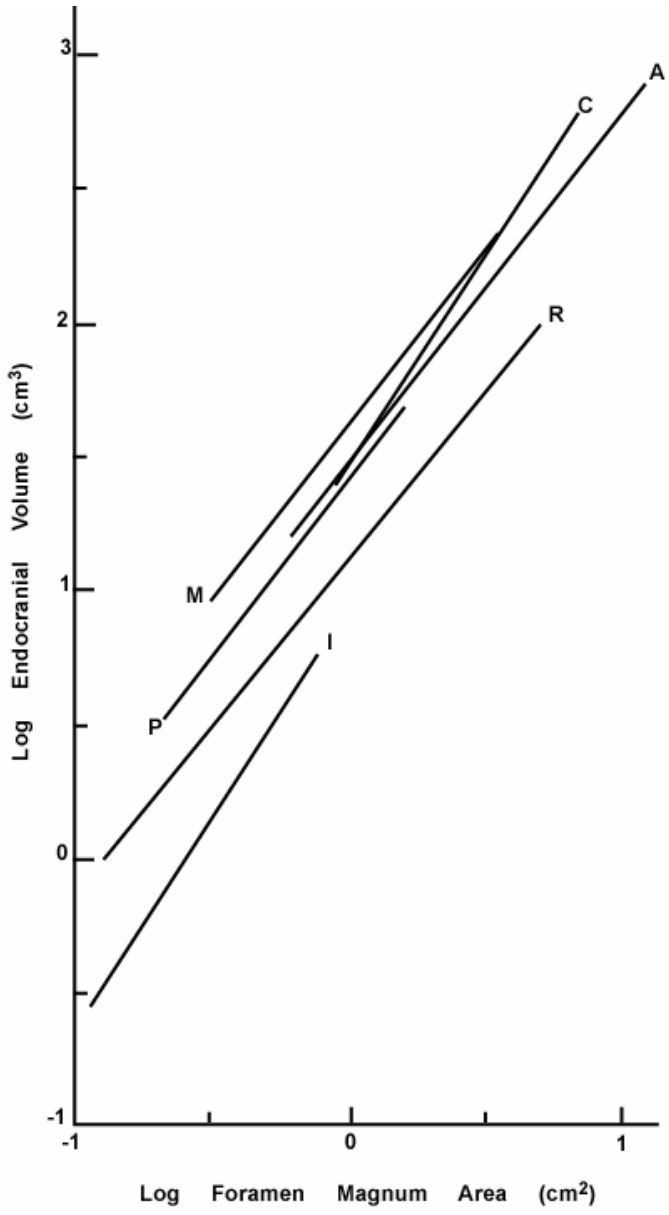

Figure 5. Graph showing the relationship between endocranial volume and area of the foramen magnum.

The lines shown are for five orders of mammals. **I**- insectivores, **R**- rodents, **P**- prosimian primates, **M**- New and Old World monkeys combined, **C**- fissiped carnivores, and **A**- artiodactyls. Redrawn based on Radinsky (1967).

carnivores and ungulates had smaller brains than Paleogene carnivores and ungulates.

In addition to the debates and disputes with Jerison and his equations, Radinsky published numerous descriptive and comparative works on mammalian endocasts (e.g., Radinsky, 1973; 1976). In one of those papers he illustrated and described a dozen endocasts of extinct and living canid genera to determine both evolutionary relationships and brain evolution (Radinsky, 1973). It is that type of work that is being continued today in various groups of animals, the present dissertation among them.

SECONDARY ENDOCAST WORKERS

Besides the four people listed above, several others studied endocasts in varying degrees of detail. Listed below are just a few select people from a long list.

Henry Fairfield Osborn

One early worker to at least illustrate and describe several endocasts was Henry Fairfield Osborn in his publication on the skulls of *Tyrannosaurus* and *Allosaurus* (Osborn, 1912). In that publication Osborn not only showed endocasts of those two particular taxa, but also that of the sauropod *Diplodocus* (Figure 6).

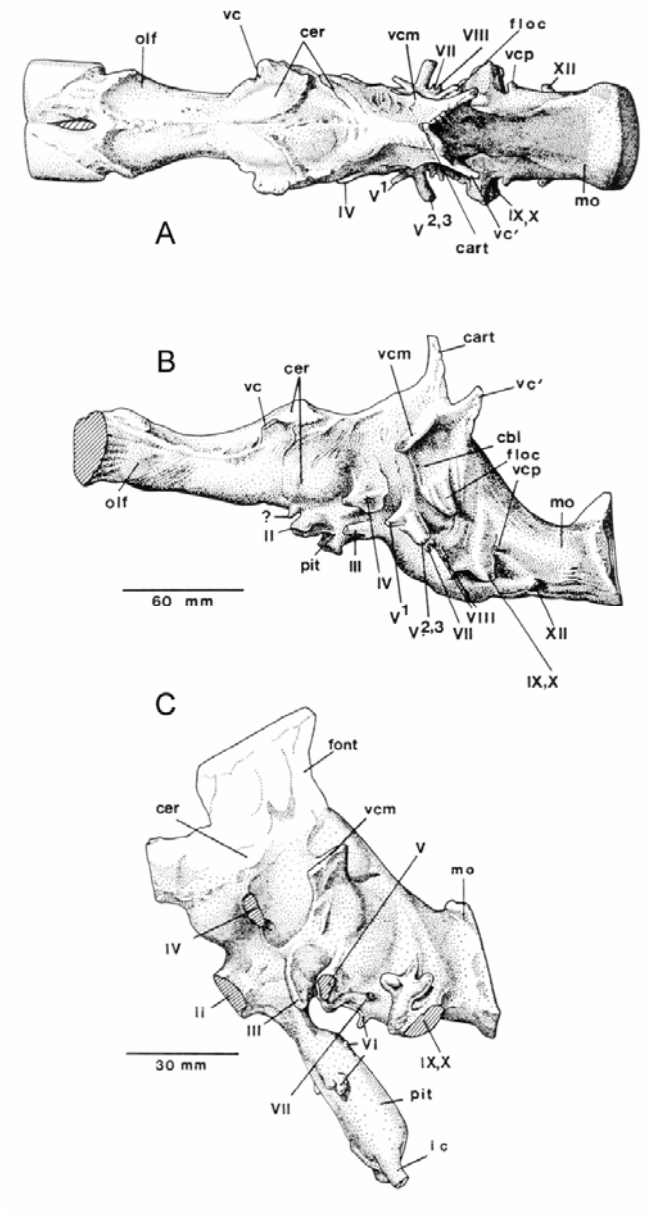

Figure 6. *Tyrannosaurus rex* endocast and *Diplodocus longus* endocast.

(A) Dorsal and (B) left lateral view of the *Tyrannosaurus rex* endocast, from AMNH 5029, illustrated by Osborn (1912). (C) Left lateral view of the *Diplodocus longus* endocast, from AMNH 694, illustrated by Osborn (1912). All three images redrawn by Hopson (1979). Permission to reprint granted by James Hopson.

Peter Galton

In 1985, Peter Galton illustrated some endocasts of the sauropodomorph *Plateosaurus* (Figure 7). In that publication, Galton also described nerves and brain regions in his description of the endocasts (Galton, 1985).

Emily Giffin

Emily Giffin (now Buchholtz) also studied endocasts. Her work centered on the ornithischian side of the dinosaur family tree, with a study of pachycephalosaur endocasts (Figure 8) (Giffin, 1989).

James Hopson

James Hopson, in *Biology of the Reptilia*, wrote a nice summary of what paleoneurology encompasses, and gave a good summary of some of the endocasts available for a wide array of taxa (Hopson, 1979). That work is vital to anyone who wants to work with endocasts. It also gave a good summary of most of the basics necessary to study an endocast and understand it. He discussed the nature of endocasts, how they are obtained, and what influences their shape. He also discussed the cranial nerves, the main divisions of the brain, and summarized some of the quantitative studies that were attempted using endocasts. He provided a review of the endocasts of turtles, lizards, crocodiles, pterosaurs, dinosaurs, and synapsids (Hopson, 1979). Although it is slightly dated and some new methods were developed later for the quantitative use of endocasts, it is still an invaluable reference.

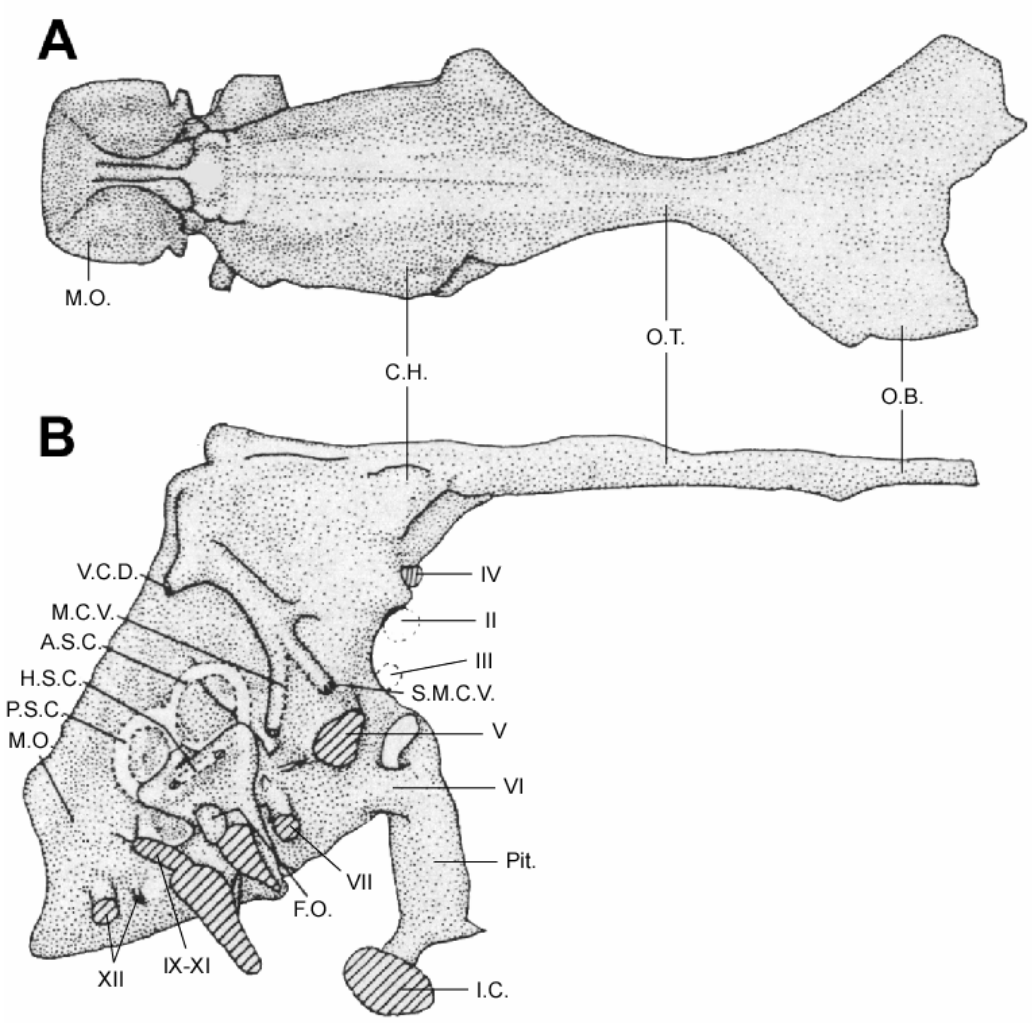

Figure 7. *Plateosaurus engelhardti* endocast.

(A) Dorsal and (B) right lateral view of an endocast of *Plateosaurus engelhardti*, AMNH 6810. Modified from Galton (1985). Permission to reprint granted by Peter Galton.

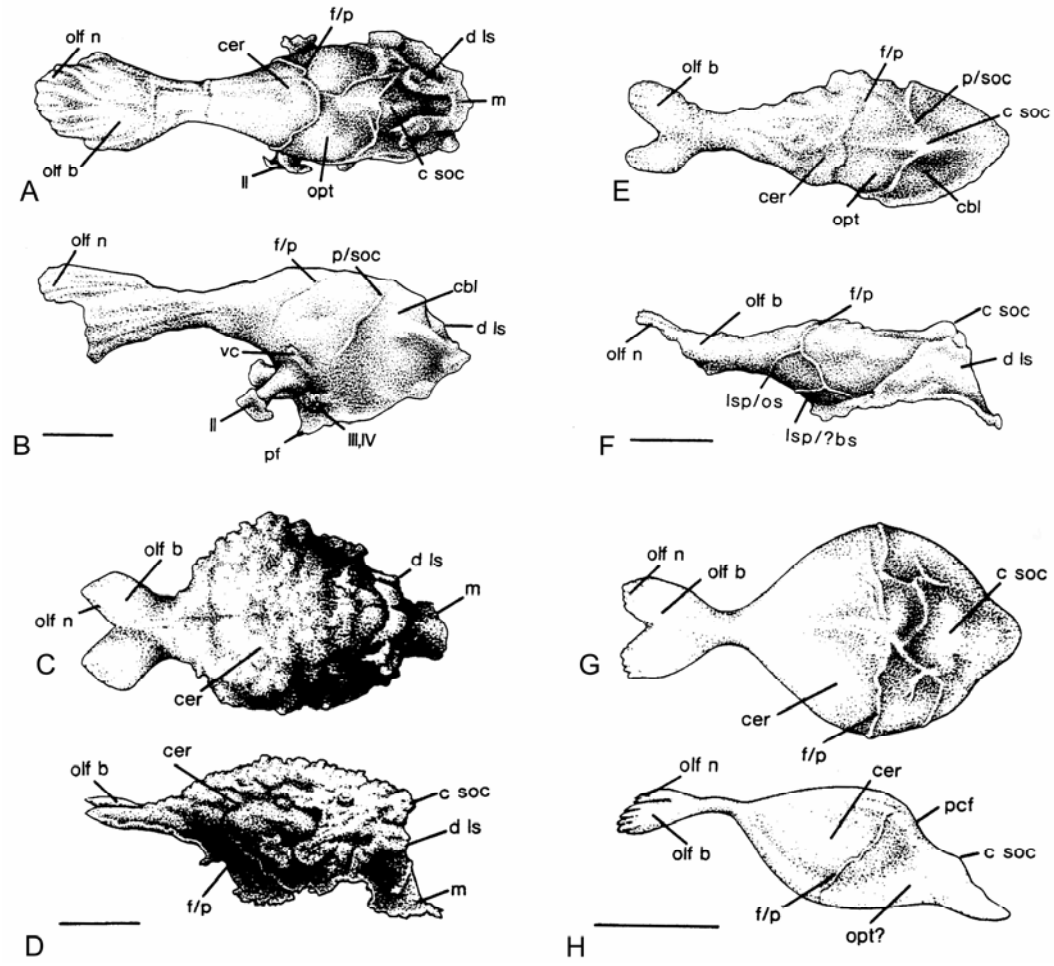

Figure 8. Endocasts of pachycephalosaurs.

(A) Dorsal and (B) lateral views of *Pachycephalosaurus wyomingensis*, USNM 264304; scale = 2 cm. (C) Dorsal and (D) lateral views of *Stegoceras sp.*, TMP 84.5.1; scale = 1 cm. (E) Dorsal and (F) lateral views of *Stenotholus kohleri*, MPM 7111; scale = 2 cm. (G) Dorsal and (H) lateral views of *Stegoceras sp.*, TMP 85.36.292; scale = 1.5 cm. From Giffin (1989). Permission to reprint granted by the Journal of Vertebrate Paleontology and Emily Buchholtz (Giffin).

In 1977, Hopson used his knowledge of endocasts and relative brain size to comment on what they might mean for dinosaur behavior. He hypothesized that the activity and behavior of taxa through evolution became more complex as their brain size increased, and he looked at different dinosaur groups to see whether that idea was consistent with the data (Hopson, 1977). Based on the data, the relationship seemed to hold true. In 1980, Hopson continued that thought by addressing the issue of dinosaur metabolism. He did that by examining where dinosaur brain sizes fell compared to the endothermic and ectothermic groups found by Jerison's encephalization quotient calculations. In that study, Hopson concluded that only coelurosaurs had a metabolism that could be considered endothermic in the same sense as birds and mammals, and that all other dinosaurs may have had an intermediate type of metabolism (Hopson, 1980). Those investigations will be elaborated upon as part of this dissertation.

Christopher Brochu

A recent advance in the study of endocasts involves the creation of digital endocasts. One of those digitally constructed endocasts is that of the *Tyrannosaurus rex* specimen known as 'Sue,' published by Christopher Brochu (Brochu, 2000). Along with his description, Brochu provided several computer-generated images of the digital endocast (Figure 9).

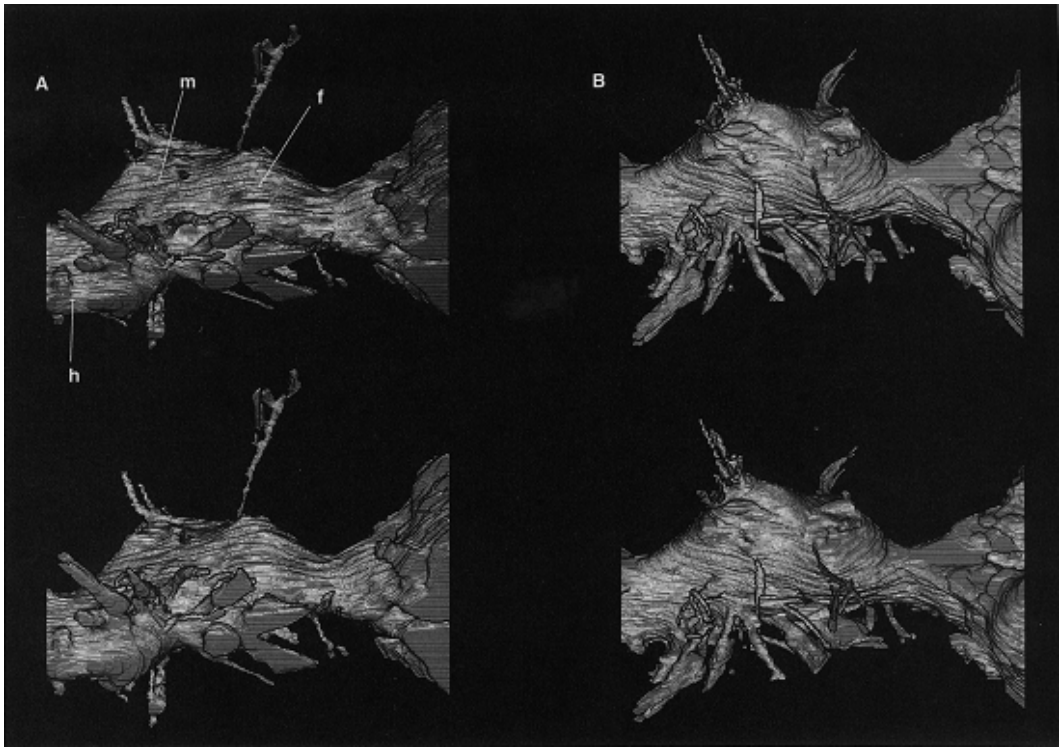

Figure 9. Digital endocast of *Tyrannosaurus rex*, FMNH PR2081.

Stereopairs in (A) ventrolateral and (B) dorsolateral views. From Brochu (2000). Permission to reprint granted by the Journal of Vertebrate Paleontology and Christopher Brochu.

Hans Larsson

Another digitally constructed, large theropod endocast was published by Hans Larsson (2001). In that paper, Larsson illustrated and described the endocast of *Carcharodontosaurus saharicus* (Figure 10). Digital construction of endocasts allows comparisons of closely related taxa that otherwise may not be possible. One of these comparisons that is now possible is that of *Carcharodontosaurus saharicus* and *Acrocanthosaurus atokensis*, for which I constructed a digital endocast as part of this dissertation (Franzosa, 2002).

John Allman

Brain size, and its evolution through time, is also being studied by neuroanatomist John Allman (1999). Allman argued that maintaining the functions of larger brains is extremely expensive energetically. In vertebrates, 2-8% of the energy used by an organism is consumed by the brain. This level of consumption holds true for ectothermic animals too, so food intake would have to increase drastically in large ectothermic animals with big brains. That may explain the lack of large-brained, ectothermic animals (Nilsson, 2000).

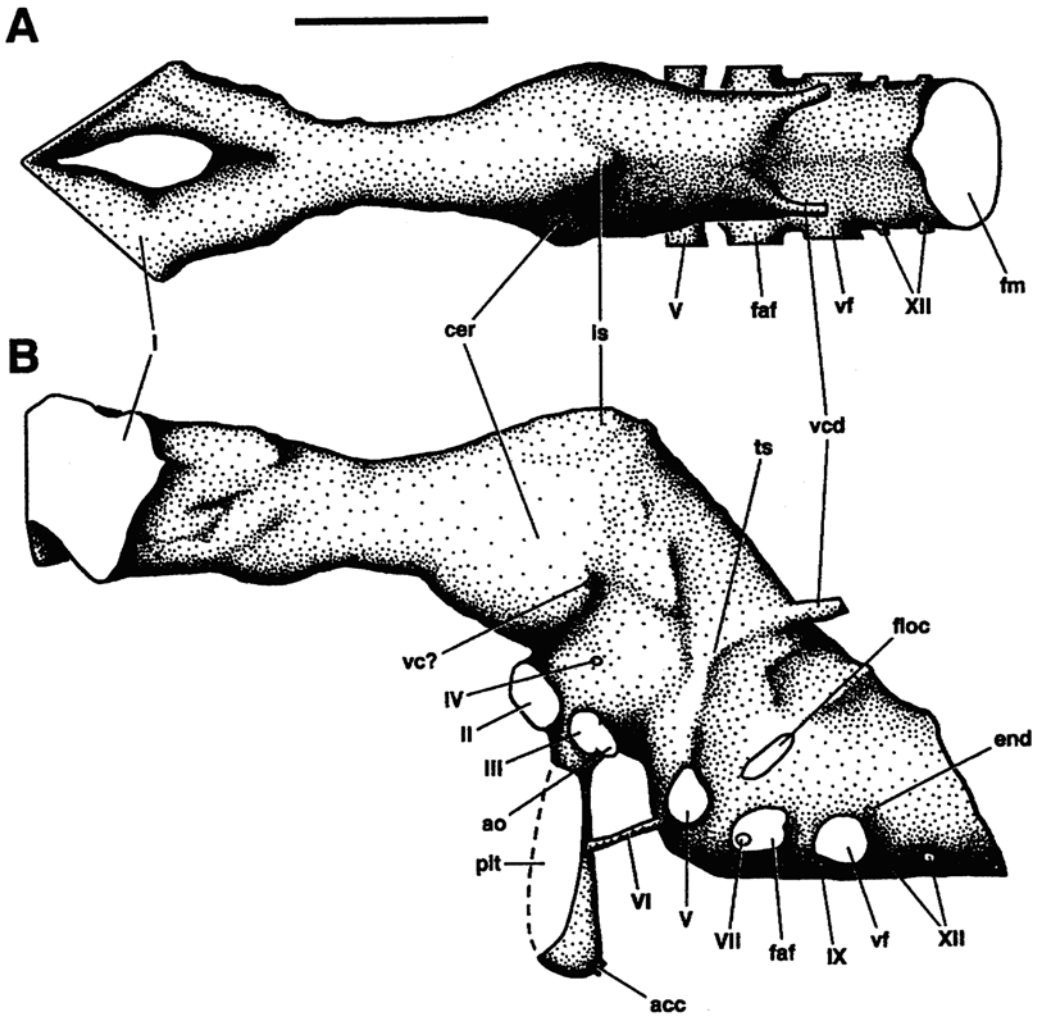

Figure 10. *Carcharodontosaurus saharicus* endocast.

(A) Dorsal and (B) lateral views of the endocast of *Carcharodontosaurus saharicus*, SGM-Din 1. Drawing from an original digital endocast. From Larsson (2001). Permission to reprint granted by Indiana University Press.

INTERPRETING ENDOCASTS

Two main factors determine the appearance of an endocast: 1) the braincase, and 2) the brain.

The Braincase

Because the size and shape of an endocast is determined by the bones that surround it, a brief review is presented here of the bones that make up the braincase in theropods, and how each one affects the part of the endocast it surrounds. It is generally accepted that the structures of the braincase are conservative, and not subject to dramatic changes in closely related taxa or over short periods of time (Gower and Sennikov, 1996). This is especially true of major structures, such as the pathways of the nerve foramina; so any changes in the location or number of these openings that does occur may be phylogenetically informative.

This review focuses on the braincase of theropod dinosaurs, the group with which I am concerned here. The bones that make up the theropod braincase are the frontals, parietals, supraoccipital, sphenethmoid, orbitosphenoids, laterosphenoids, prootics, exoccipitals, parasphenoid, basisphenoid, and basioccipital. Although not all dinosaurs have all the bones in this list, most theropods contain almost all of them (Currie, 1997). The following information on the braincase bones was obtained from Currie (1997), unless otherwise noted.

Frontals

At the anterior end of the braincase, among the anteriormost bones to house a portion of the endocast, are the frontals. On the ventral surface of the frontals are impressions of the dorsal surface of the olfactory bulbs, olfactory tracts, and the anterior portion of the cerebral hemispheres. It is these impressions that most accurately represent the actual shape and dimensions of the forebrain in maniraptoran and later theropod endocasts.

Sphenethmoid

The sphenethmoid participates in enclosing the olfactory bulbs and tracts. This bone, when preserved, forms the ventral and lateral walls of the tube formed with the frontals around the bulbs and tracts.

Orbitosphenoids

The orbitosphenoids are found posterior to the sphenethmoid. These bones contribute to the anterior wall to the endocast, and surround the single or paired opening(s) for the optic nerves (CN II). When preserved, these bones form part of the border for the oculomotor nerve (CN III), and sometimes for the trochlear nerve (CN IV).

Laterosphenoids

The laterosphenoids are located ventral to the frontals and posterior to the orbitosphenoids. The laterosphenoids form portions of the lateral and anterior walls to the endocast. These bones form the posterior border of the oculomotor foramen, and participate in, or completely enclose, the foramen for the trochlear nerve. They also form the anterior margin of the foramen for the trigeminal nerve (CN V), and in those animals in which the ophthalmic branch of the trigeminal nerve branches before leaving the braincase, the laterosphenoids either enclose its foramen and canal, or have a groove on their lateral surface marking the passage of the ophthalmic nerve anteriorly. The ventrolateral surface of the optic lobe is also reflected on the medial surface of the laterosphenoids.

Parasphenoid and Basisphenoid

Ventral to the sphenethmoid and anteroventral to the orbitosphenoids are the parasphenoid and basisphenoid, which are indistinguishably fused in almost all adult dinosaurs. This complex houses the pituitary fossa on its posterodorsal surface, just ventral to the optic foramen. The basisphenoid also forms the anteroventral wall to the endocast, encloses the abducens canal (for CN VI), and houses the abducens foramen. In some dinosaurs the abducens canal opens into the pituitary fossa, while in others the canal passes the fossa laterally. The ventrolateral surface of the basisphenoid also holds the internal carotid canal, which proceeds anterodorsomedially to unite with its counterpart in the pituitary fossa. The palatine branch of the facial nerve (CN VII), in those animals in which

it branches before exiting the braincase, also passes through the basisphenoid as it moves anteriorly through the braincase.

Parietals

The paired bones that are directly posterior to the frontals on the dorsal surface of the braincase are the parietals. Impressions of the posterodorsal surface of the cerebral hemispheres, and the dorsal surface of the cerebellum, can be seen on the ventral surface of the parietals in those animals in which the brain nearly completely fills the braincase. It can be difficult to ascertain whether or not the impressions represent the dorsal surface of the cerebellum because a large dorsal sagittal sinus overlies the median part of the cerebral hemispheres, and an occipital sinus overlies the cerebellum (Baumel et al., 1993). In some animals this is fairly small, and the actual cast of the cerebellum can be observed. In other taxa it is fairly large, and all that can be seen on the endocast is a featureless surface, which is evidence that the occipital sinus excluded the dorsal surface of the cerebellum from contact with the parietals.

Supraoccipital

Posterior to the parietals is the supraoccipital. The ventral surface of the supraoccipital also helps to delineate the posterodorsal surface to the endocast (whether it be the cerebellum or the occipital sinus). In some taxa there is also a pair of foramina that mark the exit of some branches of the occipital sinus posteriorly; in birds, these represent the passages for the external occipital veins

(Baumel et al., 1993). Again, depending on the taxa, the role that the supraoccipital plays in the formation of the foramen magnum varies from bordering most of the dorsal surface, to being entirely excluded from it by the exoccipitals.

Exoccipitals and Opisthotics

The exoccipitals are found ventrolateral to the supraoccipital. They help to form the posterolateral walls to the endocast, the lateral and dorsal margins of the foramen magnum, a portion of the occipital condyle, and are indistinguishably fused with the opisthotics to form ventrolaterally projecting paroccipital processes (Currie, 1997). Anterior to the portion of the exoccipital that participates in the occipital condyle, there is often a deep pit in the ventral surface of the exoccipital. It is in this pit that the exits for the hypoglossal nerve (CN XII) are found. Usually there are one or two foramina on either side of the skull for this nerve. Sometimes there is also a larger foramen located in this pit. This represents the jugular foramen, from which the vagus nerve (CN X), accessory nerve (CN XI), and jugular vein exit. The exoccipital also helps to form the posterior margin of the metotic fissure, from which the glossopharyngeal nerve (CN IX) exits, as well as the vagus nerve, accessory nerve, and jugular vein in those taxa that do not have a separate jugular foramen penetrating the exoccipital.

Basioccipital

The posterior floor of the braincase is formed by the basioccipital. The basioccipital participates in the ventral margin of the foramen magnum, and makes up the majority of the occipital condyle. Because most of the venous sinuses are located on the dorsal and lateral surfaces of the brain, the dorsal surface of the basioccipital provides a good representation of the ventral surface of the medulla oblongata (Hopson, 1979). The dorsolateral surface of the basioccipital also helps to form the base of the middle ear cavity and the metotic fissure, whose contents were described above.

Prootics

The final bones that help to make up the braincase are the prootics. The prootics form a large portion of the lateral walls of the braincase. Externally, the prootics form the posterior margin of the trigeminal foramen, and completely enclose the foramen for the facial nerve. They also form the anterodorsal margin of the fenestra ovalis and the fenestra pseudorotunda. Internally, the medial surface of the prootics holds the floccular recess, in which the floccular lobe was located. It is also in this area that the prootics, along with the opisthotics, enclose the osseous labyrinth, which houses the semicircular canals. These semicircular canals surrounded the floccular lobe. Beneath the osseous labyrinth and semicircular canals were the cochlea and other areas of the inner ear. It is here that the branches of the vestibulocochlear nerve (CN VIII) entered the cochlea and vestibular apparatus.

Regions of the Brain

The main mass of the endocast represents the cavity in which the brain lay while the animal was alive. This cavity may produce endocasts that do not look at all like the actual brain of the animal. The reasons for this are that a variety of structures, such as endolymphatic structures, venous sinuses, and meninges, occupied this space in addition to the brain. Plus, there are some areas seen in the endocast that may have been separated from the main cranial cavity by cartilaginous barriers (e.g., supraoccipital cartilage area) (Hopson, 1979). Consequently, the endocasts of fish, lizards, amphibians, and crocodilians do not represent the true size and shape of the animals' brains. In some animals though, such as mammals and birds, the brain almost completely fills the endocranial cavity, so their endocasts provide a better approximation of the shape and size of the brain. For non-avian theropods, it is hard to determine the degree to which their brain filled the endocranial cavity. Their extant relatives yield a phylogenetic bracket (sensu Witmer, 1995) that gives opposing stories; the brain of crocodilians does not completely fill the endocranial cavity, but bird brains do. The endocasts of more basal non-avian theropods indicate that their brains did not completely fill the endocranial cavity, as evidenced by the lack of observable cerebral hemispheres and cerebellar outlines. Endocasts from some more recent clades suggest that the brain may have come close to completely filling the cavity, as evidenced by the complete delineation of the cerebral hemispheres and cerebellum (personal observations). Depending on the degree to which the brain filled the endocranial cavity, there are several neural features that can be seen in

an endocast. Recognition of these features requires some knowledge of brain anatomy.

All vertebrate brains can be broken down into five main divisions (Hopson, 1979). These are the telencephalon, diencephalon, mesencephalon, metencephalon, and myelencephalon (Figure 11). The telencephalon and diencephalon make up what is commonly called the prosencephalon (or forebrain), the mesencephalon is the midbrain, and the metencephalon and myelencephalon make up the rhombencephalon (or hindbrain) (Hopson, 1979). The information in the following discussion will be based on Jerison (1973) unless otherwise noted. For more information on the brain and its individual regions, see references cited.

Telencephalon

The first division of the brain is the telencephalon. This consists of the olfactory bulbs, olfactory tracts (peduncles), olfactory nerves (CN I), and cerebral hemispheres. Overall, in fish, amphibians, and reptiles, the telencephalon deals with olfactory integration, while in mammals and birds it is involved in most of the advanced brain/behavior relations. The olfactory bulbs are where the olfactory nerve axons terminate, and their size often depends on the degree to which the animals relied upon smell (Butler and Hodos, 1996). The more reliant they were on smell, the larger the olfactory bulbs. Those taxa with larger olfactory bulbs also have a larger hippocampus than those with smaller bulbs (Pearson, 1972).

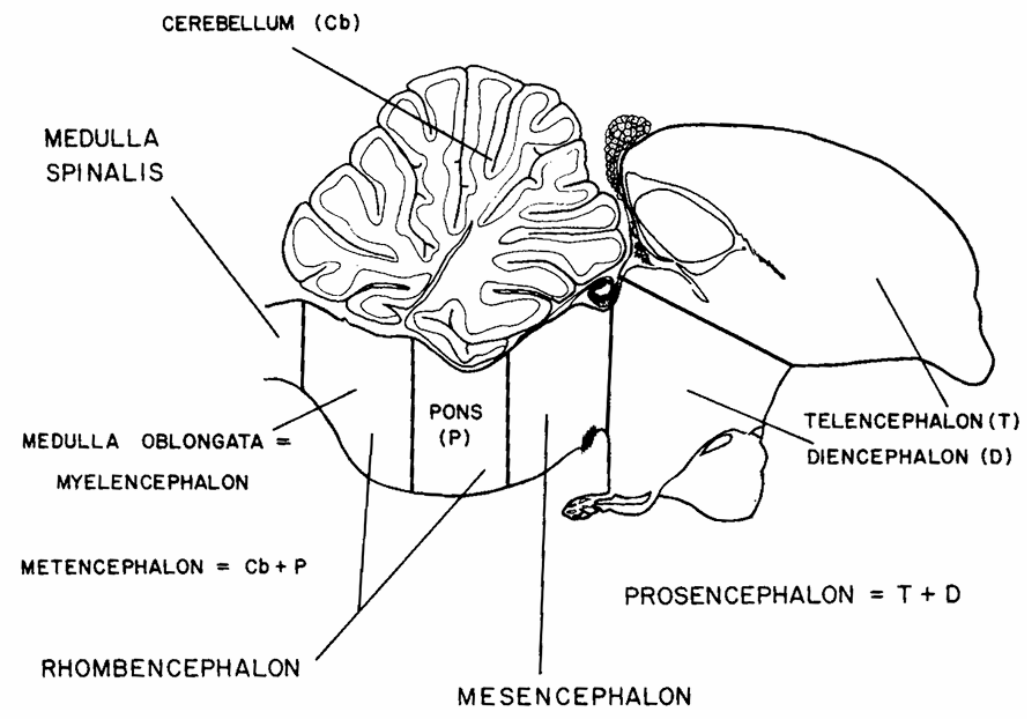

Figure 11. Five main divisions of the brain.

Median-sagittal view of the brain of a chick showing the five main divisions of the brain. From Baumel et al. (1993). Permission to reprint granted by The Nuttall Ornithological Club.

The olfactory tracts attach the olfactory bulbs to the cerebral hemispheres. The position of the olfactory bulbs and tracts can be inferred from impressions on the ventral surface of the frontals, by the positioning of the sphenethmoid, and in some cases by the orbitosphenoids (Brochu, 2003).

The cerebral hemispheres, located posterior to the olfactory bulbs and tracts, integrate information from both motor and sensory systems. In fish, amphibians, and reptiles, this information is mostly chemical and olfactory related, whereas in mammals and birds, the cerebral hemispheres also integrate tactile, auditory and visual information. The shape of the dorsal surface of the cerebral hemispheres can be inferred from the ventral surface of the frontals, and in more advanced theropods such as troodontids, the ventral surface of the parietals as well (Currie, 1997). The shape of their anterior and lateral surfaces can be inferred somewhat by the medial surfaces of the orbitosphenoids and laterosphenoids.

Diencephalon

The diencephalon consists of the pineal gland, dorsal thalamus, ventral thalamus, pituitary, optic tract, optic nerves (CN II), and hypothalamus (Butler and Hodos, 1996). Those portions of the diencephalon that can be seen in endocasts are the pituitary, pineal gland, optic tract, and optic nerves. The diencephalon is the part of the forebrain that sends information to the cerebral cortex (Butler and Hodos, 1996), and is associated with autonomic control (Pearson, 1972). The pituitary is the master gland of the body. It not only controls

the functions of many other glands, but also controls growth. It is located just ventral to the cerebral hemispheres, and is housed within the pituitary fossa, which is formed by the basisphenoid. The pineal gland is found between the cerebral hemispheres and the cerebellum, but it is not evident in theropod endocasts. It plays a role in circadian and other biological rhythms (Breazile and Hartwig, 1989; Butler and Hodos, 1996). The optic nerves and tracts relay visual information to the optic lobes and thalamus.

Mesencephalon

The mesencephalon can be divided into three major regions: the tectum, the tegmentum, and the isthmus (Butler and Hodos, 1996). The mesencephalic structures visible in an endocast consist of the optic lobes (optic tectum), oculomotor nerves (CN III), and trochlear nerves (CN IV). The mesencephalon deals with reflex controls that integrate motor behavior with auditory information, visual information, and postural reflexes. It has been greatly expanded as the optic lobes of reptiles and birds (Jerison, 1973). The mesencephalon also "links the sensory, motor, and integrative components of the hindbrain with those of the forebrain" (Butler and Hodos, 1996:201). As with the olfactory lobes, those animals that are more reliant on vision are apt to have larger optic lobes (Pearson, 1972). These lobes are located ventrolateral to the cerebral hemispheres in birds, and an idea of their size can be obtained from the medial surface of the laterosphenoids. In crocodilians and early theropods, the optic lobes are located posterior to the cerebral hemispheres and anterior to the cerebellum. The

oculomotor and trochlear nerves also attach to the brain in this region (but not to the optic lobe itself).

Metencephalon

The anterior portion of the rhombencephalon is the metencephalon. The metencephalon is composed of the cerebellum, trigeminal nerve (CN V), abducens nerve (CN VI), facial nerve (CN VII), and vestibulocochlear nerve (CN VIII). The most important component of the metencephalon is the cerebellum. The cerebellum not only coordinates movement and positioning, but also controls muscle tone (Pearson, 1972; Breazile and Hartwig, 1989). It also "has a close relationship with the vestibular, somatosensory, visual, and auditory systems" according to Butler and Hodos (1996:180). The cerebellum is located directly posterior to the cerebral hemispheres and posterodorsal to the optic lobes in birds, and can sometimes be partially represented on the ventral surface of the parietals, but this can be misleading because of the large occipital sinus that covers this region of the brain (Hopson, 1979; Baumel et al., 1993). In crocodilians and early theropods, the cerebellum is posterior to the optic lobes, which separate the cerebellum from the cerebral hemispheres. Many animals have lateral projections of the cerebellum on each side called flocculi, or floccular lobes. These lobes are hypothesized to play a role in the balance and orientation of animals as they move. The large floccular lobes of pterodactyls and birds support this suggestion, because fine control would be necessary for flying animals (Witmer et al., 2002, 2003). The floccular lobes are found within the otic capsules, and are surrounded

by the osseous labyrinths of the semicircular canals. Also found in this region are the attachment of cranial nerves V-VIII to the main body of the brain.

Myelencephalon

The posterior portion of the rhombencephalon, and final division of the brain, is the myelencephalon, which consists of the medulla oblongata, pons, glossopharyngeal nerve (CN IX), vagus nerve (CN X), accessory nerve (CN XI), and hypoglossal nerve (CN XII). The function of the myelencephalon involves the control of visceral activity, as well as a relay for information coming to, and going from, various other portions of the brain and body (Jerison, 1973; Butler and Hodos, 1996). It is along the lateral edges of the medulla that the attachment points for cranial nerves IX-XII are found. The medulla ends at the foramen magnum, but the central nervous system continues with the transition of the medulla to the spinal cord outside of the braincase.

The Cranial Nerves

Although the gross morphology of the endocast is largely explained by brain shape, another large class of features that are quite apparent in most endocasts is processes that stem from the main body of the endocast. These processes represent the locations of the foramina in the braincase bones from which the cranial nerves, as well as arteries and veins, exited the braincase.

Thirteen cranial nerves are recognized in most taxa. The terminal nerve (CN O) is not well understood, or pertinent to this discussion, so it is the

'traditional' 12 cranial nerves (CN I-XII) that are described in the text below (Figure 12). Unless otherwise noted, this summary of information on the cranial nerves is from Bubień-Waluszewska (1981). Although the information on their pathways pertains to most vertebrates, this description is based on the neuroanatomy of birds. Most of this information was also summarized by Butler and Hodos (1996).

Olfactory Nerve

The olfactory nerve (CN I) is a sensory nerve that innervates the olfactory epithelium of the nasal cavity (Butler and Hodos, 1996), and is involved in smell and chemical sensing (Jerison, 1973). It enters the olfactory bulb, which lies either directly anterior to the cerebral hemispheres, or is attached to the cerebral hemispheres via an olfactory tract that extends posteriorly from the olfactory bulb to the anterior portion of the brain. Often the entrance of the olfactory nerve into the olfactory bulb cannot be seen, but if the bulb is surrounded by bone there will be an olfactory foramen present, usually in the frontals and sphenethmoid. An impression of the dorsal surface of the olfactory bulbs and/or tracts can be seen on the ventral surface of the frontals, and often the ventral and lateral surfaces are defined by the sphenethmoid (Currie, 1997) and possibly the orbitosphenoids, as described by Brochu for tyrannosaurids (Brochu, 2003). A correlation between the thickness of the nerves and the degree of olfactory development in birds was hypothesized by Stresemann (1928-1929).

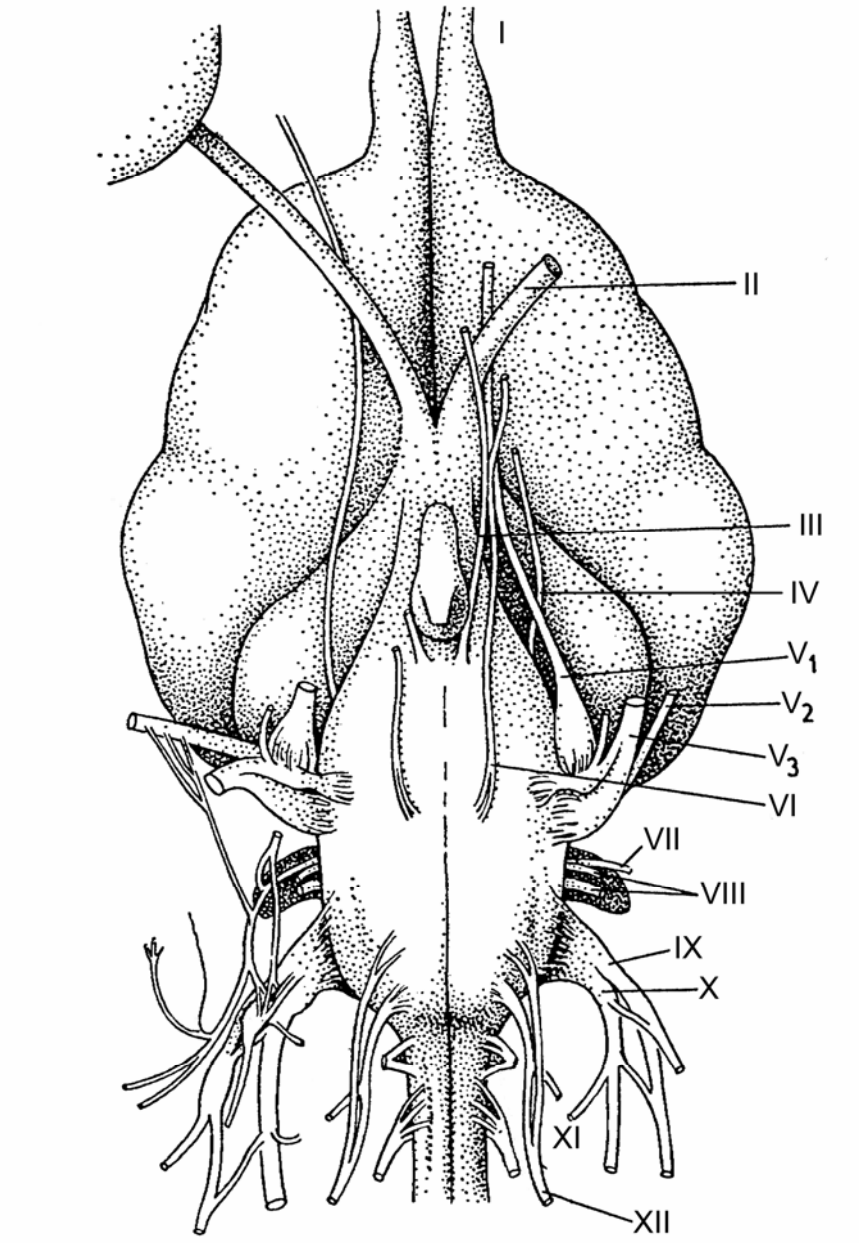

Figure 12. The cranial nerves.

Ventral view of the brain of a goose showing the 12 main cranial nerves. Cranial nerve V is shown as the three branches that comprise it. Modified from Portmann and Stingelin (1961).

Optic Nerve

The optic nerve (CN II) emerges from the braincase through the usually single, but occasionally separated, optic foramen. This foramen perforates the orbitosphenoids (Currie, 1997), but may also be bounded in part by the laterosphenoids (Brochu, 2003). The optic nerve is also a sensory nerve, involved in vision and innervating the retina (Butler and Hodos, 1996). Upon entering the braincase, the optic nerve from each side of the brain meet at the optic chiasma, before branching and criss-crossing each other en route to the thalamus (Jerison, 1973). It tends to be large in birds such as Falconiformes and Corvidae, but relatively small in nocturnal birds (Stresemann, 1928-1929).

Oculomotor Nerve

The oculomotor nerve (CN III) emerges from the braincase either through its own oculomotor foramen, or with the ophthalmic branch of the trigeminal nerve (CN V) and the abducens nerve (CN VI). If exiting by itself, the oculomotor foramen is formed anteriorly by the orbitosphenoid, and posteriorly by the laterosphenoid. It is a motor nerve that goes to the extraocular muscles of the eye, as well as the levator muscle of the upper eyelid. Within the braincase it emanates from the midbrain (mesencephalon) (Jerison, 1973).

Trochlear Nerve

The trochlear nerve (CN IV) exits the braincase through a small trochlear foramen that is usually located dorsolateral to the exit for the oculomotor nerve.

Usually the trochlear nerve is completely enclosed by the laterosphenoid, although the orbitosphenoid may participate in enclosing its anterior margin (Currie, 1997). It is a motor nerve that controls the dorsal oblique eye muscle. This nerve also emanates from the midbrain (Jerison, 1973).

Trigeminal Nerve

The trigeminal nerve (CN V) is both a sensory and a motor nerve, although its sensory functions far outweigh its motor functions. The trigeminal nerve is composed of three main branches: the ophthalmic (V_1) branch, the maxillary (V_2) branch, and the mandibular (V_3) branch. All three branches emanate from the trigeminal ganglion.

The ophthalmic branch may exit the braincase laterally with the rest of the trigeminal nerve through the maxillo-mandibular foramen, or it may branch from the rest of the nerve before leaving the braincase and exit the anterior portion of the braincase through its own ophthalmic foramen, or with the oculomotor and abducens nerves. When exiting by itself, the ophthalmic branch either runs anteriorly in a groove on the lateral surface of the laterosphenoid, or within a canal totally enclosed by the laterosphenoid (Currie, 1997). This branch is the principal sensory nerve of the orbit and nasal cavity, provides some branches to the glands in this region, and also the nictitating membrane. It serves as the sensory pathway for tactile organs of the skin of the head and the maxillary rostrum as well.

The maxillary branch exits the braincase laterally, most often with the mandibular branch before they separate. The foramen from which the nerve emerges is formed anteriorly by the laterosphenoid, and posteriorly by the prootic (Currie, 1997). The maxillary branch innervates the eyelids, skin of the dorsal orbital region and infraorbital region, the palate, and the nasal cavity.

The mandibular branch also exits the braincase laterally, often with the maxillary branch. This branch innervates jaw adductor muscles, lower eyelid muscles, salivary glands, and skin of the interramal region. In *Gallus*, it also innervates the wattle.

Abducens Nerve

The abducens nerve (CN VI) exits the anterior portion of the braincase through its own abducens foramen, or in tandem with the oculomotor nerve and the ophthalmic branch of the trigeminal nerve. When exiting alone, the abducens foramen is at the end of a canal that is enclosed by the basisphenoid. It may exit into the pituitary fossa, or lateral to the pituitary fossa as in coelurosaurs (Currie, 1997). The abducens nerve is another motor nerve that innervates the extrinsic muscles of the eye. It also emanates from the metencephalon (Hopson, 1979).

Facial Nerve

The facial nerve (CN VII), like the trigeminal nerve, is both motor and sensory, and has several branches. Overall, the nerve is responsible for innervation of glands and middle ear muscles, and deep facial sensation (Jerison,

1973). There are two main branches that comprise the facial nerve: the palatine branch, and the hyomandibular branch, both of which emanate from the metencephalon (Hopson, 1979).

The palatine branch often exits the braincase laterally with the hyomandibular branch before splitting, but in some taxa (such as *Acrocanthosaurus*) it splits before exiting the braincase, and proceeds forward to exit more anteriorly from the parasphenoid/basisphenoid complex. This branch is responsible for receiving sensory information from the nasal cavity and palate, and for innervating orbital glands.

The hyomandibular branch exits the braincase laterally, often with the palatine branch. The foramen from which it exits is entirely surrounded by the prootic (Currie, 1997). The hyomandibular branch is responsible for innervating the tympanic membrane, external acoustic meatus, depressor muscle of the mandible, and salivary glands. It also has several branches that connect to the trigeminal nerve, glossopharyngeal nerve, and cranial cervical ganglion of the sympathetic chain.

Vestibulocochlear Nerve

The vestibulocochlear nerve (CN VIII) is known by many names, some of these being the acoustic nerve (Galton, 1985), and the statoacoustic nerve (Hopson, 1979). This nerve is special sensory in function, and deals with the hearing and balance of the animal. The vestibulocochlear nerve is comprised of two branches, the vestibular branch, with a rostral and a caudal ramus, and the

cochlear branch. Each of these follows their own course from the brain, but they both emanate from the metencephalon (Hopson, 1979). Their foramina are contained within the prootic (Currie, 1997).

The two vestibular branches leave the brain laterally and enter the osseous labyrinth, where they help with balance by innervating the ampullae of the semicircular canals, utricular macula, and sacculus.

The cochlear branch also exits the brain laterally and enters the inner ear, where it helps with hearing by innervating the basilar membrane, and the macula of the lagena.

Glossopharyngeal Nerve

The glossopharyngeal nerve (CN IX) exits the braincase laterally either by itself through the metotic fissure (Hopson, 1979), or sometimes with the vagus nerve (CN X) and accessory nerve (CN XI) as well. The metotic fissure is bordered posteriorly by the exoccipital and the basioccipital (Currie, 1997). This nerve is both sensory and motor in function and emanates from the myelencephalon (Hopson, 1979). In its sensory capacity, it innervates the taste buds of the tongue, and sends afferent fibers to the whole tongue. Its motor functions control various glands, the pharynx, esophagus, crop, glottis, laryngeal muscles, and the trachea.

Vagus Nerve

The vagus nerve (CN X) exits the braincase either laterally with the accessory nerve and the glossopharyngeal nerve through the metotic fissure, or posteriorly with the accessory nerve and the jugular vein through the jugular foramen (Hopson, 1979), which is usually bordered by the exoccipital and basioccipital (Currie, 1997). This nerve is also both sensory and motor. It provides general viscero-sensory functions for the thorax and digestive tract, and somatosensory functions for the skin of the ear, glands (thymus, thyroid, etc.), esophagus, trachea, crop, and syrinx. It also provides visceromotor control for the heart, lungs, and digestive tract, usually via peripheral ganglia (Jerison, 1973). This nerve also emanates from the myelencephalon (Hopson, 1979).

Accessory Nerve

The accessory nerve (CN XI) almost always exits the braincase with the vagus nerve, whose exits are described above. This nerve is motor, innervating portions of the neck and upper body (Jerison, 1973). It, too, emanates from the myelencephalon (Hopson, 1979).

Hypoglossal Nerve

The hypoglossal nerve (CN XII) is composed of two or three branches that exit the braincase posteriorly through two or three hypoglossal foramina that penetrate the exoccipital (Currie, 1997). It is a motor nerve that controls portions

of the tongue, pharynx, larynx, syrinx, and trachea. It emanates from the myelencephalon (Hopson, 1979).

ISSUES TO BE ADDRESSED

In this dissertation, I use studies of the endocranial cavity to determine how theropod brains evolved through time, and what effects these changes may have had on the intelligence, sensory ability, and behavior of theropods. These studies are based on high-resolution X-ray computed tomographic (CT) data. The new characters I obtain from these studies are both optimized onto existing phylogenetic trees, and added to existing data matrices to see what, if any, effect they have on hypothesized relationships.

The various issues I mentioned in the discussion of Jerison's encephalization quotient (see above; and Jerison, 1969) include how much of the endocranial cavity is filled by the brain, and estimating weight in large animals, such as dinosaurs. The first issue is how much of the endocranial cavity is filled by the brain? The estimate of 50% of the endocranial volume, which was used by Jerison in his studies (1969, 1973), seems low, considering that the brain of pterosaurs, which are closely related to dinosaurs, and birds, which are dinosaurs, almost completely fill their endocranial cavities (Jerison, 1973). Even Hopson (1977) pointed out that his observations indicate that the percentage of the endocranial cavity filled by the brain never dropped below 60% in theropods. Some dinosaurs, such as *Dromaeosaurus* (Currie, 1995), *Troodon*

(=*Stenonychosaurus*), and sauropods, show features that suggest their brains almost completely filled the endocranial cavity (Hopson, 1977; 1980).

The second issue, weight estimates of dinosaurs, can be improved by using more accurately constructed models, by using the circumference of the femur to calculate weight (Anderson et al., 1985), or by trying various other methods that have been suggested for obtaining the weights of extinct organisms. One of these methods involves using graphic double integration on the picture of an entire animal rather than just the endocast (Hurlburt, 1999).

Other problems can be corrected, or at least diminished, through the use of CT scanning. CT scanning is important because it allows a new set of data, that were unattainable previously, to be used. Previous studies of endocasts relied on the availability of natural or artificial endocasts. Natural endocasts are a scarce resource, and often skulls are destroyed to obtain them. Artificial endocasts of fossils present their own problems. In order to make an artificial endocast, you must have a prepared endocranial cavity. This can be problematic due to the small size and fragile nature of many specimens. Even when well prepared, many times there are foramina and passageways that may not have been detected or cleaned. CT scanning has the potential to eliminate all of these problems. Because of the non-destructive nature of the X-rays, data about a skull and its internal structure can be obtained without sectioning it, risking damage in preparation, or taking it apart. Also, when density differences between the bone and any sediment filling the cavities is sufficient, distinguishing bony structures from sediment is much

easier than trying to do it visually. This, therefore, eliminates the problem of incompletely prepared specimens.

Several authors realized the possibilities presented by CT scanning, and many incorporated it into their studies (e.g., Currie and Zhao, 1993b; Zhao and Currie, 1993; Currie, 1995; Chure and Madsen, 1998; Knoll et al., 1999; Brochu, 2000; Larsson, 2001). Most of these studies, however, focused on the use of CT in depicting osteological characters of the specimens. Recently though, refined methods to obtain a virtual endocast from a CT dataset were achieved (Franzosa, 2001), allowing access to a large variety of specimens that were not studied before. Specimens that were too small, too fragile, or too valuable to risk the damage possible through mechanical preparation can be studied without doing any damage to the actual specimen.

In this dissertation I use digitally produced endocasts from CT datasets to investigate the evolution of the brain throughout theropod dinosaurs. My sample includes digital endocasts of a large variety of theropods, as well as those of some outgroups, such as sauropodomorphs, pterosaurs, and crocodilians. These digital endocasts allow me to describe endocasts from taxa never described before. For some specimens, such as *Herrerasaurus*, virtual endocasts may be the only way to know what their endocranial cavities look like. Endocasts also contain considerable information on the anatomy of the brain, including the position and orientation of cranial nerves, arteries, and veins; the major divisions of the brain (cerebrum, cerebellum, medulla oblongata); and even the semi-circular canals of the ear, which can be made out in good endocasts. These descriptions will provide

new data not only on morphology, but also on volumes and surface areas of different parts of the brain. These data can then be used as characters for systematic analyses.

The characters I derive from the study and description of the endocasts are examined to determine whether or not they are useful in phylogenetic analyses. These characters are evaluated based on comparable structures in birds (extant dinosaurs), and crocodiles. Following most recent literature (Gauthier, 1986; Padian and Chiappe, 1998), this dissertation considers birds to be dinosaurs. Thus, features such as the orientation of the cranial nerves, and the way the central nervous system is constructed, will be compared primarily to what is seen in modern birds rather than crocodilians, squamates, or other "reptiles."

My study differs from earlier endocast studies in which dinosaurs were viewed as reptiles, in the traditional sense of the word, which excludes birds. An example of this view was Jerison's use of *Sphenodon* brains as a correlate to dinosaurs (Jerison, 1969). Modern phylogenetic hypotheses place birds within theropod dinosaurs (Gauthier, 1986), so birds will be used as the main comparison for the non-avian theropods. Variation in size, shape, and nerve location is evaluated, and the potential significance of these variations for phylogenetic hypotheses is assessed. This study is well suited to non-avian theropod dinosaurs, because the relationships between most of the major clades are fairly well resolved. These serve as control groups against which endocast characters are tested through character optimization schemes, such as ACCTRAN and DELTRAN, which can be applied in MacClade (Maddison and Maddison, 1992).

New characters are then added to existing data matrices of the proposed phylogenies, and these matrices are rerun in PAUP (Swofford, 1993) to evaluate changes in group alignment and/or relationships.

In identifying new characters, I carefully considered the question of independence. For example- are endocast characters redundant with characters derived from braincase structure? This is a highly debated topic, and changing how characters are scored can change the output of the phylogenetic analyses, although it doesn't always cause a difference in trees (Emerson and Hastings, 1998). The phylogenies I used as controls, and with which new characters were run, are those proposed by Holtz (1998), Sereno (1999), and Rauhut (2003).

One of the more interesting things that I examined is whether or not there is a correlation between changes in the structure (size and shape) of the brain, and changes in behavior, sensory ability, and 'intelligence.' Ever since dinosaurs have been studied, paleontologists have speculated on how they lived and behaved. From pack hunting in *Deinonychus* (Ostrom, 1969), to herding and parental care in *Maiasaura* (Horner and Makela, 1979), the quest to understand extinct dinosaurs as real, living creatures has always been there. Endocasts give us a chance to explore some of these hypotheses through analyses of the size and shape of different parts of the brain. One example is the sense of smell. The shape and size of the olfactory bulbs are often preserved in an endocast, and an animal with large olfactory bulbs in relation to overall brain size is expected to have a better sense of smell than an animal with a smaller set (Jerison, 1973). Many such senses are tied to certain areas of the brain, and any changes in the size or shape

of these structures signals a shift in the importance of that sense, whether it is an increase or decrease. The same hypothesis is used when investigating behaviors such as herding, parental care, and hunting versus scavenging. Many groups, such as pachycephalosaurs, have unique endocast morphologies (Giffin, 1989), and this may be related to how the animal interacts with, and responds to, its environment. I studied behaviors previously hypothesized based on studies of tracks, bonebeds, and osteological structures, and that were supported by comparisons with modern groups showing similar data. I tested the hypothesis of a correlation between the size of the brain and 'intelligence.' Jerison addressed this subject many times with his chart, which shows some correlation between the brain/body weight ratio and intelligence (Jerison, 1973). The revision of Jerison's numbers in this study required a new set of measurements for all dinosaurs, and allowed the polygons for Jerison's "lower" vertebrates and "higher" vertebrates to be reevaluated. These studies of new endocasts add new data from more taxa to Jerison's brain/body weight chart, thereby refining and clarifying any patterns or correlations that may be present in the data.

Chapter 2: Methods and Descriptions

METHODS

CT Scanning

High-resolution X-ray Computed Tomography (CT) scanning provides reliable and non-destructive data for the internal details of fossil and recent vertebrate specimens (Rowe et al., 1993; 1995; 1997; 1999; Tykoski et al., 2002; Witmer et al., 2003). Not only can the osteology of specimens be examined in great detail, but also the foramina, canals, and fossae that are enclosed by the bony skeleton.

This is extremely useful for the study and description of the cranial cavities of theropods. Most fossil theropod skulls are rare, and short of destroying the specimens it is often difficult or impossible to obtain endocranial casts from them. The datasets that are provided by scanning the skulls can give results that are as good, if not better, than those obtained by mechanical preparation of a specimen. They are also digital, so quantitative measurements of the endocasts can be made. The reason scans are often better is that many specimens are filled with matrix, and it can be difficult to reach and prepare all of the foramina and canals within a given specimen. However, owing to differences in density and elemental composition that often exist between fossilized bone and matrix, in-filled foramina and canals are often easy to see and follow in CT datasets. It is largely this density differentiation that allows digital endocasts, 3-D

reconstructions of the cranial cavity, to be produced for specimens with intact braincases.

All but one of the specimens I describe were scanned at the UTCT. This facility uses an industrial CT scanner to produce a series of thin slices through an object. These slices can have orders of magnitude better resolution than those made using a medical CAT scan machine (Carlson et al., 2003). The parameters used for scanning the specimens described here are provided in Appendix E.

The parameters differed for each specimen, and these differences often affected the amount of anatomical detail visible in the endocast. Examination of the endocasts shows these resolution differences, as some endocasts have high resolution and exhibit smooth surfaces (e.g., *Apteryx*), while other endocasts have less resolution and exhibit a 'stair-step' pattern (e.g. *Rhamphorhynchus*). Also provided with this dissertation are QuickTime movies for all of the digital endocasts I describe. These movies are movies made from the raw slices, so no smoothing has been performed on them.

Digital Endocast Isolation

Once a dataset is created by scanning a specimen in the CT scanner, it is ready to be manipulated for the creation of a digital endocast. The method described below for creating a digital endocast was developed by Dr. Matthew Colbert, The University of Texas at Austin, and summarized elsewhere (Franzosa, 2001). Although there are better methods for digital endocast creation now available, the following method is the way I made the endocasts described.

In order to work with the created datasets, they must first be leveled for viewing. This means the grayscale values are manipulated to achieve the best image possible. The dataset is then changed from 16-bit to 8-bit in Photoshop© or a similar graphics program (Figure 13). This is done because of the inability of Photoshop and the other image processing programs to effectively work with 16-bit images. There is some loss of resolution when changing from 16-bit to 8-bit, but it is negligible, and not a concern for endocast creation purposes.

The dataset, which is composed of a series of braincase slices, is then leveled a second time. This second leveling pass is done to create maximum differentiation in the grayscale values that represent the densities of the bone and matrix. The levels chosen are somewhat subjective, and it is best to test the new levels on several slices representing different regions of the braincase. Inappropriate levels can cause areas of thin bone to be lost from the dataset, affecting foramina and other openings into the endocranial cavity, so new levels should be tested to assure necessary bone is still visible after leveling. Once this delicate balance is achieved, the new levels can be incorporated. The output levels are also changed during this pass, excluding pure black from the slices (Figure 14). This is necessary because black will be used later to fill in the endocranial space, and nothing else in the slices can have this color.

Once leveling is completed, the slices are opened in Scion Image©, Image J©, or a similar graphics program, and converted into a stack. This allowed me to scroll through all of the slices forwards and backwards. The stack is now ready

Figure 13. Transverse slice of *Allosaurus fragilis* braincase.

A transverse slice from the CT dataset for the braincase of *Allosaurus fragilis* (UUVP 5961). This slice has been leveled, and changed from 16-bit to 8-bit. Slice thickness= 1.0 mm.

Figure 14. Transverse slice of *Allosaurus fragilis* braincase.

The same slice as figure 13. In this figure it has been leveled a second time for maximum differentiation in gray-scale intensities, and to exclude pure black from the slice. Slice thickness= 1.0 mm.

for isolation of the cranial cavity. This isolation can be easy, or rather difficult, depending on the specimen being studied. If the specimen is the skeleton of an extant animal, such as the Screamer *Chauna chavaria*, the isolation of the endocranial cavity is easy because there is a large density difference between the braincase bones and the air that fills the cranial cavity, permitting selection using the magic wand tool (Figure 15). The magic wand tool will work as long as the endocranial space is completely surrounded by bone. Openings to the exterior, either foramina or other breaks in the bone, must be 'closed off' using the line tool before the magic wand tool can be used (Figure 16).

The endocranial cavity of most fossils is filled with matrix, and must be selected manually using the lasso tool (Figure 17). This is time consuming and difficult because the outline of the endocranial cavity must be traced. After the endocranial cavity and its associated foramina are selected using the magic wand tool and/or the lasso tool on each slice, the selection is filled in with the pure black that was 'set aside' earlier by changing the output levels (Figure 18). These data can then be saved in stack form, and also as individual slices.

The digital endocast can now be constructed using a volume-rendering program, such as Voxblast©, or an isosurfacing program. The black fill of the endocast is rendered opaque, and all other values as transparent (Figures 19, 20). The digital endocasts I created for this dissertation were rendered using an in-house isosurfacing program.

Figure 15. Transverse slice of *Chauna chavaria* braincase.

A transverse slice from the CT dataset for the braincase of *Chauna chavaria* (KU 81969). In this figure the cranial cavity has been selected with the magic wand tool. The outline that the wand provides has been moved away from the bone surface here for viewing purposes. When processing, it would be flush against the bone surface. Slice thickness= 0.295 mm.

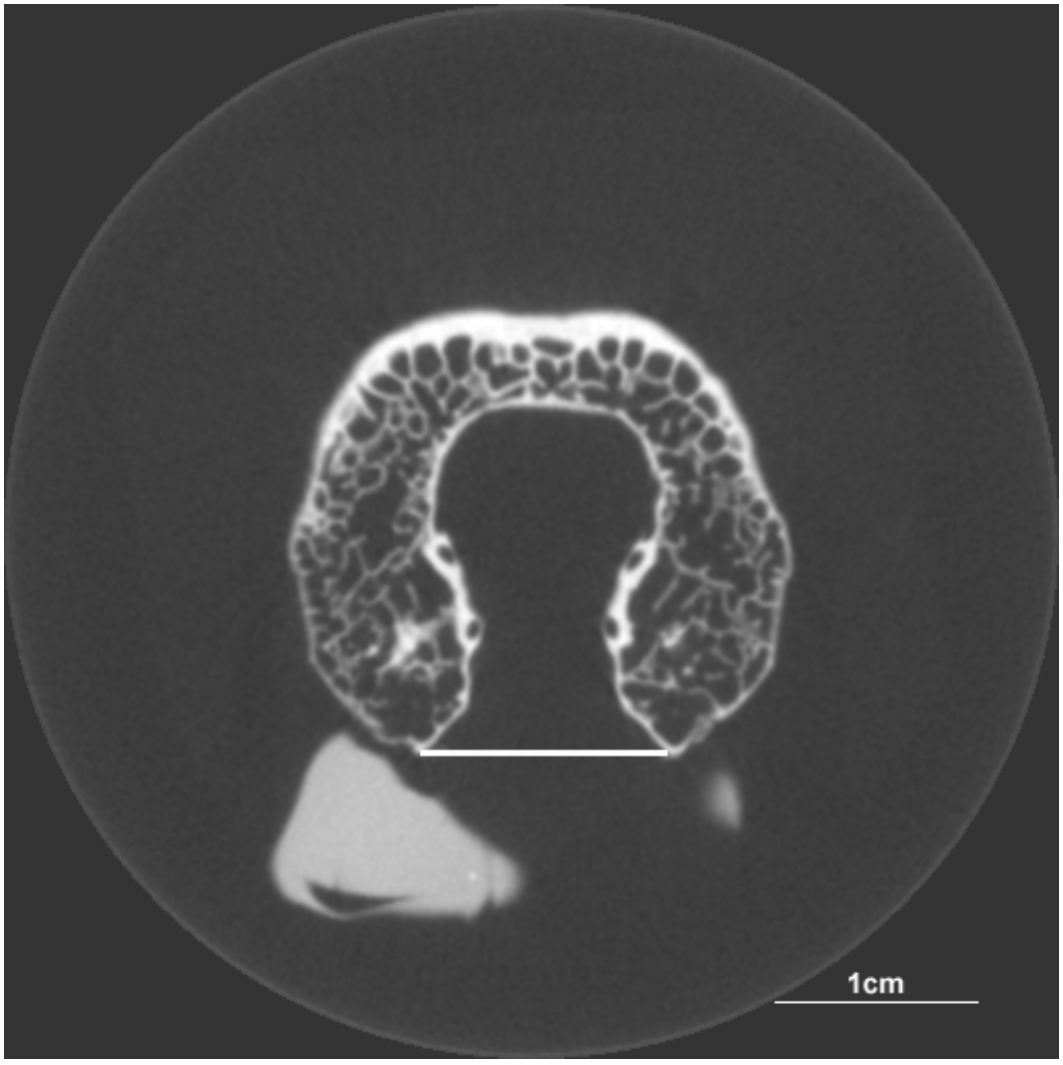

Figure 16. Transverse slice of *Chauna chavaria* braincase.

Another transverse slice from the CT dataset for the braincase of *Chauna chavaria*. In this figure the cranial cavity had to be sealed using the line tool before it could be selected with the magic wand tool. Slice thickness= 0.295 mm.

Figure 17. Transverse slice of *Allosaurus fragilis* braincase.

The same slice as figures 13 and 14. In this figure the cranial cavity had to be manually selected using the lasso tool. Slice thickness= 1.0 mm.

Figure 18. Transverse slice of *Allosaurus fragilis* braincase.

The same slice as figures 13, 14, and 17. In this figure the cranial cavity is filled with pure black after being selected manually with the lasso tool. Slice thickness= 1.0 mm.

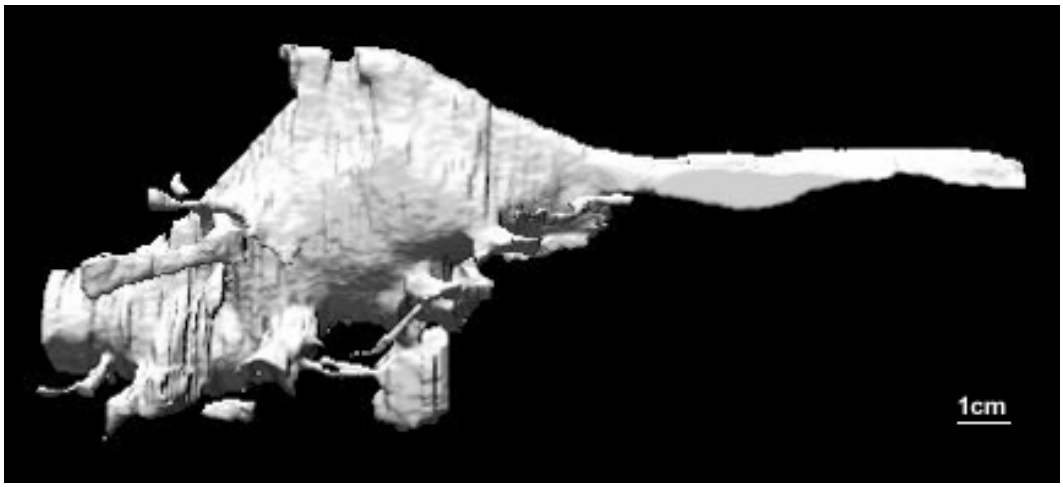

Figure 19. *Allosaurus fragilis* endocast.

Right lateral view of the digital endocast created from the CT dataset for the braincase of *Allosaurus fragilis*, specimen UUVP 5961, using an in-house isosurfacing program. Anterior is to the right.

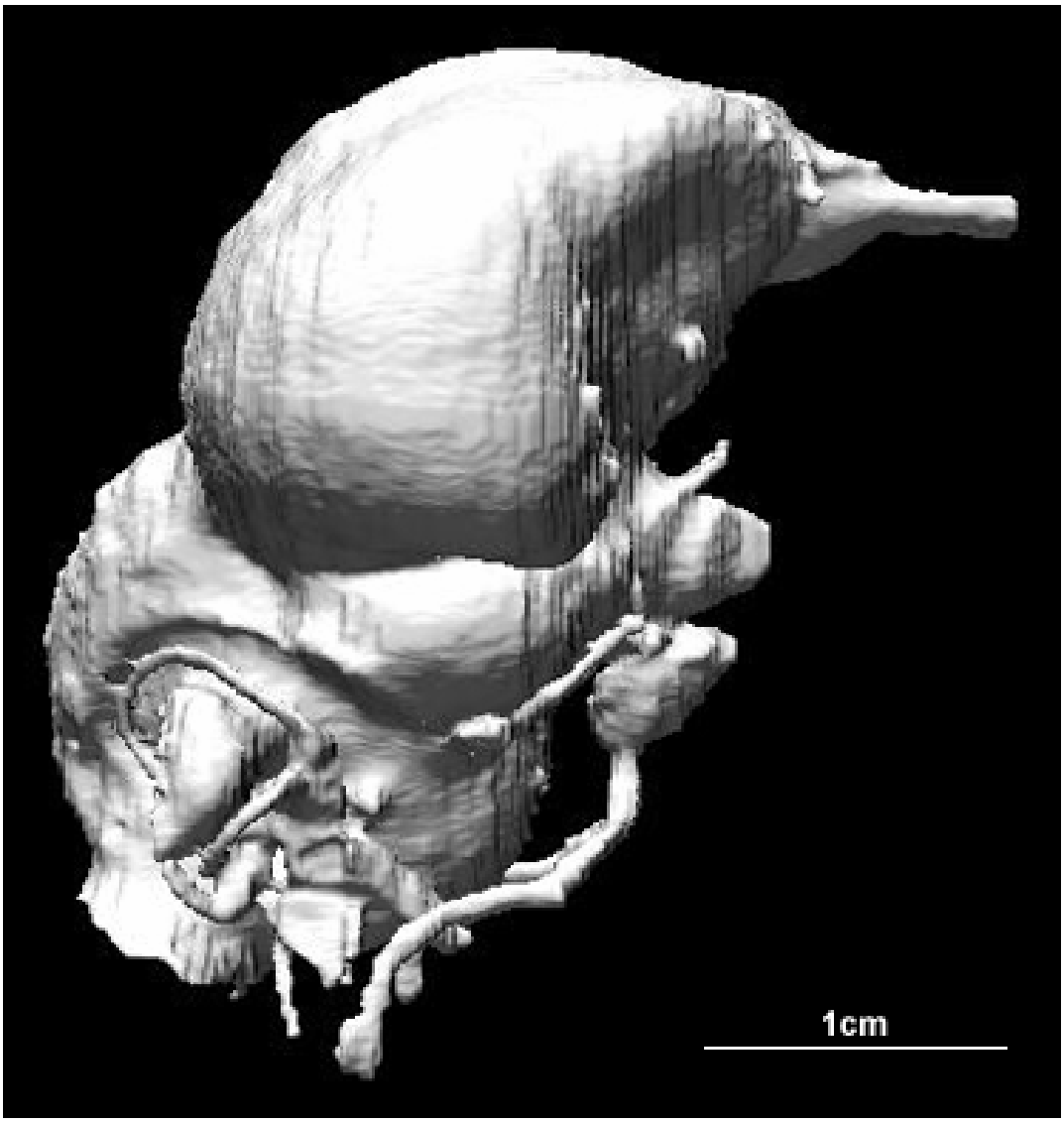

Figure 20. *Chauna chavaria* endocast.

Right lateral view of the digital endocast created from the CT dataset for the braincase of *Chauna chavaria*, specimen KU 81969, using an in-house isosurfacing program. Anterior is to the right.

Even though any slice plane through the specimen can be used to isolate a digital endocast, horizontal and transverse are the easiest to work with because of the orientation of most of the foramina. Transverse may ultimately be the best axis, because it is often the original scan plane, and usually has the largest number of slices, therefore giving better detail. It is this direction that was used to create all but one of the digital endocasts I described. The *Anhanguera santanae* endocast was scanned for another project in the horizontal plane. Other conventions used in the creation of the digital endocasts include: all cranial nerve and artery/vein foramina that open into the main cranial cavity are filled, these foramina are filled to the outer surface of the braincase bones, the medulla oblongata is represented at least until the foramen magnum has been cleared, and the olfactory bulbs and tracts are represented as far anteriorly as possible. This anterior representation varies between specimens depending on the condition of the anterior portion of the braincase, and in each specimen description below I describe how the anterior border of the endocast was chosen. The anterior extent of the pituitary is also often unclear owing to the lack of bones enclosing the front of the pituitary fossa, so representation of the pituitary is restricted to portions of the fossa that are delineated by bone.

Once created, the endocast can be used to estimate the volume and surface area of the cranial cavity. These measurements are one of the great advantages to digital endocasts, because they eliminate the uncertainties associated with graphic double integration (e.g., Jerison, 1969), water immersion methods, and other ways of calculating the endocast volume. Digital endocasts also allow individual areas

of the endocast to be measured, such as the cerebral hemispheres, olfactory bulbs, and optic lobes. Volumetric and surface area measurements were made using the in-house isosurfacing program used to create the endocasts, while linear measurements were made using either Adobe Photoshop or Illustrator©.

Lastly, a large portion of the descriptions discusses the various cranial nerve branches visible in the endocasts. As reviewed in chapter one, some of the nerves are sensory, while others are motor. This difference is important because the direction of information transmittal into or out of the brain varies depending on the type of nerve. In the endocast descriptions, however, branch directions when given are used for simplicity of description, and do not infer information transmittal direction within the actual cranial nerves. Also, endocast terminology predominately follows *Nomina Anatomica Avium* (Baumel et al., 1993), but translated into English. Endocast nomenclature traditionally uses terms that describe actual brain features. I realize that an endocast does not completely and faithfully reproduce the brain, but the use of brain terms to describe endocasts must be used to some degree. To denote the fact that the structures on the endocasts do not fully represent the actual brain features, terms such as cast of, foramen root, process, and projection are added to denote that the features are not the actual features of the brain, but only the representations of those features on the endocasts. The determination of which nerves go through certain braincase foramina, and what features various endocast structures represent was made using Witmer's Extant Phylogenetic Bracket (Witmer, 1995), with crocodilians and birds as the extant bracketing taxa.

ENDOCAST DESCRIPTIONS

In order to properly describe the features found in theropod endocasts, it is important to understand where they came from evolutionarily, and how they got to be the way they are today. I accomplished this is by looking at several successive outgroups to the group of interest to see if the ancestral condition could be ascertained, thereby giving polarity to any features that change in the group of interest. For Theropoda, three of these outgroups are Crocodylomorpha, Pterosauria, and Sauropodomorpha (Gauthier, 1986).

Crocodylomorpha

Having crocodilians as the most basal outgroup allows extinct theropods to be bracketed by a pair of extant groups: crocodilians and birds. This Extant Phylogenetic Bracket (EPB) allows several features and behaviors shared by both crocodilians and birds to be inferred in extinct theropods because of their phylogenetic position (Witmer, 1995).

Another advantage to using extant crocodilians is that the CT datasets of their skulls are much easier to interpret than the datasets from extinct groups. I also scanned a more basal member of the group, which may better represent the ancestral condition, thereby helping to polarize characters in the ingroup.

Crocodylus moreleti

I chose *Crocodylus moreleti* as the extant member of crocodilians for my study. I scanned an adult female from the collections at The University of Texas

at Austin Vertebrate Paleontology Laboratory (TMM m-4980). There are several reasons I chose this specimen. First, it was an adult, so most of the ossification and fusion of the braincase bones was complete. Second, the skull was small enough to fit in the CT scanner. Only one extant specimen is described below. I assume that extant specimens have a sufficiently similar braincase that any variation would not negatively impact the more general goals of this dissertation.

The endocast for the specimen (Figure 21) was started at the anterodorsal-most extent of the laterosphenoids. This starting point preserves a portion of the cast of the olfactory tract within the endocast, but the olfactory bulbs themselves are located more anteriorly and not indicated by bony features. The cast of the olfactory tract grades into the cast of the cerebral hemispheres posteriorly. This change is represented by the lateral and ventral expansion of the cast of the hemispheres. A large portion of the hemisphere cast is composed of the cast of the dorsal ventricular ridge (DVR; not distinguishable from other portions of the cerebral hemispheres in the crocodilian endocast). The DVR handles olfactory, visual, auditory, and somatosensory input. Each of these senses has a single region in the DVR of crocodiles (Ulinski, 1983). More detailed information and discussion about the DVR can be found in chapter 4. The single optic nerve foramen root (CN II) exits the braincase just ventral to the anterior portion of the cast of the cerebral hemispheres.

The trochlear nerve foramen root (CN IV) is posterolateral to the optic nerve foramen root, and the oculomotor nerve foramen root (CN III) is medial to

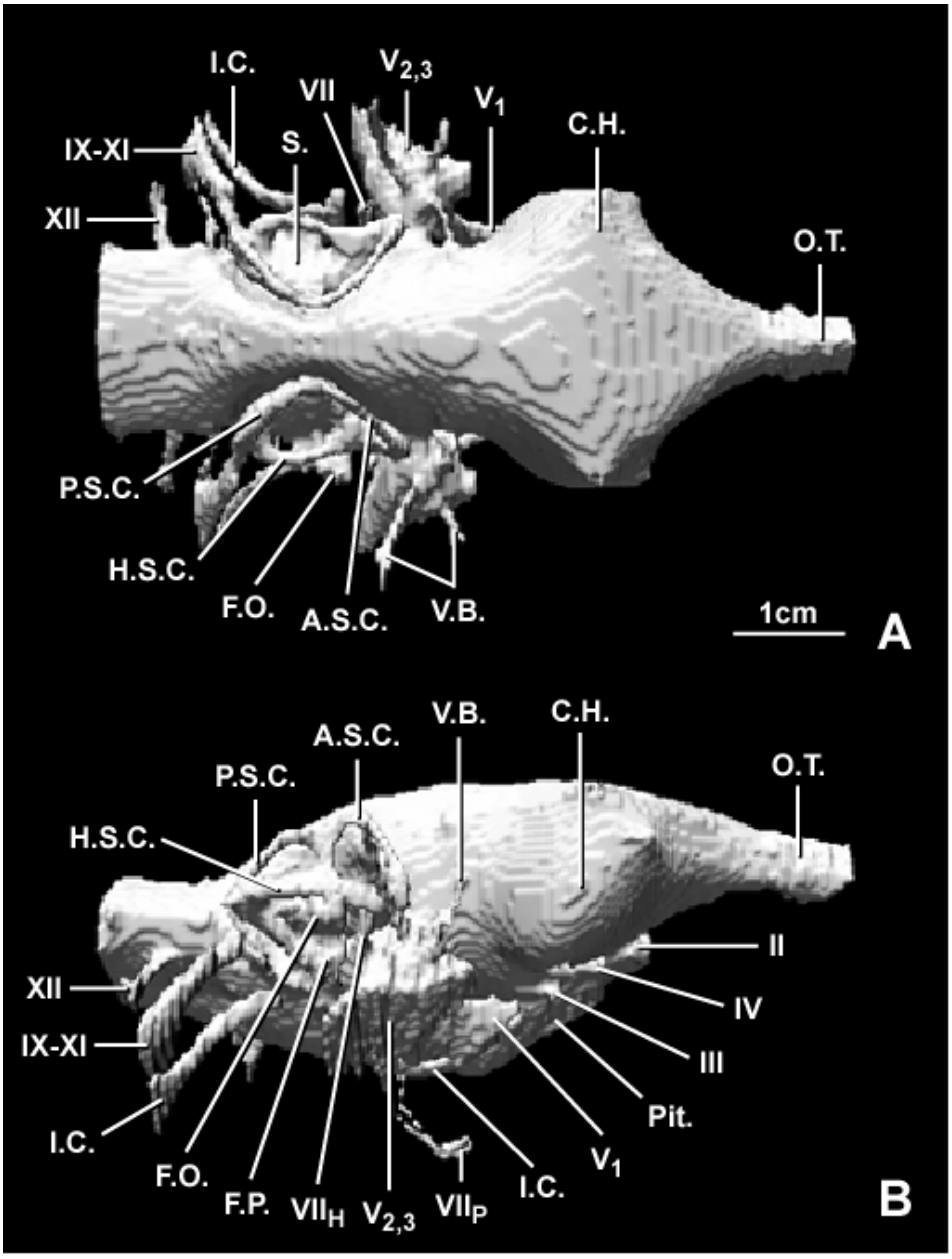

Figure 21. *Crocodylus moreleti* endocast.

(A) Dorsal, (B) right lateral, and (C) ventral (following page) views of the endocast of *Crocodylus moreleti*, TMM m-4980. Discernible cranial nerves and other features are labeled. See Appendix A for explanation of abbreviations.

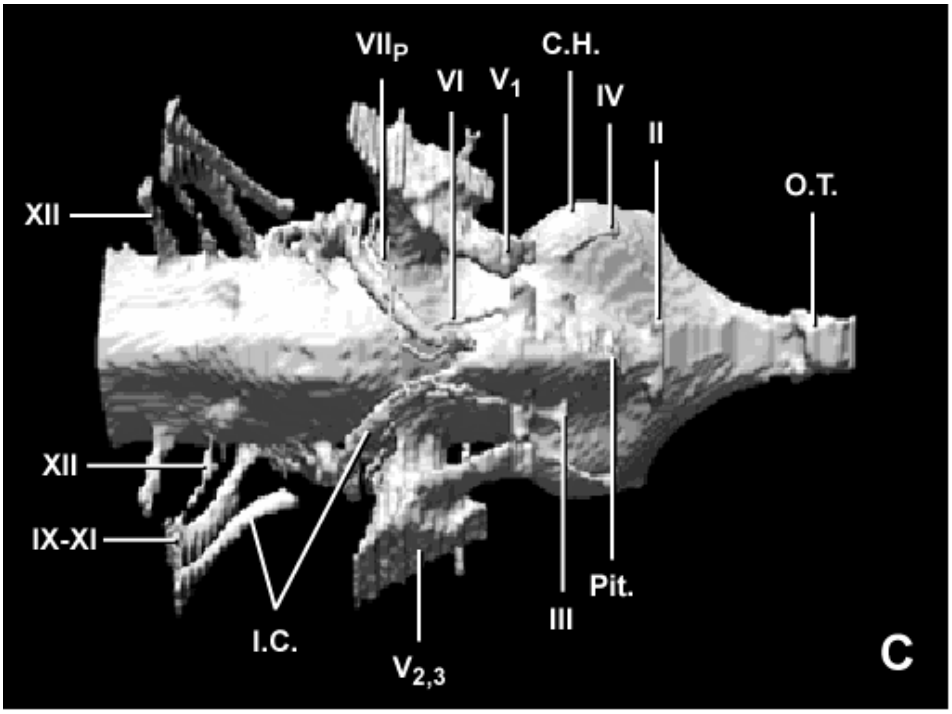

Figure 21 continued.

the trochlear nerve foramen root. The anterior portion of the abducens nerve canal process (CN VI) is posteroventral to the optic nerve foramen root. The abducens nerve canal process travels through a canal from the ventral surface of the cast of the medulla oblongata to exit anteriorly just lateral to the cast of the pituitary fossa. The cast of the pituitary fossa continues posteroventrally from this location. The process of the internal carotid canal enters the posterior end of the cast of the pituitary fossa, and can be traced posterodorsolaterally from there.

The anterior exit for the ophthalmic branch of the trigeminal nerve foramen root (CN V_1) is located just lateral to the abducens nerve canal process exit near the anterior portion of the cast of the pituitary fossa. Following the ophthalmic branch posteriorly, the combined maxillary and mandibular branches of the trigeminal nerve foramen root (CN V_2 + V_3) are encountered traveling laterally. The facial nerve foramen root (CN VII) is posterior to the trigeminal nerve foramen root. Just lateral to the single braincase exit for the facial nerve foramen root it branches into a laterally directed hyomandibular branch (CN VII_H), and an anteriorly directed palatine branch (CN VII_p) that travels anteroventromedially along a path similar to that taken by the internal carotid canal process.

The cast of the fenestra ovalis, fenestra pseudorotunda, and vestibulocochlear nerve foramen root (CN VIII) are posterior to the facial nerve foramen root. The cast of the fenestra ovalis is located dorsal to the cast of the fenestra pseudorotunda, and the two branches of the vestibulocochlear nerve foramen root, the vestibular branch and cochlear branch, exit the braincase

laterally to enter the inner ear and osseous labyrinth. The labyrinth is beautifully preserved in this well-prepared extant specimen; all three semicircular canals are preserved, as well as the cast of the sacculus between them. The orientation of the semicircular canals is the same as that of early theropods (see below). The anterior semicircular canal arches posterodorsomedially, with a short ventral turn before meeting the posterior semicircular canal. The posterior semicircular canal arches posteroventrolaterally where it meets the horizontal semicircular canal. The horizontal semicircular canal arches posterolaterally and then posteromedially from just behind the front end of the anterior semicircular canal to the back end of the posterior semicircular canal. This orientation, when viewed laterally, gives the semicircular canals a subtriangular appearance.

The glossopharyngeal (CN IX), vagus (CN X), and accessory (CN XI) nerves all exit together in a posteroventrolateral direction just ventral to the posterior end of the posterior semicircular canal, and this is seen as a cast of the metotic fissure. The posterior portion of the internal carotid canal process is just ventral to this. Two roots of the hypoglossal nerve foramina (CN XII) exit posterior to the cast of the metotic fissure. The more anterior of these emerges just behind the cast of the metotic fissure and exits through the same fissure as they do; the more posterior branch exits laterally shortly behind this. The end of the cast of the medulla oblongata, and the end of the endocast, is posterior to this.

The casts of the optic lobes, floccular lobes, and a clearly demarcated cerebellum, which are described below in some of the theropods, are obscured by the casts of large venous sinuses that cover the dorsal and lateral surfaces of the

crocodilian brain. The casts of the floccular lobes are not prominent because they do not extend between the semicircular canals as they do in theropods. A small portion of them is seen just medial to the anterior semicircular canal.

Saurosuchus galilei

With the major modifications that evolved in modern crocodilians for an aquatic lifestyle, it is useful for me to study a more basal taxon such as *Saurosuchus galilei* for use in the comparisons and analyses. *Saurosuchus galilei*, a rauisuchian from the Upper Triassic Ischigualasto Formation of Argentina (Alcober, 2000), represents a more basal member of the lineage that includes Crocodylomorpha. The specimen scanned is PVSJ 32, which includes, among other things, a braincase disassociated from the rest of the skull. The frontals were not part of the scan, so the casts of the olfactory bulbs, tract, and anterior portion of the cerebral hemispheres are not reconstructed in the endocast. The frontals and nasals are associated with the rest of the skull, and the impression of the olfactory tract is seen moving anteroposteriorly in a depression on the ventral surface of the frontals and nasals.

The most anterior portion of the endocast represents a portion of the cast of the cerebral hemispheres (Figure 22). Although incomplete, a slight lateral bulge representing the lateral edges of the hemispheres is found. The base of the optic nerve foramen roots, both of which exited through a single medial foramen, is ventral to the preserved portion of the cast of the cerebral hemispheres.

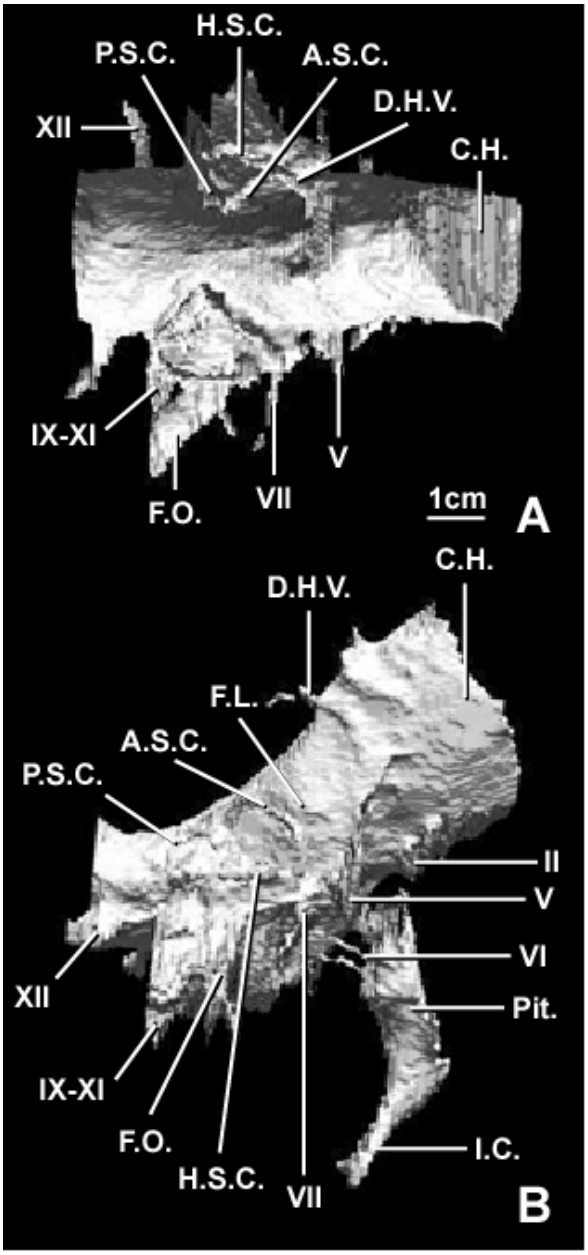

Figure 22. *Saurosuchus galilei* endocast.

(A) Dorsal, (B) right lateral, and (C) ventral (following page) views of the endocast of *Saurosuchus galilei*, PVSJ 32. Discernible cranial nerves and other features are labeled. See Appendix A for explanation of abbreviations.

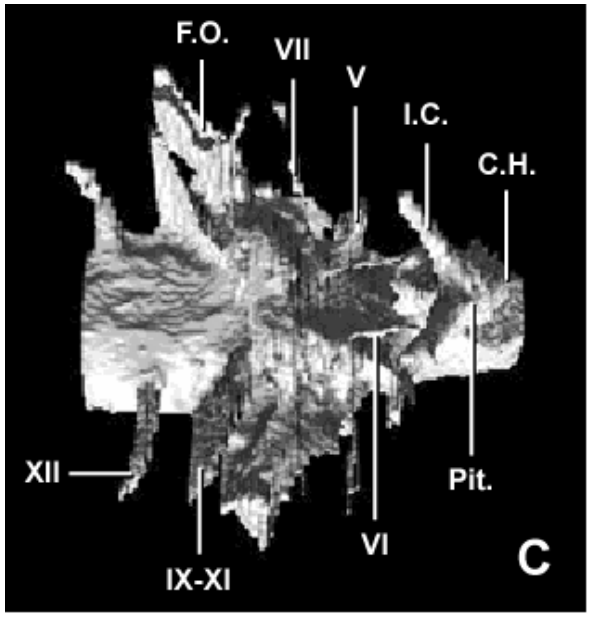

Figure 22 continued.

Foramina for the oculomotor and trochlear nerve foramen roots are not preserved in this incomplete endocast.

The cast of the pituitary fossa is directly ventral to the optic nerve foramen roots. The pituitary fossa is open anteriorly owing to a lack of ossification, or the loss, of the enclosing bones, thereby making it impossible to determine the anterior extent of the cast of the pituitary fossa. The internal carotid canal processes individually enter the posterior border of the cast of the pituitary fossa. The abducens nerve canal process also enters the cast of the pituitary fossa more dorsally and on the lateral margin.

The trigeminal nerve foramen root is posterolateral to the dorsal portion of the cast of the pituitary fossa. This nerve foramen root exits through a single foramen, so the three branches must have separated after it left the braincase. A projection labeled as the medium cephalic vein by Alcober (2000) is located dorsal to the trigeminal nerve foramen root, on the lateral border of the endocast. The foramen of this vein is located in the same position as what I call the dorsal head vein in theropods, and may be homologous.

The facial nerve foramen root is posteroventral to the trigeminal nerve foramen root, and exits just lateral to the abducens nerve canal process, which is located on the ventral surface of the endocast. The cast of the fenestra ovalis is posterior to the facial nerve foramen root. On the right side, the proximal portion of the stapes is still in place. It is within this area that the branches of the vestibulocochlear nerve foramen root enter the cochlea and the osseous labyrinth of the semicircular canals, but none of these branches are visible in the slices or

the endocast because the inner ear has no bony medial wall. The cast of the metotic fissure is posterior and slightly ventral to the cast of the fenestra ovalis. It is through this opening that the glossopharyngeal, vagus, and accessory nerves all leave the braincase laterally. Posterior to this, the hypoglossal nerve foramen roots exit the braincase through a single opening. The foramen magnum marks the end of the endocast.

Although the vestibulocochlear nerve foramen roots could not be seen, the semicircular canals that some of its branches innervated are clearly visible. The courses taken by these canals are the same as that seen in extant crocodilians. The anterior semicircular canal arches posterodorsomedially and then slightly ventrally, where it meets the posterior semicircular canal. The posterior semicircular canal arches posteroventrolaterally, eventually meeting the posterior end of the horizontal semicircular canal, which has reached a posteromedially location by arching posterolaterally and then posteromedially from just behind the front end of the anterior semicircular canal. There is also no osseous floccular fossa. There is a small projection or swelling seen in both modern crocodiles and *Saurosuchus* medial to the anterior semicircular canal which probably represents the cast of the floccular lobe, but it is nowhere near the size or extent seen in theropods and pterosaurs. The cast of the sacculus is not as visible in *Saurosuchus* as it is in *Crocodylus*.

Despite the similarities between extant crocodilians and *Saurosuchus*, there are some very obvious differences. The first of these is the overall orientation of the endocast. In modern crocodilians, such as *Crocodylus moreleti*,

there is a very slight cephalic and pontine flexure, giving the endocast a fairly 'straight tube' appearance with just a slight sinuosity to it. In *Saurosuchus*, the cephalic and pontine flexures are much more noticeable, leading to a shorter endocast anteroposteriorly, but a taller endocast dorsoventrally. Another difference lies in the orientation of the cast of the pituitary fossa. In *C. moreleti*, the cast of the pituitary fossa lies diagonally underneath the body of the endocast, and the internal carotid canal processes enter the posterior border in a nearly horizontal plane. The cast of the pituitary fossa of *Saurosuchus* is nearly vertical, and the internal carotid canal processes enter the posterior edge in a nearly dorsoventral plane. The course of the abducens nerve canal processes also varies in the two taxa. Whereas the abducens nerve canal processes enter the cast of the pituitary fossa in *Saurosuchus*, they pass just lateral to it in *C. moreleti*. The beginnings of the horizontal semicircular canals also differ somewhat, having a more lateral starting point in *Saurosuchus* than those of *C. moreleti*. Another major difference in this area is the positioning of the external opening to the ear. In modern crocodilians, the opening is closer to the dorsal surface of the skull, whereas in *Saurosuchus* it is found in a more ventral position, similar to what is seen in theropods. Lastly, the cast of the cerebral hemispheres of *C. moreleti* is much more noticeable in its endocast than those of *Saurosuchus*. Even though the anterior portion is missing in *Saurosuchus*, it is doubtful that it would approach the width seen in the extant crocodile.

Pterosauria

The second outgroup I looked at is the Pterosauria. Pterosaurs are a varied group of flying reptiles known from the Late Triassic to the Late Cretaceous (Sereno, 1991). Pterosaurs are a useful group to examine because, along with birds, they are one of only three groups of vertebrates to achieve powered flight, and, therefore, a comparison between their brains and the brains of birds can be very informative. Several pterosaur endocasts are known and have been described. The first was that of *Parapsicephalus purdoni* from the Early Jurassic (Newton, 1888; Hopson, 1979). The Late Jurassic *Pterodactylus elegans* was described by Tilly Edinger in 1941. More recently, the Cretaceous pterosaur *Tapejara wellnhoferi* was described by Wharton (2002). The two pterosaur endocasts described here are *Rhamphorhynchus muensteri* and *Anhanguera santanae*. *Rhamphorhynchus muensteri*, from the Late Jurassic of Germany, is a member of the basal rhamphorhynchoid lineage, whereas *A. santanae*, from the Early Cretaceous of Brazil, is a member of the more derived pterodactyloid lineage (Hopson, 1979; Witmer et al., 2003).

Rhamphorhynchus muensteri

Rhamphorhynchus muensteri comes from the Upper Jurassic Solnhofen Limestone of Germany. The skull scanned was CM 11434. Although the skull was filled with matrix, and the distinction between the bone and matrix was difficult at times, a fairly complete endocast was attained.

The endocast of *R. muensteri* (Figure 23) is highly apomorphic compared to the other endocasts I examined. The cast of the olfactory bulbs is either very small or absent, and the cast of the cerebral hemispheres is broad mediolaterally and narrow dorsoventrally. Their broadest point is near their posterior edge, and there is a large depression separating the two hemispheres.

The casts of the optic lobes, located at the posteroventrolateral borders of the hemispheres, are displaced ventrolaterally by the casts of the cerebral hemispheres and cerebellum, the same way as in birds. The casts of these lobes are rather large, suggesting that these animals were dependent on sight. Even at their size, they are not as large relatively as the optic lobes that are seen in birds.

The cast of the cerebellum is posterior to the cast of the cerebral hemispheres. Although its anterior extent is great enough to cause the ventrolateral displacement of the casts of the optic lobes, it is not so great that it is tightly appressed against the posterior edge of the cast of the cerebral hemispheres. The most notable features of the cast of the cerebellum are the floccular lobes, which are relatively enormous compared to those in any other taxon. Despite their size, the orientation of the casts of the floccular lobes is similar to that seen in other taxa, moving from their attachment to the cast of the body of the cerebellum posteroventrolaterally beneath the anterior semicircular canal, and ending between all three semicircular canals.

The semicircular canals are also relatively larger than those in the other taxa examined, not only in physical extent to surround the floccular lobes, but

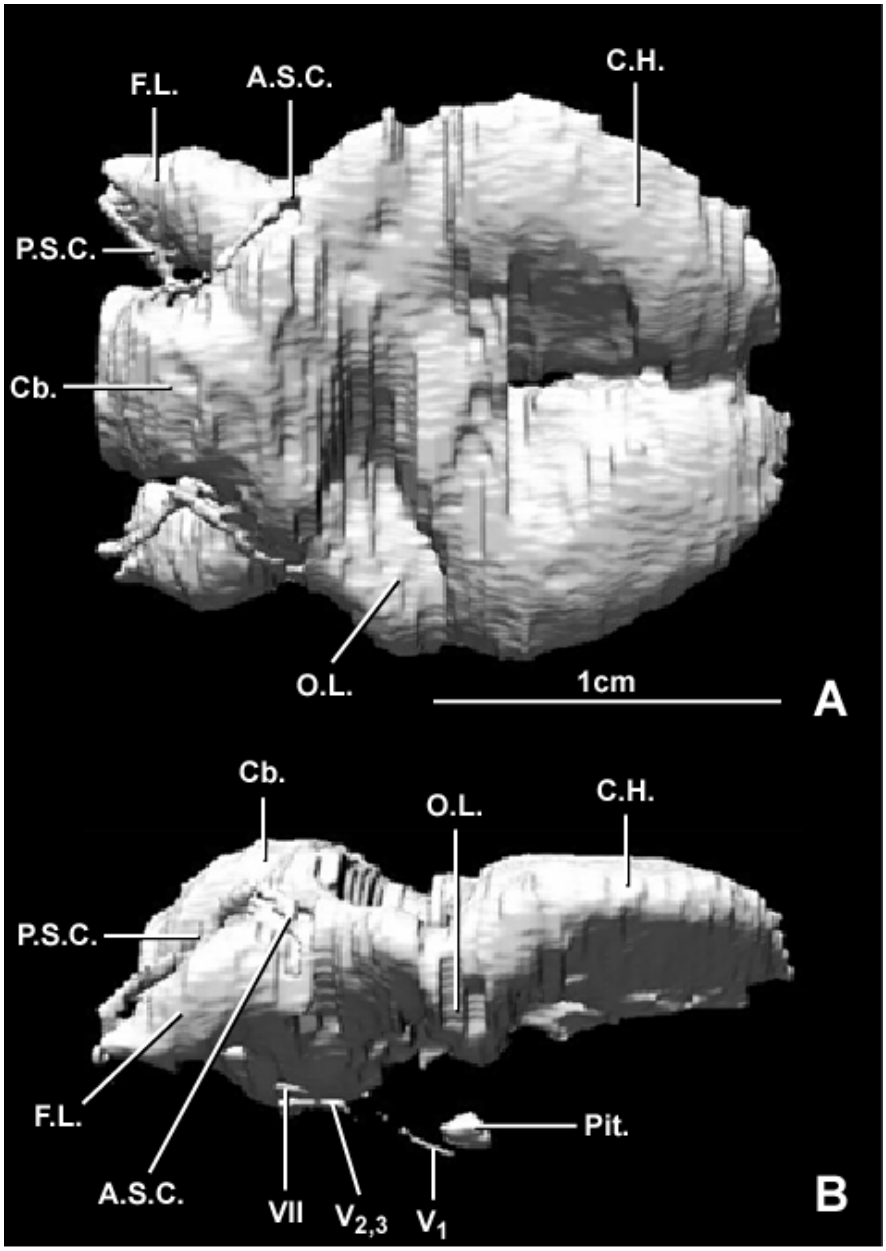

Figure 23. *Rhamphorhynchus muensteri* endocast.

(A) Dorsal, (B) right lateral, and (C) ventral (following page) views of the endocast of *Rhamphorhynchus muensteri*, CM 11434. Discernible cranial nerves and other features are labeled. See Appendix A for explanation of abbreviations.

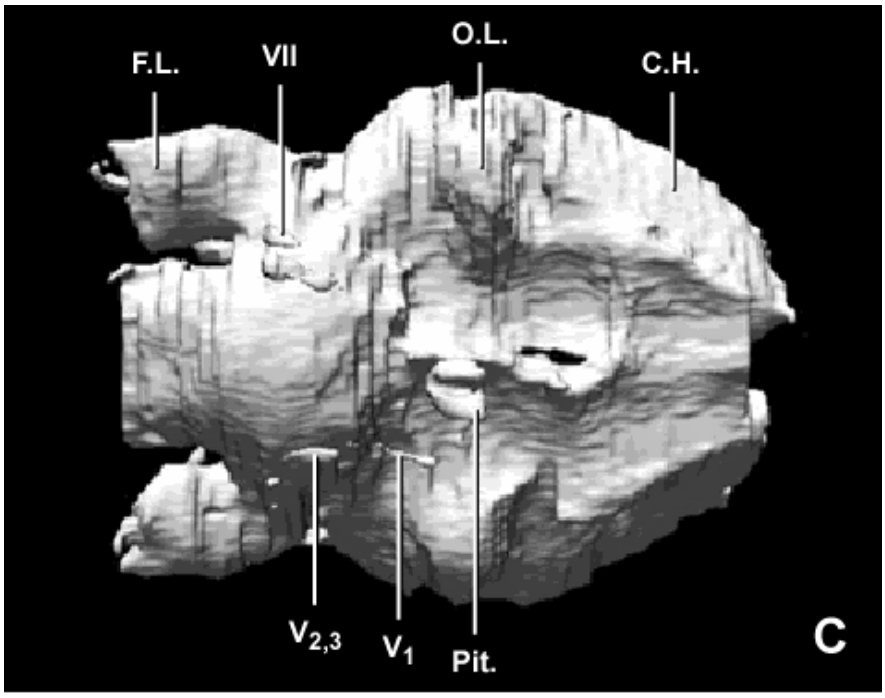

Figure 23 continued.

also in the radius of the osseous canals. The horizontal semicircular canals are not visible in the scan, although the anterior and posterior semicircular canals are fairly complete. Assuming the orientation of the endocast as reproduced here is correct, the anterior semicircular canals curve in a semicircular arch that begins by moving posterodorsomedially, and ends by moving posteroventromedially. The posterior semicircular canals meet the anterior semicircular canals at their posterior extent, and first curve posterodorsolaterally, before arching to curve posteroventrolaterally. The posterior extent of these canals could not be seen in the images.

Even though the scan is good enough to allow the main portions of the endocast to be defined, tracking the cranial nerve foramen roots and blood vessel projections is much more difficult. That said, there are some cranial nerve foramen roots that could be tentatively identified. These are the trigeminal and facial nerve foramen roots, which exit the braincase right next to each other. The anteriorly oriented ophthalmic branch of the trigeminal nerve foramen root is also visible. Also anteriorly, medial to the ophthalmic branch, a portion of the cast of the pituitary fossa can be identified. There also appears to be an opening for the optic nerve foramen root, but because I have not seen the actual specimen and this is speculative, it was not included in the endocast.

Anhanguera santanae

Anhanguera santanae is from the Lower Cretaceous Santana Formation of Brazil, and the specimen scanned was AMNH 25555. The endocast of this taxon

(Figure 24) differs markedly from *Rhamphorhynchus*, and the most obvious differences are the casts of the cerebral hemispheres. The cast of the cerebral hemispheres of *A. santanae* is much more bulbous than that of *Rhamphorhynchus*, and its broadest transverse extent is near the anterior portion of the hemispheres. There is also a trough separating these hemispheres, but it is not as distinct and broad as it is in *Rhamphorhynchus*.

The cast of the olfactory bulb, although still very small, is visible at the anteroventromedial corners of the cast of the cerebral hemispheres, and a long olfactory filament projection heads anteriorly towards the nasal cavity. The casts of the optic lobes are under the posteroventrolateral corners of the cast of the hemisphere, the same position as in *Rhamphorhynchus*, and just as in *Rhamphorhynchus*, they are relatively larger than the olfactory bulbs, but not as large relatively as the optic lobes of birds.

Another difference between *Anhanguera* and *Rhamphorhynchus* is the cast of the cerebellum. The cast of the cerebellum of *Anhanguera* is completely appressed against the posterior edge of the cast of the cerebral hemispheres, and it even begins to over-ride this posterior edge, forming a median bulge behind the hemispheres. Once again, this expanse of the cerebellar cast likely helped lead to the ventrolateral displacement of the casts of the optic lobes.

One area in which *Anhanguera* and *Rhamphorhynchus* are similar is the casts of the floccular lobes. The casts of the floccular lobes in *Anhanguera* are also huge, and oriented similarly to those in *Rhamphorhynchus*. All three

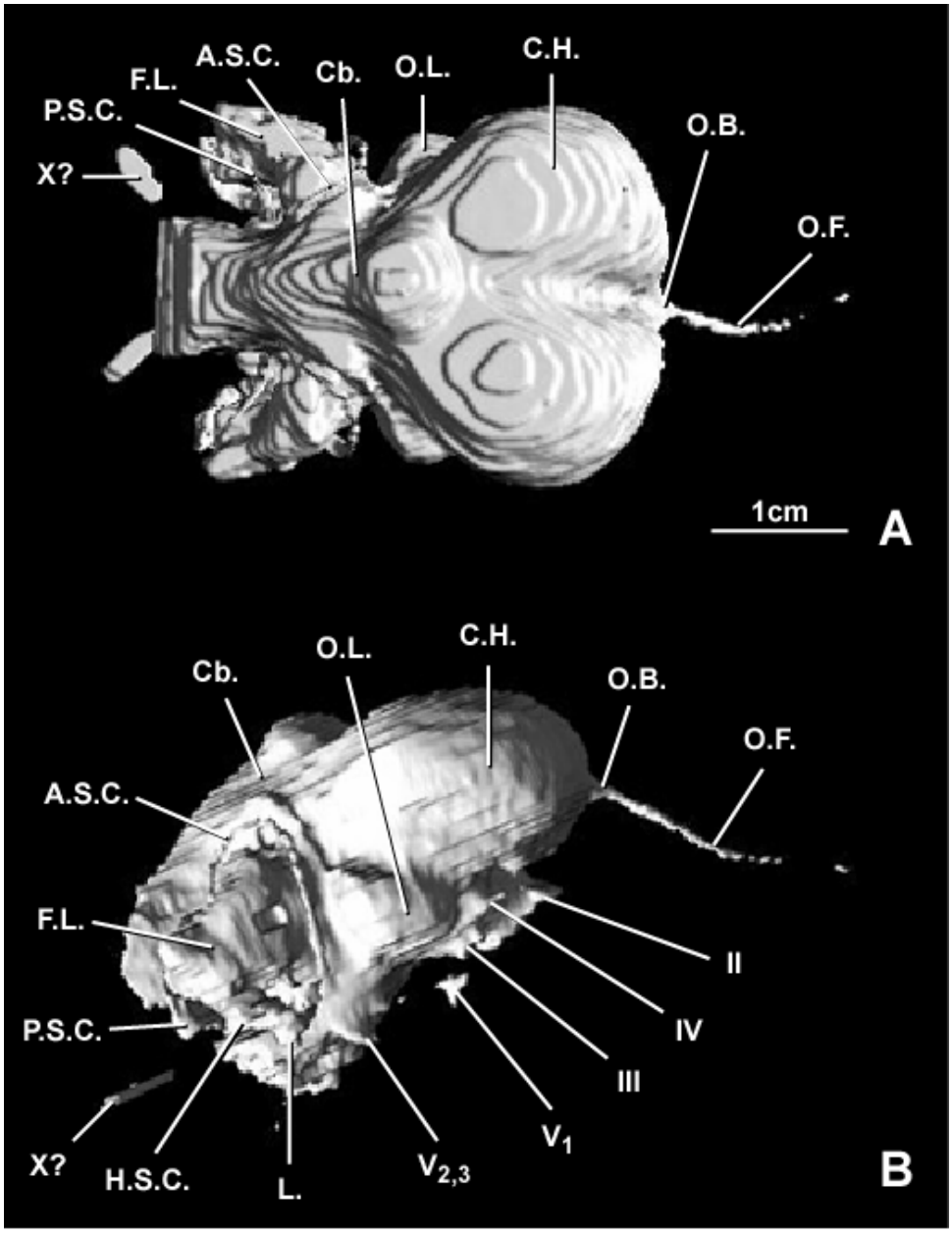

Figure 24. *Anhanguera santanae* endocast.

(A) Dorsal, (B) right lateral, and (C) ventral (following page) views of the endocast of *Anhanguera santanae*, AMNH 25555. Discernible cranial nerves and other features are labeled. See Appendix A for explanation of abbreviations.

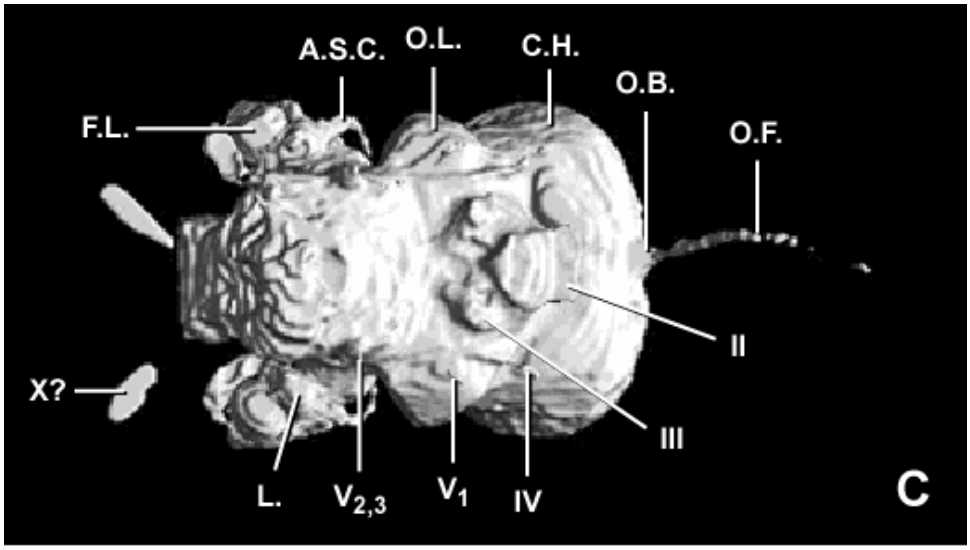

Figure 24 continued.

semicircular canals are present in *Anhanguera* and can be traced. The anterior semicircular canal first arches posterodorsomedially, and then posteroventromedially after peaking at its maximum height. The posterior semicircular canal first curves posterodorsolaterally before curving around posteroventrolaterally, and then finally anterodorsomedially. The horizontal semicircular canal curves laterally in a semicircular arch from the anterior edge of the anterior semicircular canal to the posterior edge of the posterior semicircular canal.

Unlike *Rhamphorhynchus*, several of the cranial nerve foramen roots of *Anhanguera* are traced and identified. The optic nerve foramen roots are ventral to the anterior portion of the cast of the cerebral hemispheres, and both exit from a single foramen. The base of the oculomotor nerve foramen root is posterior and slightly ventral to the optic nerve foramen root. The trochlear nerve foramen root is lateral and dorsal from the oculomotor nerve foramen root. The trigeminal nerve foramen root is posteroventral to the trochlear nerve foramen root. The trigeminal nerve foramen root exits through two separate foramina, the ophthalmic branch separating and exiting anteriorly, while the maxillary and mandibular branches exit together posteroventrolaterally. A very fine passage on the slices just posterior to this may represent the facial nerve foramen root. A bulge that represents the cast of the lagena is posterolateral to this, just beneath the anterior edge of the anterior and horizontal semicircular canals. A pair of extensions posterior to all this, and behind the rest of the endocast, may represent the vagus nerve foramen roots, but their identification is uncertain. It is possible

that they just represent a paired anomaly in the bones, but I cannot determine this from the slices.

Sauropodomorpha

Diplodocus hayi

Although *Plateosaurus* represents a more basal sauropodomorph, and therefore a less derived taxon more suitable for outgroup purposes, it is still useful to look at a more derived sauropod to have a couple of taxa from that lineage. For a description of the *Plateosaurus* endocast, see Galton (1985).

The derived sauropod specimen I examined is *Diplodocus hayi*, CM 662. Despite the large variety of sauropods known, sauropod diversity is not among the goals here, so this sauropod is the only one I described.

The anterior end of the endocast (Figure 25) represents the cast of the olfactory apparatus (i.e., olfactory bulbs and tract). How far forward these extended cannot be determined because no bone surrounded them. All that can be said is that the olfactory area entered the main portion of the cranial cavity through a single foramen dorsally. This is where the endocast was begun because it is the furthest anterior that the cast could be constructed based on corresponding bones. The optic nerve foramina roots are posteroventral to this, exiting the braincase through a pair of midline foramina. The oculomotor nerve foramen root is posterior to the optic nerve foramen root. The trochlear nerve foramen root is anterodorsal to the oculomotor nerve foramen root, and posterodorsal to the optic

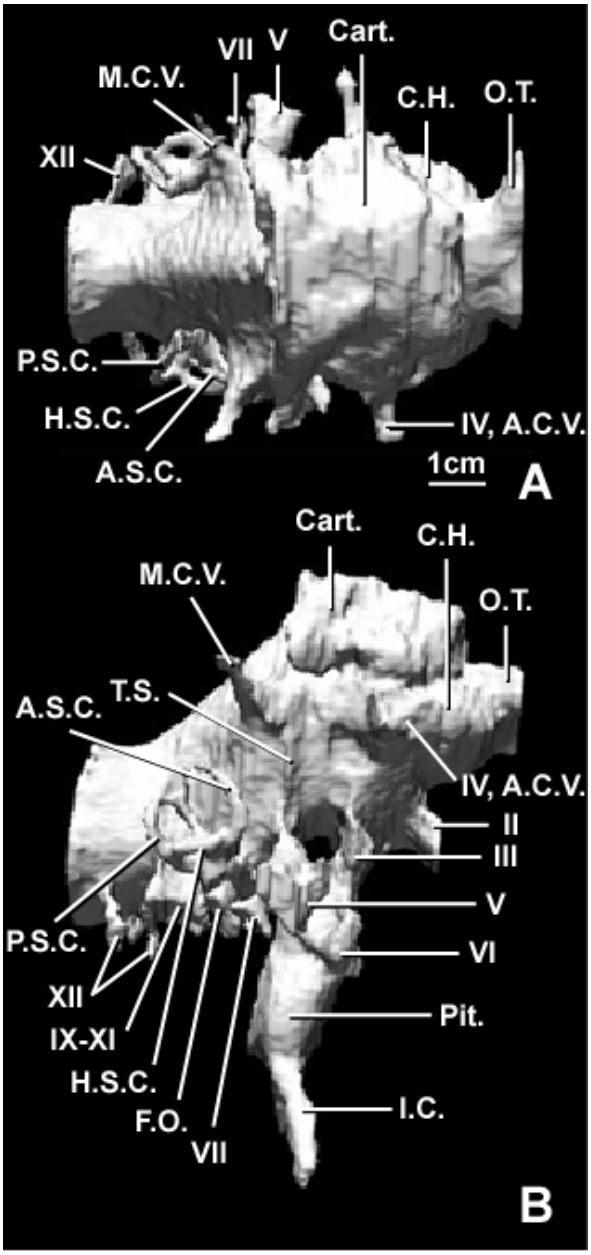

Figure 25. *Diplodocus hayi* endocast.

(A) Dorsal, (B) right lateral, and (C) ventral (following page) views of the endocast of *Diplodocus hayi*, CM 662. Discernible cranial nerves and other features are labeled. See Appendix A for explanation of abbreviations.

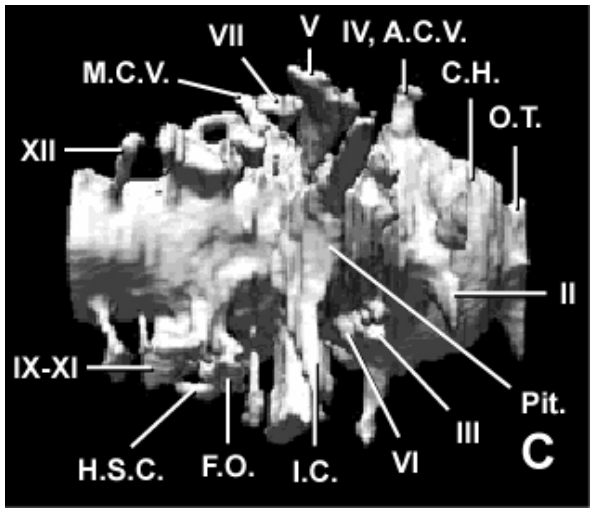

Figure 25 continued.

nerve foramen root. The foramen from which the trochlear nerve root exits probably also housed the anterior cerebral vein. Janensch (1935) suggested that this foramen is for the trochlear nerve and anterior cerebral vein in some genera, and only for the anterior cerebral vein in others, the trochlear nerve exiting from the same foramen as the oculomotor nerve in the latter taxa.

A large mass on top of the cast of the cerebral hemispheres is just dorsal to the trochlear nerve foramen and anterior cerebral vein root. This area was either separated from the cranial cavity in life by cartilage, or it may have housed a portion of the dorsal sagittal sinus. The projection of the middle cerebral vein is posteroventrolateral to this mass on top of the cast of the cerebral hemispheres, with the cast of the transverse sinus running ventrally from the anterior border of the projection of the middle cerebral vein down towards the trigeminal nerve foramen root. The cast of the optic lobe is also located in this area, but its dorsomedial location, and the cast of the sinus overlying it, accounts for its lack of expression on the endocast. The cast of the pituitary fossa is located medial and posteroventral to the oculomotor nerve foramen root. The pituitary fossa is completely encircled by bone, so a better idea of the size of the gland can be determined than in those taxa in which the anterior and lateral walls are not enclosed in bone. This area, as in other sauropods, is very large. The entrances of the internal carotid canal processes are at the posteroventral corners of the cast of the pituitary fossa, and the processes can be followed posteroventrolaterally. Although the abducens nerve canal process enters the fossa more dorsally, it stays

on the lateral margin, and its entire course into and out of the fossa is seen on the lateral side of the cast of the pituitary fossa.

The trigeminal nerve foramen root is posterior to the oculomotor nerve foramen root. There is only one foramen, indicating the nerve exited the braincase before separating and sending the ophthalmic branch anteriorly. The facial nerve foramen root is posteroventral to the trigeminal nerve foramen root. For the facial nerve root there is also only one foramen, indicating the palatine and hyomandibular branches separated after leaving the braincase. The abducens nerve canal process is ventromedial to the facial nerve foramen root. From here it exits the main body of the endocast and enters the cast of the pituitary fossa as described above. The casts of the fenestra ovalis and the fenestra pseudorotunda are posterior to the facial nerve foramen root. The actual paths of the vestibulocochlear nerve foramen branches cannot be seen, but the inner ear region and vestibular apparatus that they entered are visible. As is the case with most of the fossils studied, the cast of the cochlea cannot be seen.

The semicircular canals are beautifully preserved. Although a portion of the anterior semicircular canal is missing on the left side, it is still complete enough that its path can be traced, and the anterior semicircular canal on the right side is complete, so it can be used if there is any doubt about the positioning of the left canal. The orientation of the canals is similar to that seen in crocodilians and early theropods. The anterior semicircular canal curves posterodorsomedially and meets the posterior semicircular canal at the crus commune. The posterior semicircular canal first curves posterolaterally, and then anteroventromedially to

contact the horizontal semicircular canal, which curves posterolaterally and then posteromedially from the anterior end of the anterior semicircular canal to the posterior end of the posterior semicircular canal. The orientation of the head when *Diplodocus* is 'alert' could be determined because the horizontal semicircular canals are preserved in the endocast. The horizontal semicircular canals, when an animal is holding its head in the habitual 'alert' position, are horizontal, or possibly tilted up anteriorly between 0-5° (Witmer et al., 2002, 2003). For the *Diplodocus*, the normal head position is almost exactly the same orientation in which the skull was scanned, with possibly a 2° rotation anteriorly. A noteworthy feature of this region is the lack of prominent floccular lobe casts. There are some small swellings in the area of the vestibular apparatus that may represent them, but they are small and do not protrude between the semicircular canals as they do in theropods. The glossopharyngeal, vagus, and accessory nerve foramen roots all exit together in the cast of the metotic fissure, which is posterior to the casts of the fenestra ovalis and fenestra pseudorotunda. Two roots of the hypoglossal nerve foramina are posterior to this, the first being much thinner and slightly more ventral than the posterior one. Just posterior to this lies the foramen magnum, marking the end of the endocast.

Theropoda

The following endocast descriptions will all be from members of the ingroup for the analyses in chapter 3. In order to parallel what is found in the

analyses, the following descriptions are done in phylogenetic order, and the definition for each clade discussed is given before the appropriate descriptions.

The definition of Theropoda I use was proposed by Gauthier (1986). Theropoda are "birds and all saurischians that are closer to birds than they are to sauropodomorphs" (Gauthier, 1986:18).

Ceratosauria

The definition of Ceratosauria I use was proposed by Rowe (1989). Ceratosauria are *Ceratosaurus nasicornis* and all theropods that are more closely related to *Ceratosaurus nasicornis* than they are to birds.

Ceratosaurus magnicornis

The specimen obtained for creating the endocast of *Ceratosaurus magnicornis* was MWC 1, which consists of a complete braincase that is disarticulated from the rest of the skull (Madsen and Welles, 2000). The anterior portion of the endocast (Figure 26) begins with the casts of the olfactory bulbs. The casts of the bulbs are completely enclosed in bone, giving a good representation of their actual size. The casts of the bulbs are also separated from each other by a median sphenethmoidal septum. The septum disappears posteriorly, and the casts of the bulbs come together in the cast of a single olfactory tract. The cast of the tract merges with the cast of the cerebral hemispheres posteriorly. The cast of the hemispheres can be identified by its lateral and dorsoventral expansion.

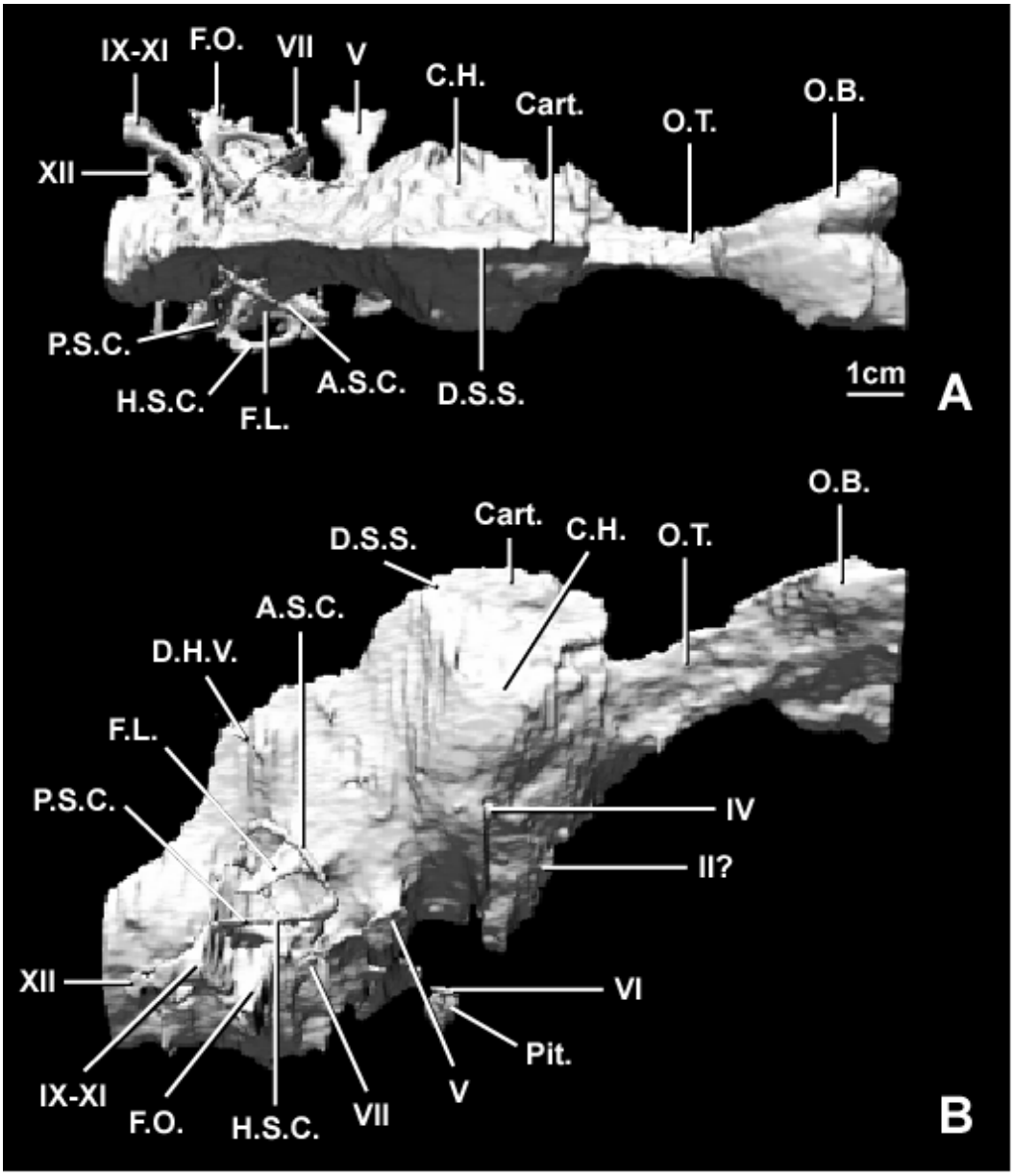

Figure 26. *Ceratosaurus magnicornis* endocast.

(A) Dorsal, (B) right lateral, and (C) ventral (following page) views of the endocast of *Ceratosaurus magnicornis*, MWC 1. Discernible cranial nerves and other features are labeled. See Appendix A for explanation of abbreviations.

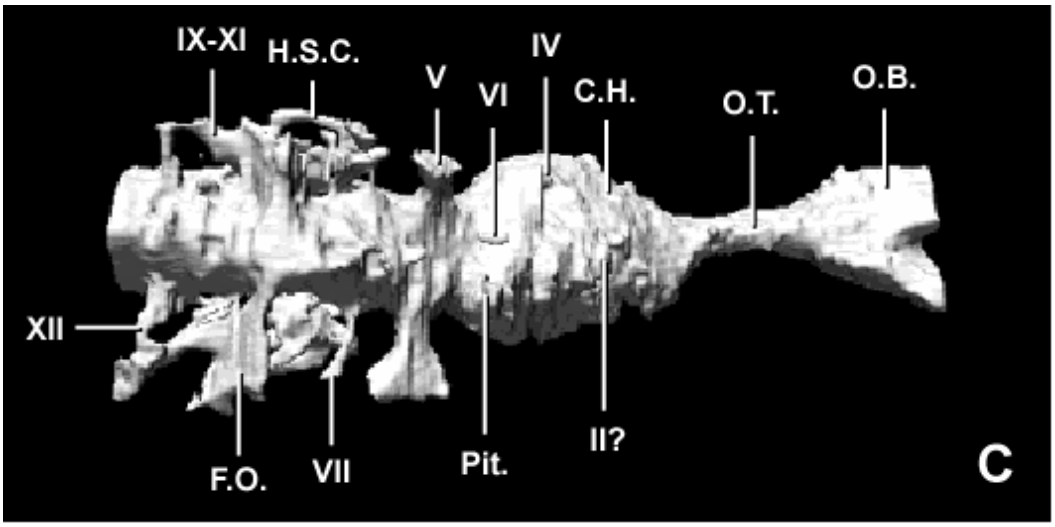

Figure 26 continued.

The optic nerve foramen root is ventral to the cast of the hemispheres, but it is difficult to identify owing to the matrix in this area of the braincase. The trochlear nerve foramen root can be identified posterodorsal to the optic nerve foramen root. The cast of the pituitary fossa is ventral to the optic nerve foramen root. The cast of the pituitary fossa is also difficult to identify owing to the large amount of pneumatic space found within the braincase bones. The attachment of the cast of the pituitary fossa to the rest of the endocast cannot be seen, so it appears to be contained completely within the bones, just as the pneumatic spaces, which invade the bones but are usually not connected to the cranial cavity proper. The area thought to be the cast of the pituitary fossa was found by following the internal carotid canal processes, which appear to meet in the area that is identified as the cast of the pituitary fossa. Once again though, even following the internal carotid canal processes was difficult given the amount of pneumaticity present. Also helping with the identification of the cast of the pituitary fossa was the presence of what appears to be one of the abducens nerve canal processes. This nerve canal process is found lateral to the cast of the pituitary fossa, and although it cannot be traced continuously to its exit from the ventral surface of the endocast, the very beginning of it leaving the ventral surface is present, as well as the anterior end where it exits the braincase lateral to the cast of the pituitary fossa.

The trigeminal nerve foramen root is situated posteroventral to the trochlear nerve foramen root, and exits ventrolaterally as a single root, not branching until after it exits the braincase. A thin vascular projection dorsal to the

trigeminal nerve also exits ventrolaterally. This projection is also seen in various other taxa that will be described below. The facial nerve foramen root is posteroventral to the trigeminal nerve foramen root, and exits the endocast posteroventrolaterally. Just dorsal to the facial nerve foramen root, and using a portion of the same stem, is a thin connection with the semicircular canals. This connection may represent one of the vestibular rami of the vestibulocochlear nerve. Another connection that may be the cochlear branch of the vestibulocochlear nerve foramen root is posterior to this. The cast of the fenestra ovalis is the next root found posteroventrally. The cast representing the glossopharyngeal, vagus, and accessory nerves leaving the metotic fissure is posterior to the cast of the fenestra ovalis. A shorter root, which may represent the glossopharyngeal nerve foramen, a hypoglossal nerve foramen branch, or just a pneumatic structure not related to the cranial nerves, is ventral to the metotic fissure cast. The hypoglossal nerve foramen roots, which exit laterally through a single foramen, are posterior to the combined nerve cast. Behind the hypoglossal nerve foramen root is the end of the endocast.

A large ridge dorsal to the cast of the cerebral hemispheres may represent an area that was dorsal to the cranial cavity and covered by cartilage in life. This area also housed the dorsal sagittal sinus. A large projection representing the foramen of the dorsal head vein exits posterodorsolaterally from the dorsolateral surface of the endocast posteroventral to the cast of the dorsal sagittal sinus. The cast of the floccular lobe of the cerebellum stretches in a posteroventrolateral direction ventral to the dorsal head vein foramen projection. The cast of the lobe

passes underneath the anterior semicircular canal, and ends in the area bracketed by all three canals. The orientation of the semicircular canals is the same as that seen in the crocodile. The anterior semicircular canal first arches posterodorsomedially, and just after turning ventrally meets the posterior semicircular canal, which arches posteroventrolaterally, where it meets the horizontal semicircular canal. This canal begins just posterior to the front of the anterior semicircular canal and arches posterolaterally before going posteromedially to meet the posterior semicircular canal. This orientation of the canals gives the same subtriangular appearance as in the crocodile.

Majungatholus atopus

Majungatholus atopus is a Cretaceous ceratosaur from Madagascar. The endocast described is from FMNH PR 2100. This specimen was CT scanned for Larry Witmer, and the dataset was graciously lent to me for the creation of the endocast and description. A complete description of the specimen is currently underway by Scott Sampson and Larry Witmer (pers. comm.).

The endocast (Figure 27) begins with the casts of the olfactory bulbs anteriorly, which are separated by a median sphenethmoidal septum. The anterior portion of the casts of the olfactory bulbs are not ventrally or laterally encased by bone, but as the endocast is followed posteriorly, the casts of the bulbs give way to the casts of the olfactory tracts, which merge, because of the loss of the median septum, and they are completely encased by bone. The cast of the tract continues

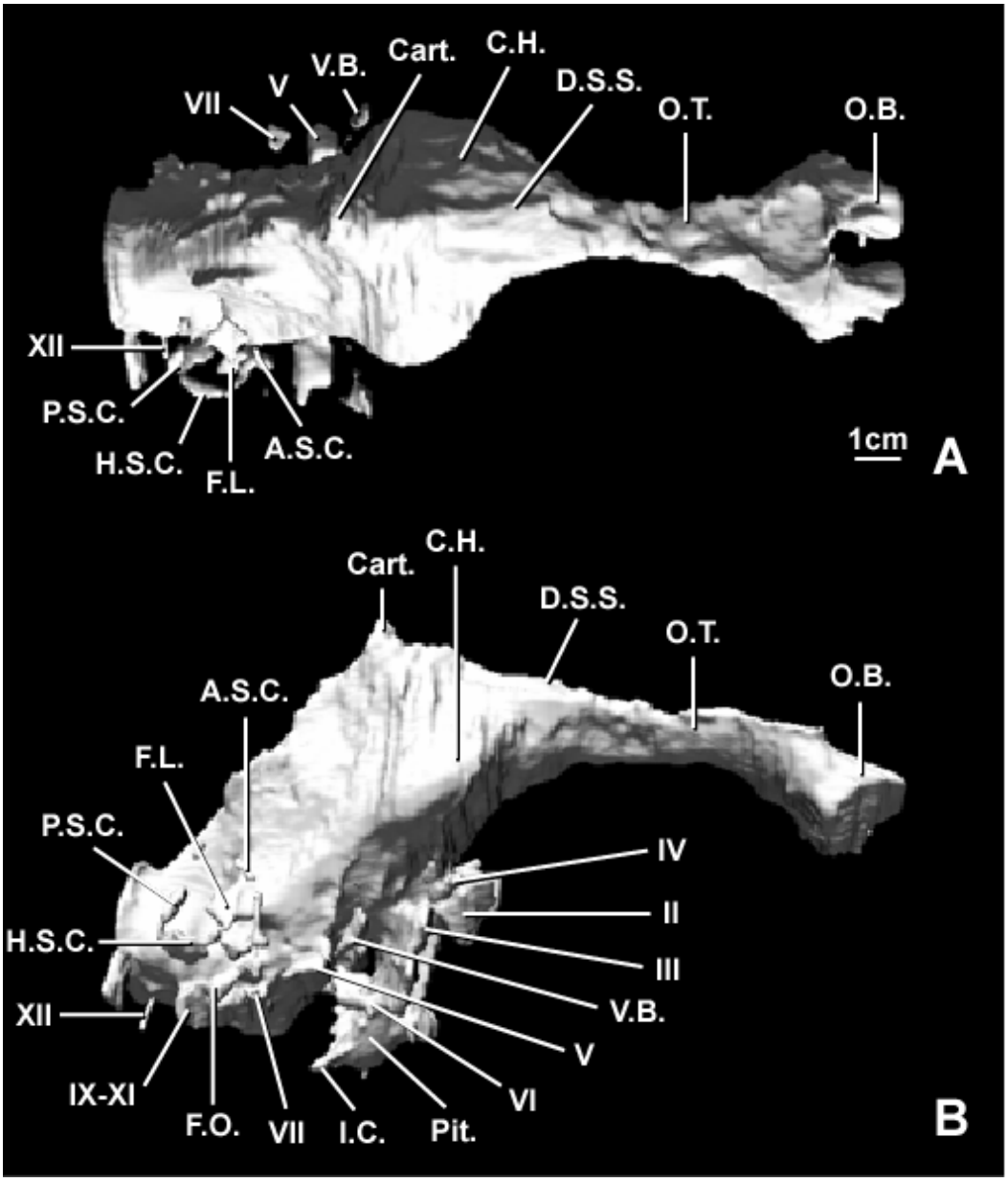

Figure 27. *Majungatholus atopus* endocast.

(A) Dorsal, (B) right lateral, and (C) ventral (following page) views of the endocast of *Majungatholus atopus*, FMNH PR 2100. Discernible cranial nerves and other features are labeled. See Appendix A for explanation of abbreviations.

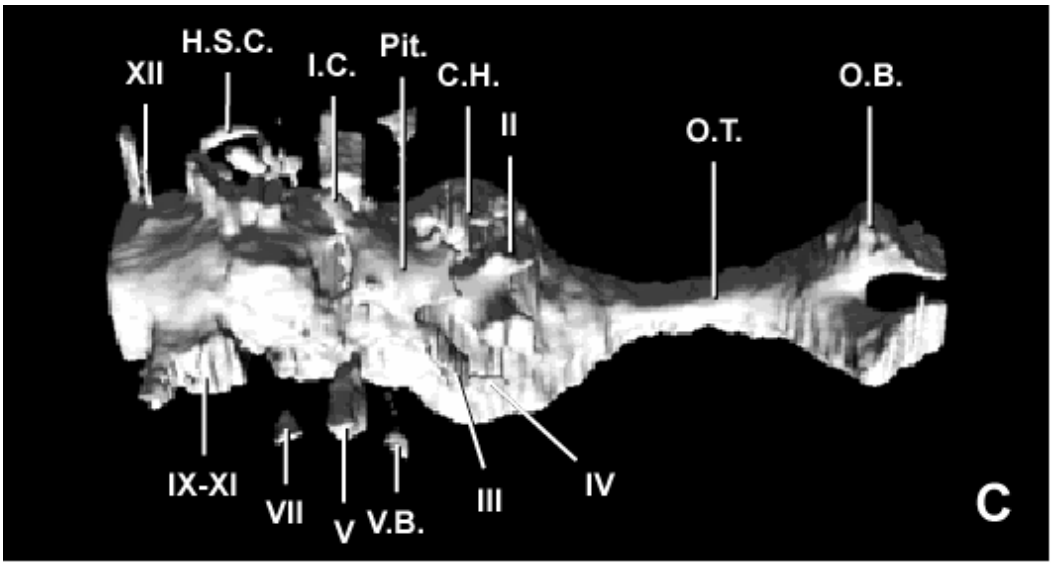

Figure 27 continued.

posteriorly until it meets the cast of the cerebral hemispheres, which broadens posteriorly in all directions.

The optic nerve foramen roots, each of which exits through its own foramen, are ventral to the anterior portion of the cast of the cerebral hemispheres. The trochlear nerve foramen root is posterolateral to the optic nerve foramen root. The oculomotor nerve foramen root is slightly posteroventral to the trochlear nerve foramen root. A long posteroventrally oriented ridge, whose posterior portion represents the anterior boundary of the abducens nerve canal process where it exits the braincase, is continuous with the ventral edge of the oculomotor nerve foramen root. The abducens nerve canal process can be followed posteriorly, through the lateral margins of the cast of the pituitary fossa, to its exit from the ventral surface of the endocast. The cast of the pituitary fossa is medial to the anterior end of the abducens nerve canal process, and is completely enclosed in bone. A process exiting the anteroventrolateral corner of the cast of the pituitary fossa may represent the anterior exit of the internal carotid canal. The abducens nerve canal process passes through the lateral margin of the cast of the pituitary fossa dorsal to the internal carotid canal process, as described above. The internal carotid canal process enters the posteroventrolateral corner of the cast of the pituitary fossa from a posteroventrolateral direction.

The trigeminal nerve foramen root is located posteroventral to the oculomotor nerve foramen root, and exits the endocast before separating into its three constituent branches. A projection most likely representing a vascular pathway is anterodorsal to the trigeminal nerve foramen root, and exits the

endocast in a ventrolateral direction. A similar projection is present in *Ceratosaurus*. A thin root representing the facial nerve foramen is posterior to the trigeminal nerve foramen root. The cast of the fenestra ovalis is posterior to the facial nerve foramen root. I would expect to find the branches of the vestibulocochlear nerve foramen root medial to this cast of the fenestra ovalis, but the preservation and scan quality make it impossible to locate any of these branches with certainty. It is also not possible to accurately identify some of the cranial nerve foramen roots posterior to the cast of the fenestra ovalis. Owing to fractures in this area, the exact exit point of the glossopharyngeal, vagus, and accessory nerve roots in the cast of the metotic fissure cannot be accurately determined. The last roots posteriorly represent the hypoglossal nerve foramen, although on the right side, where there are two roots, the most posterior one may actually be a fracture rather than a nerve foramen exit. Posterior to this the endocast ends at the foramen magnum.

Although the braincase is fractured in the area around the fenestra ovalis, the right side of the endocast does preserve the semicircular canals and cast of the floccular lobe. This lobe cast exits the endocast in the typical posteroventrolateral direction, passing underneath the anterior semicircular canal and ending in the area created by the location of all three canals. The anterior semicircular canal arches in a posterodorsomedial direction, but its meeting point with the posterior semicircular canal is not preserved. The latter canal arches posteroventrolaterally until it meets the horizontal semicircular canal. The horizontal semicircular canal arches posterolaterally from its starting point just posterior to the front of the

anterior semicircular canal, before changing direction to arch posteromedially to its meeting point with the back of the posterior semicircular canal. This orientation of the canals gives the same subtriangular appearance found in other early theropods and crocodilians.

Despite the landmark of the cast of the floccular lobe, the rest of the cast of the cerebellum cannot be seen in the endocast, nor can the cast of the optic lobes, which is located anterior to the cast of the cerebellum. Both of these features, as well as the dorsal surface of the cast of the cerebral hemispheres, are covered by the casts of the dorsal sagittal sinus and occipital sinus that run along the dorsal surface of the endocast. Also located near the posterodorsal edge of the cast of the cerebral hemispheres is a peak, which most likely represents an area that was separated from the cranial cavity in life by cartilage.

Tetanurae

The definition I use for Tetanurae was proposed by Gauthier (1986). Tetanurae are birds and all other theropods that are more closely related to birds than they are to Ceratosauria.

Carnosauria

The definition I use for Carnosauria was proposed by Padian et al. (1999). Carnosauria are all avetheropods that are more closely related to *Allosaurus* than to Neornithes.

Allosaurus fragilis

One of the better-known theropods is *Allosaurus fragilis*, thanks to the large number of specimens that were recovered from the Cleveland-Lloyd Dinosaur Quarry in Utah (Madsen, 1976). Along with those specimens, several well-preserved braincases, and even a natural endocast, were recovered. The braincase used to create the endocast described here is UUVP 5961, which represents a complete braincase that is disarticulated from the anterior portion of the skull.

The endocast (Figure 28) begins at the anterior portion of the braincase, which is the frontal and possibly the posterior end of the nasal. On the underside of these bones is a depression for the dorsal surface of the olfactory tract. Unfortunately there are no lateral or ventral bones to complete the enclosure of the tract, so only the upper surface can confidently be reproduced. Moving posteriorly, the cast of the olfactory tracts merge with the cast of the cerebral hemispheres, a transition marked by the dorsal and lateral expansion of the cast of the hemispheres.

The root for the trochlear nerve foramen is found at the anteroventrolateral border of the lateral expansion of the cast of the cerebral hemisphere. The single root for the optic nerve foramen is ventromedial to the trochlear nerve foramen root. The oculomotor nerve foramen root is posterolateral to the optic nerve foramen root. The cast of the pituitary fossa is posteroventral to the optic nerve foramen root. Only the posterior border of the pituitary fossa is preserved, so the

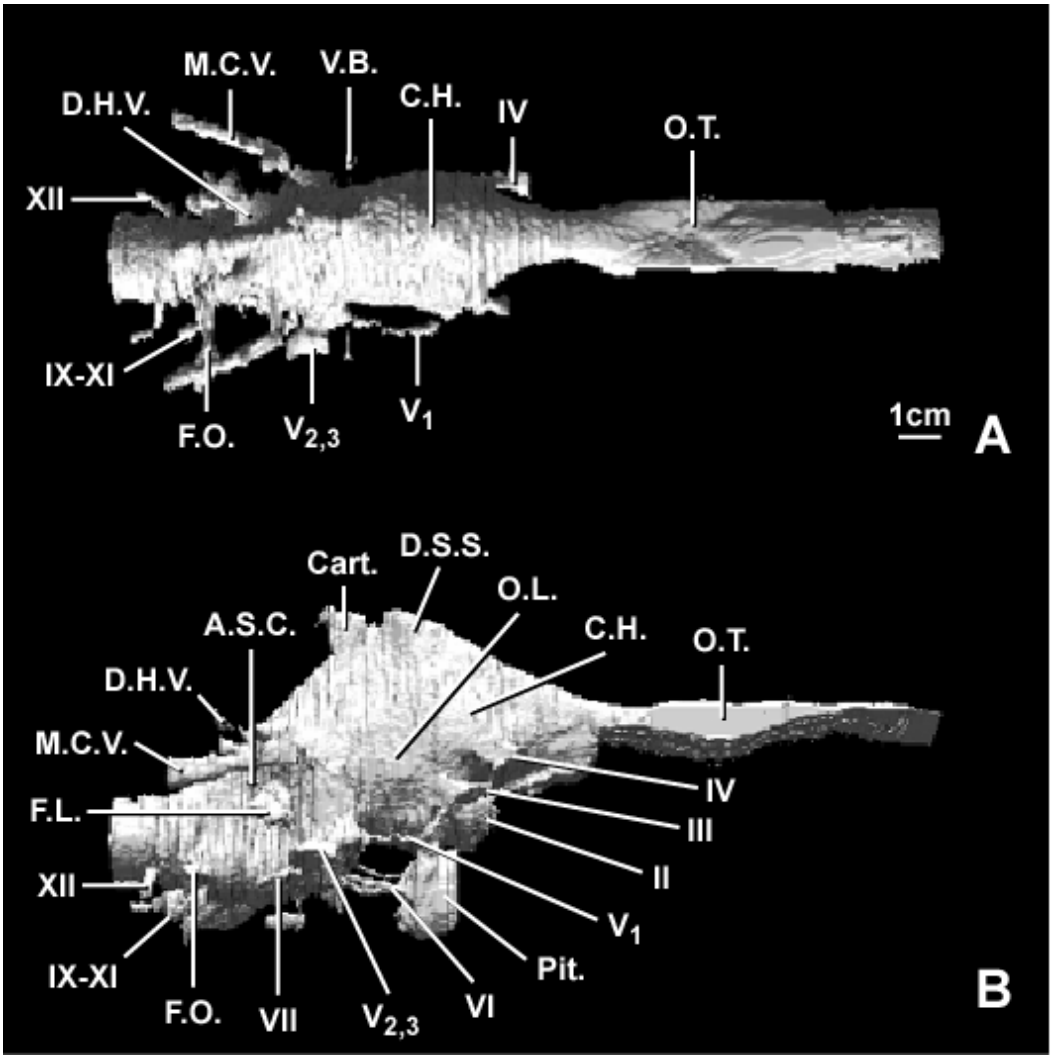

Figure 28. *Allosaurus fragilis* endocast.

(A) Dorsal, (B) right lateral, and (C) ventral (following page) views of the endocast of *Allosaurus fragilis*, UUVP 5961. Discernible cranial nerves and other features are labeled. See Appendix A for explanation of abbreviations.

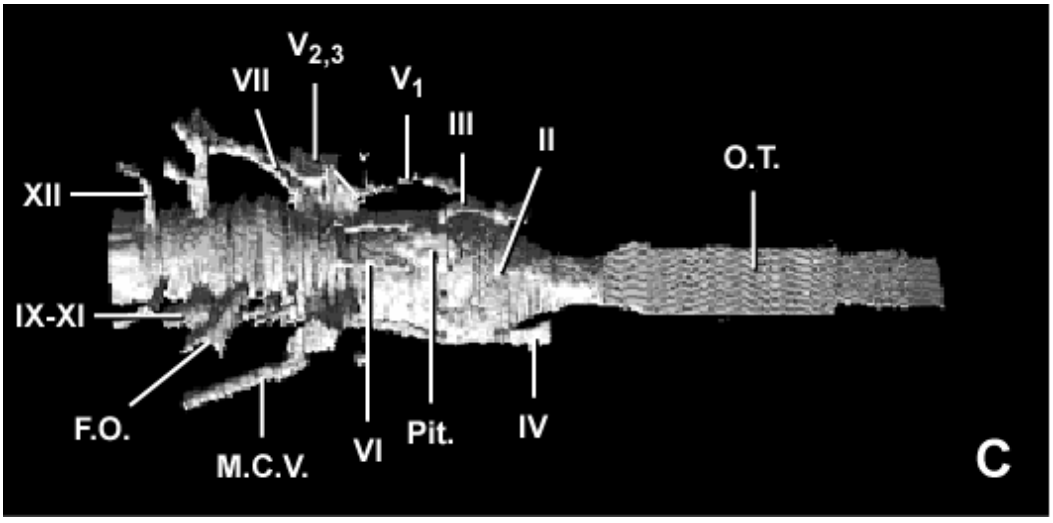

Figure 28 continued.

anterior and lateral extent of the cast of the pituitary fossa cannot be accurately determined. The abducens nerve canal process enters the posterolateral edge of the cast of the pituitary fossa at the midpoint of its dorsoventral extent. The posterior portion of this nerve canal process can be followed posteriorly to its connection on the ventral surface of the endocast. The anterior exit from the braincase of the ophthalmic branch of the trigeminal nerve foramen root is ventrolateral to the oculomotor nerve foramen root. The ophthalmic branch can be followed posteriorly to the rest of the trigeminal nerve foramen root, whose other two branches exit the braincase together ventrolaterally. A vascular projection anterodorsolateral to this is seen exiting the endocast in a ventrolateral direction. A slight ledge on the lateral surface of the endocast that may represent the transverse sinus is found posterior to this vascular projection, and directly dorsal to the trigeminal nerve foramen root. The middle cerebral vein foramen projection exits, and continues posteriorly, immediately posterolateral to the cast of the transverse sinus. Posteromedial to the base of the middle cerebral vein foramen projection, the dorsal head vein foramen projection leaves the endocast posteriorly.

The facial nerve foramen root is located posteroventral to the base of the trigeminal nerve foramen root. The cast of the fenestra ovalis is posterior to the facial nerve foramen root. Unfortunately, the actual branches of the vestibulocochlear nerve foramen root cannot be seen. The combined branches representing the glossopharyngeal, vagus, and accessory nerves leave the endocast in the cast of the metotic fissure in a posteroventrolateral direction just

posterior to the cast of the fenestra ovalis. The hypoglossal nerve foramen roots leave the endocast together ventrolaterally posterior to the cast of the metotic fissure. Posterior to the hypoglossal nerve foramen root is the foramen magnum and the end of the endocast.

Several additional features representing the actual brain are found. First, just posteroventral to the cast of the cerebral hemispheres, a slight outline of what may be the cast of the optic lobe is found. Dorsal to this and the cast of the cerebral hemispheres, forming a peak in the endocast, is a structure that represents an area of the braincase that was probably covered with cartilage that was lost after the death of the animal. Also covering the dorsal surface of the casts of the cerebral hemispheres and cerebellum in this area are the casts of the dorsal sagittal sinus and occipital sinus. More posteriorly, the cast of the floccular lobe of the cerebellum is just posteroventral to the middle cerebral vein foramen projection. This lobe cast stretches away from the endocast in a posteroventrolateral direction. The anterior semicircular canal is also visible, arching in a posterodorsomedial direction over the floccular lobe. The other canals cannot be discerned in the specimen, although they must be present because of the completeness of the specimen in this area. A natural *Allosaurus* endocast (UUVP 294) (Madsen, 1976) preserves all the semicircular canals, revealing the subtriangular orientation found in crocodilians and other early theropods.

Carcharodontosauridae

The definition I use for Carcharodontosauridae was proposed by Sereno et al. (1996). Carcharodontosauridae are all descendants of the most recent common ancestor of *Giganotosaurus* and *Carcharodontosaurus*.

Acrocanthosaurus atokensis

The *Acrocanthosaurus atokensis* specimen used for scanning was the complete, uncrushed braincase of the type specimen, OMNH 10146 (formerly MUO 8-0-S9) (Stovall and Langston, 1950). The anteriormost portion of the endocast (Figure 29) is composed of the casts of the olfactory bulbs and tracts, which are completely encased in bone, with a median sphenethmoidal septum separating the two bulb casts. The casts of the olfactory tracts extend posteriorly from the bulbs, and merge along the midline with the loss of the median septum. The cast of the common tract continues posteriorly to the anterior margin of the cast of the cerebral hemispheres. The transition to these hemispheres is seen as a ventral, as well as a gradual lateral, expansion of the endocast.

Overlying the cast of the cerebral hemispheres is a ridge that represents the dorsal sagittal sinus. A small extension moving ventrally from this that looks like it is going to run down between the cast of the floccular lobe and the trigeminal nerve foramen root represents the transverse sinus. The optic nerve foramen roots lie just ventral to the cast of the cerebral hemispheres, and exit the braincase together through a single optic foramen. Although it is a single opening,

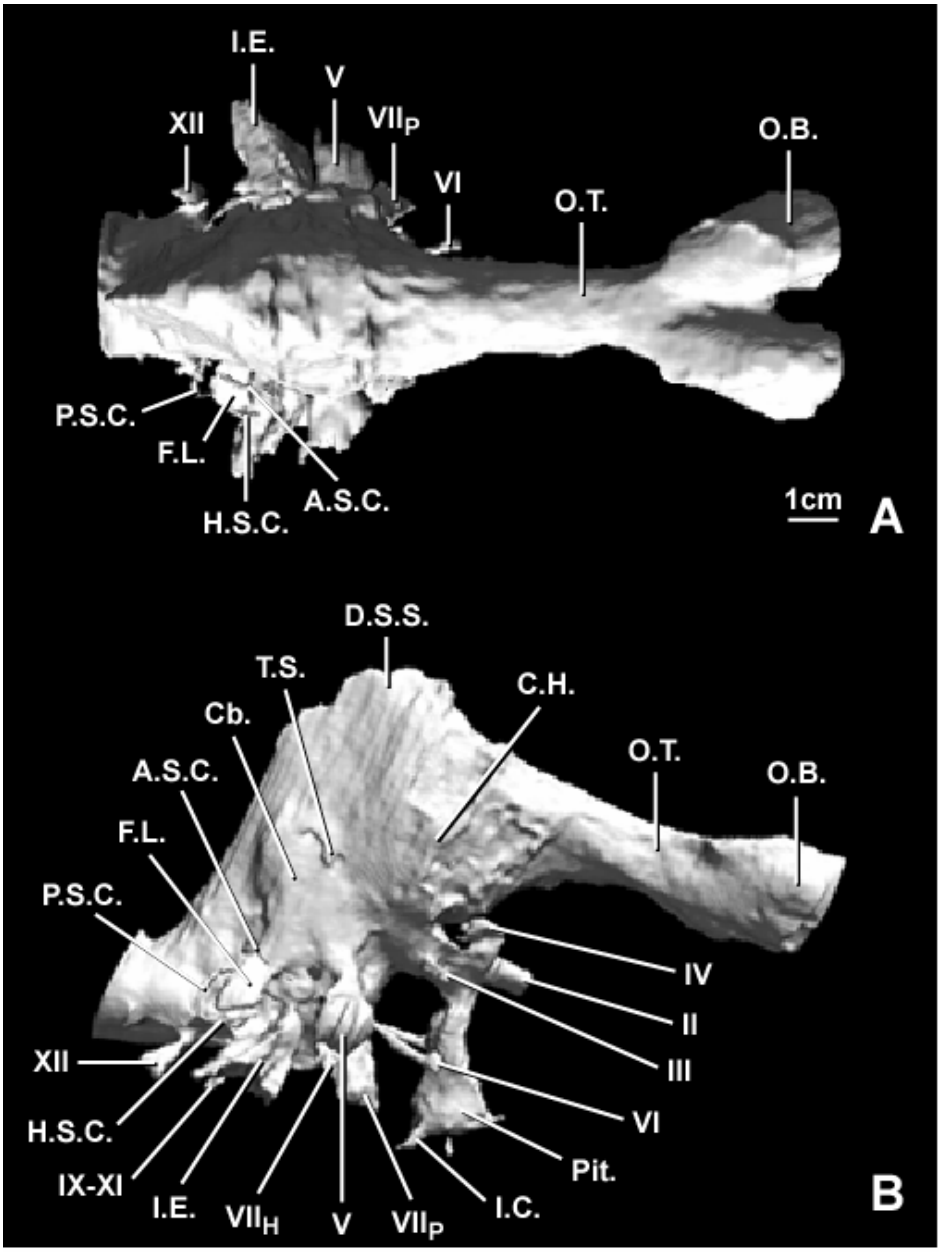

Figure 29. *Acrocanthosaurus atokensis* endocast.

(A) Dorsal, (B) right lateral, and (C) ventral (following page) views of the endocast of *Acrocanthosaurus atokensis*, OMNH 10146. Discernible cranial nerves and other features are labeled. See Appendix A for explanation of abbreviations.

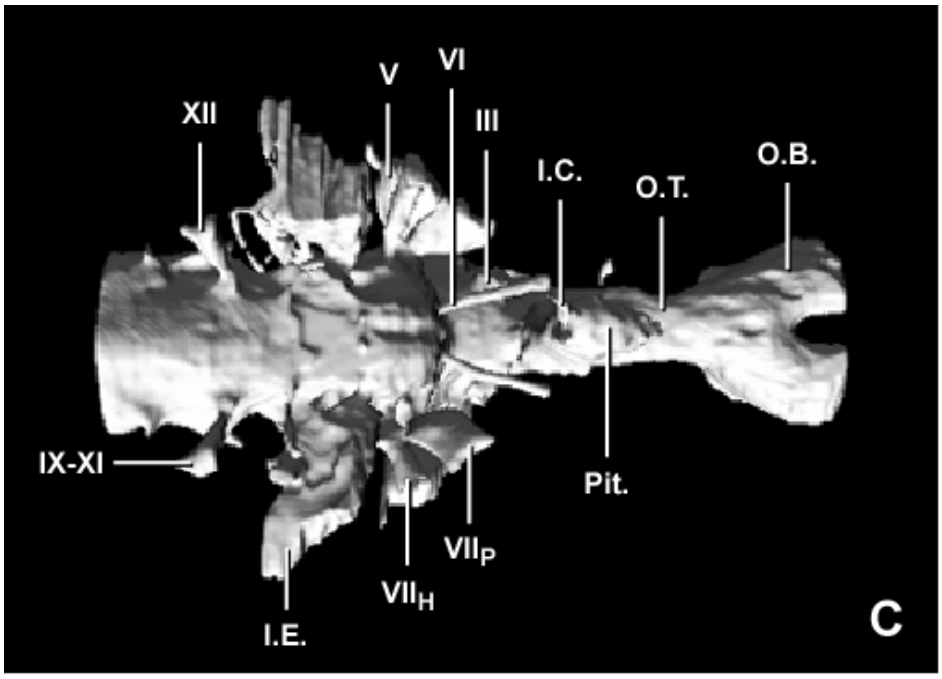

Figure 29 continued.

there is a portion of the orbitosphenoid that hangs down medially within the foramen, but whether this actually divided it in two and is broken, or did not divide the foramen, could not be determined.

Located posterior and dorsal to the optic nerve foramen root is an oval foramen root that is connected to the optic nerve foramen root. Whether this is a part of the optic nerve foramen root, or the trochlear nerve foramen root, cannot be stated with certainty. The oculomotor nerve foramen root exits the endocast ventrolateral to the oval foramen root, and if this oval foramen root is part of the optic nerve foramen root, then the oculomotor nerve foramen root probably represents the trochlear nerve root as well. The cast of the pituitary fossa extends ventrally beneath the optic nerve foramen root, and medial to the oculomotor nerve foramen root. The anterior border of the pituitary fossa is not ossified, so the anterior extent of the cast of the pituitary fossa cannot be accurately determined. The entrances for the internal carotid canal processes are found within the ossified ventral portion of the pituitary fossa. These artery canal processes can be followed posteroventrally from the cast of the pituitary fossa. The abducens nerve canal process is just lateral to the cast of the pituitary fossa, its posterior end leaving the ventral surface of the endocast just ventromedially to the exit for the trigeminal nerve foramen root.

The trigeminal nerve foramen root exits near the anteroventral border of this portion of the endocast. Only one is present, indicating that the ophthalmic branch did not diverge from the maxillary and mandibular branches until they exited the braincase. Several small projections dorsal and posterodorsal to the

trigeminal nerve foramen root exit the endocast in a posteroventrolateral direction. These most likely represent vascular branches.

The facial nerve foramen root is posterior and ventral to the trigeminal nerve foramen root. Unlike the trigeminal nerve foramen root, the facial nerve foramen root branches before exiting the endocast, sending the palatine branch anteriorly before the hyomandibular branch exits laterally, ventral to the trigeminal nerve foramen root. The cast of the inner ear lies just posterior to the facial nerve foramen root. Owing to the degree of fracturing present, the exact paths of the vestibular and cochlear branches of the vestibulocochlear nerve foramen root cannot be established. This fracturing, and possibly some over-preparation, also makes the exact size, shape, and extent of the inner ear impossible to determine.

The cast of the floccular lobe is posterodorsal to this area. It extends posteroventrolaterally from the endocast, between the semicircular canals. It moves beneath the anterior semicircular canal, and ends near the posterior corner of the horizontal semicircular canal and the ventral edge of the posterior semicircular canal. Although preserved on both sides of the endocast, the floccular lobe cast and semicircular canals are more complete on the right side.

If the endocast is situated with the cast of the olfactory tract horizontal, the semicircular canals are incorrectly oriented. The anterior semicircular canal is horizontal, rather than sloping dorsally, as it moves posteriorly, and the other canals are similarly incorrectly oriented (Witmer et al., 2002, 2003). In order to correct this, the endocast needs to be rotated in an anterior direction

approximately 25°. The anterior semicircular canal travels posterodorsally, passing lateral to the cast of the floccular lobe. The anterior edge of the posterior semicircular canal begins near the posterior edge of the anterior semicircular canal, and travels posteroventrally. The horizontal semicircular canal begins ventral to the anterior edge of the anterior semicircular canal, and travels posteriorly just ventral to the cast of the floccular lobe. After traveling past the posterior edge of the cast of the floccular lobe, the horizontal semicircular canal meets the posterior semicircular canal. This orientation gives the same subtriangular shape to the semicircular canals described for previous theropods and the crocodile.

The vagus, accessory, and hypoglossal nerve foramen roots are on the ventrolateral surface of the endocast, directly behind the cast of the inner ear. The foramina for these nerves are found in a deep pit lateral to the occipital condyle. On the left-hand side there is a third foramen, which is not found on the right-hand side. The positioning of this foramen is what would be expected if there was a separate exit for the glossopharyngeal nerve, or it could have transmitted the external ophthalmic artery and vein. The glossopharyngeal nerve root exited with the vagus and accessory nerve roots if the third foramen mentioned above was not for the glossopharyngeal nerve. The foramen magnum is just posterior to these nerve roots, marking the end of the endocast.

Although a large amount of information can be taken from this endocast, there are some major features of the brain that cannot be discerned. One of these features is the cast of the optic lobes. The optic lobes in *Acrocanthosaurus*

probably had not yet obtained the ventrolateral position seen in modern birds, and owing to the dorsal sagittal sinus and occipital sinus, the optic lobes did not leave any impressions on the medial walls of the braincase. They were most likely positioned dorsally and posterior to the cerebral hemispheres, like what is seen in modern crocodiles. Also indiscernible in the endocast is the cast of the main body of the cerebellum. Some of the lateral margins are seen, and the general position of the main body can be inferred based on the casts of the floccular lobes, but, just as with the optic lobes, a large portion of it was covered with the occipital sinus.

Coelurosauria

The definition I use for Coelurosauria was proposed by Gauthier (1986). Coelurosauria are birds and all other theropods that are more closely related to birds that they are to Carnosauria.

Maniraptora

The definition I use for Maniraptora was also proposed by Gauthier (1986). Maniraptora are birds and all coelurosaurs that are more closely related to birds than they are to Ornithomimidae.

Citipati osmolskae

The *Citipati osmolskae* specimen used for this scan, IGM 100/978, was found in the Djadokhta Formation of Ukhaa Tolgod, Mongolia. It is a complete skeleton, but only the skull was scanned (Clark et al., 2001).

This specimen was complete, and as such a complete endocast (Figure 30) was recovered. The anterior portion of the endocast consists of the cast of the olfactory tract, which is enclosed by bone, permitting a good reconstruction of its size and shape. Anterior to this the skull opens completely, making the position and size of the olfactory bulbs impossible to determine. Posteriorly the cast of the tract merges with the cast of the cerebral hemispheres, which expands mainly dorsally and laterally. These hemispheres are quite well defined, and the depression representing the interhemispherical fissure is seen between the two. The increase in size of the cast of the hemispheres may be owing to an increase in the sensory reception areas of the dorsal ventricular ridge. In modern birds, there are three auditory, two visual, and two somatosensory centers (Ulinski, 1983). In *Citipati*, there doesn't appear to be an increase in optic lobe size, but there is a change in semicircular canal orientation, and *Caudipteryx*, which is closely related to *Citipati*, had feathers (Padian et al., 2001b). This means that *Citipati* also probably had feathers, and would require extra somatosensory receptors in the brain for processing information from these feathers. The increase in cerebral hemisphere size may therefore be related to the addition of an extra somatosensory and/or one or two of the extra auditory centers found in birds but not crocodilians. Posteroventral to the cast of the hemisphere is a slight bulge that may represent a portion of the cast of the optic lobe. This lobe is still mostly in the dorsomedial position seen in early theropods and crocodilians, and has not yet achieved the ventrolateral position found in birds. A single root for the optic nerve

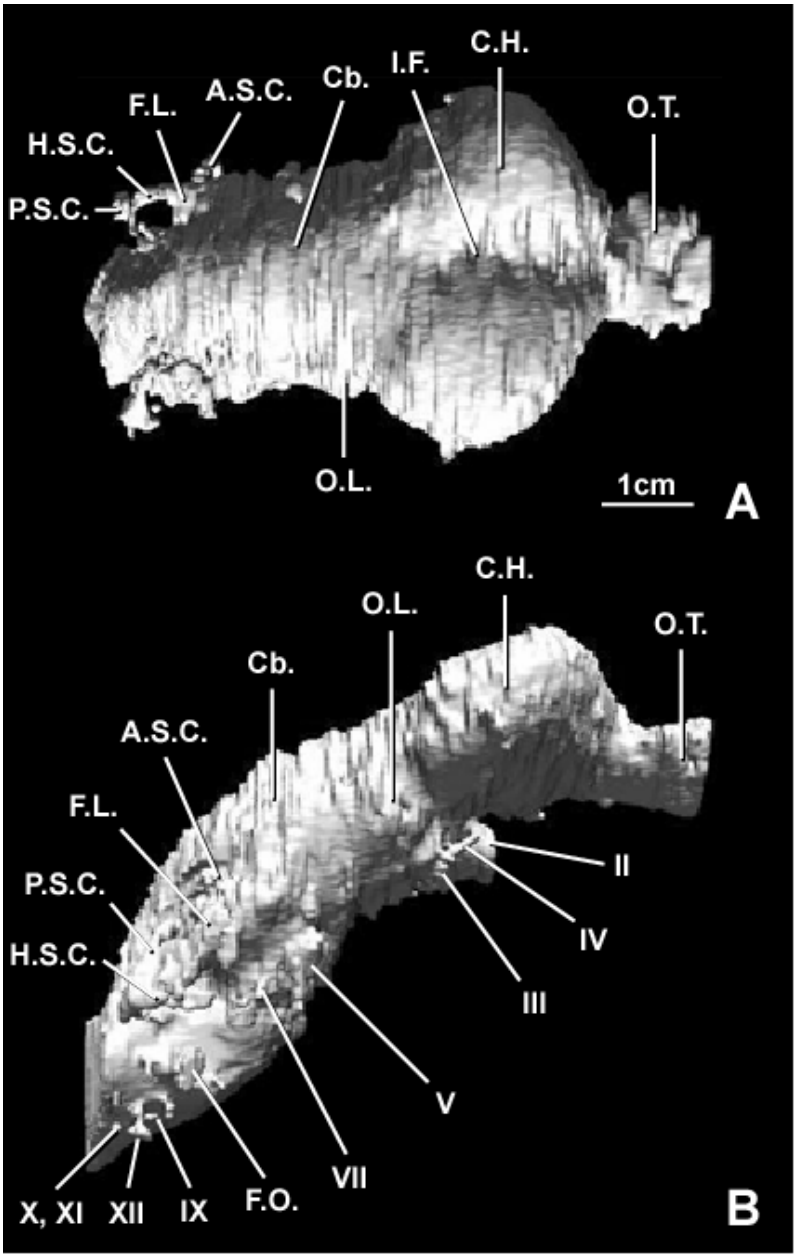

Figure 30. *Citipati osmolskae* endocast.

(A) Dorsal, (B) right lateral, and (C) ventral (following page) views of the endocast of *Citipati osmolskae*, IGM 100/978. Discernible cranial nerves and other features are labeled. See Appendix A for explanation of abbreviations.

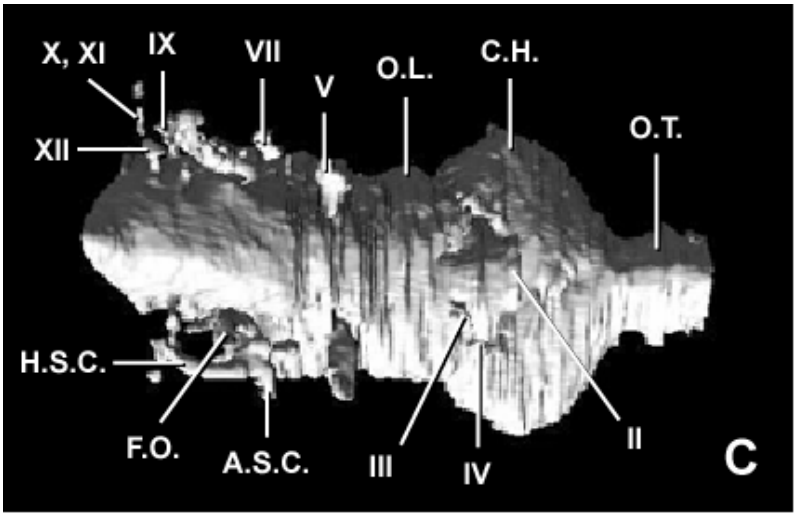

Figure 30 continued.

foramen is present ventral to the cast of the cerebral hemispheres. The trochlear nerve foramen root is lateral to the optic nerve foramen root, and a root that may represent the oculomotor nerve foramen is posteromedial to the trochlear nerve foramen root.

Some of the features that must be present, but cannot be seen, are the cast of the pituitary fossa and the abducens nerve canal processes. These cannot be found because of the difficulty in distinguishing between the matrix and the bone. This difficulty is not only because of the density of the matrix, but also the fact that the bone is very thin, adding to the difficulty in the distinction. Unfortunately this led to my inability to find the cast of the pituitary fossa and abducens nerve canal processes, even though they should be present owing to the fact that the braincase is complete.

The trigeminal nerve foramen root is posteroventrolateral to the trochlear and oculomotor nerve foramen roots. The trigeminal nerve foramen root exits the endocast ventrolaterally, with no sign that any of the branches diverge before it has left the braincase. The facial nerve foramen root is posteroventral to the trigeminal nerve foramen root. Posteroventral to the facial nerve foramen root are a variety of projections, the identities of which are difficult to determine. The two posteriormost roots represent the hypoglossal nerve foramina, and there are several roots at the base of the paroccipital process that were identified by Clark et al. (2002) as the glossopharyngeal and vagus nerve foramen roots. The root representing the accessory nerve, as in all the other taxa I examined, exits with the vagus nerve root. A cast that may represent the fenestra ovalis is anterior to the

glossopharyngeal and vagus nerve foramen roots, but as was previously mentioned, this cannot be substantiated. Several small branches are seen in the osseous labyrinth region posterior to the facial nerve foramen root, and these may represent various branches of the vestibulocochlear nerve foramen root. Just posterior to the hypoglossal nerve foramina roots the foramen magnum marks the end of the endocast.

One region that is well preserved in this specimen, but not on some of the specimens described later, is the osseous labyrinth and cast of the floccular lobe. The cast of the floccular lobe emerges from the main endocast dorsal to the facial nerve foramen root, and extends almost straight posteriorly, with very small amounts of ventral and lateral movement. The orientation of the semicircular canals differs from what I described in previous taxa. The anterior semicircular canal arches dorsomedially before changing direction to move posteroventromedially. In this posteroventromedial position the anterior semicircular canal meets the posterior semicircular canal. The posterior semicircular canal arches primarily ventrolaterally, with only slight posterior movement. After meeting the horizontal semicircular canal, it continues in a dorsomedial direction with slight anterior movement, coming to an end near the location where it began. The orientation of the horizontal semicircular canal is more usual, arching posterolaterally from its beginning just posterior to the anterior semicircular canal, and then moving posteromedially to its contact with the posterior semicircular canal. This change in semicircular canal orientation

may be the first step in the transformation of the ear from one like a crocodilian to one like a bird.

Troodontidae

The definition I use for Troodontidae was proposed by Xu et al. (2002). Troodontidae are *Saurornithoides junior* (=*Mongolodon junior*) and all Deinonychosauria that are more closely related to *Saurornithoides junior* than they are to Dromaeosauridae. In this study, that includes *Mongolodon junior, Byronosaurus jaffei*, and the Zos Canyon troodontid.

Mongolodon junior

Mongolodon junior is a member of the clade Troodontidae, which is variably placed as the closest non-avian relative to birds (Forster et al., 1998), or as one of the closest outgroups (Holtz, 1998). Although there are a fair number of troodontids known (Currie, 1985; Currie and Peng, 1993; Currie and Zhao, 1993b; Russell and Dong, 1993), most of them have only fragmentary or partially complete braincases. One of the most complete braincases for a troodontid is that of *Mongolodon junior*, IGM 100/1, which was described by Barsbold (1974).

The anterior portion of the endocast (Figure 31) consists of the cast of the olfactory tract. Owing to the lack, or loss, of the sphenethmoid bones that would have enclosed the ventral portion of the olfactory bulbs and tract, the exact length and shape of this region cannot be determined. The ventral surface of the frontal

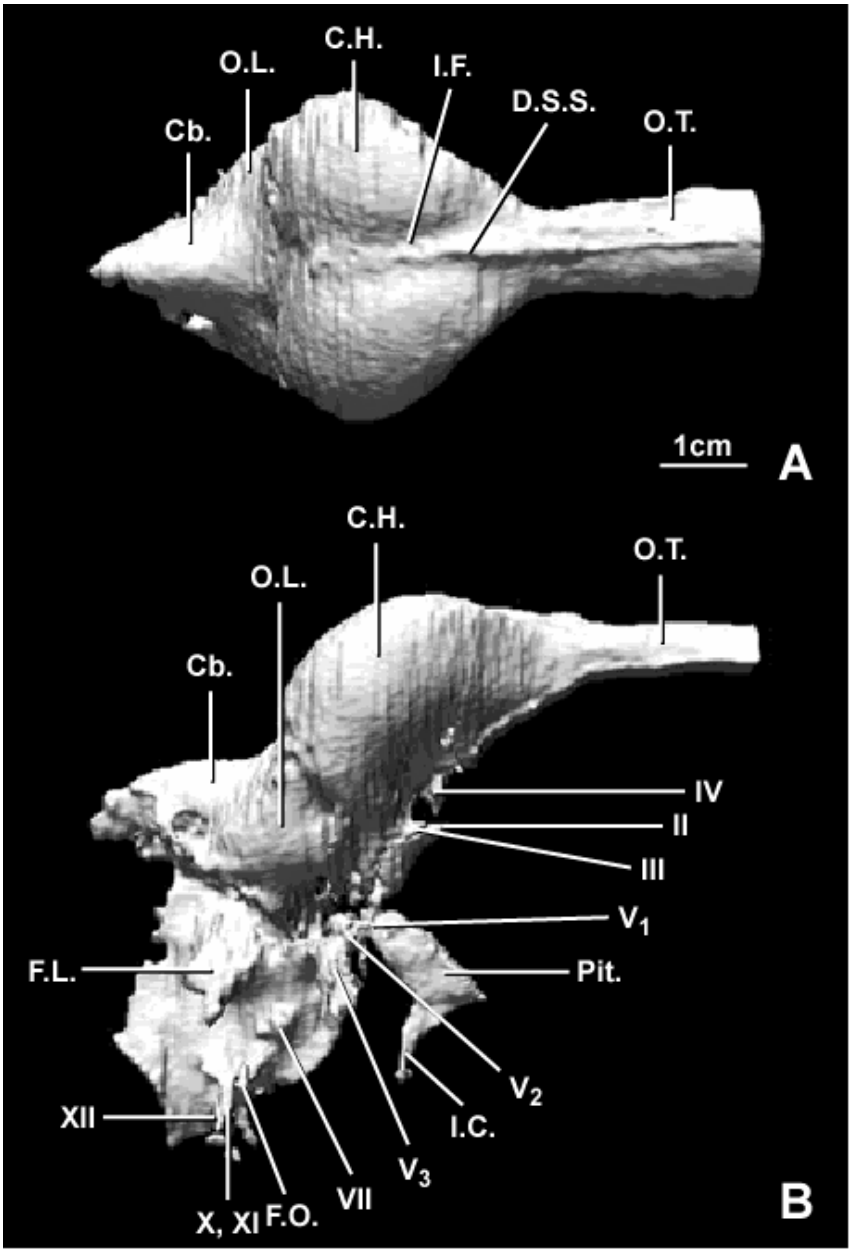

Figure 31. *Mongolodon junior* endocast.

(A) Dorsal, (B) right lateral, and (C) ventral (following page) views of the endocast of *Mongolodon junior*, IGM 100/1. Discernible cranial nerves and other features are labeled. See Appendix A for explanation of abbreviations.

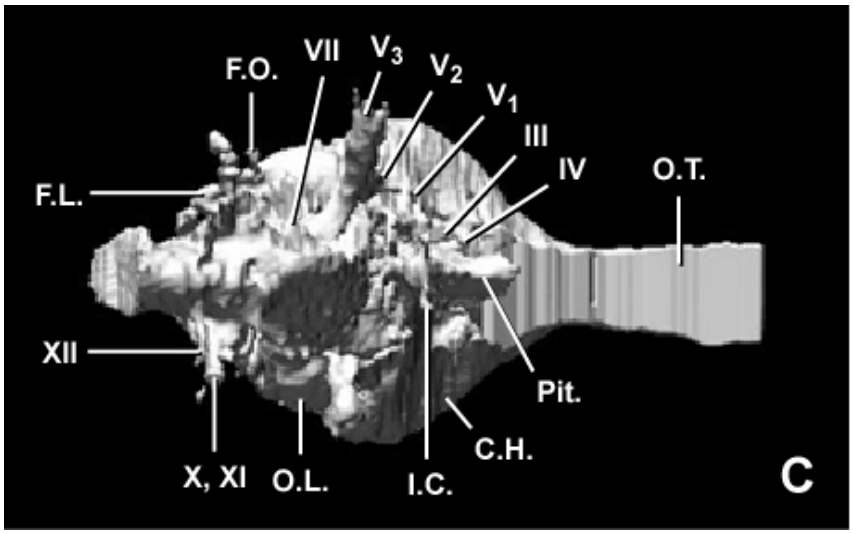

Figure 31 continued.

does have an impression of what the upper surface of the tract looks like, however, and I therefore chose to begin the illustration of the endocast with that bone. The frontal extends forward of where the endocast begins, but there is a natural break in the skull separating the snout region from the braincase region, and it is behind this break that the endocast was started. This decision was arbitrary though, and the olfactory region may well have extended more anteriorly than is depicted. The posterior border of the cast of the olfactory tract is found where the expansion of the cast of the cerebral hemispheres begins.

Cortical expansion is quite apparent, and the lateral extent of the cast of the cerebral hemispheres is great enough that it is forced posteroventrally by the eyeball, as is reflected in the shape of the laterosphenoid and other bones that participate in forming the posterior wall of the orbit. This expansion and diversion of the cast of the cerebral hemispheres is much more similar to what is seen in extant birds than more basal theropods such as *Acrocanthosaurus* and *Tyrannosaurus* (personal observation). The depression representing the interhemispherical fissure is seen on the dorsal surface of the endocast between the casts of the two hemispheres, suggesting that the hemispheres completely filled the endocranial cavity. Also present on the dorsal surface of the endocast is the cast of the dorsal sagittal sinus, which is confined to a narrow canal in the depression representing the interhemispherical fissure owing to the expansion of the cerebral hemispheres. The increase in size of the cerebral hemispheres may be a result of the addition of the second visual center seen in the DVR of birds (Ulinski, 1983). The increase in the size of the optic lobes may have accompanied

the addition of this second area. The cast of the cerebellum comes in contact with the posterior edge of the cast of the cerebral hemispheres, and this may have, in part, led to the ventrolateral migration of the casts of the optic lobes.

Ventral to the cortical expansion, remnants of what may have been the trochlear nerve foramen root leave the main body of the endocast. The optic nerve foramen root exits the braincase through a single optic foramen ventromedial to the trochlear nerve foramen root. The oculomotor nerve foramen root is posterior and ventrolateral to the optic nerve foramen root. The lateral surface of the cast of the optic lobe is seen posterior to the oculomotor nerve foramen root, and posteroventral to the cast of the cerebral hemisphere. As seen with the cerebral hemispheres, the optic lobes are much more similar in orientation and development to modern birds than basal theropods, where the optic lobes were positioned dorsomedially and effectively hidden from view (personal observation).

The cast of the pituitary fossa is directly ventral, and slightly anterior, to the optic nerve foramen root. No anterior or lateral borders to the pituitary fossa are preserved, so the anterior and lateral extent of the cast of the pituitary fossa cannot be determined with certainty. The foramina and canals for the abducens nerves are also not discernible in the slices, although they should be present owing to the complete and uncrushed nature of the specimen. The internal carotid canal process enters the ventral portion of the cast of the pituitary fossa from a more posterior position.

One of the more obvious roots exiting the endocast is for the trigeminal nerve foramen. All three of the trigeminal nerve foramen root branches leave the main body of the endocast together. The first to separate is the ophthalmic branch. This branch is seen as a very thin projection that passes anteriorly from the other two branches to exit on the anterior face of the braincase. The forward path of this branch is completely encased in bone, and is clearly seen on both sides of the endocast. The maxillary branch exits laterally from a small foramen dorsal to a larger foramen from which the mandibular branch exits ventrolaterally.

The facial nerve foramen root is located posteroventral to the trigeminal nerve foramen root, and exits the endocast posteroventrolaterally. The facial nerve foramen root is visible on the left side of the endocast, but its path on the right side cannot be followed.

The vestibulocochlear nerve foramen roots enter the inner ear posteroventral to the facial nerve foramen root, and innervate the vestibular and cochlear regions, which are involved in balance and hearing. The direct paths of the various branches are difficult to follow, but the cast of the fenestra ovalis is in the posterior portion of the lateral depression. Also found in this region of the endocast is the cast of the floccular lobe, which exits the endocast in a ventrolateral direction. In this particular specimen, only the right floccular lobe cast is completely represented owing to the presence of some very dense mineral deposits in this area on the left side of the skull. This allows only the base of the cast of the floccular lobe to be shown on this side of the specimen. Also unrepresented in this specimen are the semicircular canals. Just like the abducens

nerve canals and foramina, the semicircular canals are undoubtedly present within the specimen, but owing to their small diameter, lack of density difference from the surrounding bone, and the presence of dense mineral deposits in the area, they are not visible in the CT scan. This means that the habitual orientation of the head cannot be known with certainty because the horizontal semicircular canal, which tells us how the brain, and thus the head, would have been positioned (Witmer et al., 2002, 2003), is not visible.

The foramina of the final cranial nerves are located posteroventral to the lateral depression. In this area three roots are seen, two small median ones, and a larger lateral one. The large lateral one represents the vagus and accessory nerve foramen roots. A small root that exits dorsal to this larger root on the left side may be the glossopharyngeal nerve foramen root. The two smaller median roots are for the hypoglossal nerve foramina.

Byronosaurus jaffei

Byronosaurus jaffei, IGM 100/983, was discovered at Ukhaa Tolgod in 1993 (Norell et al, 2000; Makovicky et al, 2003). The scan consists of a partial braincase that is disassociated from the rest of the skull. The bones that form the roof of the braincase are missing, and this has revealed the eroded remains of a natural endocast.

Because of the incomplete nature of the braincase, most of the anterior portion of the endocast is not present (Figure 32). There are no casts of the

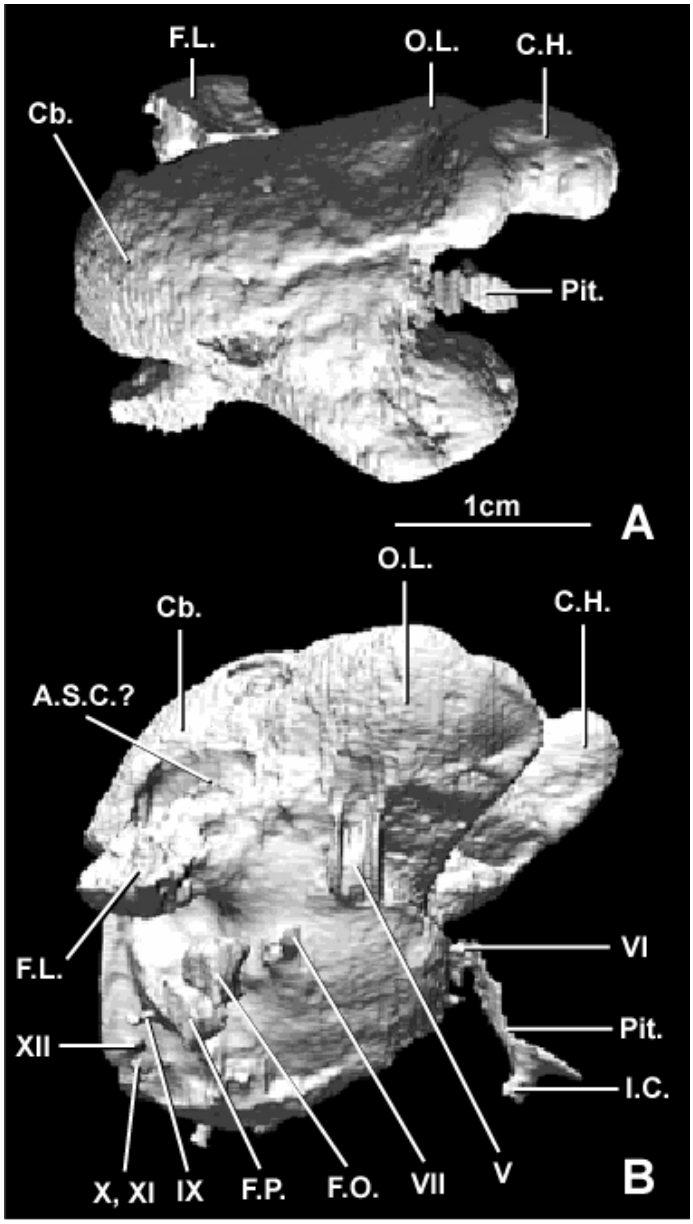

Figure 32. *Byronosaurus jaffei* endocast.

(A) Dorsal, (B) left lateral, and (C) ventral (following page) views of the endocast of *Byronosaurus jaffei*, IGM 100/983. The images have been inverted for comparison purposes with the other figures. Discernible cranial nerves and other features are labeled. See Appendix A for explanation of abbreviations.

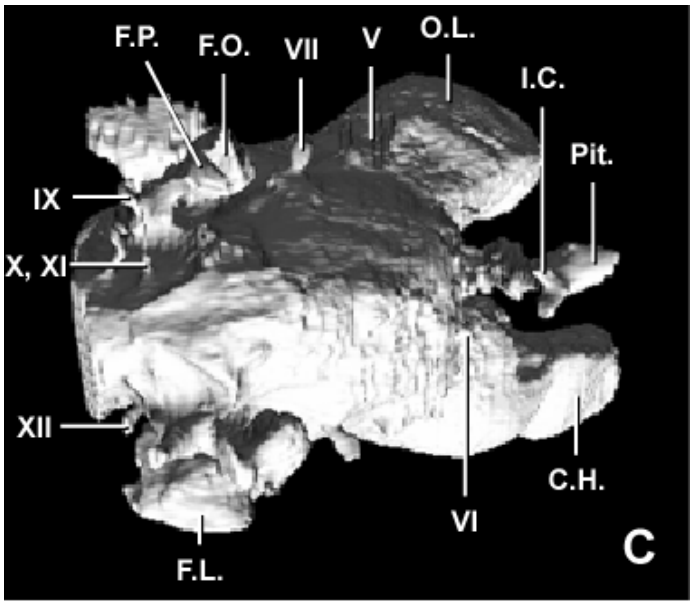

Figure 32 continued.

olfactory bulbs or tracts, and most of the cast of the cerebral hemispheres is missing. Also, the exits for cranial nerves II, III, and IV are missing. The most recognizable structure near the front of the braincase is the pituitary fossa. There are no anterior or lateral borders present, so the size and extent of the cast of the pituitary fossa are uncertain. The internal carotid canal processes are present, and they merge with each other before entering the posteroventral border of the cast of the pituitary fossa. The anterior end of the abducens nerve canal process is lateral to the cast of the pituitary fossa, and this process can be traced posteriorly to its exit from the ventral surface of the endocast. The posterior portion of the trigeminal nerve foramen root is found posterodorsolateral to the abducens nerve canal process. Whether it branched or not before exiting the braincase cannot be determined because of the missing anterior braincase bones. The lateral border of the cast of the optic lobe is dorsal to the trigeminal nerve foramen root. The facial nerve foramen root, which exits the endocast anterolaterally, is posteroventral to the trigeminal nerve foramen root.

Posterior to the facial nerve foramen root is the cast of the fenestra ovalis, followed by the cast of the fenestra pseudorotunda. Although difficult to discern in the transverse slices, it appears that the two branches of the vestibulocochlear nerve foramen root are present, and enter the inner ear. The glossopharyngeal nerve root, which exits the endocast in the cast of the metotic fissure, is posterior to this area. One root representing the location of the vagus and accessory nerve foramen is posteroventral to the glossopharyngeal nerve foramen root, followed

by two roots of the hypoglossal nerve foramina. Just posterior to this the endocast ends abruptly.

The main body of the endocast is composed not only of the open endocranial cavity space, but dorsally there is a partially eroded natural endocast in the specimen. As mentioned previously, this does not include the casts of the olfactory bulbs or tract, and almost the entire cast of the cerebral hemispheres is missing. The lateral borders of the casts of the optic lobes are visible, but owing to the lack of enclosing bones their exact size cannot be ascertained. A prominent cast for the cerebellum is posterior to the casts of the optic lobes. Once again, the exact size of the cerebellum cannot be determined because of the absence of the roofing bones, but it appears to have been large. The endocast in this area is also very deep, suggesting to Makovicky et al. (2003) a large pons and medulla oblongata. Also in this cerebellar region, beneath the dorsal extent of the cast of the cerebellum and above the casts of the deep pons and medulla oblongata, the casts of the floccular lobes are preserved. As has been seen with other portions of the endocast, the lateral walls of these areas are missing, so the exact size and extent of the casts of the optic lobes cannot be determined, but they appear to be rather large, and extend in the standard posteroventrolateral direction. Unfortunately the preservation is such that the semicircular canals cannot be identified with any certainty. There are however, some faint areas in the bones around the floccular lobes that may represent portions of the posterior and horizontal canals, but these are too faint and debatable to include in the endocast. What is in the endocast is a ridge dorsal to the floccular lobes that appears to be

the anterior semicircular canal. However, this ridge was attached to the rest of the endocast, so whether it is actually a canal or just a lateral portion of the cerebellum is unsure.

Zos Canyon troodontid

This troodontid, specimen IGM 100/1005, was also collected from Ukhaa Tolgod, Mongolia in 1997. The scanned portion of the specimen consists of a complete skull encased within a nodule. It is difficult to differentiate between the matrix and bone. Thus, the only thing that could be reconstructed from the scan was the main endocranial cavity itself, no nerve foramen roots or vascular projections could be identified leaving the endocast. Despite the lack of cranial nerve and vascular information, the information provided by the endocranial cavity is considerable because it allows measurements related to volume, length, and width to be made. It also shows the relative position of certain features to each other.

The anterior extent of the endocast (Figure 33) consists of the posterior portion of the cast of the olfactory tract. This cast of the tract had no ventral bones enclosing it, so only the dorsal surface is confidently reconstructed based on the depression in the ventral surface of the frontals. The cast of the olfactory tract merges with the cast of the cerebral hemispheres where it begins to expand laterally, ventrally, and even slightly dorsally. The lateral portions curve ventrally around the posterior margin of the orbit, as in the hemispheres of modern birds.

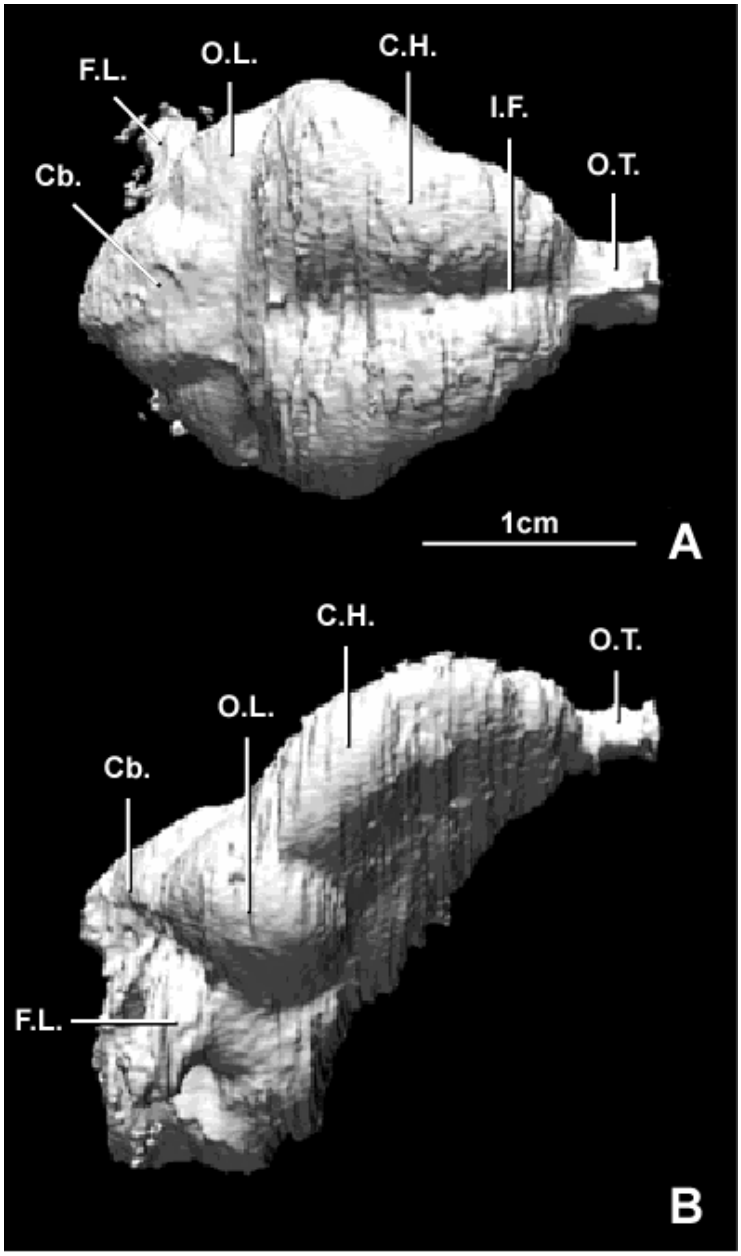

Figure 33. Zos Canyon troodontid endocast.

(A) Dorsal, (B) right lateral, and (C) ventral (following page) views of the endocast of Zos Canyon troodontid, IGM 100/1005. Discernible cranial nerves and other features are labeled. See Appendix A for explanation of abbreviations.

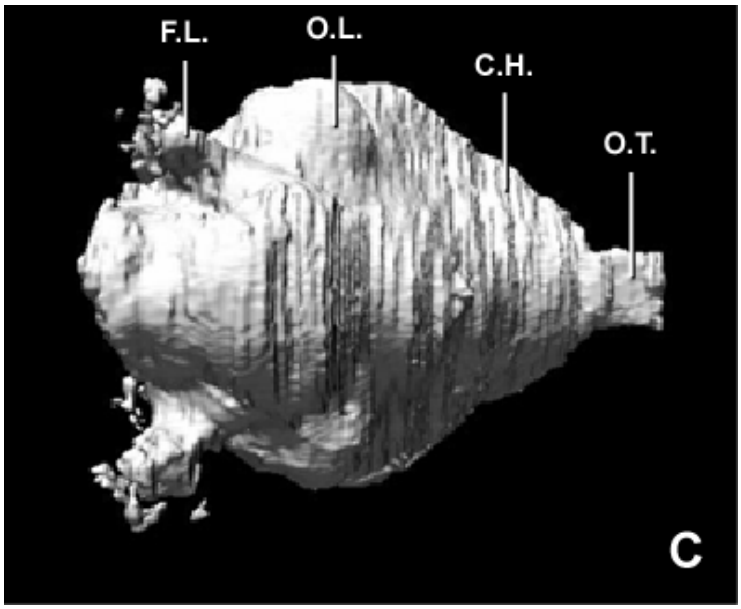

Figure 33 continued.

Dorsally, the depression representing the interhemispherical fissure is clearly visible. The casts of the optic lobes are clearly visible behind the posteroventrolateral portion of the cast of the cerebral hemispheres. The casts of these optic lobes are in the ventrolateral position found in birds, and completely visible. This is a change from the basal theropods and crocodilians in which the optic lobes are dorsomedial and difficult to see, if they can be seen at all. Medial to the cast of the optic lobes, the cast of the cerebellum contacts the posterior edge of the cast of the cerebral hemispheres. Another portion of the cast of the cerebellum, the casts of the floccular lobes, is visible posteroventral to the casts of the optic lobes. The casts of the floccular lobes extend in a posteroventrolateral direction, and would have terminated within an area whose boundaries are formed by the semicircular canals. Unfortunately the canals could not be traced, although some of the pneumaticity in that area may represent portions of the canals. Just posterior to this area is the end of the endocast.

Aves

The definition I use for Aves was proposed by Gauthier (1986). Aves are "all descendants of the most recent common ancestor of Ratitae, Tinami, and Neognathae" (Gauthier, 1986:14).

The phylogenetic picture becomes very muddled when we move into extant birds. There is a central division into neognaths and paleognaths that is not disputed. Examining neognaths can be intimidating however, because the most common cladogram shows a large unresolved polytomy for almost all neognaths.

This polytomy is slowly being resolved, and most cladograms show the Anseriformes and Galliformes being the first to branch off, together forming an outgroup to the rest of the neognaths (Cracraft, 1988; van Tuinen et al., 2000). Because this clade is thought to be the most basal within Neognathae, I used the Northern Screamer, *Chauna chavaria*, a member of the Anseriformes, as the extant representative of theropods.

Neognathae

The definition I use for Neognathae was proposed by Cracraft (1986). Neognathae are *Chauna* and all Aves (Neornithes in Cracraft) that are more closely related to *Chauna* than they are to Paleognathae.

Chauna chavaria

In modern birds, the brain fills the entire endocranial cavity, and the endocast accurately represents the size and shape of the brain itself. The endocasts are also complete and undistorted because the specimens are extant, and the skulls are not subjected to burial and fossilization.

The first extant bird I studied was *Chauna chavaria* (KU 81969). Beginning at the anterior end of the endocast (Figure 34), the first structures encountered are the casts of the olfactory filaments. They leave the casts of the olfactory bulbs anteriorly, and continue until the canals in which they were housed began to open into the larger spaces of the nasal cavity. Unlike some non-

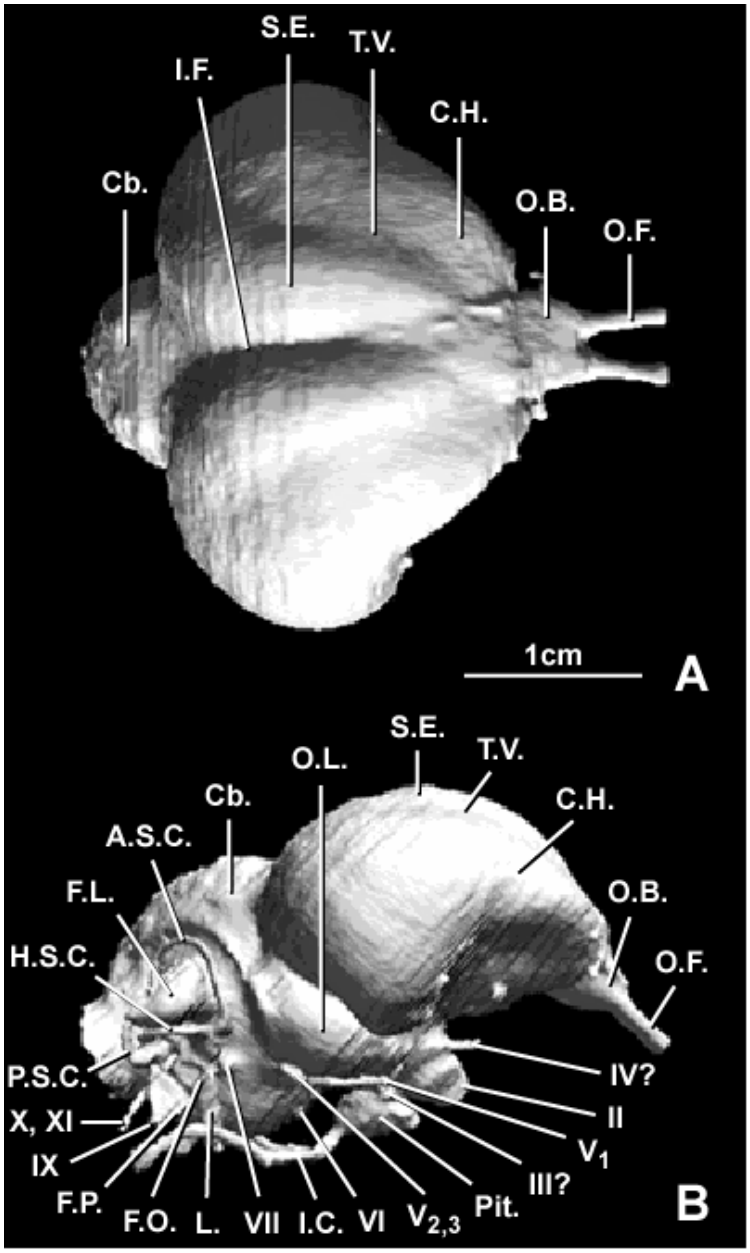

Figure 34. *Chauna chavaria* endocast.

(A) Dorsal, (B) right lateral, and (C) ventral (following page) views of the endocast of *Chauna chavaria*, KU 81969. Discernible cranial nerves and other features are labeled. See Appendix A for explanation of abbreviations.

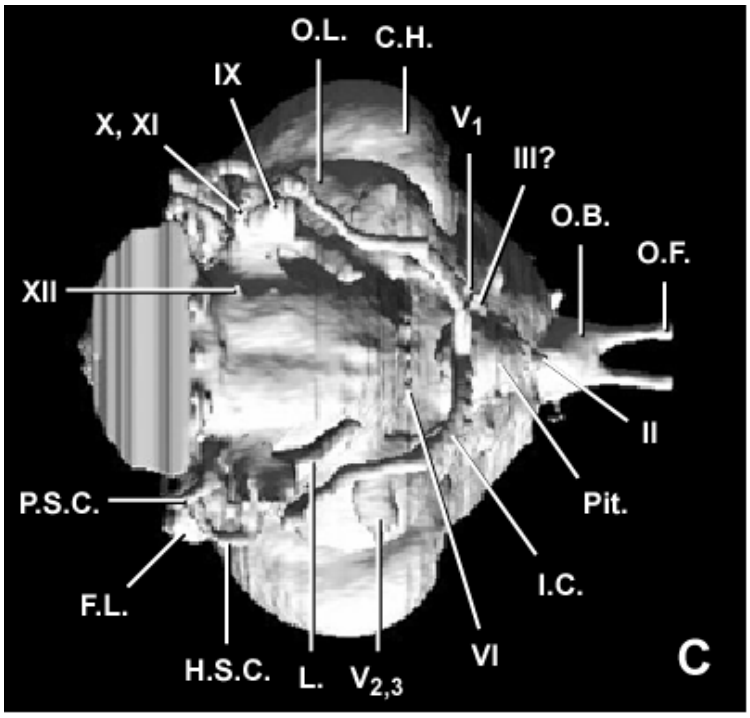

Figure 34 continued.

avian theropod dinosaurs, no cast for the olfactory tract is found between the casts of the olfactory bulbs and the cerebral hemispheres, because the casts of the olfactory bulbs are directly anterior to the cast of the cerebral hemispheres, and are actually appressed against the anterior end of the cast of cerebral hemispheres.

The cast of the cerebral hemispheres expands posteriorly and laterally from its anterior contact with the casts of the olfactory bulbs. As was the case in *Mongolodon*, the eye and bones forming the posterior wall of the orbit confine the expansion to a postorbital position. Several features of the cerebral hemispheres that were not visible in the taxa discussed earlier can now be described. First are the casts of the telencephalic vallecula, and the sagittal eminence (Baumel et al., 1993). Most modern taxa possess these features, although they are not visible in the endocast of *Apteryx* (personal observation). Another feature that is visible is the depression representing the interhemispherical fissure (Baumel et al., 1993), which can also be seen in *Mongolodon*, *Citipati*, and the Zos Canyon troodontid. The fact that this feature is not visible in earlier taxa such as *Acrocanthosaurus* suggests that the cerebral hemispheres did not completely fill the endocranial cavity. The reason for this suggestion is that in taxa where the brain completely fills the endocranial cavity, the interhemispherical fissure is visible, along with the dorsal sagittal sinus and occipital sinus, which are confined to narrow channels in the interhemispherical fissure owing to the expansion of the cerebral hemispheres. In earlier taxa, however, the dorsal sagittal sinus and occipital sinus obscure the entire dorsal surface of the brain, suggesting that there is no pressure applied to confine them into small channels, meaning that the brain did not

completely fill the endocranial cavity. As was seen in the endocasts of *Citipati* and *Mongolodon*, part of the reason for the large size of the cerebral hemispheres in birds is the expansion of the DVR. By the time the modern avian brain is achieved, the sensory regions expanded from one of each, as is seen in crocodilians, to three auditory, two visual, and two somatosensory, each being important to an animal that depends heavily on these senses for its survival (Ulinski, 1983).

The trochlear nerve foramen root is ventral to the cast of the cerebral hemispheres, and passes anterolaterally. The optic nerve foramen roots are directly ventral to the trochlear nerve foramen root, and both exit through a single foramen before separating to go to their respective eyes. The oculomotor nerve foramen root is posteroventral to the optic nerve foramen root, and exits the main body of the endocast just lateral to the cast of the pituitary fossa.

The cast of the pituitary fossa is located ventral to the optic nerve foramen root. The anterior wall of the pituitary fossa in completely ossified, so the exact shape and size of the cavity can be determined. This is contrary to what I saw in most of the non-avian theropods I examined, in which the anterior border of the pituitary fossa was either unossified or lost so that the anterior extent of this cavity could not be accurately determined. The internal carotid canal processes enter the cast of the pituitary fossa on its posteroventral borders. Followed posteriorly, these artery canal processes continue ventrolateral to the endocast to eventually exit the braincase beneath the otic region.

The abducens nerve canal process is also just lateral to the cast of the pituitary fossa. Extending posteriorly through the canal, the abducens nerve process enters the ventral border of the main body of the endocast.

The ophthalmic branch of the trigeminal nerve foramen root is located dorsolateral to the anterior end of the abducens nerve canal process, and travels posterolaterally in its canal until meeting up with the rest of the trigeminal nerve foramen root. The other two branches of this nerve foramen root, the maxillary and mandibular, exit the endocast together laterally.

The casts of the optic lobes are located dorsal to the trigeminal nerve foramen root. The casts of these lobes are well defined in the endocast, only their medial border obscured in the main body of the endocast. They are less well defined further down the theropod lineage. In *Mongolodon*, they are slightly less well defined, and in *Acrocanthosaurus* it is difficult to identify them at all. In the extant taxa they are also pushed further ventrally and laterally to accommodate the expansion of the cerebral hemispheres and cerebellum.

The facial nerve foramen root is posterior and slightly ventral to the trigeminal nerve foramen root. It exits through a narrow canal, and does not split into its primary branches, the palatine and hyomandibular, until it exits the braincase.

The casts of the fenestra ovalis and fenestra pseudorotunda are immediately posterior to the facial nerve foramen root. Also discernible in the transverse CT slices are the cochlear and vestibular branches of the vestibulocochlear nerve foramen root. Because the specimen is extant and was

prepared in a laboratory, all of the delicate bones and structures within the ear are still intact as well. This allows the casts of the lagena, utriculus, and other structures within the inner ear to be recognized for the first time. Often these structures are destroyed or lost in the fossilization process. The semicircular canal system is also intact, and its entire course can be traced. The anterior semicircular canal arches posterodorsomedially before turning ventrally just before meeting the posterior semicircular canal. The posterior semicircular canal arches mainly ventrolaterally, and slightly posteriorly, before looping around to arch anterodorsomedially. The horizontal semicircular canal first arches posterolaterally from just posterolateral to the anterior semicircular canal, and then arches posteromedially before meeting the posterior end of the posterior semicircular canal. The arrangement is typical of that in modern birds (Baumel et al., 1993). It differs from that seen in basal theropods however, in which the semicircular canal system had a subtriangular appearance when viewed laterally. This is also found in the extant crocodilian *Crocodylus moreleti*. Both the *Acrocanthosaurus* braincase and the *Chauna chavaria* specimen were originally scanned in an orientation such that the olfactory filaments are horizontal. The semicircular canals, with the endocast in this orientation, are not correctly aligned, meaning that the endocast is not oriented in the same way that the bird would habitually hold its head, with the horizontal semicircular canal horizontal, or slightly elevated in front (Witmer et al., 2002, 2003). In order to achieve this horizontal posture, the endocast must be rotated rostrally approximately 38°. The cast of the floccular lobe protrudes from the endocast posterolaterally beneath the

arch of the anterior semicircular canal, and terminates at the lateral extent of the horizontal semicircular canal; it is situated just dorsal to the horizontal semicircular canal and anterior to the posterior semicircular canal.

The glossopharyngeal nerve foramen root extends ventral to the inner ear region. This is followed by the vagus nerve foramen root posteriorly. The accessory nerve root is transmitted with the vagus nerve foramen root. The two roots of the hypoglossal nerve foramina are medial to the vagus nerve foramen root. The endocast ends just posterior to this, where the medulla oblongata would exit the braincase through the foramen magnum and continue on as the spinal cord.

Anas platyrhynchos

Even though *Chauna chavaria* was chosen to be described in depth as the extant representative of Theropoda, there is a wide range of variation present within Recent avian brains that cannot be ignored (Pearson, 1972; personal observation). This variation is obvious even in the other extant birds I examined, *Anas platyrhynchos, Apteryx sp., Crypturellus cinnamomeus,* and *Dinornis giganteus*, which went extinct about 2000 years ago (Fenton and Fenton, 1958).

A skull of *Anas platyrhynchos* is the only other neognath that I examined. The specimen is an unnumbered TMM specimen, and consisted of a frozen head, with all flesh, feathers, and organs intact. In most ways, the endocast of this specimen (Figure 35) and that of the *Chauna chavaria* are similar. However, in

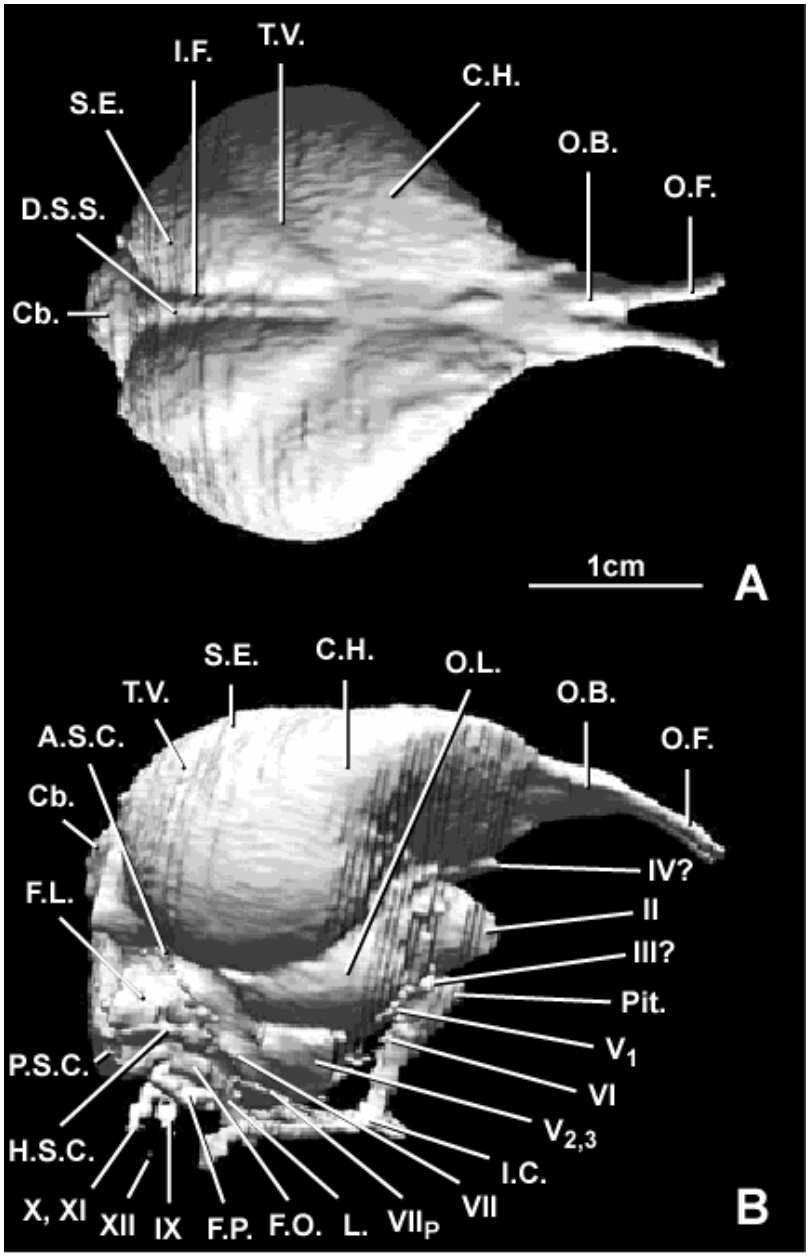

Figure 35. *Anas platyrhynchos* endocast.

(A) Dorsal, (B) right lateral, and (C) ventral (following page) views of the endocast of *Anas platyrhynchos*, unnumbered TMM specimen. Discernible cranial nerves and other features are labeled. See Appendix A for explanation of abbreviations.

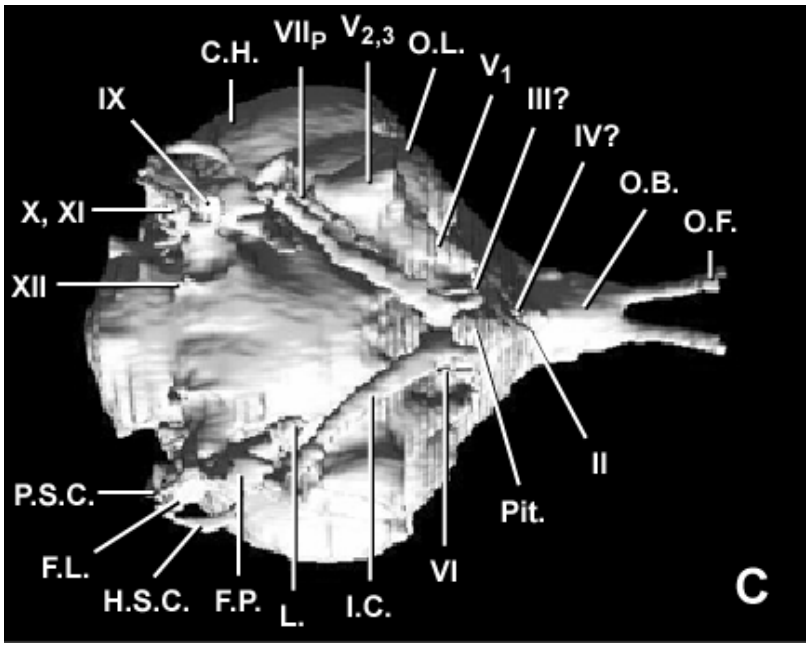

Figure 35 continued.

the *Anas* endocast, the palatine branch of the facial nerve foramen root can be traced forward, whereas this branch of the facial nerve foramen root cannot be seen in the *Chauna* endocast. Another difference is the orientation of the endocast. Both specimens were scanned such that the casts of the olfactory filaments were in a fairly horizontal position. With this being the case, the screamer had to be rotated approximately 38° anteriorly in order to bring its horizontal canal into a horizontal orientation. To bring this canal into a horizontal position in the duck, the specimen only had to be rotated about 10°. Other than these two differences, the endocasts of the *Chauna* and *Anas* are almost the same.

Paleognathae

The definition I use for Paleognathae was proposed by Cracraft (1986). Paleognathae are *Crypturellus* and all Aves (Neornithes in Cracraft) that are more closely related to *Crypturellus* than to Neognathae.

Ratitae

The definition I use for Ratitae was also proposed by Cracraft (1986). Ratitae are *Apteryx* and all Paleognathae that are more closely related to *Apteryx* than to Tinamidae.

Apteryx sp.

I examined several paleognath skulls, and most of them vary from *C. chavaria* in fundamental ways. One of the taxa that exemplifies this is *Apteryx* (AMNH 18456). The kiwi is a flightless bird that is naturally found only in New Zealand. One feature of the endocast (Figure 36) that differs from *C. chavaria* is the size of the casts of the floccular lobes. The casts of the floccular lobes in the kiwi are smaller than those seen in *C. chavaria*. Because these lobes are thought to be important for orientation and balance in regards to the demands of flight, this decrease in size may not seem too abnormal for a flightless animal. The most obvious difference in the kiwi however is the enormous size of its cerebral hemisphere casts. These hemisphere casts completely dominate the lateral and dorsal views of the endocast. Posteriorly they meet the cast of the cerebellum, so the casts of the optic lobes are ventrolaterally located as in all extant birds, but the casts of the cerebral hemispheres are so large that no indications of the optic lobes are found in the endocast. The casts of the olfactory bulbs are appressed against the anterior edge of the cerebral hemispheres, and they are larger than those found in many other avian taxa, suggesting a larger reliance on smell than most other birds (Bang and Cobb, 1968).

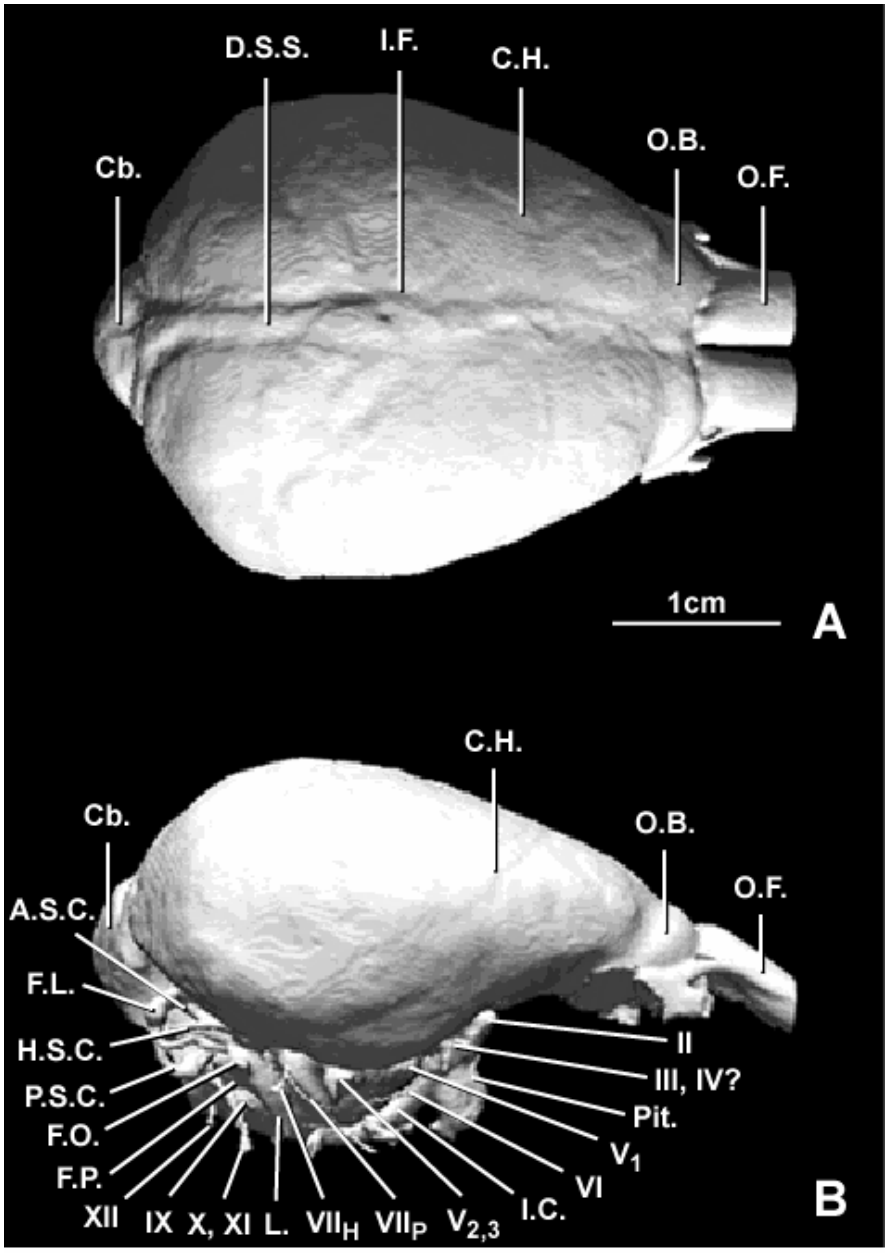

Figure 36. *Apteryx sp.* endocast.

(A) Dorsal, (B) right lateral, and (C) ventral (following page) views of the endocast of *Apteryx sp.*, ANMH 18456. Discernible cranial nerves and other features are labeled. See Appendix A for explanation of abbreviations.

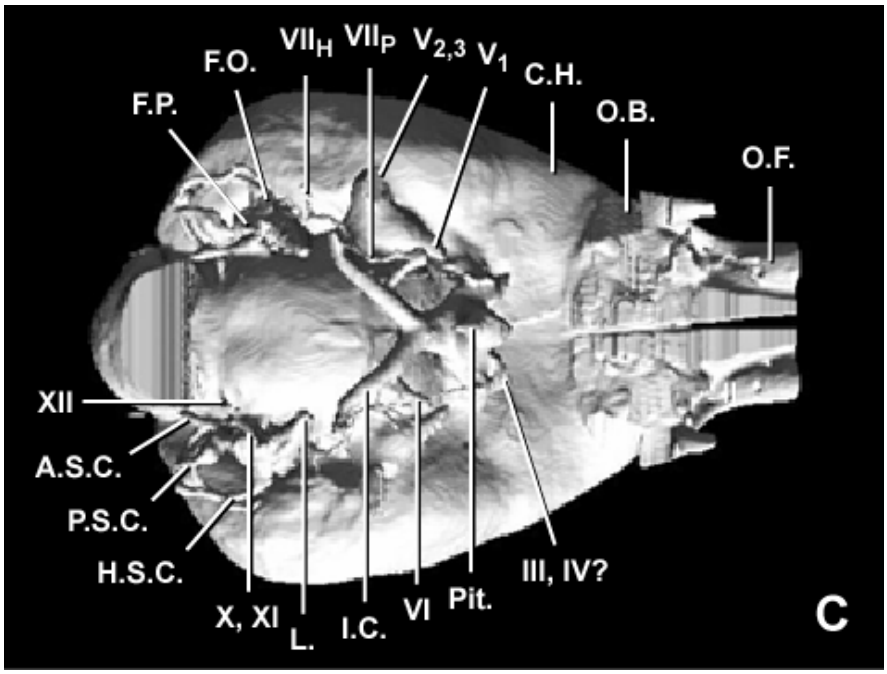

Figure 36 continued.

Dinornis giganteus

One recently extinct clade of birds that is related to the kiwi is *Dinornis*. The moas were also flightless birds that inhabited New Zealand, ranging in size from that of a turkey to more than 3.3 m (10 feet) in height. These birds were hunted to extinction by the ancestors of the Maoris, but because this happened less than 2000 years ago, there are many well-preserved specimens that can be studied (Fenton and Fenton, 1958). My examination of a moa endocast (Figure 37), taken from AMNH FR1000001, revealed several differences from the *C. chavaria* endocast. First, the moa completely lacks any osseous evidence of floccular lobes. I would expect the lobes to be smaller than in *C. chavaria*, similar to the decrease seen in the kiwi because the moa was also flightless, but the complete lack of any fossae is unique among the avian taxa I studied. Also, as with the kiwi, the optic lobes did not leave any impressions on the braincase and cannot be identified in the endocast. The cast of the cerebellum does meet the posterior end of the cast of the cerebral hemispheres, however, so the position of optic lobes is ventrolateral. Another feature that deserves mention is the huge size of the cast of the sagittal eminence. This feature is present in *C. chavaria*, but it is not as prominent as it is in the moa.

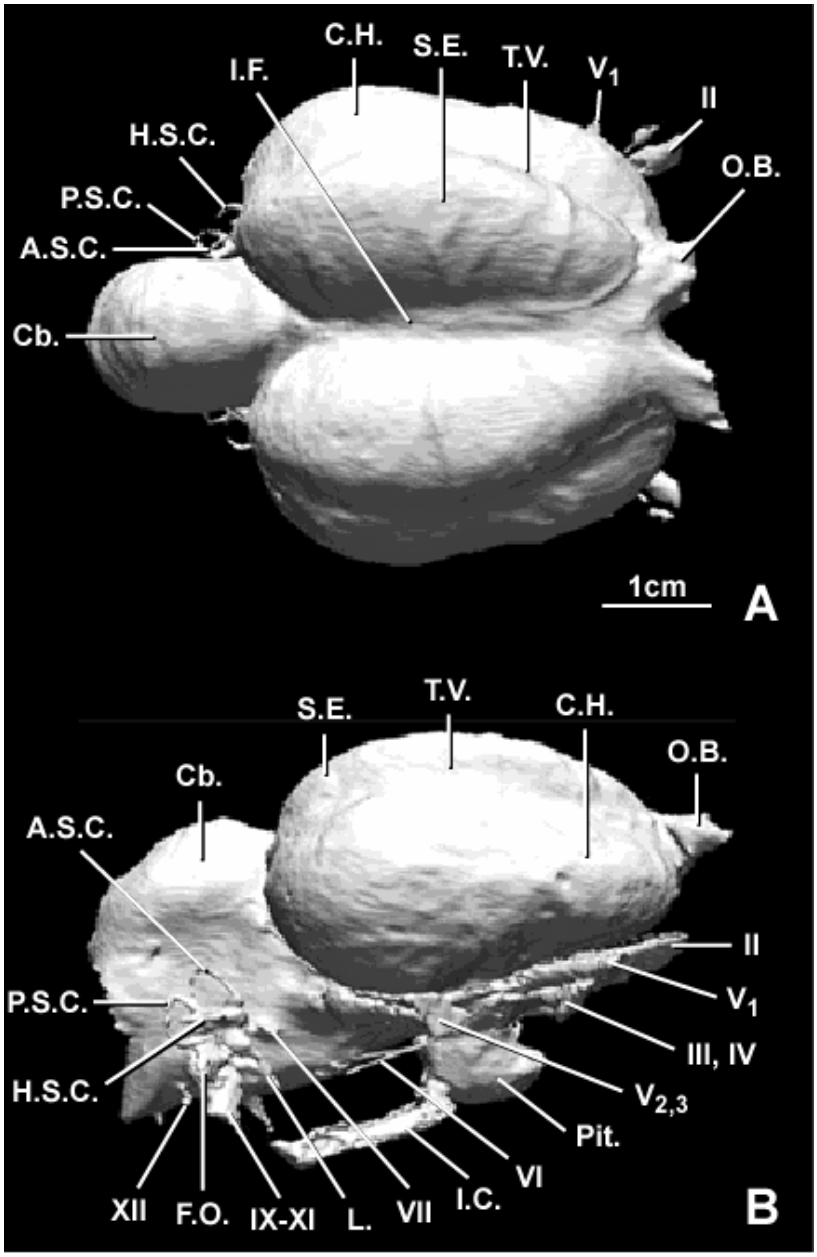

Figure 37. *Dinornis giganteus* endocast.

(A) Dorsal, (B) right lateral, and (C) ventral (following page) views of the endocast of *Dinornis giganteus*, AMNH FR1000001. Discernible cranial nerves and other features are labeled. See Appendix A for explanation of abbreviations.

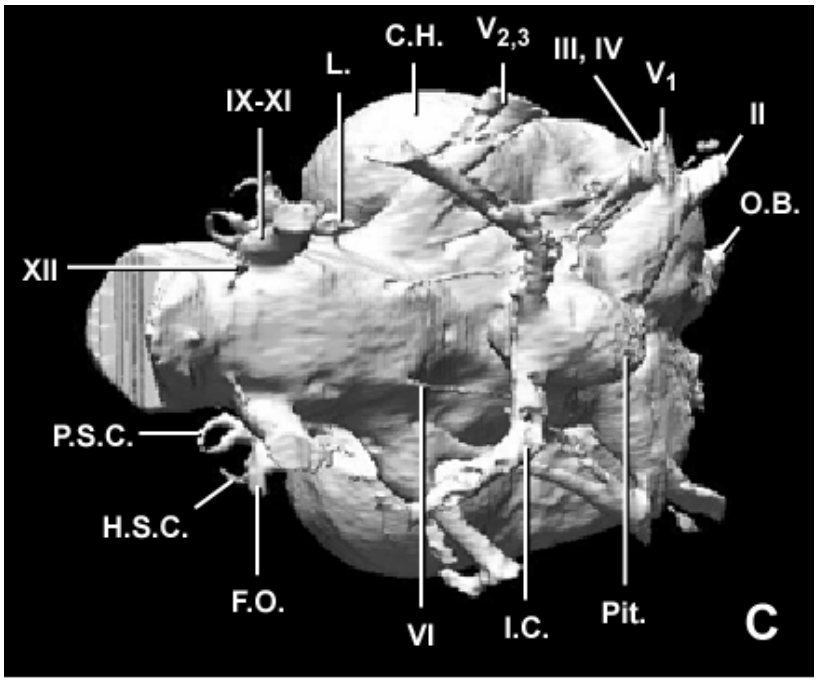

Figure 37 continued.

Tinamidae

Crypturellus cinnamomeus

Within paleognaths but outside Ratitae, another bird that shows some significant differences from *C. chavaria* is the tinamou, *Crypturellus cinnamomeus* (KU 34658). Tinamous are small birds found in Central and South America. Although they are capable of flight, it is very short in duration and erratic, and they prefer to walk or run (Parkes, 1995). The first major difference in its endocast (Figure 38) compared to that of *C. chavaria* is lack of large floccular lobe casts. There is a small bulge in the appropriate area, but it is not very big, and it does not become a flange-like structure typical of the floccular lobe casts in other birds. Also in this region, the semicircular canals have a broad area of curvature (see canals in figure 38). Although the size of these canals varies from taxon to taxon, no other bird I examined has anything even remotely similar in extent to what I found in the tinamou. It may be this combination of small floccular lobes and oversized semicircular canals that make it a very erratic flyer. One difference from the other paleognaths I examined is the recognition of the cast of the optic lobes. Not only can the optic lobes be identified on the endocast, they are enormous. No other bird in my study has optic lobe casts even approaching the relative size of those seen in the tinamou. These enormous optic lobe casts suggest that eyesight is very important to the tinamou, and probably their dominant sense. The casts of the optic lobes are still in the

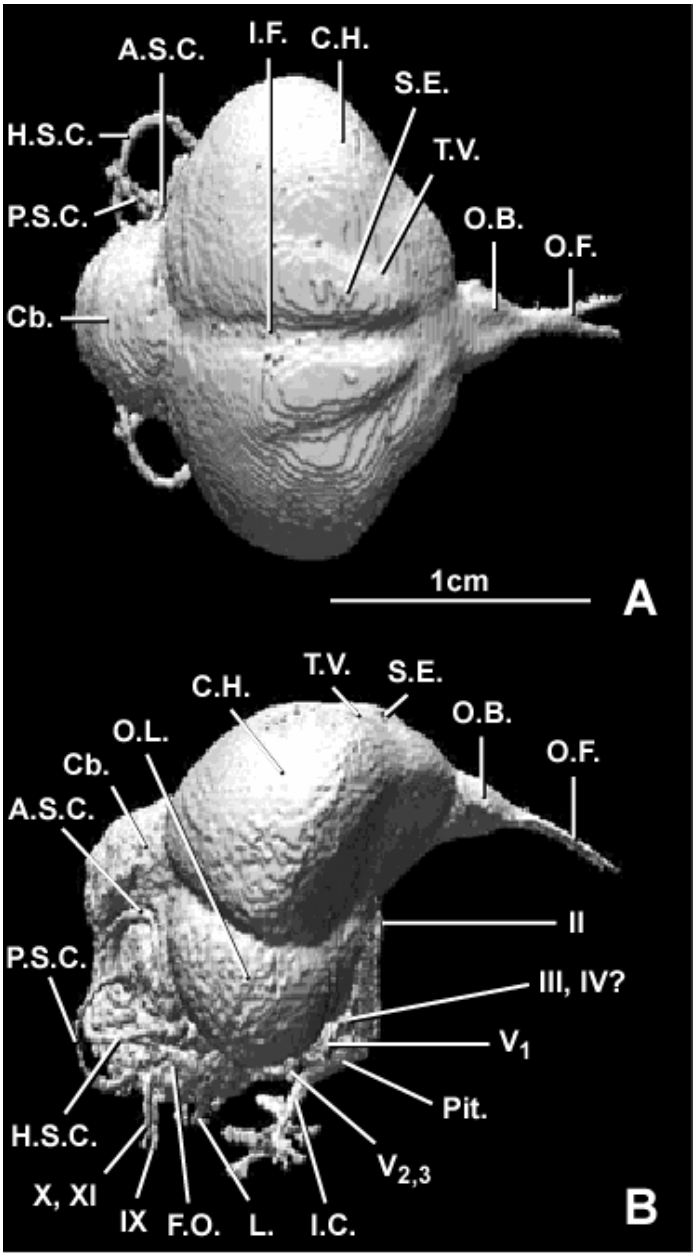

Figure 38. *Crypturellus cinnamomeus* endocast.

(A) Dorsal, (B) right lateral, and (C) ventral (following page) views of the endocast of *Crypturellus cinnamomeus*, KU 34658. Discernible cranial nerves and other features are labeled. See Appendix A for explanation of abbreviations.

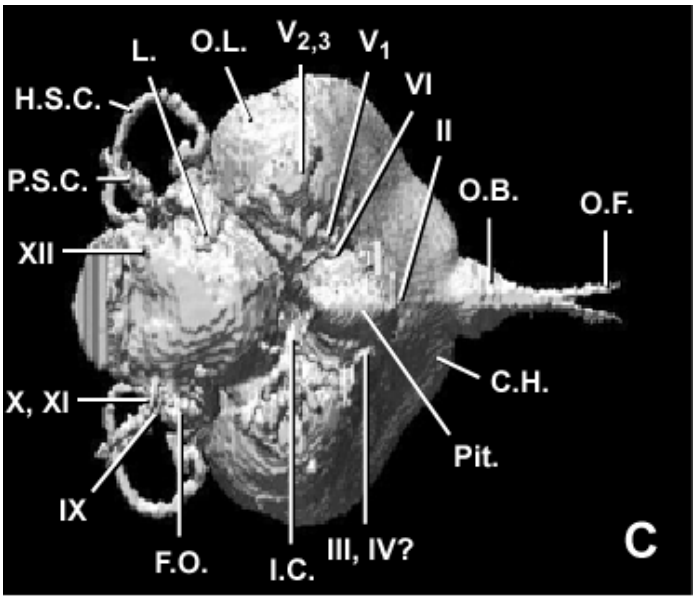

Figure 38 continued.

ventrolateral position found in all birds, as the cast of the cerebellum touches the posterior edge of the cast of the cerebral hemispheres.

Chapter 3: Character Analyses

INTRODUCTION

After describing the digital endocasts, I used them and their accompanying braincases as a source of characters for phylogenetic analyses. Only phylogenetically informative characters were considered.

The taxa that I analyzed consisted mainly of those theropod taxa that were described in chapter two. There were, however, several endocasts not described in chapter two that I used. Those endocasts were: (1) *Carcharodontosaurus saharicus* (Sereno et al., 1996; Larsson et al., 2000; Larsson, 2001); (2) *Tyrannosaurus rex* (Osborn, 1912; Brochu, 2000; 2003); and (3) *Archaeopteryx lithographica* (Domínguez-Alonso et al., in review). These endocasts were chosen for use in the analyses because they are figured in other sources, and therefore available for character determinations. These taxa also helped to fill some of the areas on the tree that are not well represented by the taxa I had access to.

I used the characters I found to construct a data matrix, which I analyzed using PAUP 4.0b10(Altivec) (Swofford, 1993). I optimized the acquired trees using DELTRAN and ACCTRAN in MacClade 4.04PPC (Maddison and Maddison, 1992). After this initial analysis, I added the characters to three recently published data matrices used for resolving theropod systematics: (1) Holtz (1998); (2) Rauhut (2003); and (3) Sereno (1999). After incorporating the characters into these data matrices, I reran the analyses in PAUP, and analyzed them in MacClade, to determine the impact, if any, of endocast characters on the

original tree topologies. My examination of the trees in MacClade also provided insight on the distribution of the new characters after inclusion into a larger phylogenetic analysis.

CHARACTERS

1.) Median septum of the sphenethmoid dividing the sphenethmoidal fossa: present (0), absent (1).

2.) Olfactory bulb position: anterior to cerebral hemispheres and olfactory tract (0), appressed against anterior border of the cerebral hemispheres (1).

3.) Cerebral hemispheres: slight oval expansion visible (0), broad ventrolateral expansion against the posterior orbital wall (1).

4.) Cerebral hemispheres: occupy less than 35% of the total volume of the endocranial cavity (0), occupy more than 35% of the total volume of the endocranial cavity (1) (Modified from Larsson et al., 2000).

5.) Maximum width of the endocast: less than 45% of the length of the endocast (0), greater than 45% of the length of the endocast (1) (Modified from Wharton, 2002).

6.) Optic lobe: positioned dorsomedially (not visible in endocast) (0), visible and lying in a ventrolateral position (1) (Wharton, 2002).

7.) Number of trigeminal nerve foramina: 1 (0), 2 to 3 (1) (Wharton, 2002).

8.) Abducens nerve canal: enters pituitary fossa (0), passes lateral to the pituitary fossa (1).

9.) Internal carotid canals: separate canals entering the pituitary fossa (0), confluent canals entering the pituitary fossa (1) (Holtz, 1998).

10.) Floccular fossa (cerebellar auricular fossa): absent or very small (0), present and very noticeable (1).

11.) Shape of the floccular lobe: narrow and knifeblade-like (0), thicker and bulbous (1).

12.) Posterior semicircular canal orientation: mostly lies in a parasagittal plane with a slight lateral component (0), mostly lies in a transverse plane with a slight posterior component (1).

13.) Number of hypoglossal nerve foramina: 1 (0), 2 to 3 (1).

14.) Reptile Encephalization Quotient: less than 6 (0), greater than 6 (1) (Modified from Wharton, 2002).

CHARACTER POLARITY

I determined the polarity of the characters listed above by looking at the character states in a series of outgroups, those states found being considered primitive and scored as 0. The outgroups I used were those for which I made endocasts, or those that had endocasts available for them in the literature. The two outgroups that I examined for all the characters were *Plateosaurus engelhardti* and *Saurosuchus galilei*. I used *Plateosaurus* because it is a basal member of Sauropodomorpha, which is the closest outgroup to Theropoda. Although I did not create a digital endocast for this taxon, Galton described and figured an endocast in a 1985 article. *Saurosuchus*, for which I did create a digital endocast,

was used because it is a basal member of the lineage that includes crocodiles, a group that helps to form the Extant Phylogenetic Bracket around non-avian theropods (Witmer, 1995). If there were characters that could not be scored in either of these outgroups, other taxa, such as *Diplodocus hayi* and *Crocodylus moreleti*, other members of the lineages including the two main outgroup taxa, were employed. These taxa were only employed when necessary, because they are more derived members of their lineages, making them more removed from the ancestral condition.

The pterosaurs that I described in this study, *Rhamphorhynchus muensteri* and *Anhanguera santanae*, were not used in the outgroup comparisons because they are specialized for flight, and one area in which these specializations are found is the brain. This means they are far removed from the ancestral archosaur condition, and will only be used for comparisons with avian endocasts when I discuss flight in chapter 4.

DISCUSSION OF CHARACTERS

Character 1- Sphenethmoidal septum dividing the sphenethmoidal fossa.

This character was difficult to study, because it requires the walls of the sphenethmoidal fossa to be completely ossified and preserved, something that was not seen in several taxa because of incomplete ossification or loss during the fossilization process. In those taxa that preserve this fossa, there are two character states. Some taxa have a median sphenethmoidal septum in the anterior portion of the fossa. This septum divides the olfactory bulbs. In other taxa with a fossa, the

septum is absent. *Saurosuchus* does not preserve this character, and neither do *Plateosaurus* or *Diplodocus*, so I examined the modern crocodile. In *Crocodylus moreleti* the sphenethmoidal fossa is partially preserved, but the portion that would preserve the septum is not present, so the polarity cannot be determined based on these outgroups. Another taxon has an endocast that hints at the presence of this septum. Within pachycephalosaurs, the olfactory bulbs are often well separated, and *Gravitholus* has a deep groove separating the bulbs (Giffin, 1989). This separation by a deep groove suggests the presence of a median septum in the skull. Because ornithischians are the sister group to saurischians, I used the presence of a median septum as the primitive state. This decision was later confirmed based on its presence in basal theropods, and absence in more derived theropods.

The members of the ingroup that show the primitive state are *Acrocanthosaurus atokensis, Carcharodontosaurus saharicus, Ceratosaurus magnicornis, Majungatholus atopus,* and *Tyrannosaurus rex*. The only member of the ingroup to show the derived state is *Citipati osmolskae*. The character state could not be determined in *Allosaurus fragilis, Archaeopteryx lithographica, Byronosaurus jaffei, Mongolodon junior,* and the Zos Canyon troodontid. Some taxa do not contain an ethmoidal fossa, so the character state could not be scored. The taxa that do not have the character are *Anas platyrhynchos, Apteryx sp., Chauna chavaria, Crypturellus cinnamomeus,* and *Dinornis giganteus*. Although only one taxon is positive for the derived character state, I kept the character in the analyses because there are several taxa in which the character state is

uncertain, and the addition of better fossils may help to clarify the character state in those taxa. I therefore did not want to discard this character.

Character 2- Olfactory bulb position.

The olfactory bulbs are either attached to the cerebral hemispheres by way of a visible olfactory tract, or appressed against the anterior edge of the cerebral hemispheres, thereby obscuring the olfactory tract. The outgroups exhibit the former condition, making that the primitive character state.

The ingroup taxa showing the primitive state are *Acrocanthosaurus atokensis, Allosaurus fragilis, Archaeopteryx lithographica, Carcharodontosaurus saharicus, Ceratosaurus magnicornis, Citipati osmolskae, Majungatholus atopus, Mongolodon junior, Tyrannosaurus rex,* and the Zos Canyon troodontid. The ingroup taxa showing the derived character state are *Anas platyrhynchos, Apteryx sp., Chauna chavaria, Crypturellus cinnamomeus,* and *Dinornis giganteus*. In one taxon, *Byronosaurus jaffei*, the character state could not be determined.

Character 3- Cerebral hemisphere shape.

The cast of the cerebral hemispheres can be seen to varying degrees in the endocasts of archosaurian taxa. In some taxa, the cerebral hemispheres are only slightly visible, and have an oval appearance in lateral view. In other taxa, the cerebral hemispheres are clearly visible, and exhibit a broad ventrolateral expansion, giving a very distinctive shape caused in part by the presence of the posterior orbital wall.

The outgroups for this study exhibit the slightly visible, oval-shaped cerebral hemispheres, making this the primitive character state. The ingroup taxa showing this state are *Acrocanthosaurus atokensis, Allosaurus fragilis, Carcharodontosaurus saharicus, Ceratosaurus magnicornis, Majungatholus atopus,* and *Tyrannosaurus rex*. The clearly visible, broad, ventrolaterally expanded cerebral hemispheres are the derived character state. The ingroup taxa showing this state are *Anas platyrhynchos, Apteryx sp., Archaeopteryx lithographica, Chauna chavaria, Citipati osmolskae, Crypturellus cinnamomeus, Dinornis giganteus, Mongolodon junior,* and the Zos Canyon troodontid. Once again, the character state could not be determined in *Byronosaurus jaffei*.

Character 4- Volume of the cerebral hemispheres.

The amount of the total endocast volume occupied by the cerebral hemispheres varies widely among the taxa I studied. I estimated the volume of the cerebral hemispheres by measuring the maximum length, width, and height of one cerebral hemisphere in the endocast, and using that to calculate the volume of two ellipses, one for each hemisphere (Larsson et al., 2000). I then divided this volume by the entire endocast volume, which includes the olfactory bulbs and tracts. The volumes of the cerebral hemispheres measured can be divided into two groups, those whose volume is less than 35% of the total endocast volume, and those whose volume is more than 35% of the total endocast volume. This percentage is modified slightly from that suggested in Larsson et al. (2000). Although he did not use this as a strict binomial character, Larsson et al. (2000) suggested that a notable change occurs around a cerebral hemisphere volume that

is 30% of the total endocast volume. When calculating this percentage in my taxa, several came out with values right at 30%, but there was a distinct gap between 30% and 39%, so a midpoint value of 35% was used. The outgroups have cerebral hemisphere volumes that are less than 35% of the total endocast volume, which is considered the primitive character state. Any taxa with a cerebral hemisphere volume that is greater than 35% of the total endocast volume show the derived character state.

The ingroup taxa showing the primitive state are (calculated values given parenthetically) *Acrocanthosaurus atokensis* (29%), *Allosaurus fragilis* (25%), *Carcharodontosaurus saharicus* (24%), *Ceratosaurus magnicornis* (30%), *Majungatholus atopus* (30%), and *Tyrannosaurus rex* (26%). The ingroup taxa showing the derived state are *Anas platyrhynchos* (73%), *Apteryx sp.* (86%), *Archaeopteryx lithographica* (44%), *Chauna chavaria* (80%), *Citipati osmolskae* (39%), *Crypturellus cinnamomeus* (65%), *Dinornis giganteus* (74%), *Mongolodon junior* (50%), and the Zos Canyon troodontid (50%). The character state could not be determined in *Byronosaurus jaffei*.

Character 5- Width of the endocast.

This character was also determined using measurements from the endocasts. The maximum width of the endocast is usually found across the cerebral hemispheres, and the length of the endocast is taken from the front of the olfactory bulbs to the back of the endocast, which is where the medulla oblongata leaves the foramen magnum. The taxa were separated into two groups: those with endocast widths less than 45% the length of the endocast, and those with endocast

widths greater than 45% the length of the endocast. This percentage was used rather than 30%, which Wharton used (2002). For the same reason as the previous character; 30% was a little low, and there is a nice gap between the taxa with values below 35% and taxa with values above 52%, so a midpoint value of 45% was chosen. The outgroups have an endocast width that is less than 45% of the endocast length. Thus, a narrow endocast is considered the primitive character state, and those with an endocast width greater than 45% the length of the endocast exhibit the derived character state.

The ingroup taxa that exhibit the primitive character state are *Acrocanthosaurus atokensis* (29%), *Allosaurus fragilis* (19%), *Carcharodontosaurus saharicus* (19%), *Ceratosaurus magnicornis* (25%), *Majungatholus atopus* (32%), and *Tyrannosaurus rex* (34%). The ingroup taxa that exhibit the derived character state are *Anas platyrhynchos* (72%), *Apteryx sp.* (71%), *Archaeopteryx lithographica* (53%), *Chauna chavaria* (94%), *Citipati osmolskae* (61%), *Crypturellus cinnamomeus* (89%), *Dinornis giganteus* (76%), *Mongolodon junior* (53%), and the Zos Canyon troodontid (73%). The character state could not be determined in *Byronosaurus jaffei*.

Character 6- Optic lobe position.

The position of the casts of the optic lobes shifts from being dorsomedial and not visible in the outgroups and basal members of the ingroup, to being ventrolateral and visible in the more derived ingroup members. The outgroups have non-visible optic lobes in a dorsomedial position, hence, this is the primitive

character state, while the taxa that have visible optic lobes in a ventrolateral position show the derived character state.

The ingroup in which the primitive state is found are *Acrocanthosaurus atokensis, Allosaurus fragilis, Carcharodontosaurus saharicus, Ceratosaurus magnicornis, Majungatholus atopus,* and *Tyrannosaurus rex*. The ingroup taxa with the derived character state are *Anas platyrhynchos, Apteryx sp., Archaeopteryx lithographica, Byronosaurus jaffei, Chauna chavaria, Citipati osmolskae, Crypturellus cinnamomeus, Dinornis giganteus, Mongolodon junior,* and the Zos Canyon troodontid.

Character 7- Number of trigeminal nerve foramina.

The number of foramina for the trigeminal nerve changes from only one foramen, found in the outgroups and basal-most members of the ingroup, to two or three foramina in more derived ingroup taxa. For this reason, I chose 'one trigeminal foramen' as the primitive character state, and 'two or three trigeminal foramina' as the derived character state.

The ingroup taxa showing the primitive character state are *Acrocanthosaurus atokensis, Carcharodontosaurus saharicus, Ceratosaurus magnicornis, Citipati osmolskae,* and *Majungatholus atopus*. The ingroup taxa showing the derived character state are *Allosaurus fragilis, Anas platyrhynchos, Apteryx sp., Chauna chavaria, Crypturellus cinnamomeus, Dinornis giganteus, Mongolodon junior,* and *Tyrannosaurus rex*. Ingroup taxa for which the character state could not be determined are *Archaeopteryx lithographica, Byronosaurus jaffei,* and the Zos Canyon troodontid.

Character 8- Abducens nerve canal.

The abducens nerve canal either passes lateral to the pituitary fossa, or opens into the pituitary fossa. This character can be somewhat difficult to assess. In some of the taxa the abducens nerve canal opens into the fossa, but stays on the very lateral edge. These are still considered to open into the fossa, and only those canals that completely avoid the fossa and open lateral to it are considered the derived state. The abducens nerve canal opens into the pituitary fossa in the outgroups, and that is considered the primitive state, while the derived state is seen in those taxa in which the abducens nerve canal pass lateral to the pituitary fossa.

The ingroup taxa with the primitive character state are *Allosaurus fragilis, Carcharodontosaurus saharicus,* and *Majungatholus atopus*. The ingroup taxa with the derived character state are *Acrocanthosaurus atokensis, Anas platyrhynchos, Apteryx sp., Byronosaurus jaffei, Ceratosaurus magnicornis, Chauna chavaria, Crypturellus cinnamomeus, Dinornis giganteus,* and *Tyrannosaurus rex*. The ingroup taxa for which the character state could not be determined are *Archaeopteryx lithographica, Citipati osmolskae, Mongolodon junior,* and the Zos Canyon troodontid.

Character 9- Internal carotid canals.

The right and left internal carotid canals either enter the pituitary fossa separately, or join before entering the fossa, thereby entering the fossa through a single foramen. In the outgroups the internal carotid canals each open separately into the pituitary fossa, making this the primitive character state. The derived

character state is found in those taxa in which the internal carotid canals join prior to entering the pituitary fossa, thereby opening into the pituitary fossa through a single foramen.

The taxa having the primitive character state are *Acrocanthosaurus atokensis, Allosaurus fragilis, Carcharodontosaurus saharicus, Ceratosaurus magnicornis, Chauna chavaria, Dinornis giganteus,* and *Majungatholus atopus.* Taxa having the derived character state are *Anas platyrhynchos, Apteryx sp., Archaeopteryx lithographica, Byronosaurus jaffei, Crypturellus cinnamomeus, Mongolodon junior,* and *Tyrannosaurus rex*. The taxa in which the character state could not be determined in are *Citipati osmolskae*, and the Zos Canyon troodontid.

Character 10- Floccular fossa.

The floccular fossa is the depression on the inside of the braincase in which the floccular lobe sits. In some animals this depression is either absent or very small, while in others it is present and noticeable. The outgroups in this study lack or have a small and nearly indistinguishable floccular fossa, here taken as the primitive state. The presence of a noticeable fossa is the derived state of the character.

The ingroup taxa that show the primitive character state are *Crypturellus cinnamomeus,* and *Dinornis giganteus*. The ingroup taxa that show the derived character state are *Acrocanthosaurus atokensis, Allosaurus fragilis, Anas platyrhynchos, Apteryx sp., Archaeopteryx lithographica, Byronosaurus jaffei, Carcharodontosaurus saharicus, Ceratosaurus magnicornis, Chauna chavaria,*

Citipati osmolskae, Majungatholus atopus, Mongolodon junior, Tyrannosaurus rex, and the Zos Canyon troodontid.

Character 11- Floccular lobe shape.

In those taxa that have a very noticeable floccular fossa, the cast of the floccular lobe can take on two general shapes. Either the lobe is thin and knifeblade-like, or it is thicker and more bulbous. The outgroups for this study lack, or have a small, floccular fossa. In the outgroup taxon *Plateosaurus*, which has a small floccular fossa, it is thin; therefore a thin and knifeblade-like lobe is considered the primitive state, whereas a thicker and more bulbous lobe is the derived character state.

The ingroup taxa that exhibit the primitive character state are *Acrocanthosaurus atokensis, Allosaurus fragilis, Carcharodontosaurus saharicus, Ceratosaurus magnicornis, Majungatholus atopus,* and *Tyrannosaurus rex*. The ingroup taxa that exhibit the derived character state are *Anas platyrhynchos, Apteryx sp., Archaeopteryx lithographica, Byronosaurus jaffei, Chauna chavaria, Citipati osmolskae, Mongolodon junior,* and the Zos Canyon troodontid. Two ingroup taxa (*Crypturellus cinnamomeus* and *Dinornis giganteus*) do not have the character, and therefore cannot be scored with a character state.

Character 12- Posterior semicircular canal orientation.

The orientation of the posterior semicircular canal is either mainly in a parasagittal plane with a slight lateral component, or in a mostly transverse plane with a slight posterior component. In those taxa exhibiting the former, the space

between the three semicircular canals has a subtriangular appearance in lateral view. The taxa that exhibit the latter condition have lost that appearance, because the posterior canal moves laterally at an almost 90° angle to the rest of the endocast. The outgroups exhibit the former condition, so I considered this the primitive state.

The ingroup taxa exhibiting the primitive state are *Acrocanthosaurus atokensis, Allosaurus fragilis, Carcharodontosaurus saharicus, Ceratosaurus magnicornis, Majungatholus atopus,* and *Tyrannosaurus rex*. The ingroup taxa exhibiting the derived state are *Anas platyrhynchos, Apteryx sp., Archaeopteryx lithographica, Chauna chavaria, Citipati osmolskae, Crypturellus cinnamomeus,* and *Dinornis giganteus*. The character state could not be determined in *Byronosaurus jaffei*, *Mongolodon junior*, and the Zos Canyon troodontid.

Character 13- Number of hypoglossal nerve foramina.

The number of hypoglossal nerve foramina varies within the ingroup as well as the outgroups. When variation is found within the outgroups, a primitive character state can be decided upon by using a method devised by Maddison et al. (1984). This method stated that when various outgroups show differing character states, it may be equivocal whether one state or the other is used as the primitive state. This is the situation that I found myself in, and because the basal-most member of the outgroups, *Saurosuchus*, has only one hypoglossal foramen, this was chosen as the primitive character state.

The ingroup taxa in which the primitive state is found are *Acrocanthosaurus atokensis, Allosaurus fragilis, Ceratosaurus magnicornis,*

Majungatholus atopus, and *Tyrannosaurus rex*. The ingroup taxa in which the derived state is found are *Anas platyrhynchos, Apteryx sp., Archaeopteryx lithographica, Byronosaurus jaffei, Carcharodontosaurus saharicus, Chauna chavaria, Citipati osmolskae, Crypturellus cinnamomeus, Dinornis giganteus,* and *Mongolodon junior*. The character state could not be determined in the Zos Canyon troodontid.

Character 14- Reptile Encephalization Quotient.

The Reptile Encephalization Quotient (REQ) is a revision of Jerison's "lower" vertebrate equation, and was devised by Hurlburt (1996) for non-avian reptiles. The equation is: $REQ=M_{Br}/(0.0155 \times M_{Bd}^{0.553})$. M_{Br} is the mass of the brain (or endocast) in grams, and M_{Bd} is the mass of the body in grams. For M_{Br}, I used the entire volume of the endocast, and a specific gravity of 1g/mL to obtain the volume in grams. I obtained the body masses for the different taxa from a variety of sources (see Appendix C for a detailed description). The REQ scores span a broad spectrum, and they were ultimately divided almost halfway between the highest and the lowest REQs, which was an REQ of 6 (this is why the REQ was modified from the 5.5 of Wharton (2002)). The outgroups have REQs under 6, so that is the primitive character state, and REQs of greater than 6 are the derived character state.

The ingroup taxa with the primitive character state are *Acrocanthosaurus atokensis, Allosaurus fragilis, Archaeopteryx lithographica, Carcharodontosaurus saharicus, Ceratosaurus magnicornis, Citipati osmolskae, Crypturellus cinnamomeus,* and *Dinornis giganteus*. The ingroup taxa with the

derived character state are *Anas platyrhynchos, Apteryx sp., Chauna chavaria,* and *Tyrannosaurus rex*. For several ingroup taxa the character state could not be determined. Those ingroup taxa are *Byronosaurus jaffei, Majungatholus atopus, Mongolodon junior,* and the Zos Canyon troodontid.

CHARACTER ANALYSES

Data Matrix

Taxa	Characters													
	1	**2**	**3**	**4**	**5**	**6**	**7**	**8**	**9**	**10**	**11**	**12**	**13**	**14**
Acrocanthosaurus atokensis	0	0	0	0	0	0	0	1	0	1	0	0	0	0
Allosaurus fragilis	?	0	0	0	0	0	1	0	0	1	0	0	0	0
Anas platyrhynchos	-	1	1	1	1	1	1	1	1	1	1	1	1	1
Apteryx sp.	-	1	1	1	1	1	1	1	1	1	1	1	1	1
Archaeopteryx lithographica	?	0	1	1	1	1	?	?	1	1	1	1	1	0
Byronosaurus jaffei	?	?	?	?	?	1	?	1	1	1	1	?	1	?
Carcharodontosaurus saharicus	0	0	0	0	0	0	0	0	0	1	0	0	1	0
Ceratosaurus magnicornis	0	0	0	0	0	0	0	1	0	1	0	0	0	0
Chauna chavaria	-	1	1	1	1	1	1	1	0	1	1	1	1	1
Citipati osmolskae	1	0	1	1	1	1	0	?	?	1	1	1	1	0
Crypturellus cinnamomeus	-	1	1	1	1	1	1	1	1	0	-	1	1	0
Dinornis giganteus	-	1	1	1	1	1	1	1	0	0	-	1	1	0
Majungatholus atopus	0	0	0	0	0	0	0	0	0	1	0	0	0	?
Mongolodon junior	?	0	1	1	1	1	1	?	1	1	1	?	1	?
Tyrannosaurus rex	0	0	0	0	0	0	1	1	1	1	0	0	0	1
Zos Canyon troodontid	?	0	1	1	1	1	?	?	?	1	1	?	?	?

Table 1. Data matrix for the 16 ingroup taxa and 14 characters utilized in this study.

0 represents the primitive character state, 1 represents the derived character state, ? means the character state cannot be determined from the specimen, and - means the character in question is not a character the specimen possesses, so the specimen cannot be scored for the character.

My Data Alone

The first analysis I performed was a simple parsimony analysis run with only the taxa and characters given in table 1 above. The test was run in PAUP 4.0b10(Altivec). It was run using the heuristic mode, with the starting tree gained through stepwise addition. Swapping was done on the best tree only using tree bisection-reconnection (TBR), and it was run randomly with 10 repetitions. The analysis produced 4,215 most parsimonious trees of 21 steps. I also generated a strict consensus tree (Figure 39), as well as a 50% majority tree (Figure 40). The strict consensus tree had a CI of 0.70, an RI of 0.91, and an RC of 0.63, while the 50% majority tree had a CI of 0.67, an RI of 0.89, and an RC of 0.59.

Despite the fact that I used only 14 characters and 16 taxa, some resolution was obtained. The strict consensus tree resolved three nodes within the ingroup. The basal polytomy, Theropoda (node A), consists of *Acrocanthosaurus, Allosaurus, Carcharodontosaurus, Ceratosaurus*, *Majungatholus*, and a clade containing the rest of the ingroup taxa. Following the basal polytomy is node B (Coelurosauria; *Tyrannosaurus* and node C). Above node B is another polytomy, Maniraptora (node C), consisting of *Anas, Apteryx, Archaeopteryx, Byronosaurus, Chauna, Citipati,* (*Crypturellus* + *Dinornis*)*, Mongolodon,* and the Zos Canyon troodontid. Within this polytomy, a partial resolution of paleognaths is discernable.

The 50% majority rule tree includes an unexpected grouping of *Acrocanthosaurus* with *Ceratosaurus*, and did not resolve the positions of

My Data Only- Strict Consensus Tree

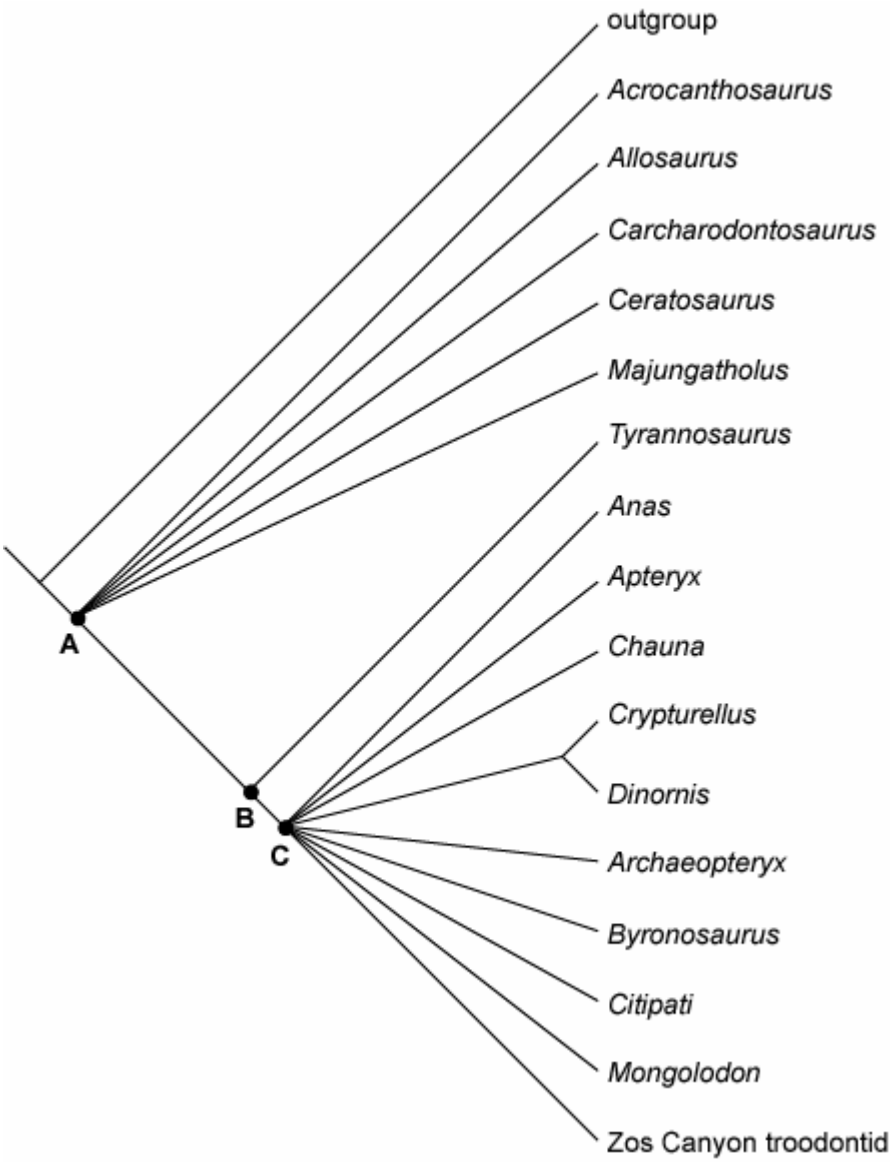

Figure 39. Strict consensus tree of taxa examined in my study and 14 characters. **A**, **B**, and **C** serve to distinguish nodes mentioned in the accompanying text.

My Data Only- 50% Majority Rule Tree

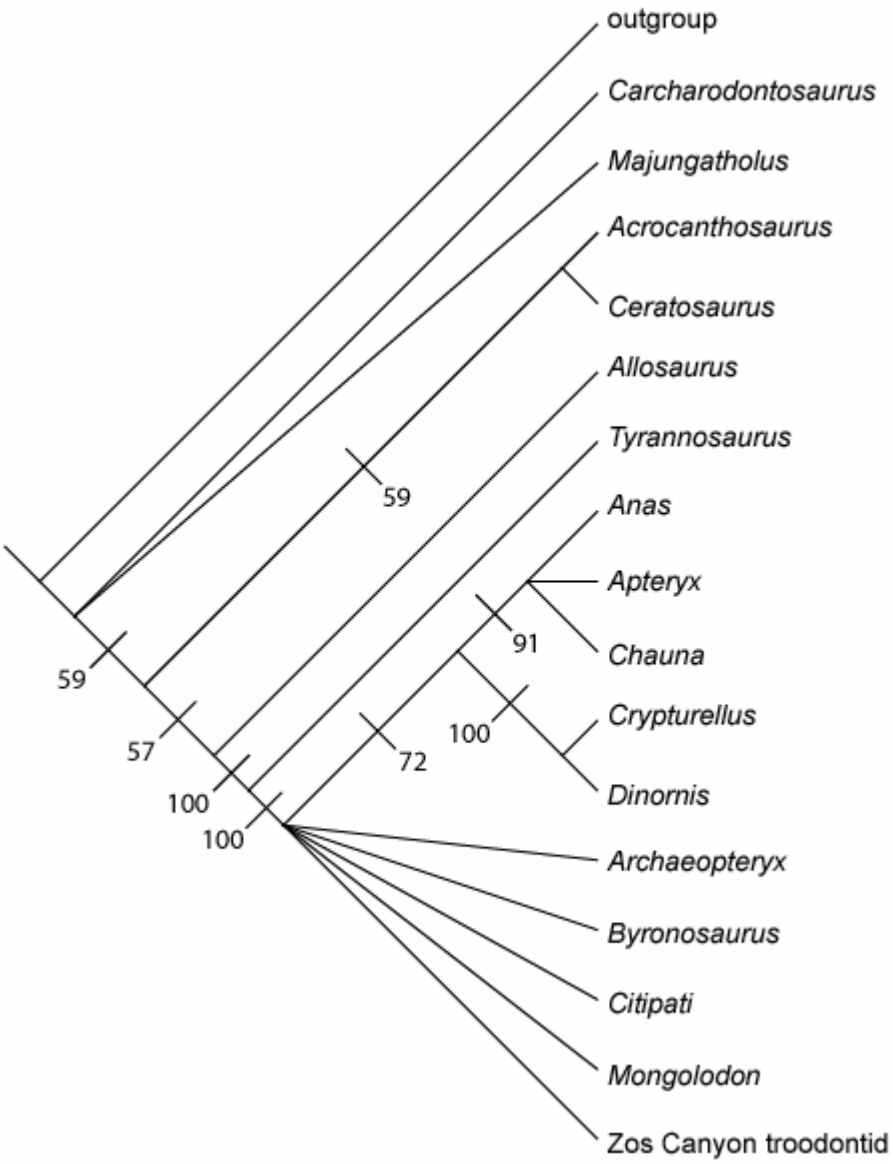

Figure 40. 50% majority rule tree of taxa examined in my study and 14 characters.

Majungatholus and *Carcharodontosaurus*. *Allosaurus* is depicted as the sister taxon to a clade including *Tyrannosaurus* + the more derived coelurosaurs. These groupings were found in less than 60% of the recovered trees. Above *Allosaurus*, all of the groupings are 69% or higher. Although a large polytomy is still found among coelurosaurs, all of the modern avian taxa are on a branch of their own, and this was found in 72% of the trees. Within this branch, 91% of the trees preserved *Anas*, *Apteryx,* and *Chauna* as a clade, with *Crypturellus* + *Dinornis* as the sister clade. Although these avian clades are inconsistent with previous findings, in which *Apteryx* is a paleognath, while here being placed within the neognaths, it is encouraging that all the avian taxa were separated from the non-avian theropods.

Character Tracing and Optimization

The strict consensus tree obtained by PAUP was opened in MacClade 4.04PPC for character tracing and optimization. Owing to the polytomies that are present, MacClade would not perform ACCTRAN and DELTRAN optimizations on the tree.

The 14 characters and their transition points on the consensus tree can be seen in figures 41-54. The distribution of the character states for the median septum of the sphenethmoid dividing the sphenethmoidal fossa (character 1) is straightforward (Figure 41). The definite lack of the septum is found in only one taxon, *Citipati*. This would seem to make it an autapomorphy, and therefore

My Data Only- Sphenethmoidal Septum Dividing Sphenethmoidal Fossa (Character 1) Resolution

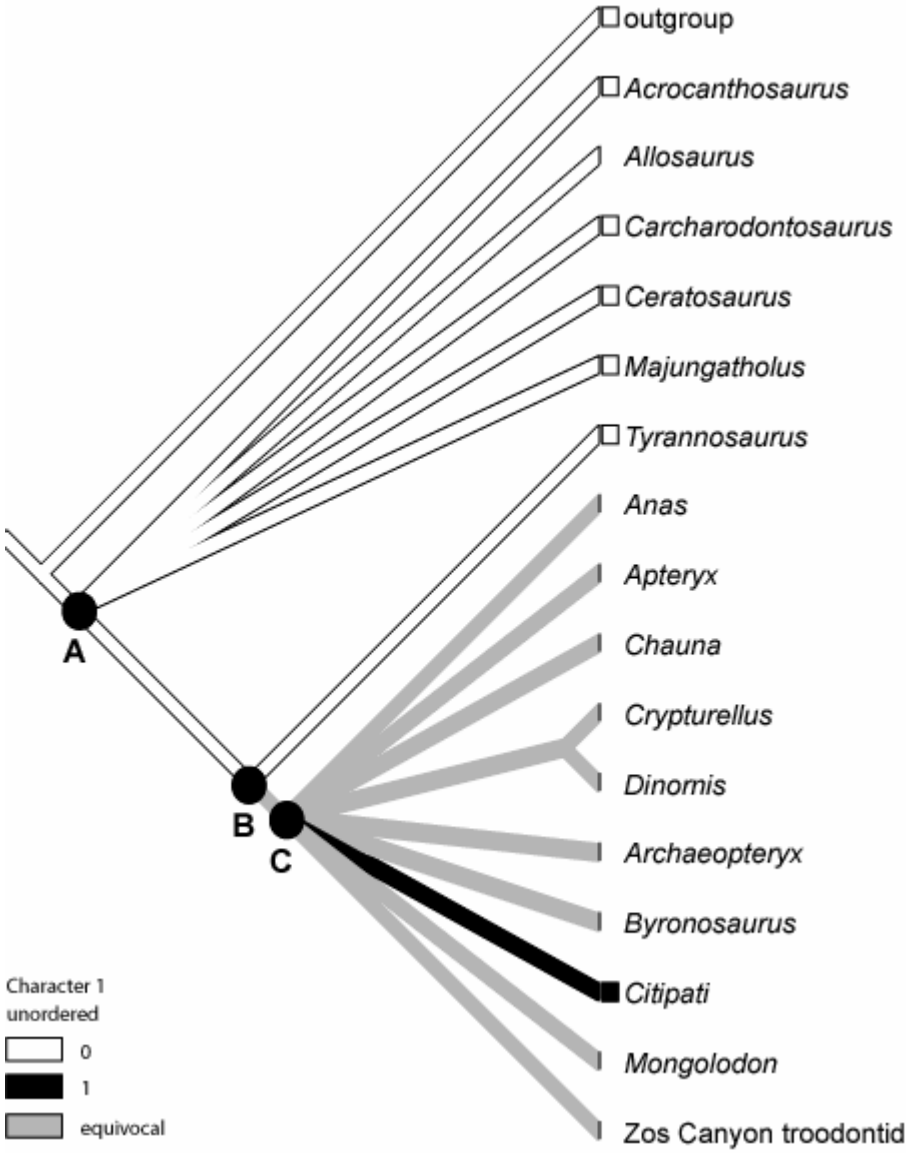

Figure 41. Resolution of character 1 (derived condition: median septum of the sphenethmoid dividing the sphenethmoidal fossa absent) on my strict consensus tree.

A, **B**, and **C** serve to distinguish nodes mentioned in the accompanying text.

uninformative, but the small number of taxa that I was able to examine led me to include this character because the study of more taxa may lead to the discovery of others having the derived state.

All the taxa showing the derived state for character 2, having the olfactory bulbs appressed against the anterior border of cerebral hemispheres, are modern avians, while those taxa preserving the primitive state (olfactory bulbs anterior to the cerebral hemispheres and olfactory tract) are not (Figure 42). This implies that the acquisition of the derived state occurred somewhere along the lineage to modern birds, but the lack of additional taxa in this study make the exact position at which it was attained impossible to determine.

The derived conditions of character 3, the shape of the cerebral hemispheres, character 4, the volume of the cerebral hemispheres, character 5, the width of the endocast, and character 6, the optic lobe position, are found in the taxa stemming from node C (Figures 43, 44, 45, 46). Characters 3, 4, and 5 are not preserved in *Byronosaurus* because the anterior portion of the braincase was eroded away. The fact that the same distribution is seen in all these characters begs the question, are they correlated? This is a possibility. I kept the characters separate in these analyses because of the small number of taxa examined. If a larger study consisting of more taxa still shows these characters together, then they should probably be combined and scored as a single character.

The number of trigeminal nerve foramina (character 7) have a fairly simple character distribution, with two exceptions (Figure 47). Within the group

My Data Only- Olfactory Bulb Position (Character 2) Resolution

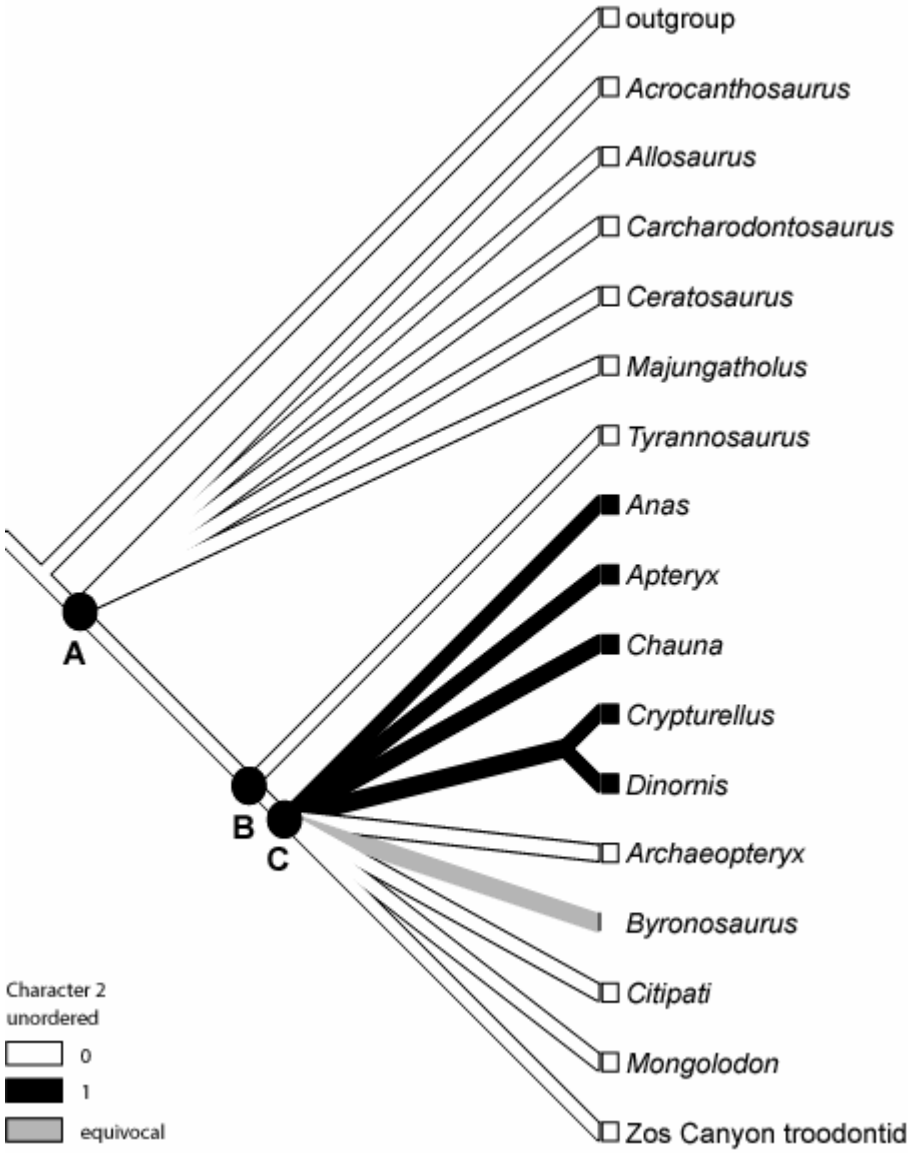

Figure 42. Resolution of character 2 (derived condition: olfactory bulbs appressed against anterior border of cerebral hemispheres) on my strict consensus tree.

A, **B**, and **C** serve to distinguish nodes mentioned in the accompanying text.

My Data Only- Cerebral Hemisphere Shape (Character 3) Resolution

Figure 43. Resolution of character 3 (derived condition: cerebral hemispheres broad ventrolateral expansion against posterior orbital wall) on my strict consensus tree.

A, **B**, and **C** serve to distinguish nodes mentioned in the accompanying text.

My Data Only- Volume of the Cerebral Hemispheres (Character 4) Resolution

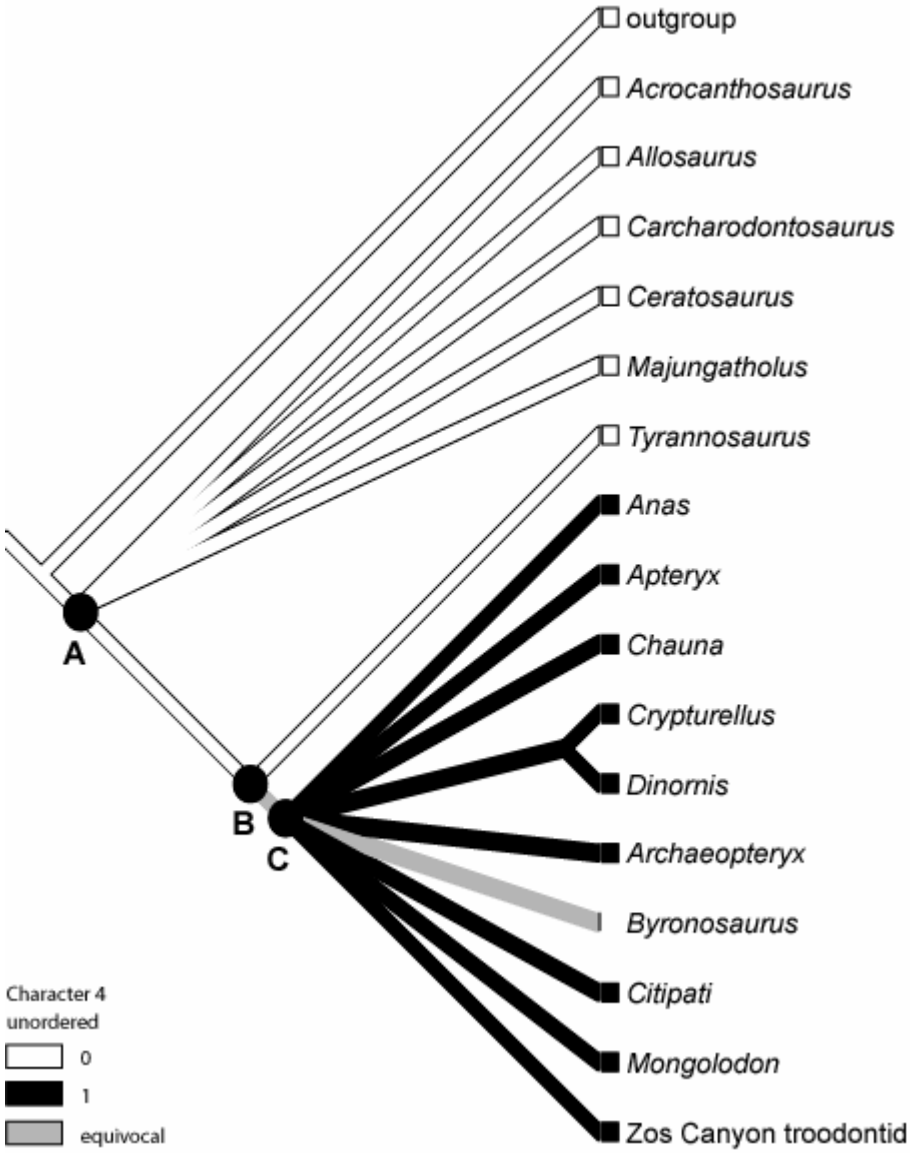

Figure 44. Resolution of character 4 (derived condition: cerebral hemispheres occupy greater than 35% of the volume of the endocranial cavity) on my strict consensus tree.

A, **B**, and **C** serve to distinguish nodes mentioned in the accompanying text.

My Data Only- Width of Endocast (Character 5) Resolution

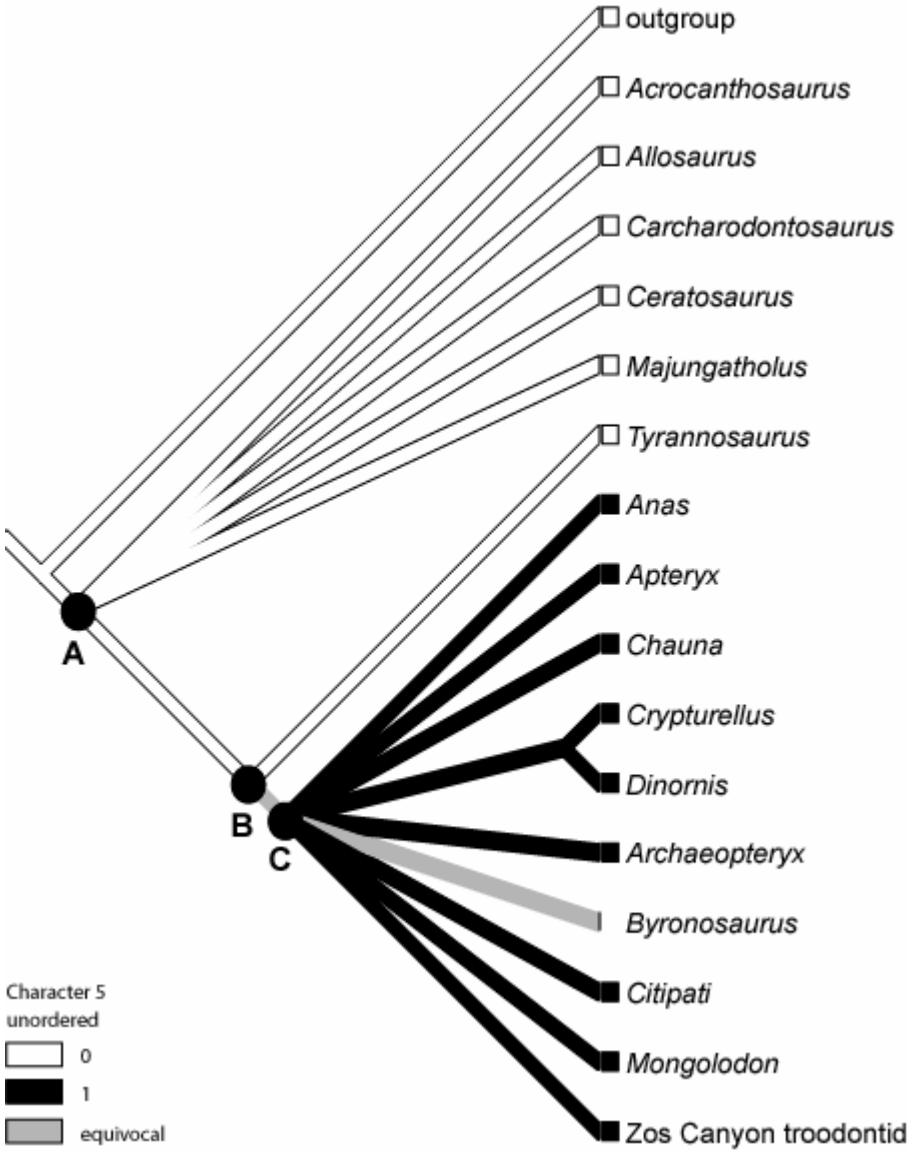

Figure 45. Resolution of character 5 (derived condition: maximum width of endocast greater than 45% of the length of the endocast) on my strict consensus tree.

A, **B**, and **C** serve to distinguish nodes mentioned in the accompanying text.

My Data Only- Optic Lobe Position (Character 6) Resolution

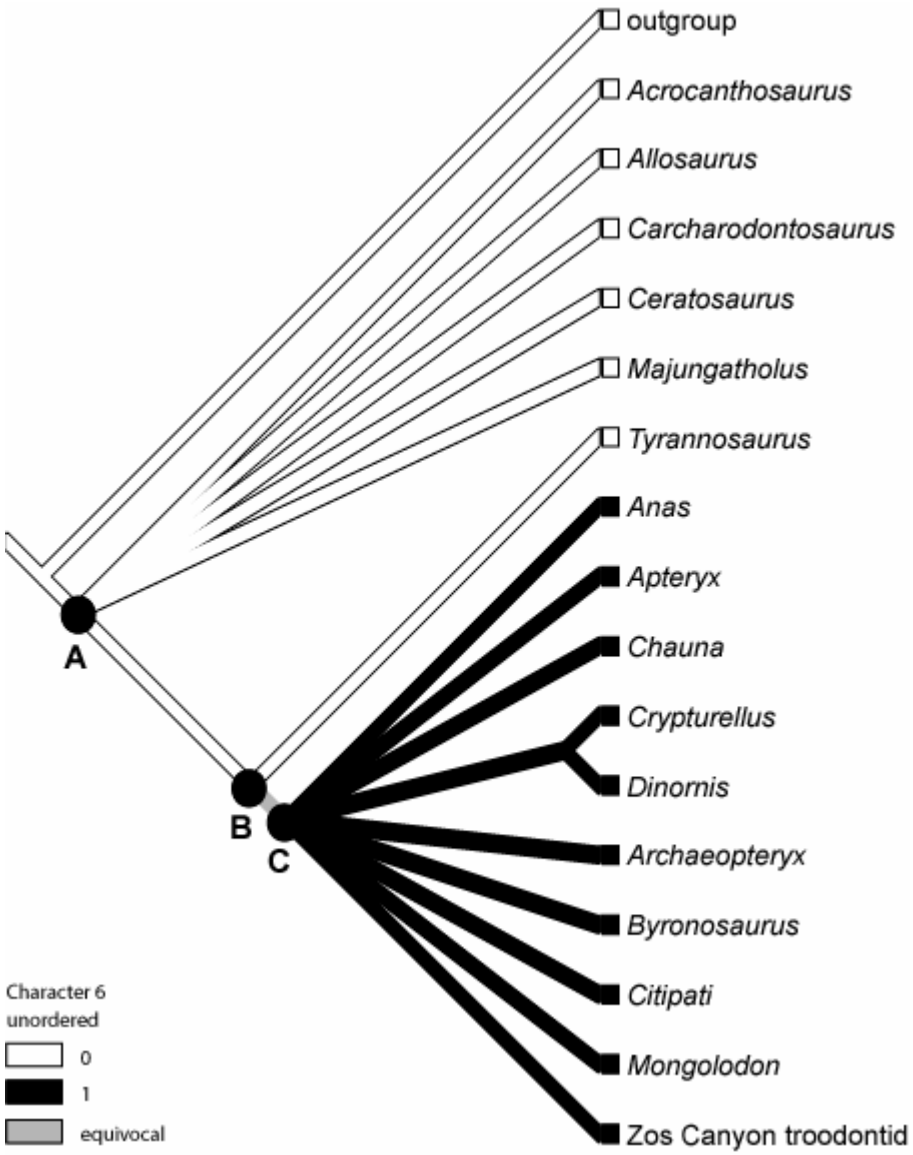

Figure 46. Resolution of character 6 (derived condition: optic lobe visible and lying in a ventrolateral position) on my strict consensus tree.

A, **B**, and **C** serve to distinguish nodes mentioned in the accompanying text.

My Data Only- Number of Trigeminal Nerve Foramina (Character 7) Resolution

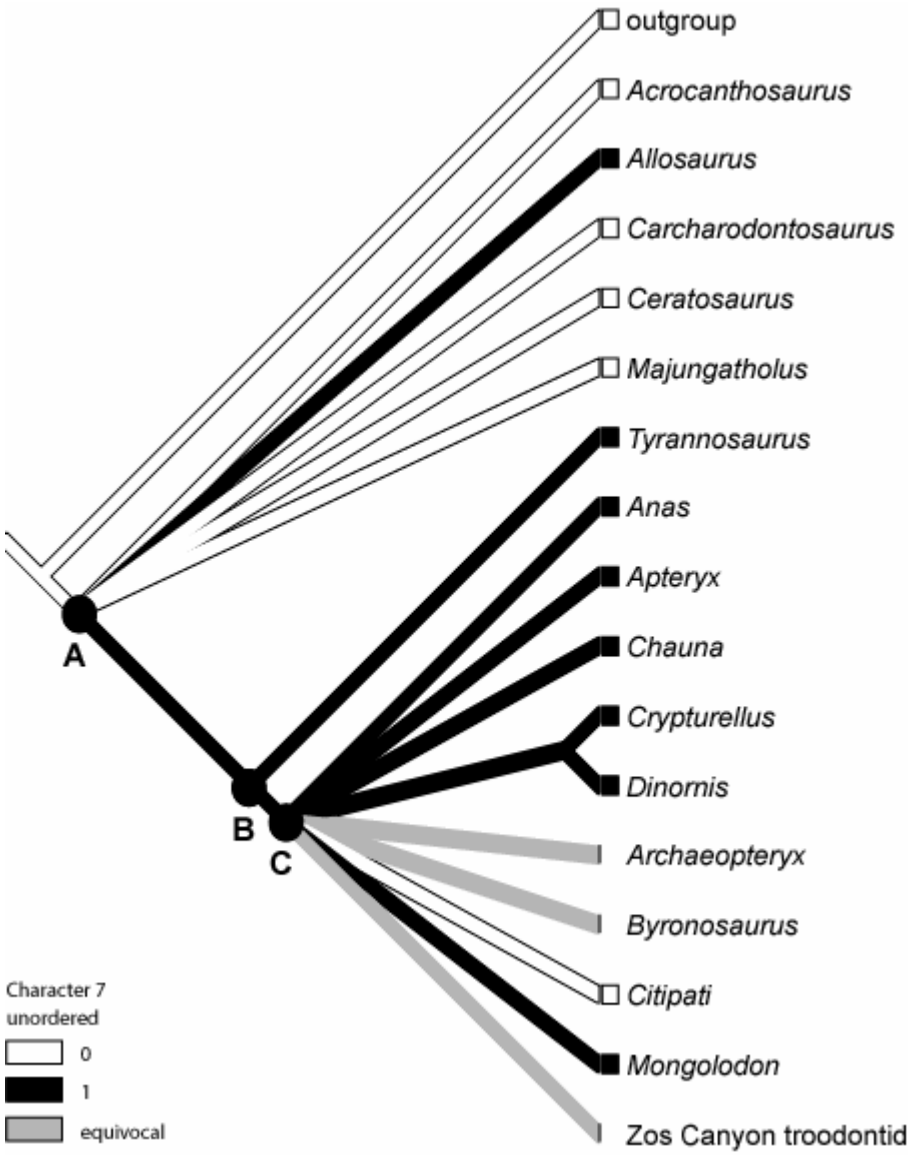

Figure 47. Resolution of character 7 (derived condition: 2 to 3 trigeminal nerve foramina) on my strict consensus tree.

A, **B**, and **C** serve to distinguish nodes mentioned in the accompanying text.

stemming from node A, all of the taxa have the primitive character state (1 trigeminal nerve foramen) except for *Allosaurus* and taxa stemming from node B. All the taxa stemming from node B have the derived character state (2 or 3 trigeminal nerve foramina), except for *Citipati*. The character state is unknown in *Archaeopteryx, Byronosaurus*, and the Zos Canyon troodontid.

The derived condition for character 8, having the abducens nerve canal passing lateral to the pituitary fossa, is found in *Acrocanthosaurus*, *Ceratosaurus*, and taxa stemming from node B (Figure 48). When discernible, the derived condition for the internal carotid canals (character 9; confluent canals entering the pituitary fossa) is found in all taxa stemming from node B except *Chauna* and *Dinornis*. Because of this distribution, the character is marked as equivocal for those taxa in which it could not be scored (Figure 49).

The floccular fossa (character 10) is found in its derived character state (present and noticeable) in all ingroup taxa except *Crypturellus* and *Dinornis*, where it is optimized as a reversal (Figure 50). The floccular lobe shape (character 11) transforms to its derived condition (thicker and bulbous) in the taxa stemming from node C. It is scored as equivocal at node C, however, because both *Crypturellus* and *Dinornis* are missing the floccular fossa seen in the other taxa (Figure 51).

The derived condition for the posterior semicircular canal orientation (character 12; mostly lies in a parasagittal plane with a slight lateral component) is found in all taxa stemming from node C where it is preserved. Once again there

My Data Only- Abducens Nerve Canal (Character 8) Resolution

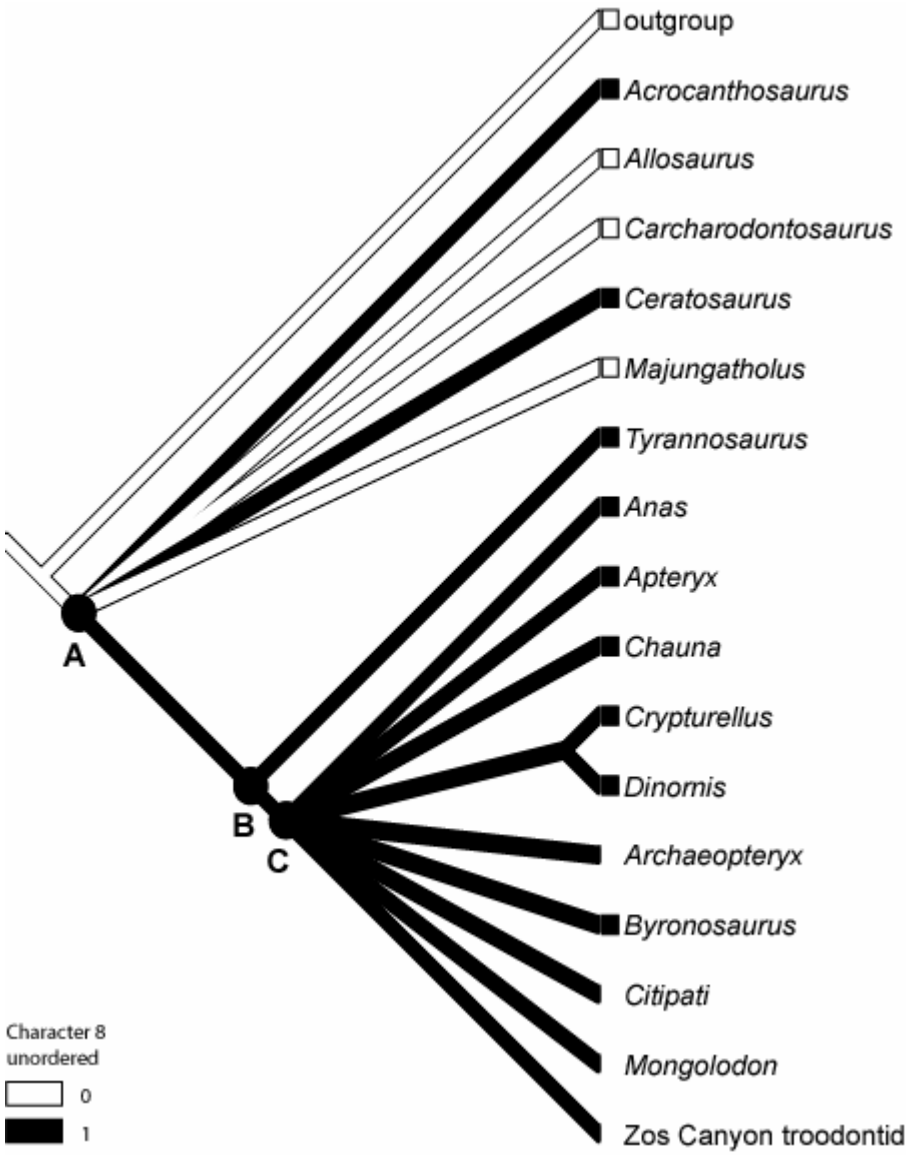

Figure 48. Resolution of character 8 (derived condition: abducens nerve canal passes lateral to pituitary fossa) on my strict consensus tree.

A, **B**, and **C** serve to distinguish nodes mentioned in the accompanying text.

My Data Only- Internal Carotid Canals (Character 9) Resolution

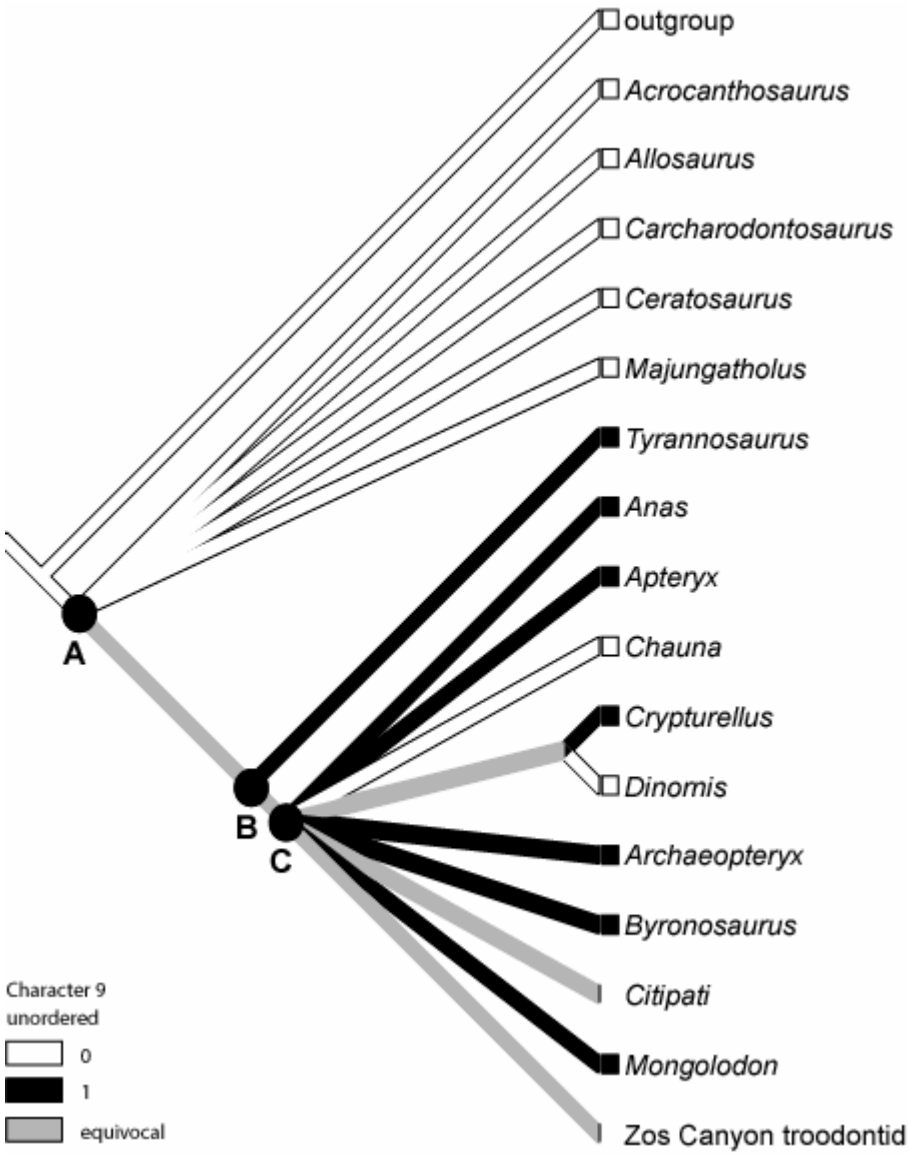

Figure 49. Resolution of character 9 (derived condition: internal carotid canals confluent entering pituitary fossa) on my strict consensus tree.

A, **B**, and **C** serve to distinguish nodes mentioned in the accompanying text.

My Data Only- Floccular Fossa (Character 10) Resolution

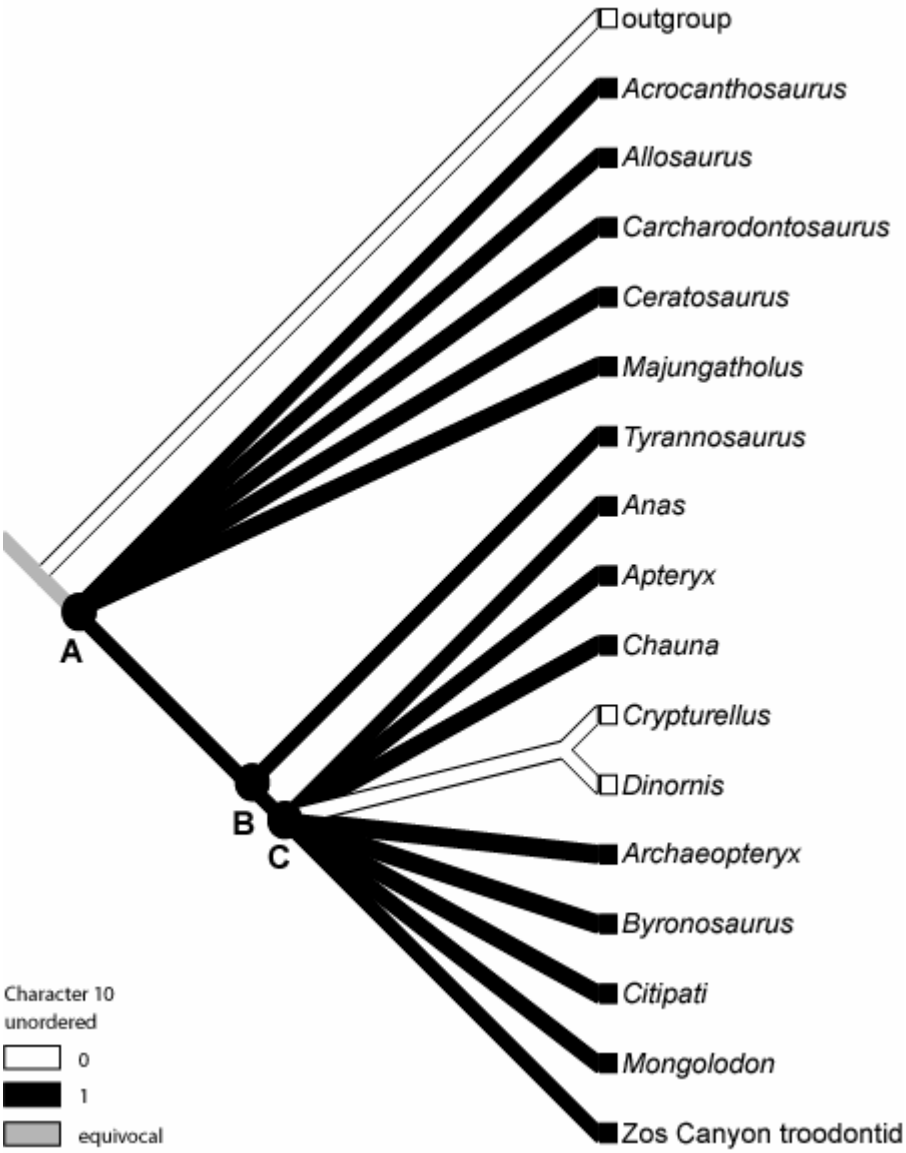

Figure 50. Resolution of character 10 (derived condition: floccular fossa present and noticeable) on my strict consensus tree.

A, **B**, and **C** serve to distinguish nodes mentioned in the accompanying text.

My Data Only- Floccular Lobe Shape (Character 11) Resolution

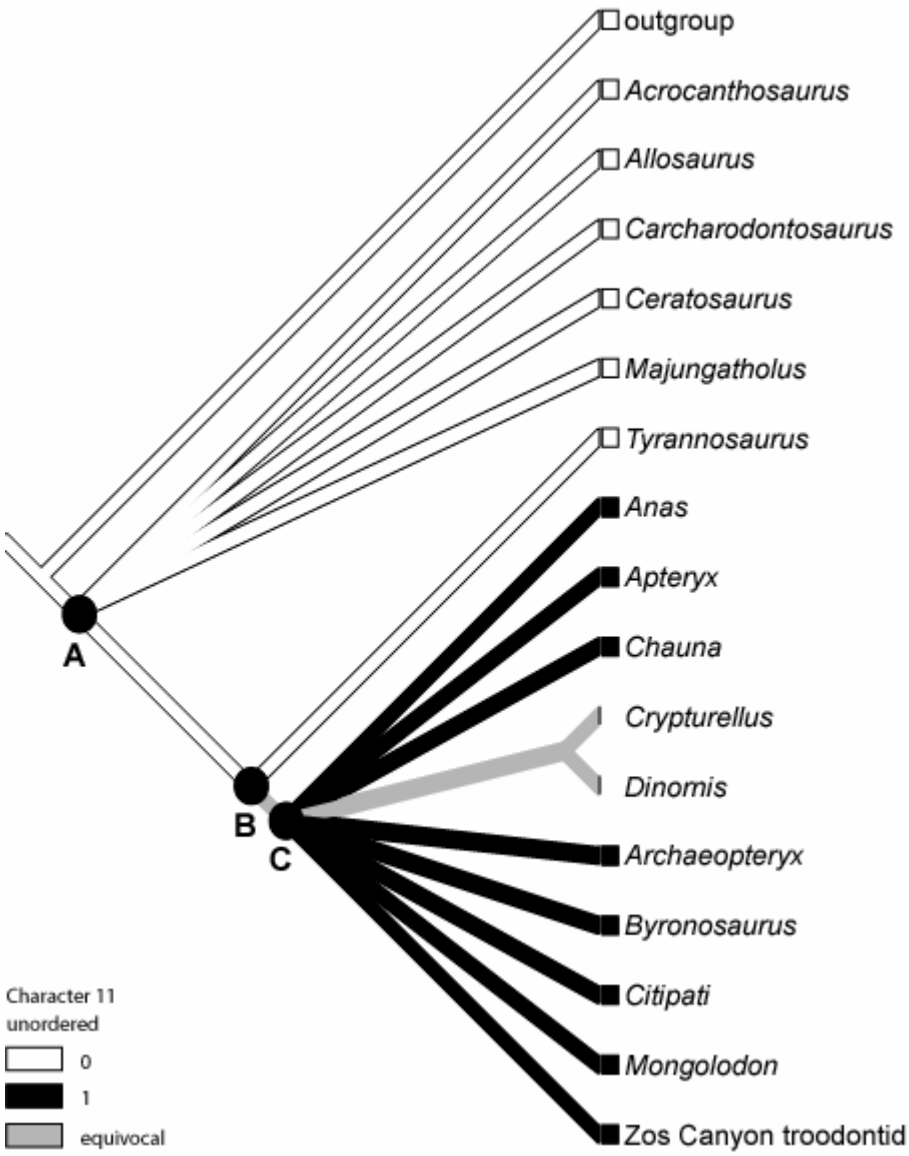

Figure 51. Resolution of character 11 (derived condition: shape of floccular lobe thicker and bulbous) on my strict consensus tree.

A, **B**, and **C** serve to distinguish nodes mentioned in the accompanying text.

is some equivocation in the taxa stemming from node C, this time owing to the lack of preservation of the posterior semicircular canals in *Byronosaurus, Mongolodon,* and the Zos Canyon troodontid (Figure 52).

The derived state of character 13 (2 to 3 hypoglossal nerve foramina) is found in *Carcharodontosaurus* and the taxa stemming from node C, except for the Zos Canyon troodontid, where the character cannot be seen in the scan data. For this reason, the condition of the character state along the branch leading from node A to the Zos Canyon troodontid is listed as equivocal (Figure 53).

The Reptile Encephalization Quotient (REQ) (character 14) has a complex distribution of states (Figure 54). All taxa in the basal polytomy possess the primitive character state (less than 6), except for *Majungatholus*, which is equivocal because an REQ cannot be measured owing to the lack of a body mass for this taxon. *Tyrannosaurus* shows the derived character state (greater than 6), as do *Anas, Apteryx,* and *Chauna*, but *Archaeopteryx, Citipati, Crypturellus*, and *Dinornis* show the primitive character state. The rest of the taxa stemming from node C (*Mongolodon, Byronosaurus*, and the Zos Canyon troodontid) could not be scored for this character because the REQ requires a body mass in order to be calculated. Many of the taxa consist only of a skull and scattered postcranial remains. Often, these remains are not those required for estimating mass. Even with the lack of REQs for the studied troodontid taxa, there is a troodontid taxon with an REQ high enough to be derived, and this means that the troodontids in these analyses would also most likely possess the derived character state.

My Data Only- Posterior Semicircular Canal Orientation (Character 12) Resolution

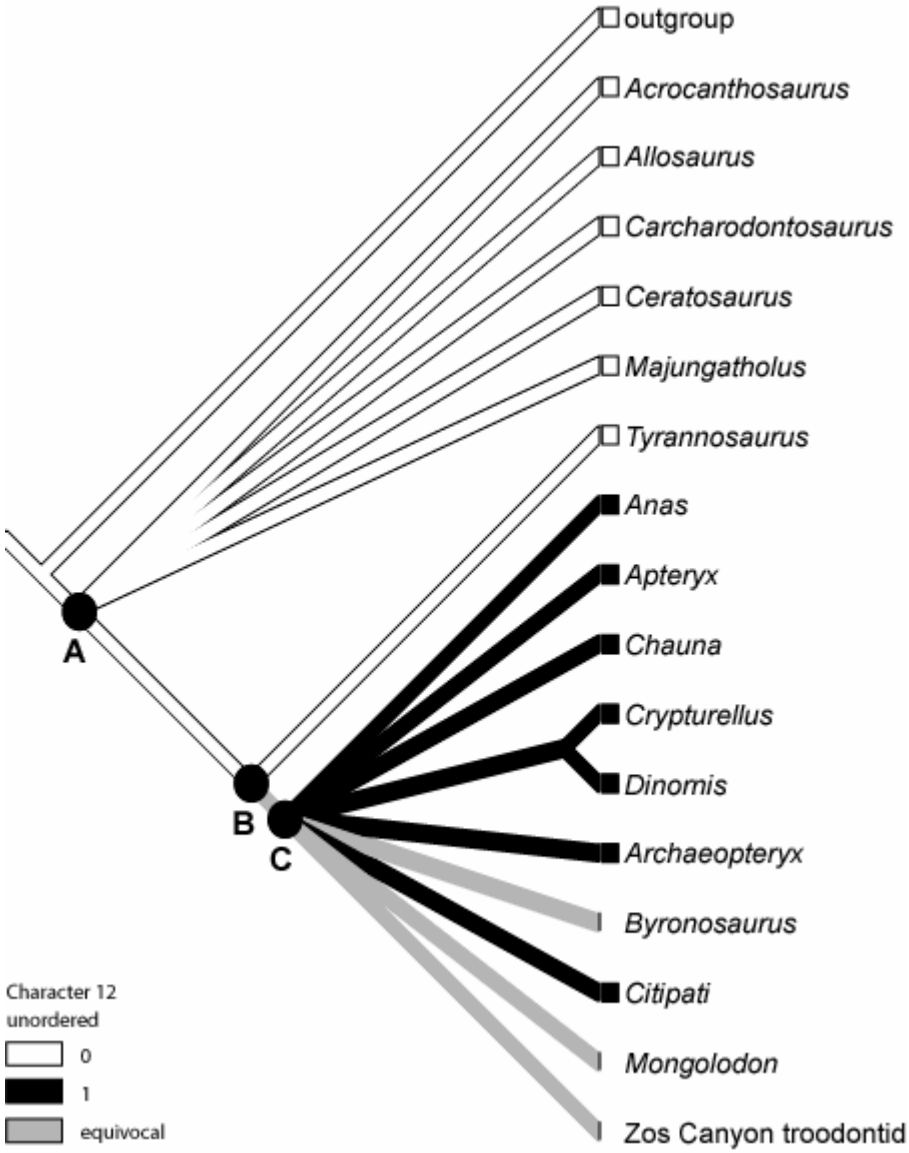

Figure 52. Resolution of character 12 (derived condition: posterior semicircular canal mostly lies in a transverse plane with a slight posterior component) on my strict consensus tree.

A, **B**, and **C** serve to distinguish nodes mentioned in the accompanying text.

My Data Only- Number of Hypoglossal Nerve Foramina (Character 13) Resolution

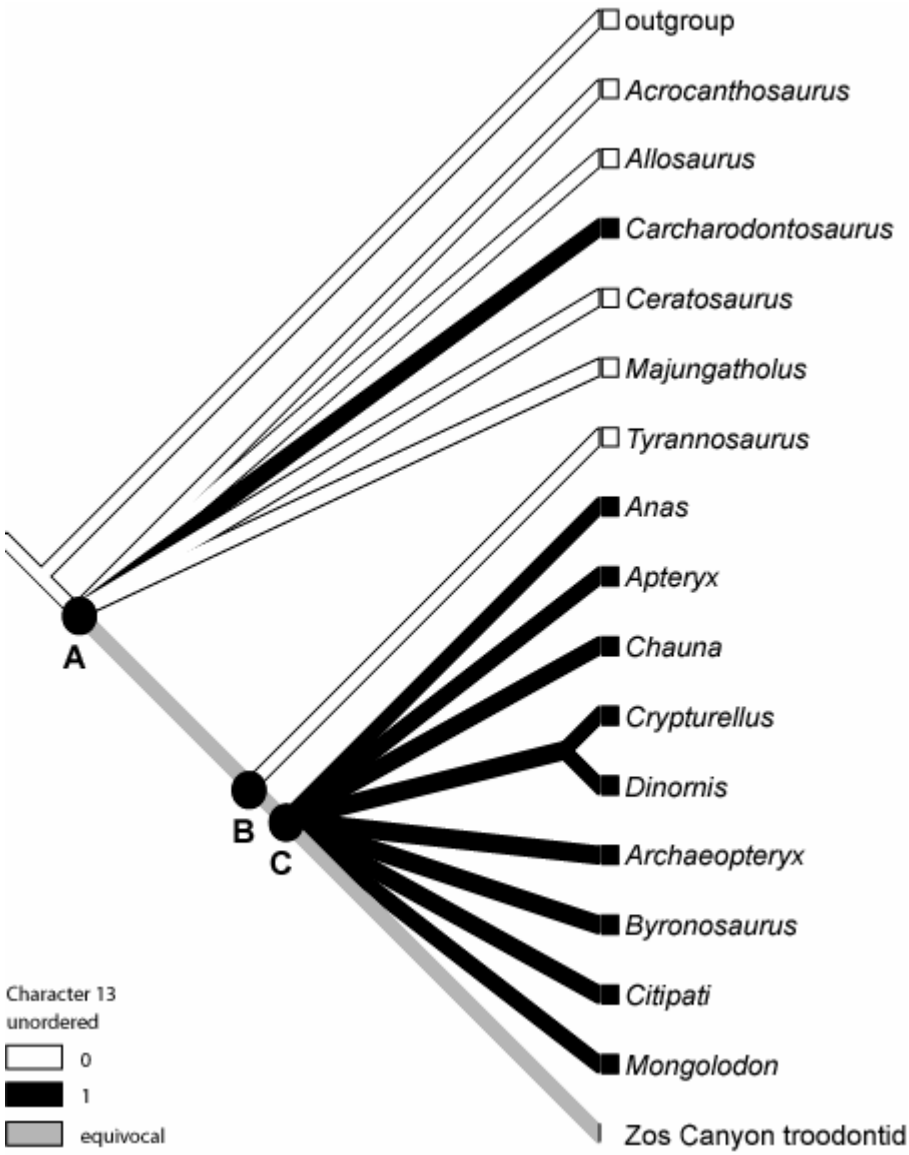

Figure 53. Resolution of character 13 (derived condition: 2 to 3 hypoglossal nerve foramina) on my strict consensus tree.

A, **B**, and **C** serve to distinguish nodes mentioned in the accompanying text.

My Data Only- Reptile Encephalization Quotient (Character 14) Resolution

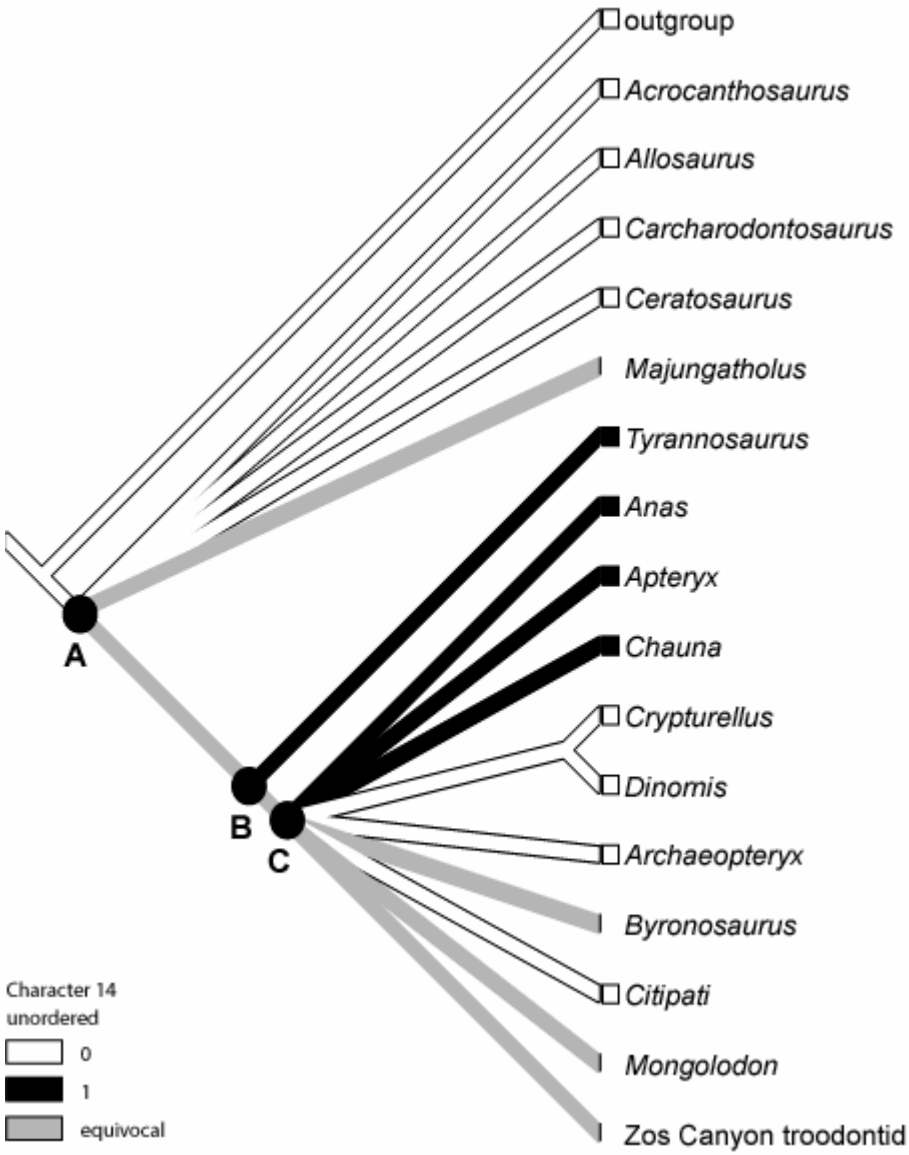

Figure 54. Resolution of character 14 (derived condition: Reptile Encephalization Quotient greater than 6) on my strict consensus tree.

A, **B**, and **C** serve to distinguish nodes mentioned in the accompanying text.

Holtz's Data + My Data

The second analysis that I performed used the phylogenetic tree and data published by Holtz in 1998, which consisted of 41 ingroup taxa and 386 characters. I reran Holtz's original analysis in order to confirm his results, and the consensus tree obtained differed from Holtz's in having *Elaphrosaurus* in a polytomy with *Dilophosaurus*/Coelophysidae and (*Ceratosaurus* (*Carnotaurus*, *Abelisaurus*)) instead of having *Elaphrosaurus* more closely related to (*Ceratosaurus* (*Carnotaurus*, *Abelisaurus*)) (Figure 55). The total tree length was 1412 steps with an all zero outgroup, and a consensus tree was calculated from the 40 equally most-parsimonious trees. I used the same parameters that Holtz used, (a heuristic search option, random branch addition with 30 replicates, and TBR branch swapping). The consensus tree was opened in MacClade, and a C.I. of 0.48, an R.I. of 0.66, and an R.C. of 0.32 were calculated.

After confirming the original Holtz tree, I added the 14 endocast characters described above to the Holtz data matrix. Before running the analysis, several adjustments had to be made. First, my character 9 was left out of the matrix because it is identical to Holtz's internal carotid canals character (his character 91). Second, *Majungatholus* was omitted because Holtz did not have it in his study. Third, some of the taxa used in the first analysis had to be entered as a combination. *Mongolodon, Byronosaurus,* and the Zos Canyon troodontid were entered as Troodontidae, *Citipati* was added under Oviraptoridae, and the bird taxa were added under Ornithothoraces. The combined data matrix was run in

Holtz's 1998 Data Only- Strict Consensus Tree

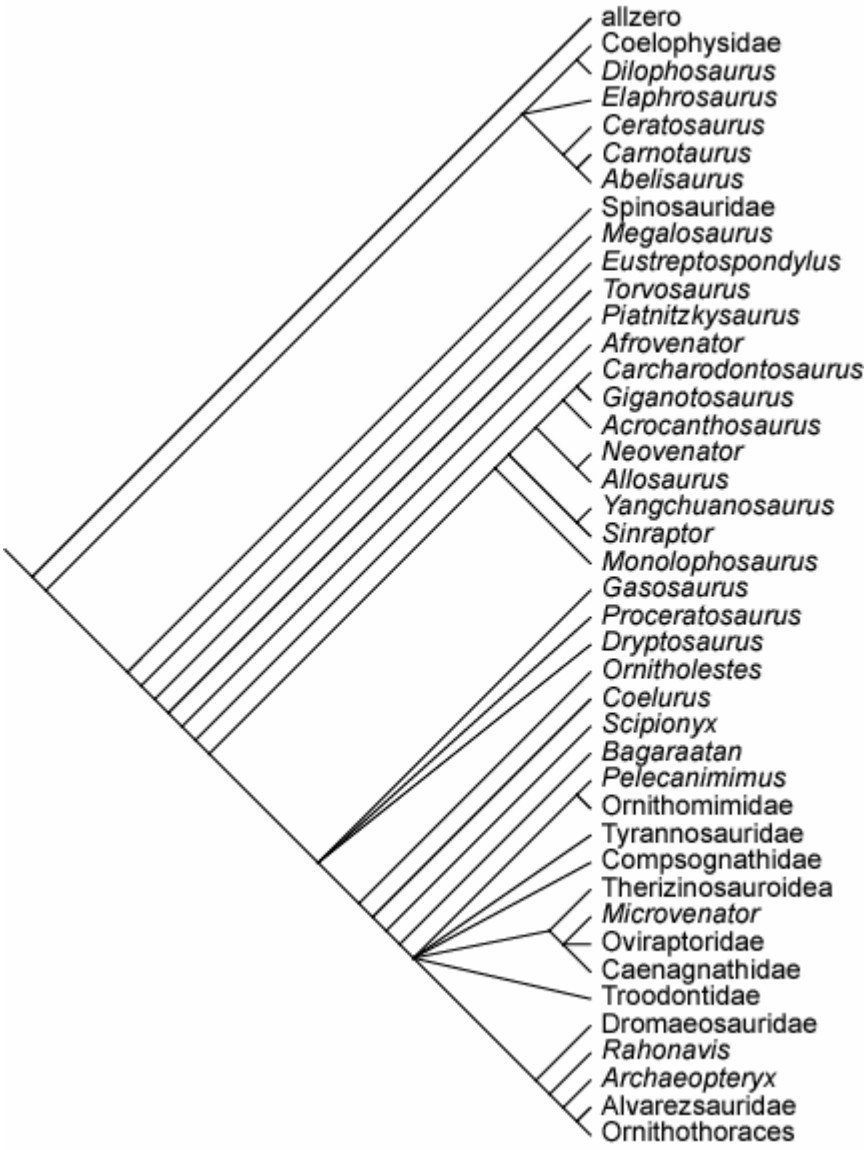

Figure 55. Strict consensus tree of Holtz's taxa and characters.

PAUP, using the same parameters that were used to run Holtz's data alone. This resulted in 20 equally most-parsimonious trees of 1431 steps (Figure 56). A strict consensus tree with a C.I. of 0.44, an R.I. of 0.62, and an R.C. of 0.28 was derived from these 20 trees, and compared to the consensus tree from the original Holtz data. Some differences between Holtz's strict consensus tree and the strict consensus tree containing my data were found. A 50% majority tree based on the results was nearly identical to the strict consensus tree. The only difference was that the polytomy comprised of *Gasosaurus, Proceratosaurus,* and *Dryptosaurus* was resolved (Figure 57).

Returning to the two strict consensus trees, the new consensus tree showed more resolution than the original strict consensus tree. The two trees show the exact same relationships through *Bagaraatan*, but a large polytomy in the original strict consensus tree consisting of (*Pelecanimimus,* Ornithomimidae), Compsognathidae, Tyrannosauridae, (Therizinosauroidea (*Microvenator,* Oviraptoridae, Caenagnathidae)), and Troodontidae is resolved in the combined data strict consensus tree. Tyrannosauridae is resolved as the sister group to the *Pelecanimimus*/Ornithomimidae clade, Compsognathidae alone forms the next branch up the tree, followed by the branch containing (Therizinosauroidea (*Microvenator,* Oviraptoridae, Caenagnathidae)), and lastly, a branch of only Troodontidae. Above this, the two trees again show the same relationships.

Holtz's Data + My Data- Strict Consensus Tree

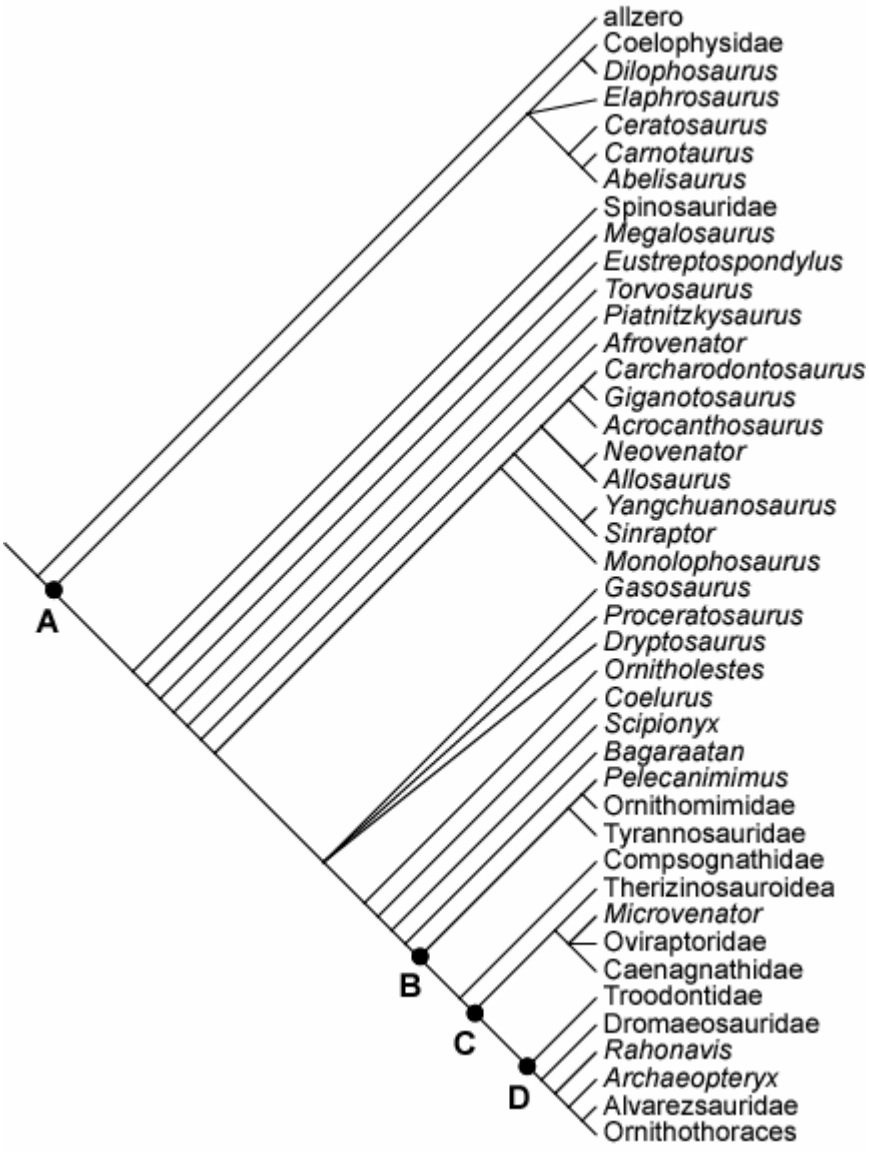

Figure 56. Strict consensus tree of Holtz's taxa and characters + taxa and characters used in my study.

A, **B**, **C**, and **D** serve to distinguish nodes mentioned in the accompanying text.

Holtz's Data + My Data- 50% Majority Rule Tree

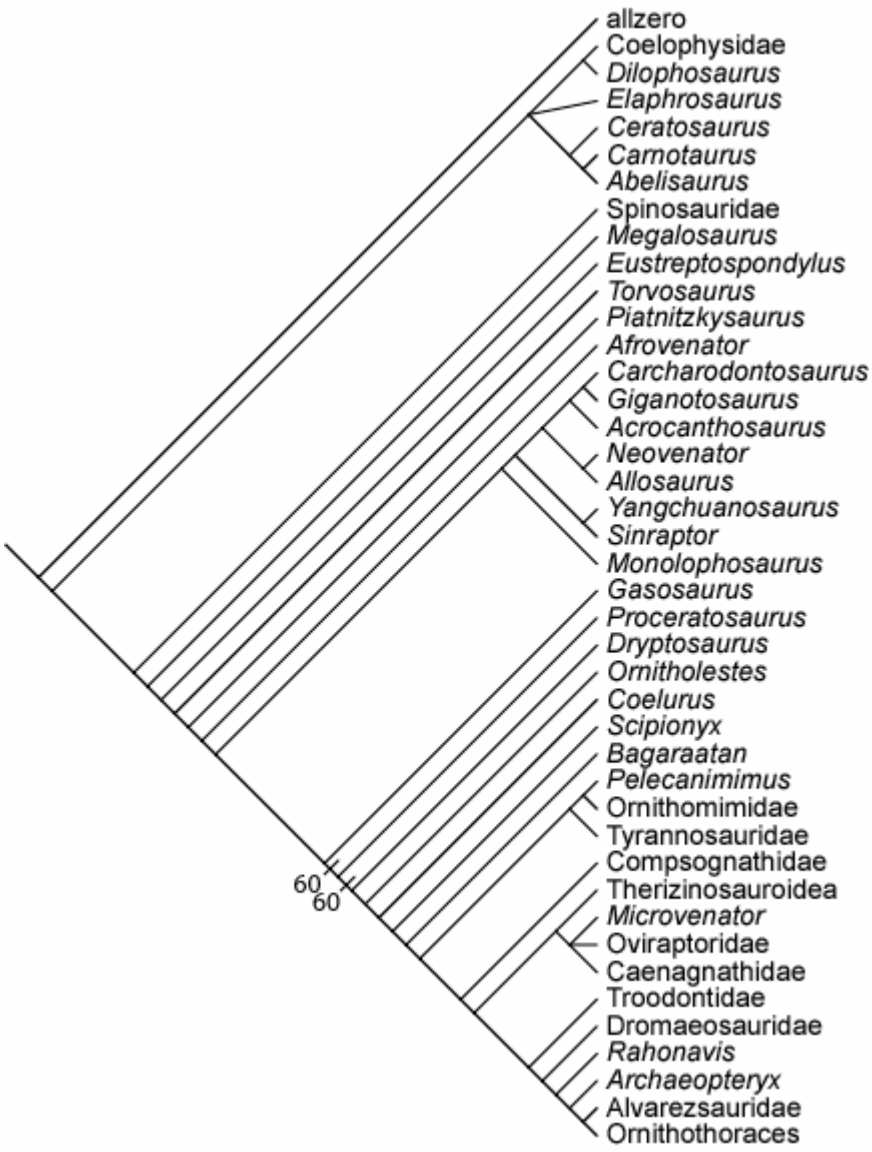

Figure 57. 50% majority rule tree of Holtz's taxa and characters + taxa and characters used in my study.

Character Tracing and Optimization

The combined strict consensus tree was opened in MacClade to investigate character transformations and optimizations. ACCTRAN and DELTRAN could not be applied by MacClade once again owing to the polytomies present in the tree, so any reference to ACCTRAN and DELTRAN below is based on my application of these optimizations.

The distribution of the character states for the median septum of the sphenethmoid dividing the sphenethmoidal fossa (character 1) remains uninformative, the derived condition only being known for *Citipati* (Figure 58). If ACCTRAN optimization is employed, the derived character state is assigned at Compsognathidae onwards, whereas DELTRAN optimizes it as an autapomorphy of Oviraptoridae.

The olfactory bulb position (character 2) is also uninformative, with the derived character state exhibited only in Ornithothoraces (Figure 59). Its occurrence in Alvarezsauridae is equivocal.

The character for the shape of the cerebral hemispheres (character 3) shows the same distribution of states (Figure 60) as the character for the volume of the cerebral hemispheres (character 4) (Figure 61), the character for the width of the endocast (character 5) (Figure 62), and the optic lobe position (character 6) (Figure 63). These distributions show an equivocal state for Compsognathidae, and the derived character state for taxa stemming from node C. Compsognathidae would show the derived character state with ACCTRAN optimization, and the primitive character state with DELTRAN optimization.

Holtz's Data + My Data- Sphenethmoidal Septum Dividing Sphenethmoidal Fossa (Character 1) Resolution

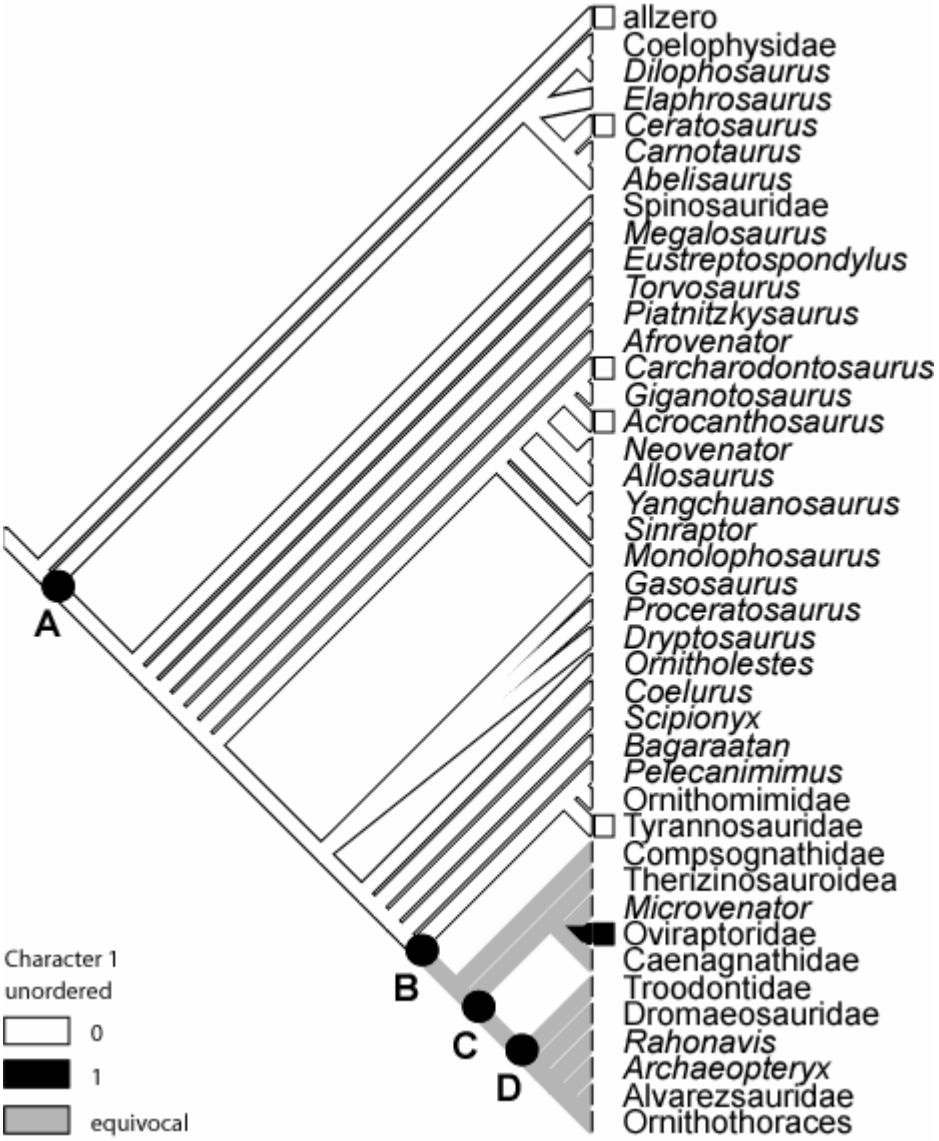

Figure 58. Resolution of character 1 on Holtz's data + my data strict consensus tree.

A, **B**, **C**, and **D** serve to distinguish nodes mentioned in the accompanying text.

Holtz's Data + My Data- Olfactory Bulb Position (Character 2) Resolution

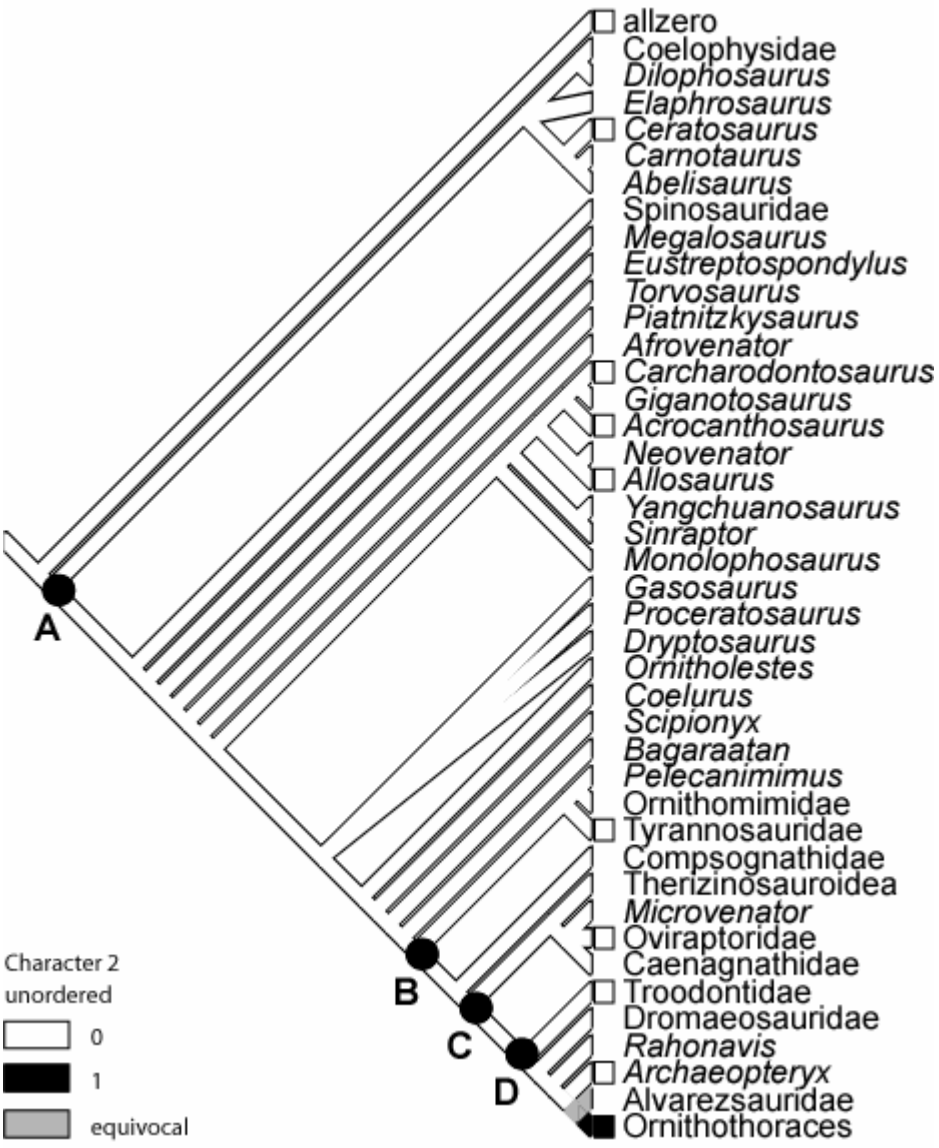

Figure 59. Resolution of character 2 on Holtz's data + my data strict consensus tree.

A, **B**, **C**, and **D** serve to distinguish nodes mentioned in the accompanying text.

Holtz's Data + My Data- Cerebral Hemisphere Shape (Character 3) Resolution

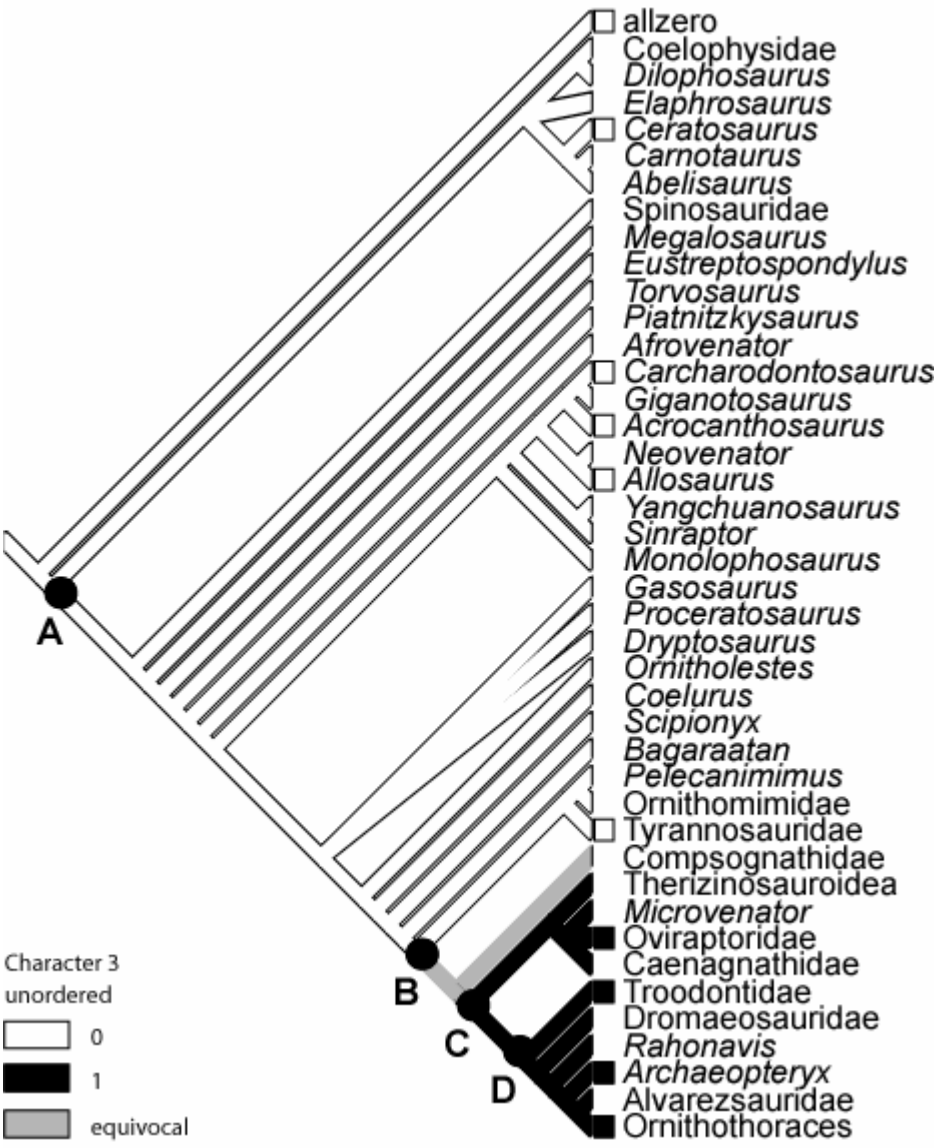

Figure 60. Resolution of character 3 on Holtz's data + my data strict consensus tree.

A, **B**, **C**, and **D** serve to distinguish nodes mentioned in the accompanying text.

Holtz's Data + My Data- Volume of the Cerebral Hemispheres (Character 4) Resolution

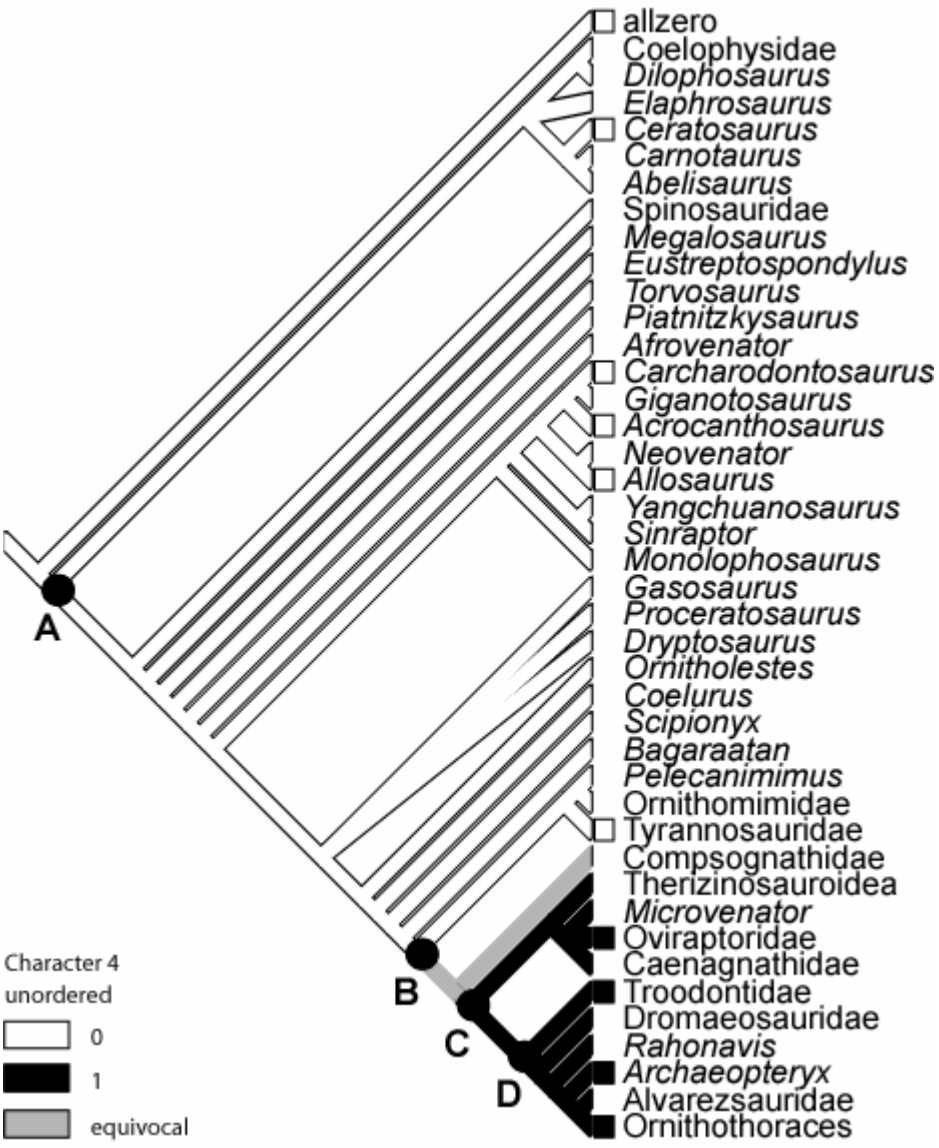

Figure 61. Resolution of character 4 on Holtz's data + my data strict consensus tree.

A, **B**, **C**, and **D** serve to distinguish nodes mentioned in the accompanying text.

Holtz's Data + My Data- Width of Endocast (Character 5) Resolution

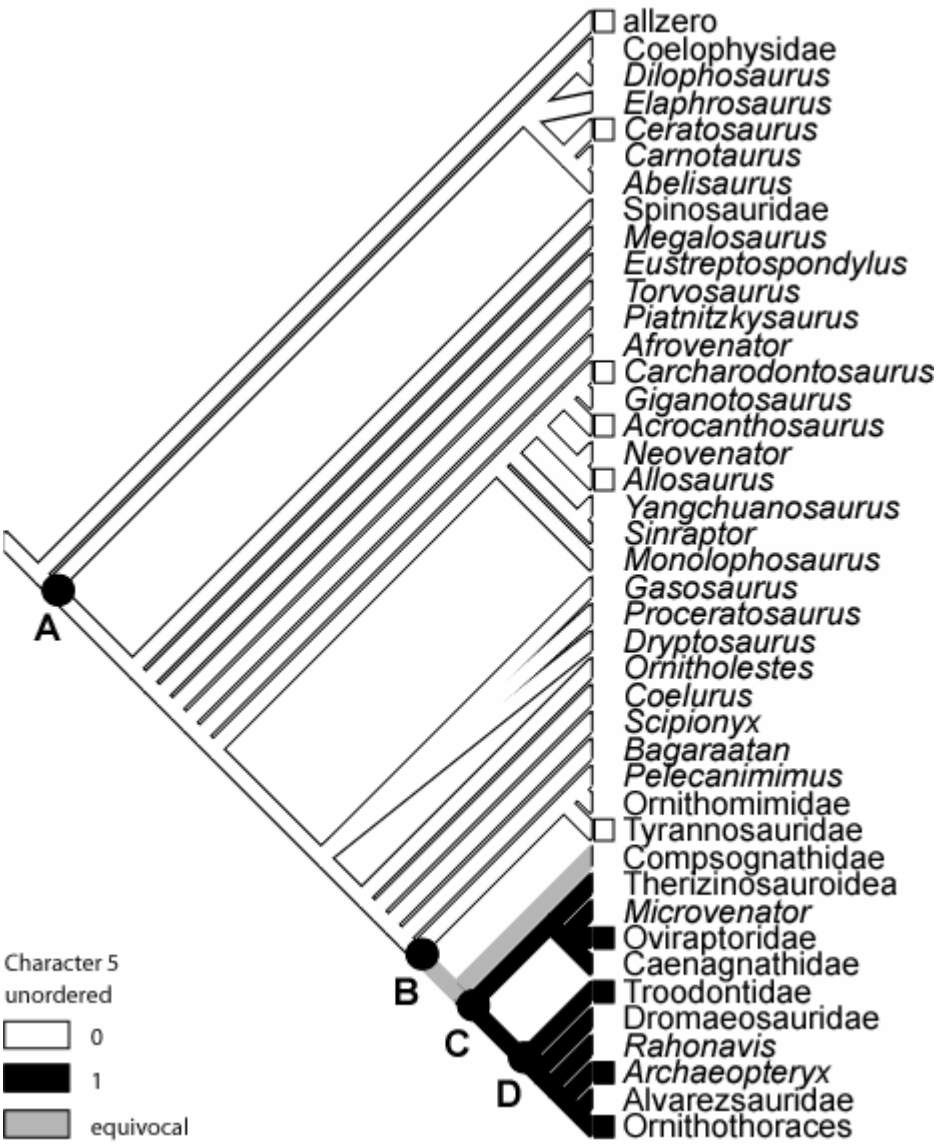

Figure 62. Resolution of character 5 on Holtz's data + my data strict consensus tree.

A, **B**, **C**, and **D** serve to distinguish nodes mentioned in the accompanying text.

Holtz's Data + My Data- Optic Lobe Position (Character 6) Resolution

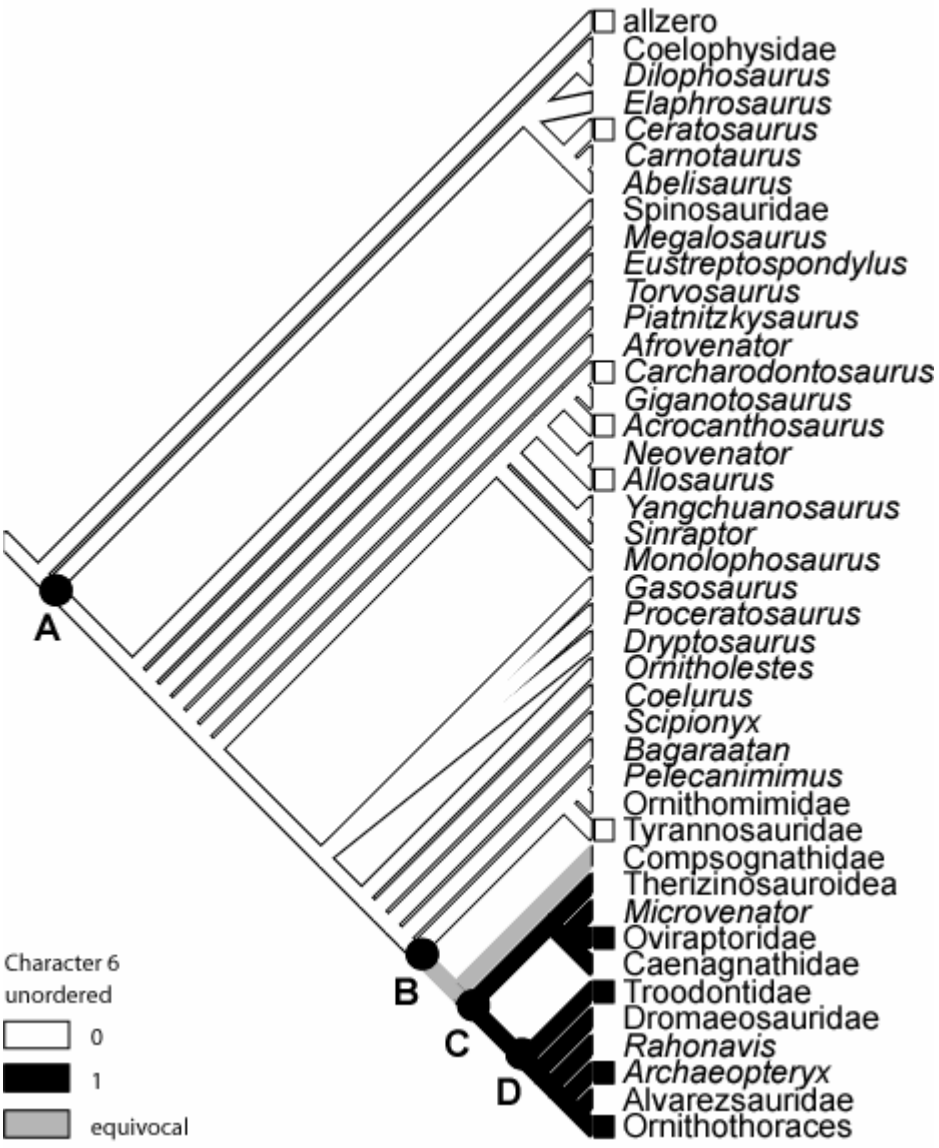

Figure 63. Resolution of character 6 on Holtz's data + my data strict consensus tree.

A, **B**, **C**, and **D** serve to distinguish nodes mentioned in the accompanying text.

The number of trigeminal nerve foramina (character 7) exhibits very little consistency on the tree, with the exception of taxa stemming from node D, which are optimized with the derived character state (Figure 64). The clade containing *Allosaurus, Acrocanthosaurus,* and *Carcharodontosaurus* shows both states, indicating homoplasy. The same is true for the Ornithomimidae/Tyrannosauridae clade. As it now stands this character is not very useful, but scoring of this character in other taxa may help to clarify where the character state transitions occur.

The abducens nerve canal (character 8) also has low consistency, with only the taxa stemming from node B showing no homoplasy and the derived character state (Figure 65). One area containing conflicting character states, as with character 7, is the clade containing *Allosaurus, Acrocanthosaurus,* and *Carcharodontosaurus*. *Allosaurus* and *Carcharodontosaurus* exhibit the primitive character state, while *Acrocanthosaurus* shows the derived character state.

Holtz's internal carotid canals (character 91), which is the same as character 9 in my data matrix, contains a large equivocal area in the central portion of the tree because of the contradictory states seen in the Ornithomimidae/Tyrannosauridae clade (Figure 66). The derived character state is found in taxa stemming from node C, with the exception of the equivocation found within Ornithothoraces.

The floccular fossa (character 10) nearly shows complete consistency on the cladogram, with all of the taxa stemming from node A having the derived

Holtz's Data + My Data- Number of Trigeminal Nerve Foramina (Character 7) Resolution

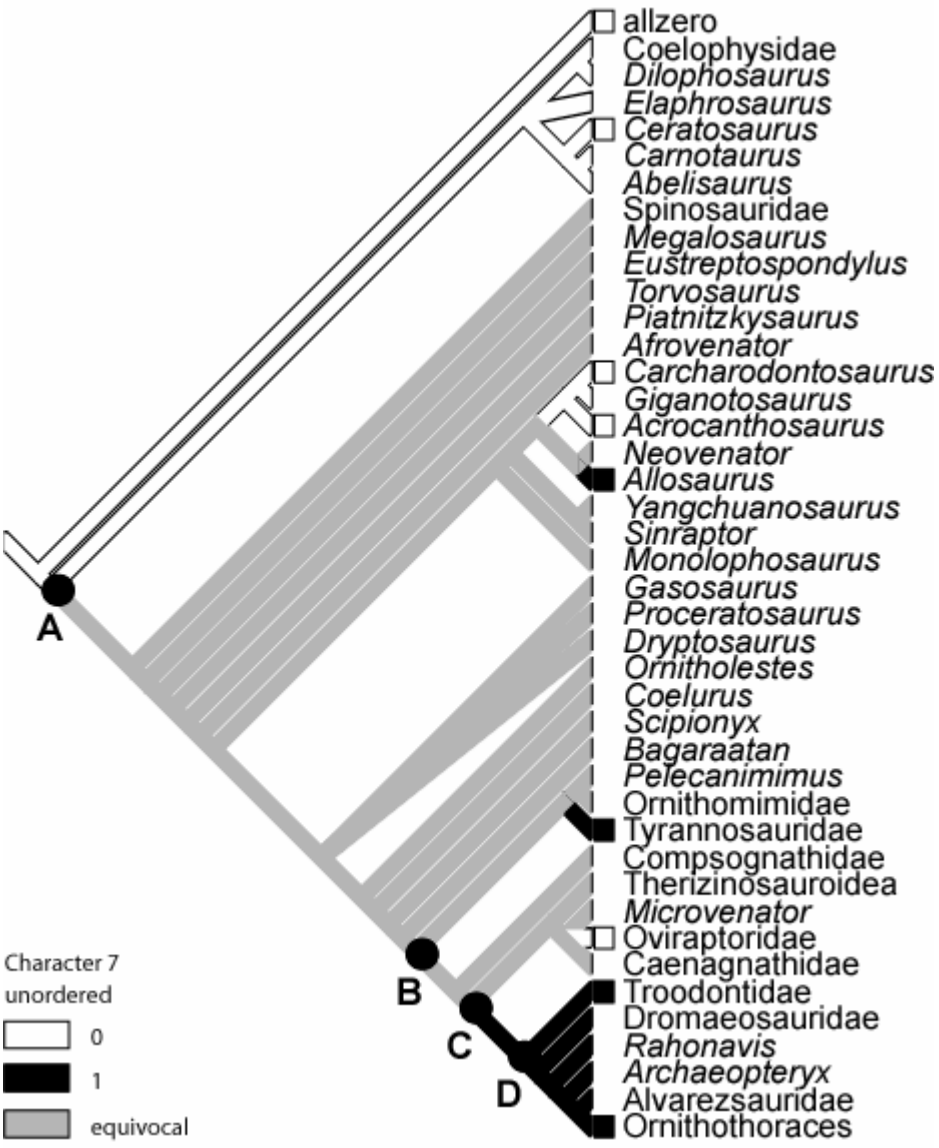

Figure 64. Resolution of character 7 on Holtz's data + my data strict consensus tree.

A, **B**, **C**, and **D** serve to distinguish nodes mentioned in the accompanying text.

Holtz's Data + My Data- Abducens Nerve Canal (Character 8) Resolution

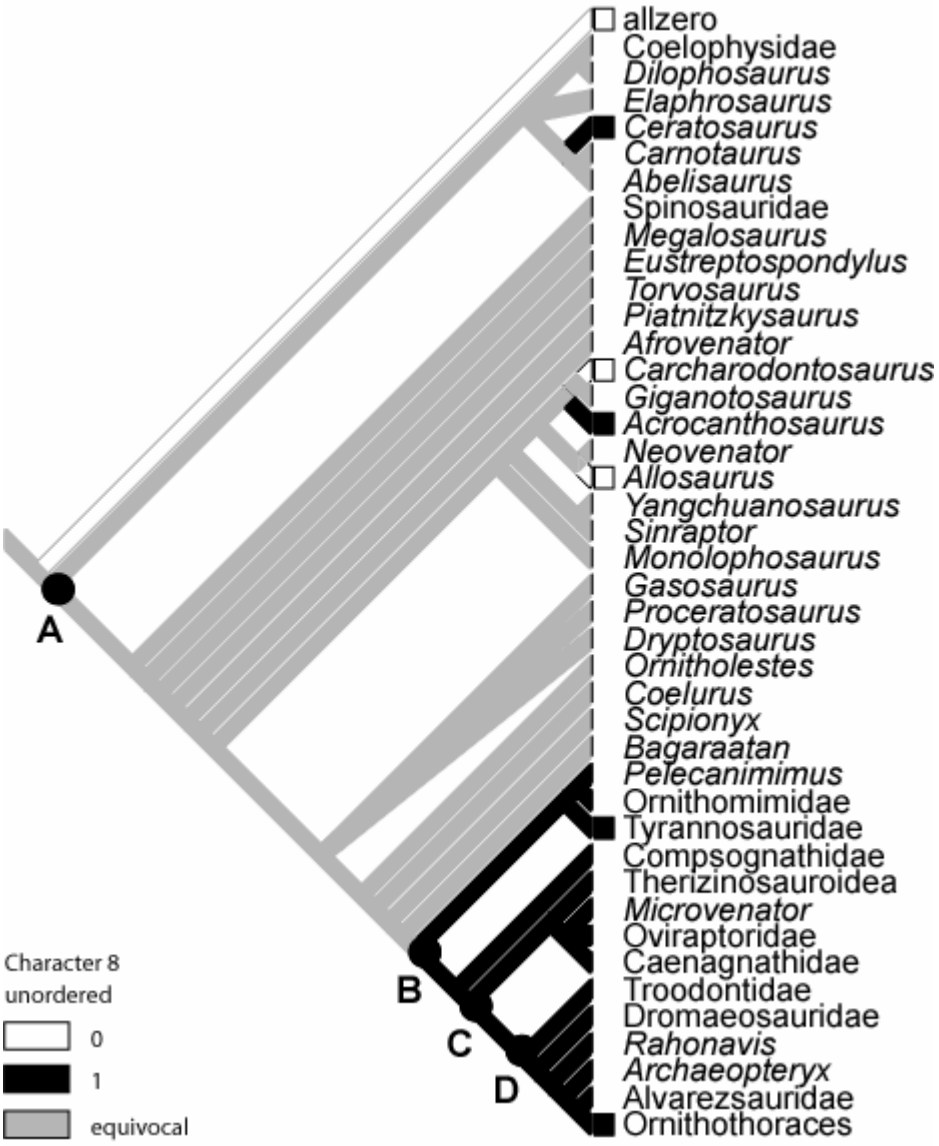

Figure 65. Resolution of character 8 on Holtz's data + my data strict consensus tree.

A, **B**, **C**, and **D** serve to distinguish nodes mentioned in the accompanying text.

Holtz's Data + My Data- Internal Carotid Canals (Holtz's Character 91/My Character 9) Resolution

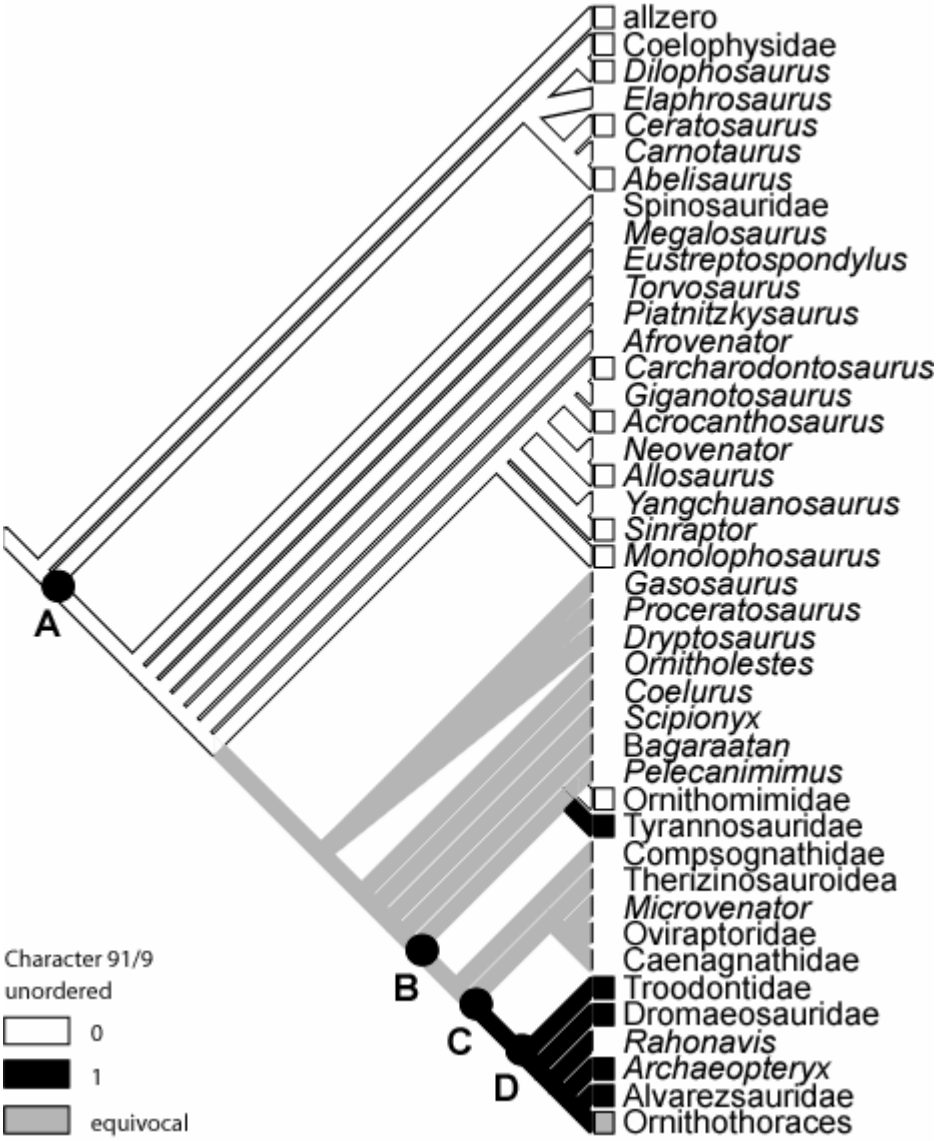

Figure 66. Resolution of Holtz's character 91/my character 9 on Holtz's data + my data strict consensus tree.

A, **B**, **C**, and **D** serve to distinguish nodes mentioned in the accompanying text.

character state, except for the equivocation found in Ornithothoraces (Figure 67). The floccular lobe shape (character 11) (Figure 68), and the posterior semicircular canal orientation (character 12) (Figure 69), both show the same distribution of character states as characters 3-6. This distribution is the primitive state through Tyrannosauridae, an equivocal state in Compsognathidae, and taxa stemming from node C with the derived character state. The ACCTRAN and DELTRAN optimizations are also the same, with Compsognathidae having the derived character state in ACCTRAN, and the primitive character state in DELTRAN.

The distribution of the character states for the number of hypoglossal nerve foramina (character 13) is also the same as for characters 3-6 and 11-12, with one exception (Figure 70). In character 13, the derived character state is found in *Carcharodontosaurus,* whereas the primitive character state is found in this taxon for the other characters. This derived state in *Carcharodontosaurus* leads to an equivocal optimization in *Giganotosaurus* because of the primitive state found in *Acrocanthosaurus*.

The REQ character states (character 14) are unequivocal on most of the tree, with nearly all of the taxa showing the primitive state (Figure 71). The Ornithomimidae/Tyrannosauridae clade shows equivocation for *Pelecanimimus* and Ornithomimidae, and the derived character state for Tyrannosauridae. The state for Ornithothoraces is equivocal. Although not present in this study, there is a troodontid (*Troodon formosus*) and an ornithomimid (*Dromiceiomimus brevitertius*) that have endocast REQs within the derived range (Hurlburt, 1996).

Holtz's Data + My Data- Floccular Fossa (Character 10) Resolution

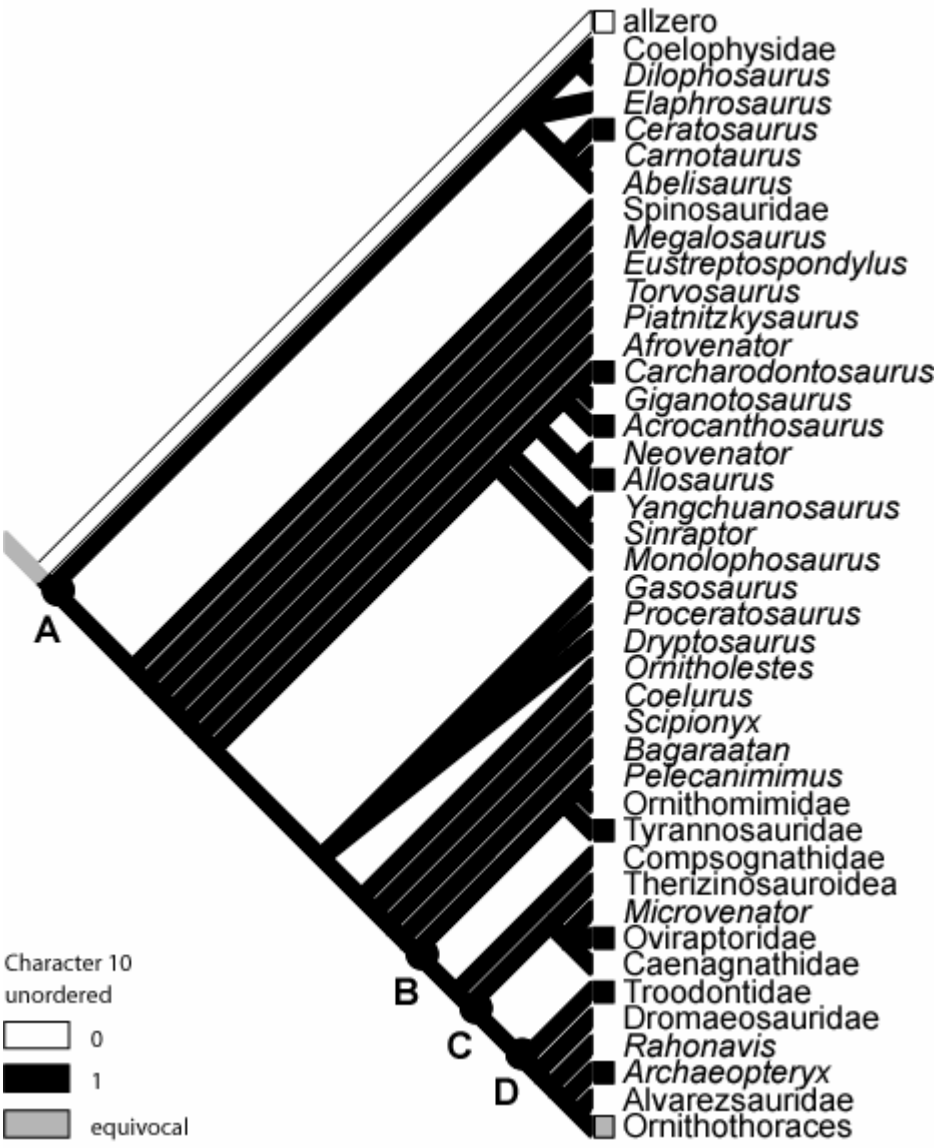

Figure 67. Resolution of character 10 on Holtz's data + my data strict consensus tree.

A, **B**, **C**, and **D** serve to distinguish nodes mentioned in the accompanying text.

Holtz's Data + My Data- Floccular Lobe Shape (Character 11) Resolution

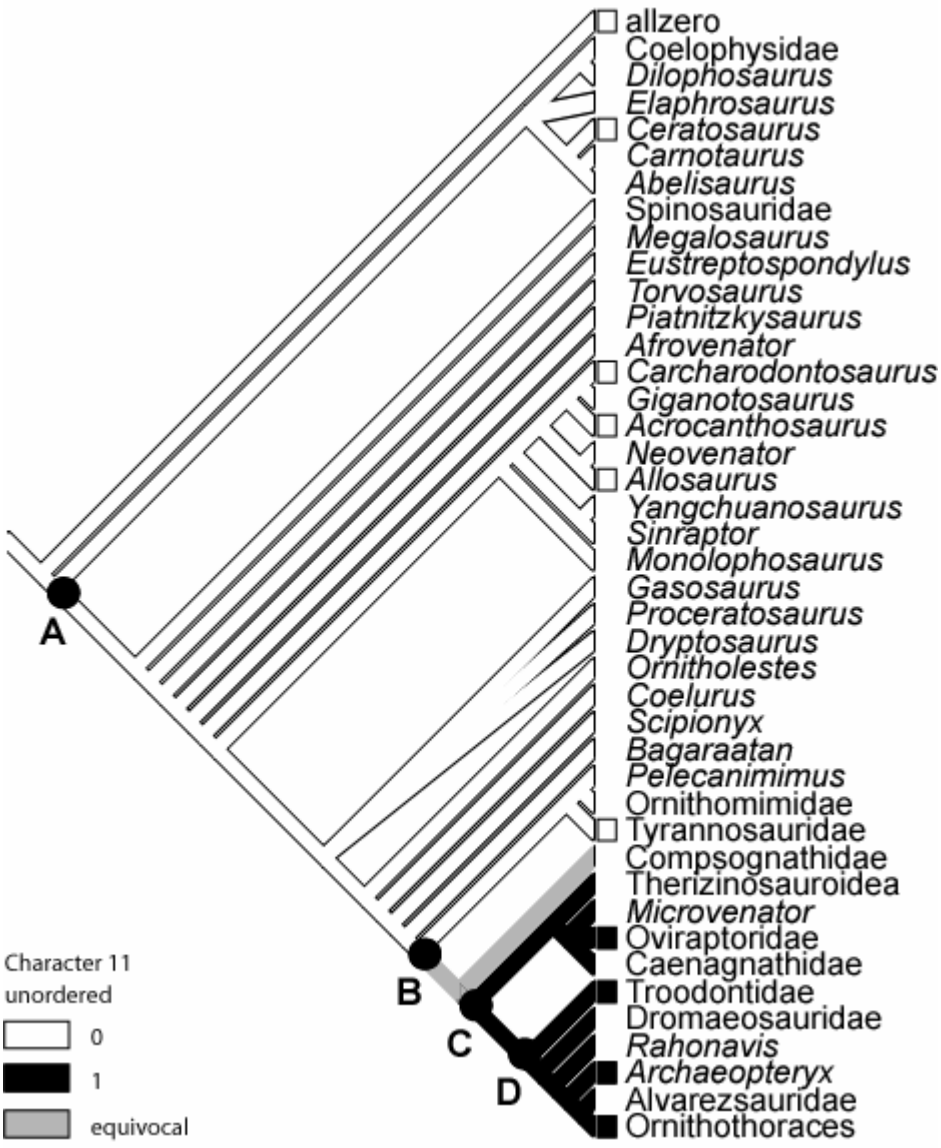

Figure 68. Resolution of character 11 on Holtz's data + my data strict consensus tree.

A, **B**, **C**, and **D** serve to distinguish nodes mentioned in the accompanying text.

Holtz's Data + My Data- Posterior Semicircular Canal Orientation (Character 12) Resolution

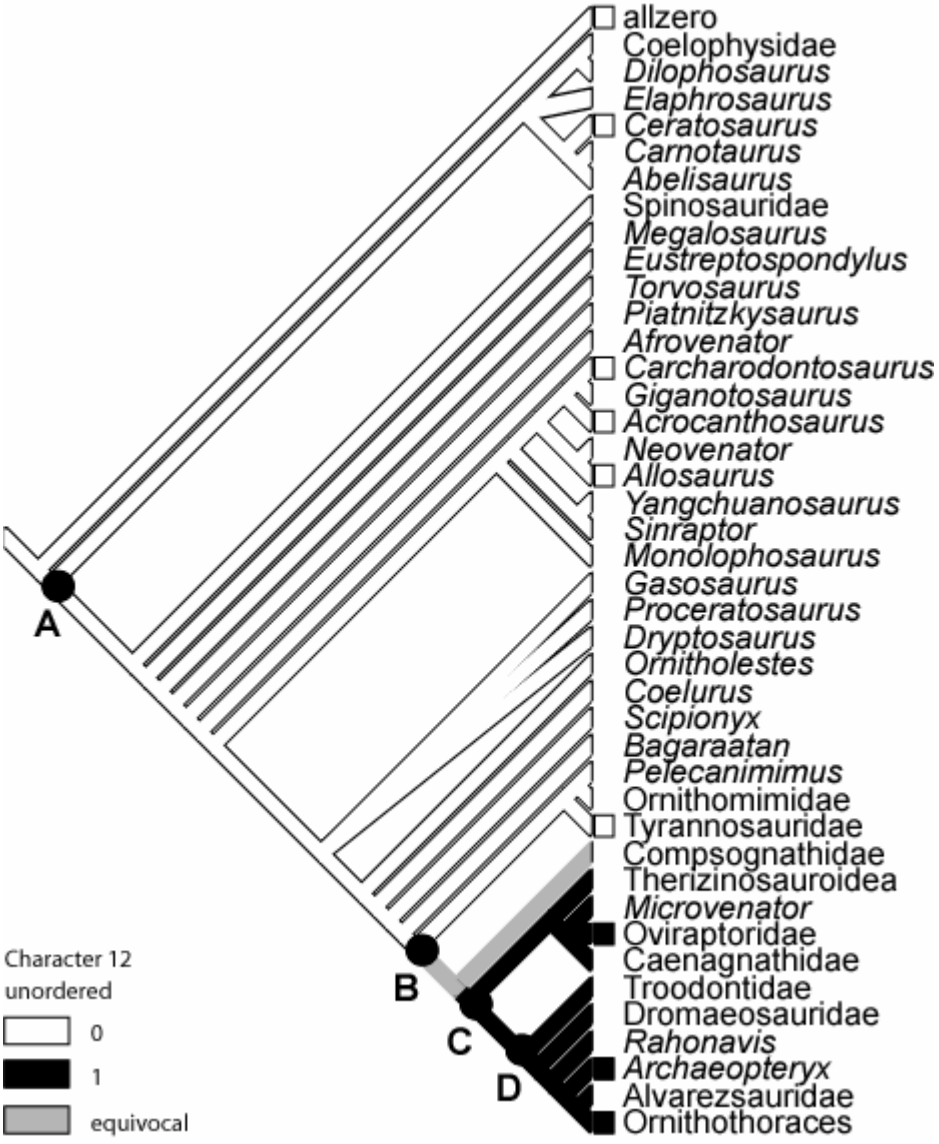

Figure 69. Resolution of character 12 on Holtz's data + my data strict consensus tree.

A, **B**, **C**, and **D** serve to distinguish nodes mentioned in the accompanying text.

Holtz's Data + My Data- Number of Hypoglossal Nerve Foramina (Character 13) Resolution

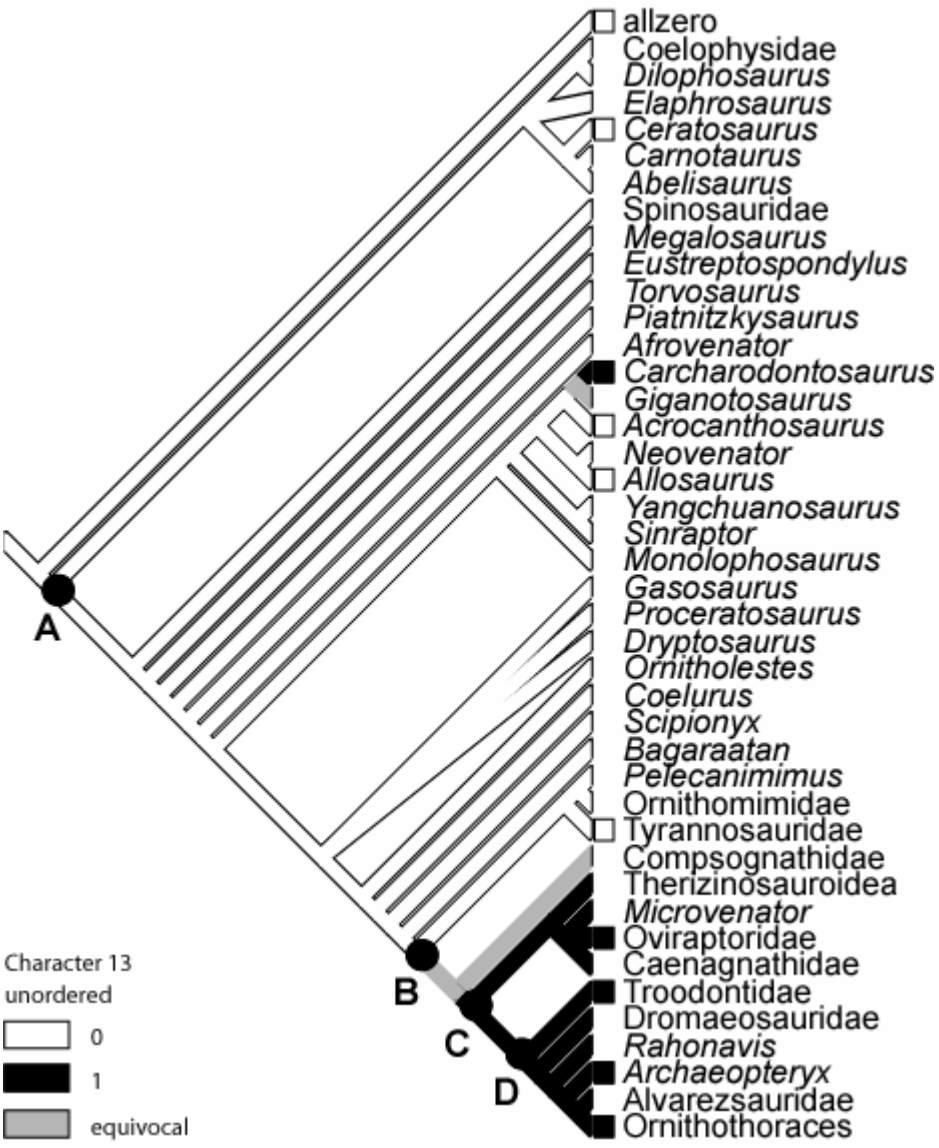

Figure 70. Resolution of character 13 on Holtz's data + my data strict consensus tree.

A, **B**, **C**, and **D** serve to distinguish nodes mentioned in the accompanying text.

Holtz's Data + My Data- Reptile Encephalization Quotient (Character 14) Resolution

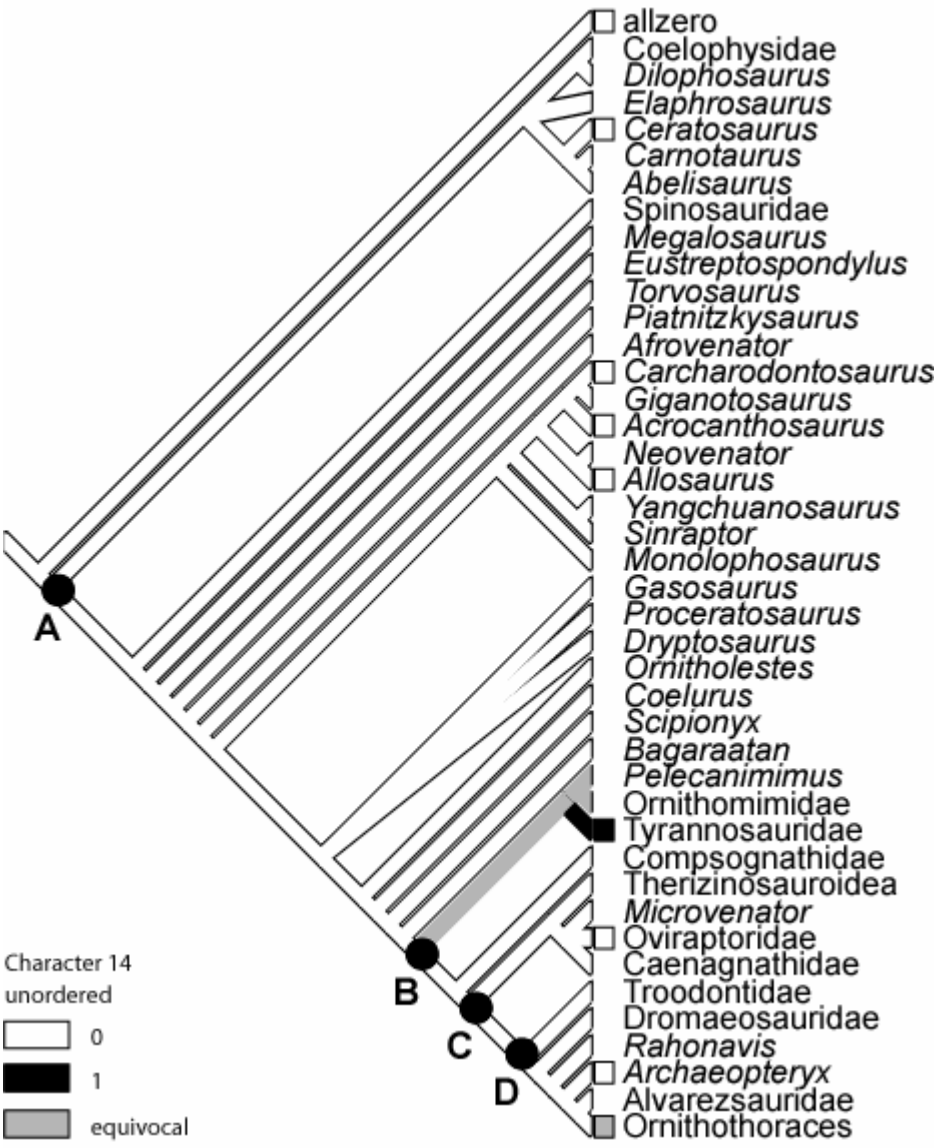

Figure 71. Resolution of character 14 on Holtz's data + my data strict consensus tree.

A, **B**, **C**, and **D** serve to distinguish nodes mentioned in the accompanying text.

Rauhut's Data + My Data

In the third analysis I used Rauhut's (2003) phylogenetic tree and data matrix, which contained 47 ingroup taxa (in its final run by Rauhut) and 224 characters. As in the analysis with Holtz's data, I reran the matrix to verify the original data and parameters. One difference in the settings I used versus Rauhut's analysis was that I ran only 30 replicates instead of 100 to expedite the analysis. Even with this change, the same number of equally most-parsimonious trees, 5,544, was obtained. There was a difference in the number of steps required, however. The original analysis was reported by Rauhut to be 652 steps, whereas my analysis resulted in 750 steps. Despite this difference, the strict consensus tree is the same for both (Figure 72). The tree was opened in MacClade, and a C.I. of 0.42, an R.I. of 0.75, and an R.C. of 0.32 were obtained.

After I verified the original tree, my endocranial characters were added to Rauhut's data matrix. Some changes and deletions were necessary. First, Rauhut's cerebral hemisphere shape character (character 64), and mine (character 3) were basically the same, so my character was left out of the analysis. Also, Rauhut's EQ character (character 63) used Jerison's EQ equation, which I consider unreliable, so it was deleted from the matrix. Some of my taxa also had to be combined, deleted, or referred to a more inclusive taxon. All the bird taxa and *Archaeopteryx* were combined as Aves. *Majungatholus* was under the heading Abelisauridae. *Carcharodontosaurus* and *Acrocanthosaurus* were in Carcharodontosauridae. *Citipati* was within Oviraptorosauria. Lastly,

Rauhut's Data + My Data- Strict Consensus Tree

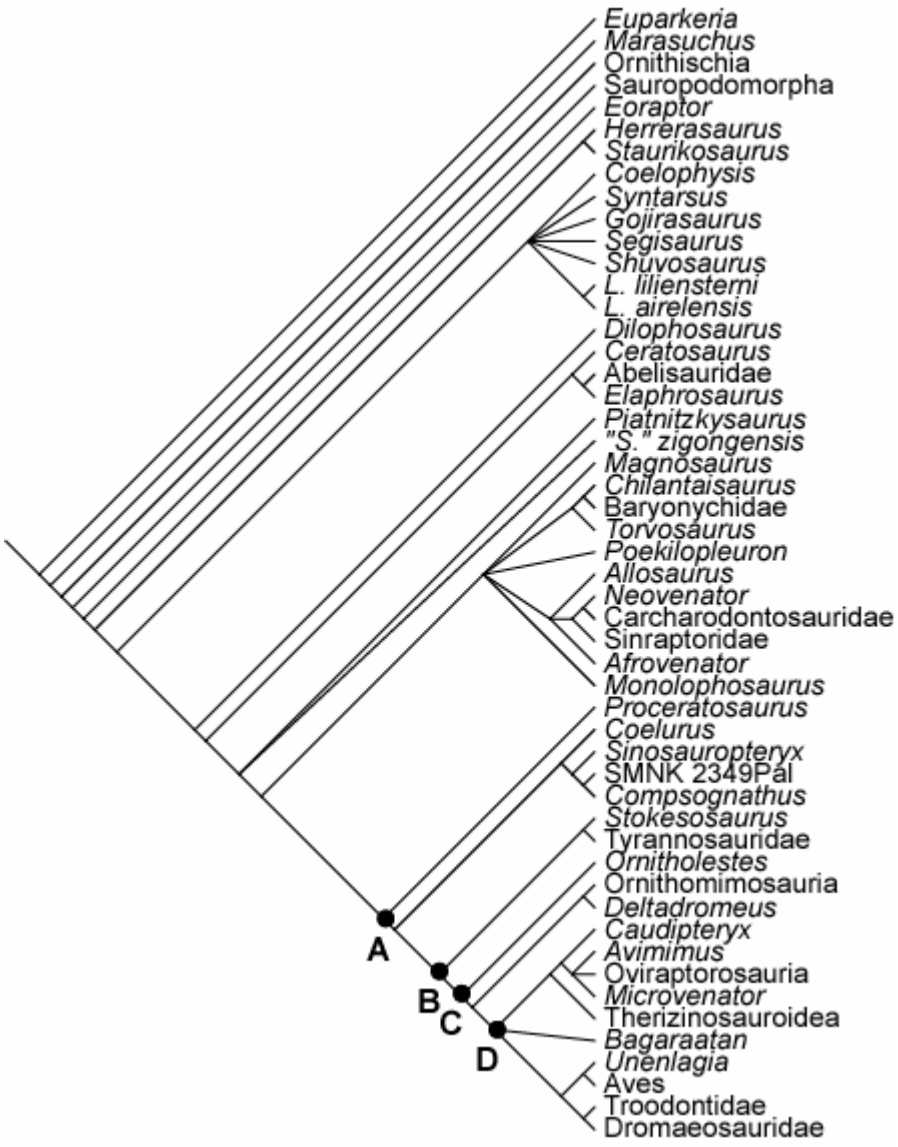

Figure 72. Strict consensus tree of Rauhut's taxa and characters + taxa and characters used in my study.

A, **B**, **C**, and **D** serve to distinguish nodes mentioned in the accompanying text.

Byronosaurus, Mongolodon, and the Zos Canyon troodontid were combined under Troodontidae.

Once these changes were made, I reran the data using the same parameters as Rauhut with the exception of running only 30 replicates. The same 5,544 trees were found, with a length of 767 steps. The strict consensus tree is also the same. The only change to the measurements performed in MacClade was in the C.I., which went from 0.42 to 0.43. A 50% majority tree was also retained to examine the differences between it and the strict consensus tree (Figure 73). The 50% majority tree did show some slight resolution in two of the polytomies found in the strict consensus tree. The lower polytomy, which contained, among other taxa, *Syntarsus*, was slightly resolved. *Liliensternus liliensterni* and *L. airelensis* were still found together 100% of the time, but they were now a sister group to the rest of the taxa in the polytomy 82% of the time. Within this smaller polytomy, *Coelophysis* and *Syntarsus* were placed together 82% of the time. Some resolution was also gained in the polytomy that contains *Poekilopleuron*. The resolution gained was the movement of *Magnosaurus* to become the closest outgroup to (*Torvosaurus* (*Chilantaisaurus*, Baryonychidae)) 71% of the time, and the movement of *Monolophosaurus* to become the closest outgroup to the clade containing *Allosaurus* 71% of the time. Other than these few things, no other changes were found.

Rauhut's Data + My Data- 50% Majority Rule Tree

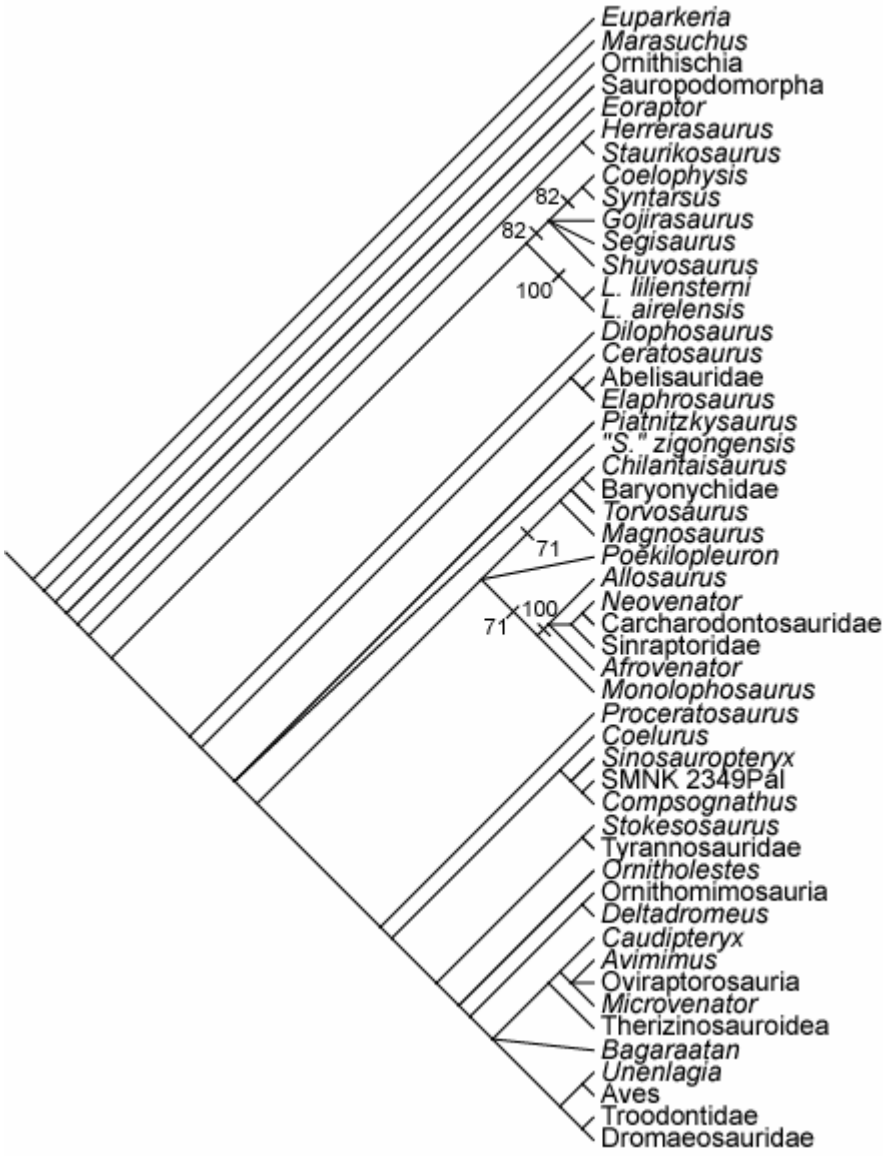

Figure 73. 50% majority rule tree of Rauhut's taxa and characters + taxa and characters used in my study.

Character Tracing and Optimization

I opened the strict consensus tree based on the combined data in MacClade to allow character tracing and optimization. Once again, ACCTRAN and DELTRAN could not be performed by MacClade owing to the polytomies present in the tree.

The distribution of the character states for the median septum of the sphenethmoid dividing the sphenethmoidal fossa (character 1) shows resolution on the lower portion of the tree, where all the taxa have the primitive character state, but the taxa stemming from node C lack this resolution (Figure 74). The lack of recognition of this character in all the taxa stemming from node C, with the exception of Oviraptorosauria, leads to the equivocation seen.

The olfactory bulb position (character 2) is found in the primitive state throughout the entire tree, except in Aves, which is equivocal (Figure 75). The attainment of the derived state occurs somewhere between *Archaeopteryx* and modern birds, but the lack of data on taxa in this area leaves its place of attainment on the cladogram uncertain.

Rauhut's character on the shape of the cerebral hemispheres (Character 64), which is basically the same as my character 3, shows largely unequivocal optimization of the primitive and derived character states (Figure 76). The primitive character state is exhibited in the clades through Tyrannosauridae, and the derived character state is exhibited in the taxa stemming from node D and their sister group. The only area of equivocation is in *Ornitholestes*. ACCTRAN

Rauhut's Data + My Data- Sphenethmoidal Septum Dividing Sphenethmoidal Fossa (Character 1) Resolution

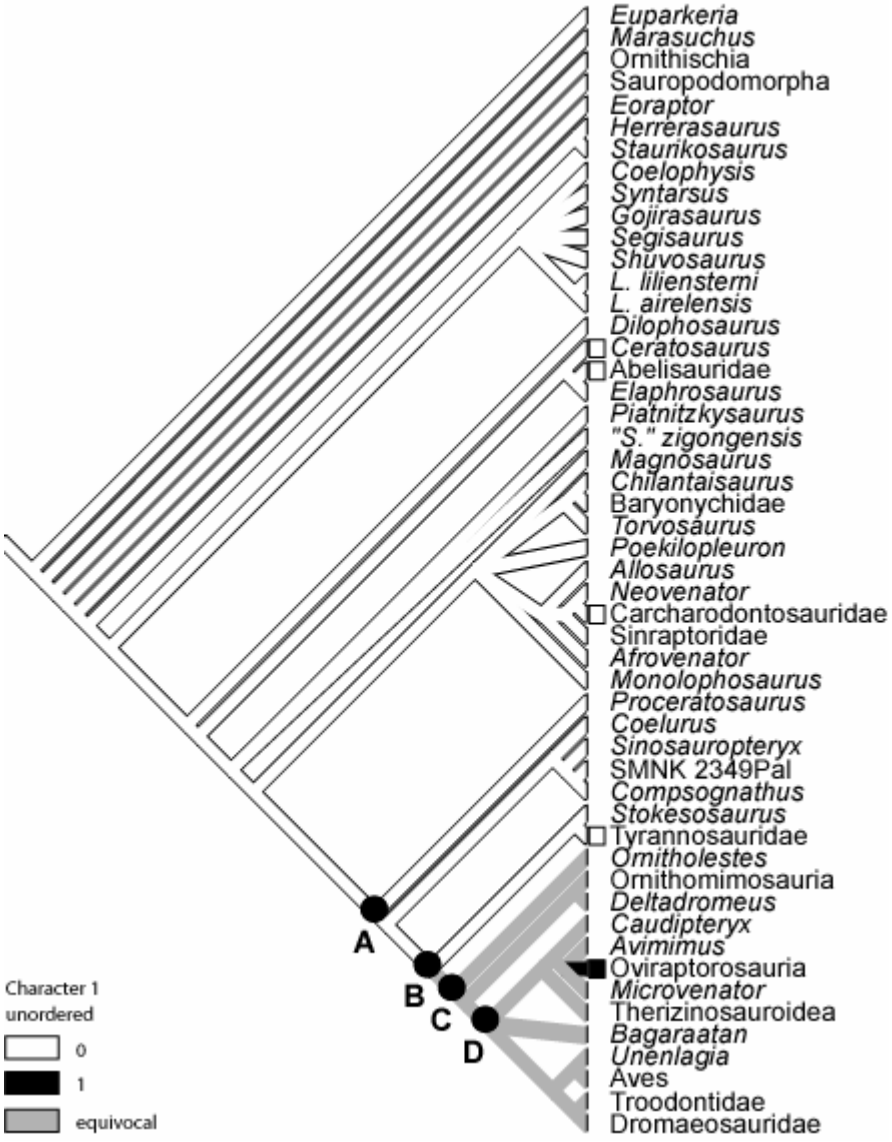

Figure 74. Resolution of character 1 on Rauhut's data + my data strict consensus tree.

A, **B**, **C**, and **D** serve to distinguish nodes mentioned in the accompanying text.

Rauhut's Data + My Data- Olfactory Bulb Position (Character 2) Resolution

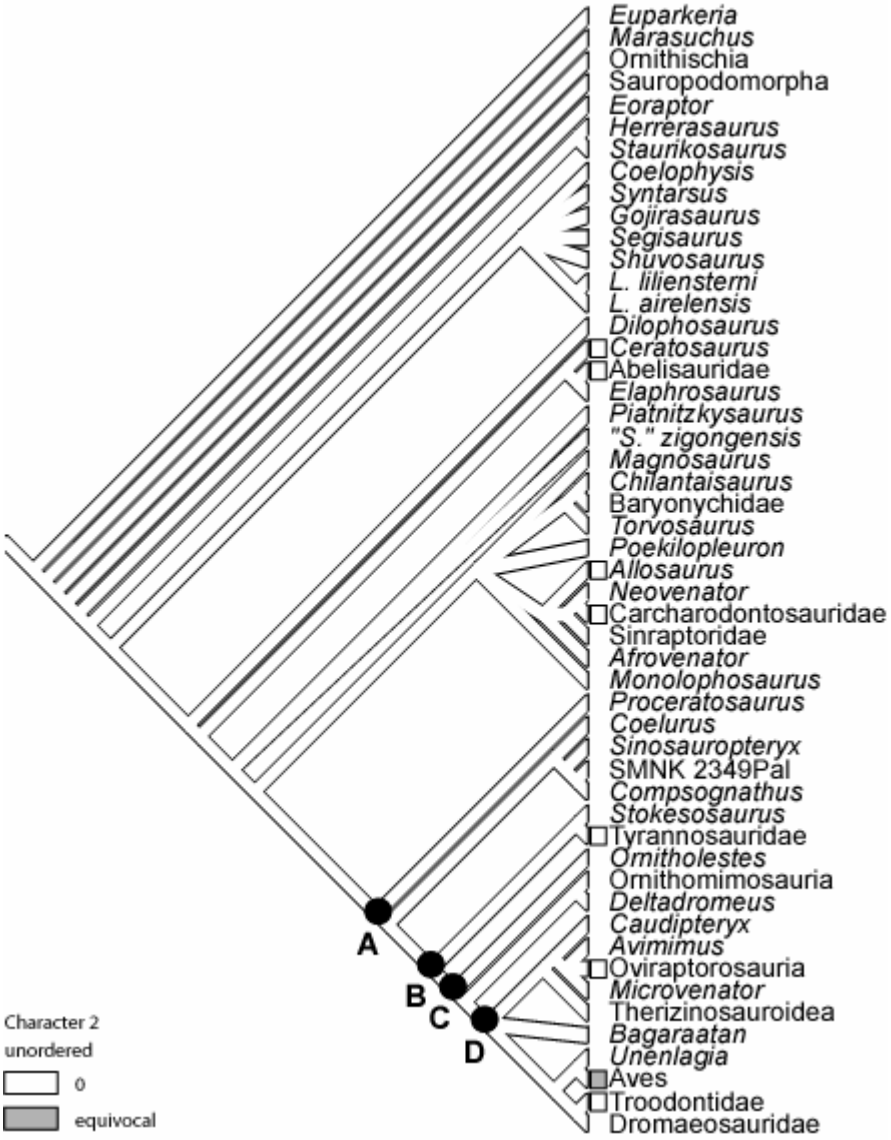

Figure 75. Resolution of character 2 on Rauhut's data + my data strict consensus tree.

A, **B**, **C**, and **D** serve to distinguish nodes mentioned in the accompanying text.

Rauhut's Data + My Data- Cerebral Hemisphere Shape (Rauhut's Character 64/My Character 3) Resolution

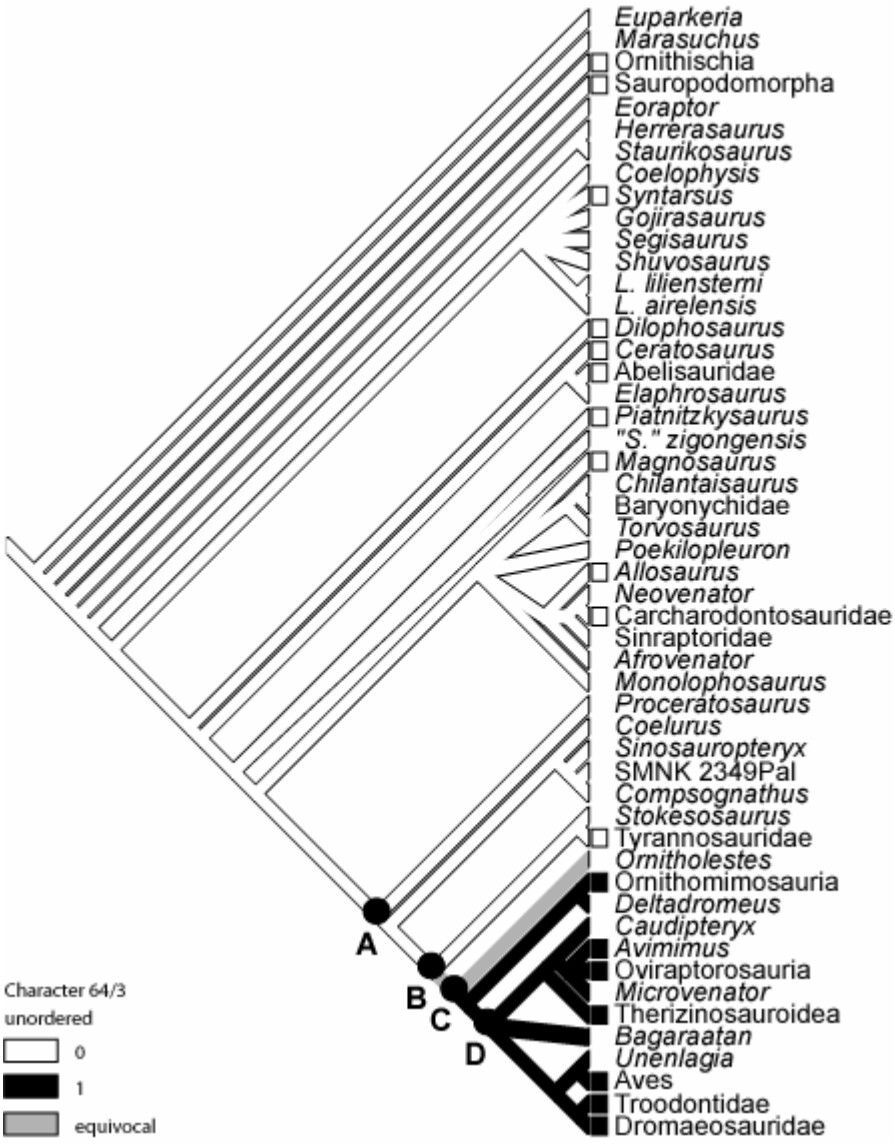

Figure 76. Resolution of Rauhut's character 64/my character 3 on Rauhut's data + my data strict consensus tree.

A, **B**, **C**, and **D** serve to distinguish nodes mentioned in the accompanying text.

optimization would show this taxon with the derived character state, and DELTRAN optimization would show it with the primitive character state.

The volume of the cerebral hemispheres (character 4), width of the endocast (character 5), and optic lobe position (character 6) characters show the same distribution of character states (Figures 77, 78, 79). The primitive character state is found through Tyrannosauridae, the derived character state is found in the taxa stemming from node D, and an equivocal state is found between Tyrannosauridae and the taxa stemming from node D, as well as *Bagaraatan*.

The number of trigeminal nerve foramina (character 7) shows very little consistency. The addition of my data demonstrating the primitive state in the outgroups, however, causes the primitive state to be seen from the bottom of the tree through the branch containing *Ceratosaurus* (Figure 80). The central portion of the tree is hard to unequivocally optimize with the data given. *Allosaurus* and Tyrannosauridae show the derived condition, while Carcharodontosauridae and Oviraptorosauria exhibit the primitive character state. It is not until the clade consisting of Aves, *Unenlagia*, Troodontidae, and Dromaeosauridae is reached that the derived state is consistently present.

The abducens nerve canal character states (character 8) have near total equivocation on the tree (Figure 81). It is not until that taxa stemming from node B that the derived character state is permanently attained. Basal to node B, *Ceratosaurus* exhibits the derived character state, as well as *Acrocanthosaurus* within Carcharodontosauridae. Abelisauridae and *Allosaurus* exhibit the primitive character state, as does *Carcharodontosaurus* within Carcharodontosauridae.

Rauhut's Data + My Data- Volume of the Cerebral Hemispheres (Character 4) Resolution

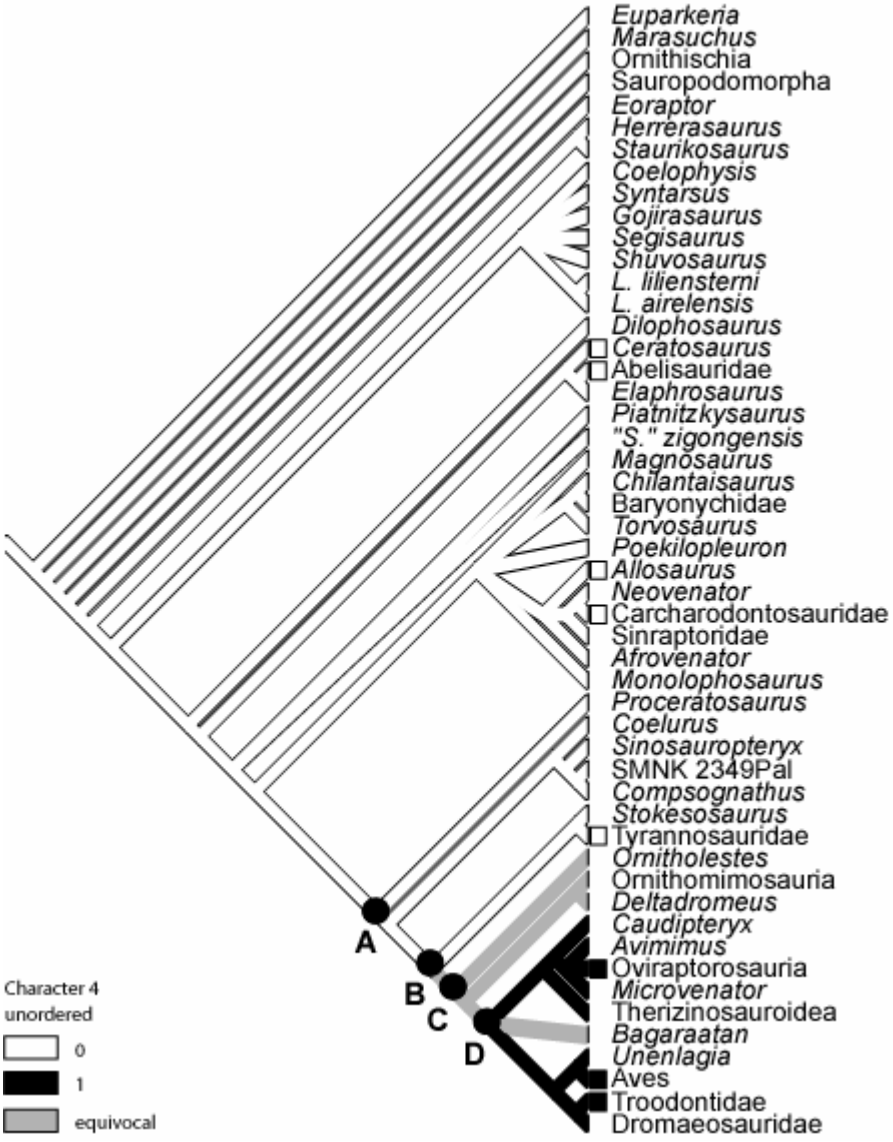

Figure 77. Resolution of character 4 on Rauhut's data + my data strict consensus tree.

A, **B**, **C**, and **D** serve to distinguish nodes mentioned in the accompanying text.

Rauhut's Data + My Data- Width of Endocast (Character 5) Resolution

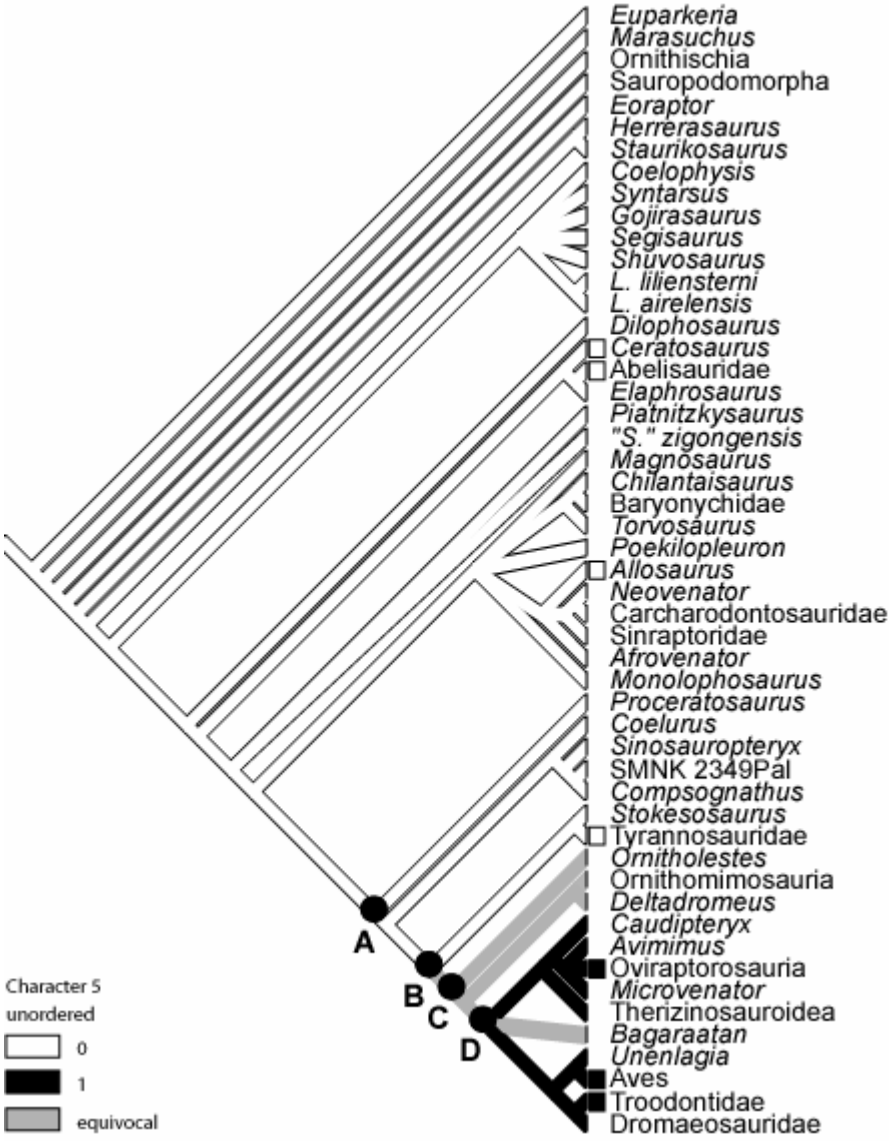

Figure 78. Resolution of character 5 on Rauhut's data + my data strict consensus tree.

A, **B**, **C**, and **D** serve to distinguish nodes mentioned in the accompanying text.

Rauhut's Data + My Data- Optic Lobe Position (Character 6) Resolution

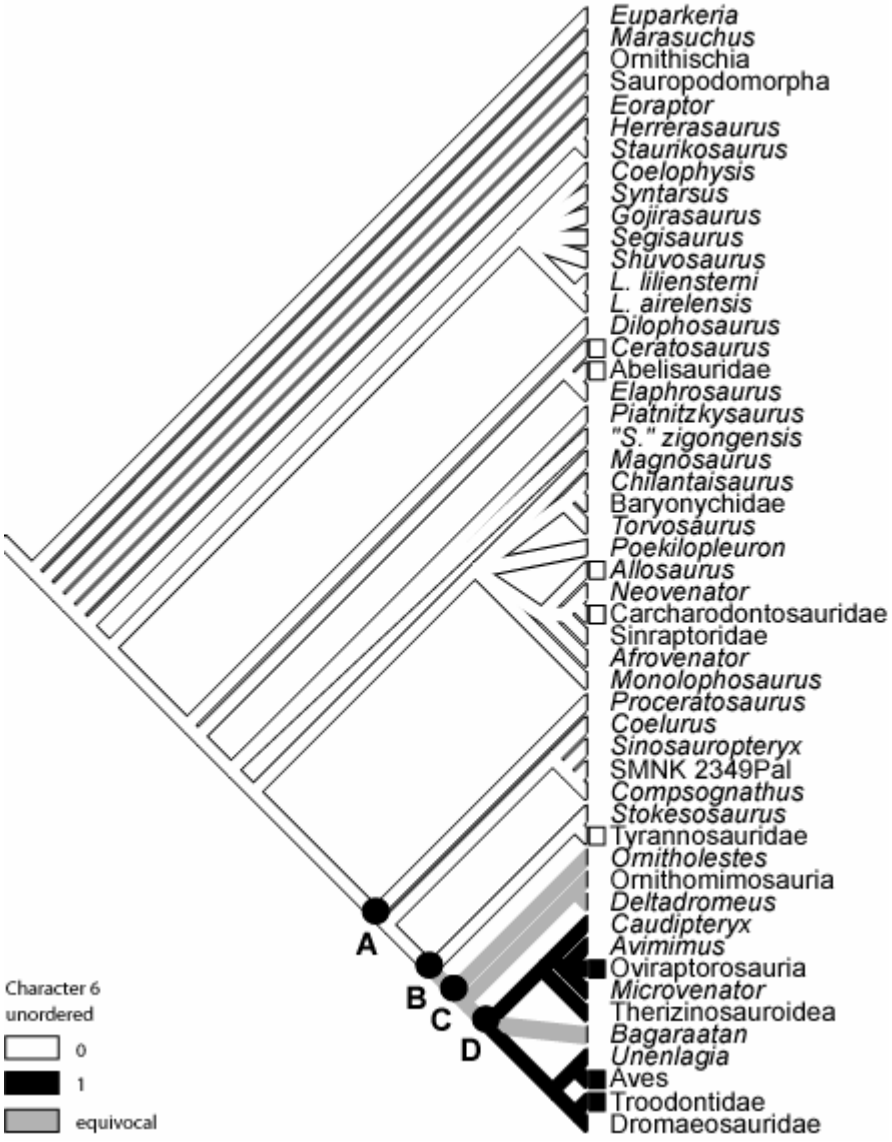

Figure 79. Resolution of character 6 on Rauhut's data + my data strict consensus tree.

A, **B**, **C**, and **D** serve to distinguish nodes mentioned in the accompanying text.

Rauhut's Data + My Data- Number of Trigeminal Nerve Foramina (Character 7) Resolution

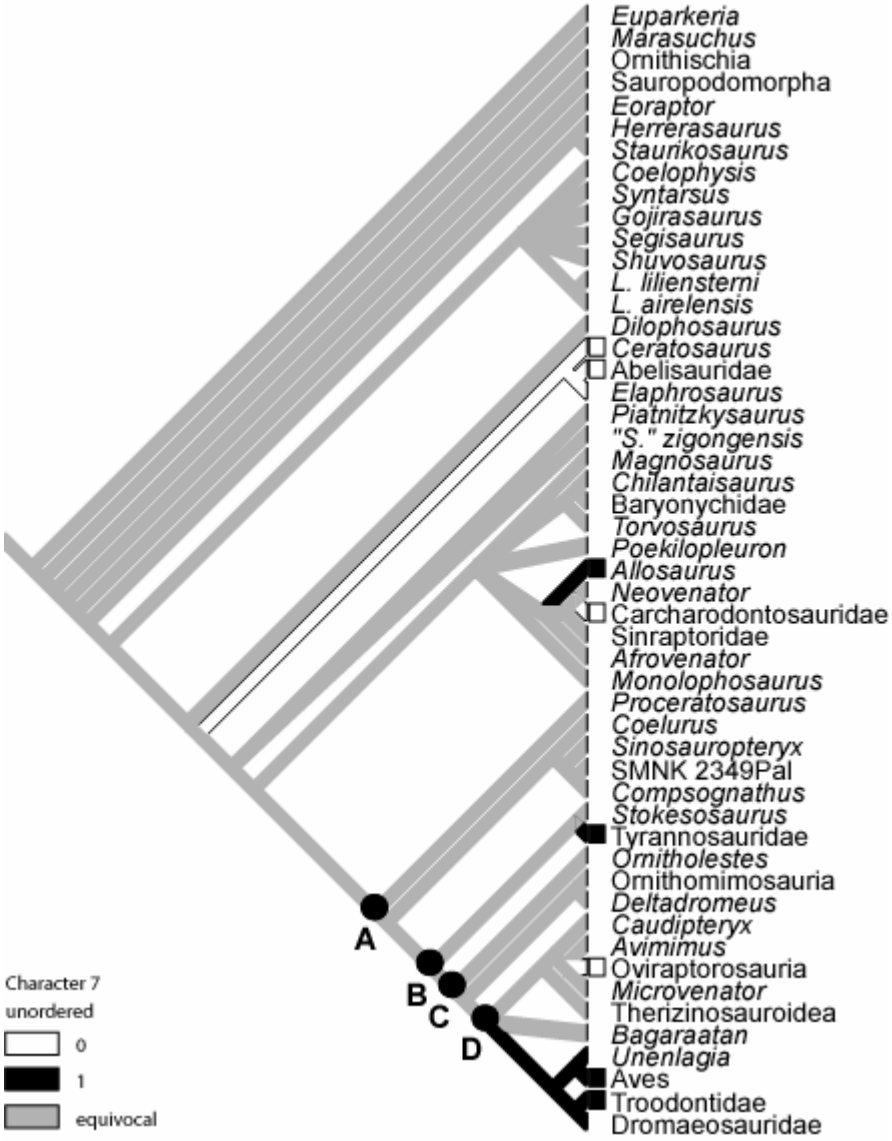

Figure 80. Resolution of character 7 on Rauhut's data + my data strict consensus tree.

A, **B**, **C**, and **D** serve to distinguish nodes mentioned in the accompanying text.

Rauhut's Data + My Data- Abducens Nerve Canal (Character 8) Resolution

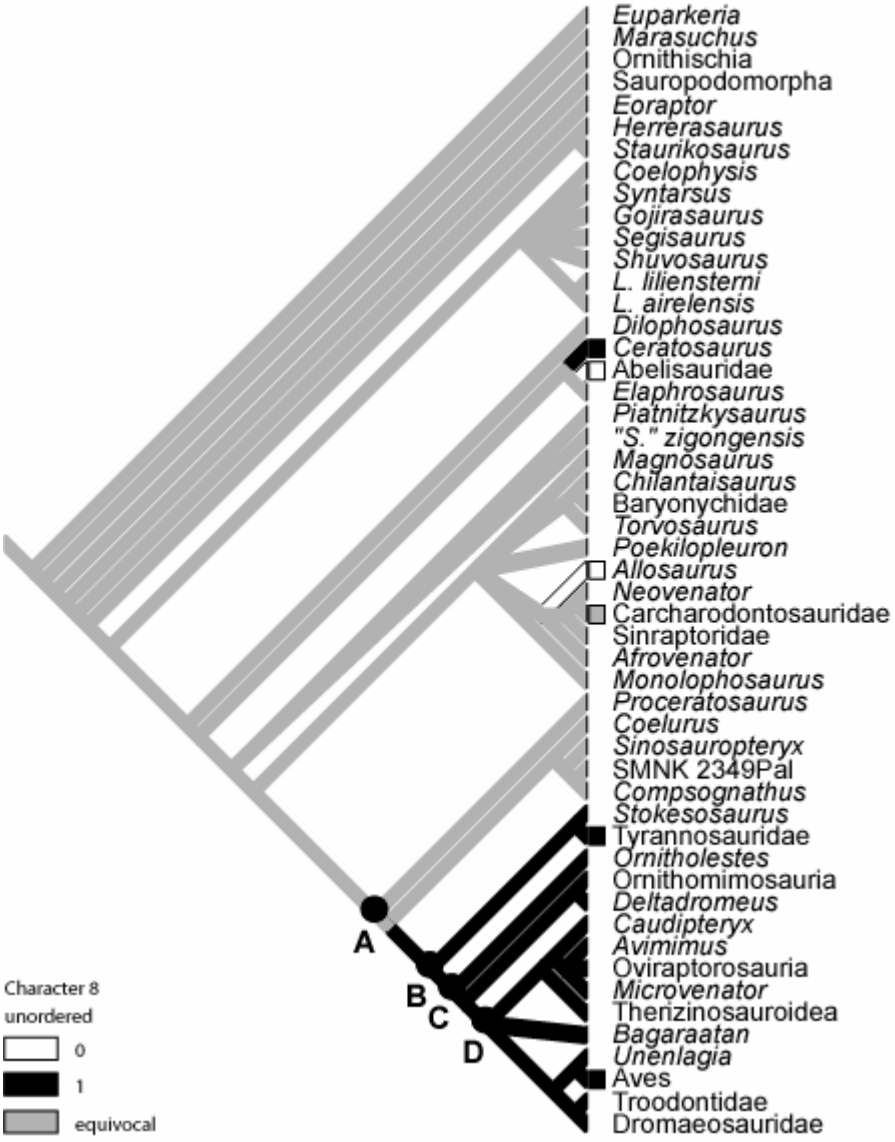

Figure 81. Resolution of character 8 on Rauhut's data + my data strict consensus tree.

A, **B**, **C**, and **D** serve to distinguish nodes mentioned in the accompanying text.

The internal carotid canals character states (character 9) are fairly consistent, with a small area of equivocation between the basal portion of the tree that shows the primitive character state, and taxa stemming from node B, which show the derived character state (Figure 82). There is also equivocation within Aves, because it contains taxa showing both the primitive and derived character states.

The floccular fossa (character 10) is shown in the derived state in most of the taxa given. It is equivocal is seen in Aves, which has both the primitive and derived character states as in character 9 (Figure 83).

The floccular lobe shape (character 11) (Figure 84), and the posterior semicircular canal orientation (character 12) (Figure 85) have the same distributions as characters 4, 5, and 6. The number of hypoglossal nerve foramina (character 13) is fairly consistent, with most of the tree showing the primitive character state until the taxa stemming from node D, which show mostly the derived character state (Figure 86). There is some equivocation in two small areas of the tree. The first area is within Carcharodontosauridae, which contains taxa with the primitive and the derived character states. The second area of equivocation is found in the clades between nodes B and D, and with *Bagaraatan*.

The REQ (character 14) is unequivocally optimized for most of the tree (Figure 87). Two clades show equivocation. The (*Stokesosaurus* + Tyrannosauridae) clade shows equivocation for *Stokesosaurus* and the derived character state for Tyrannosauridae, and Aves exhibits equivocation because it

Rauhut's Data + My Data- Internal Carotid Canals (Character 9) Resolution

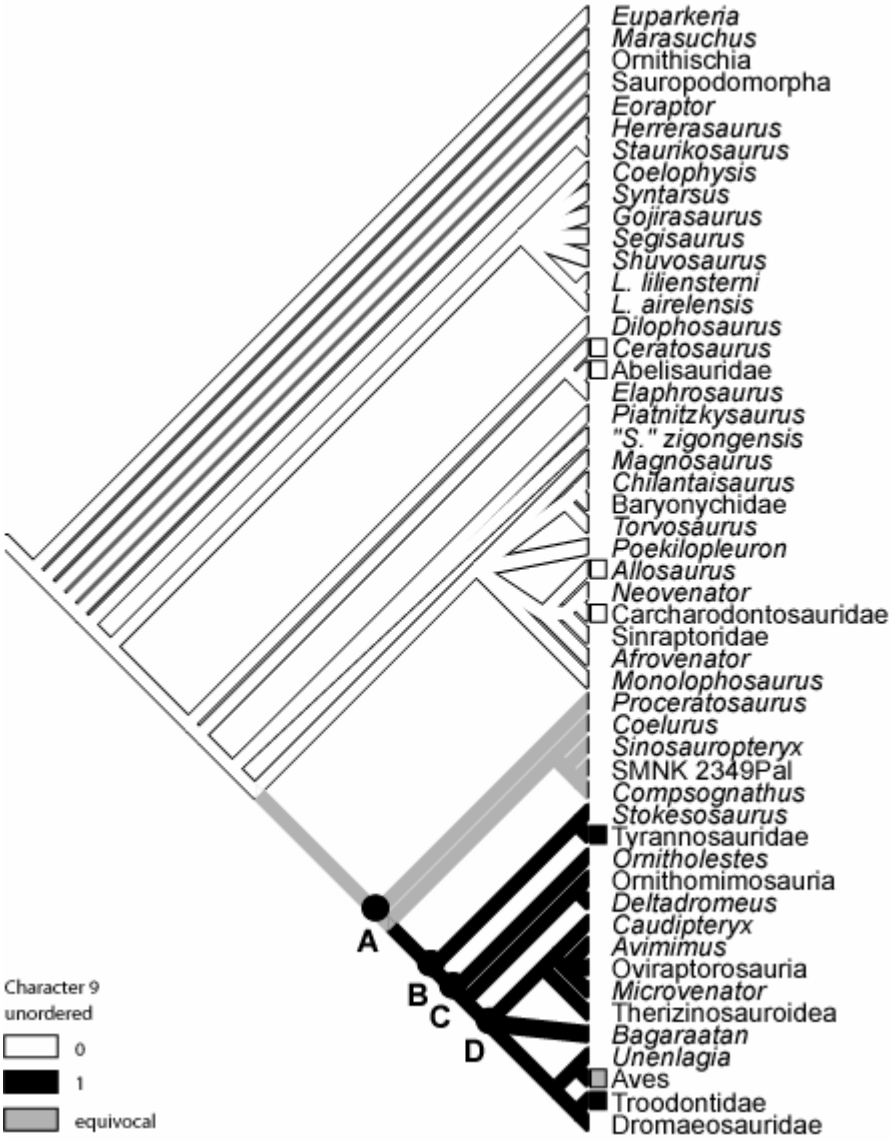

Figure 82. Resolution of character 9 on Rauhut's data + my data strict consensus tree.

A, **B**, **C**, and **D** serve to distinguish nodes mentioned in the accompanying text.

Rauhut's Data + My Data- Floccular Fossa (Character 10) Resolution

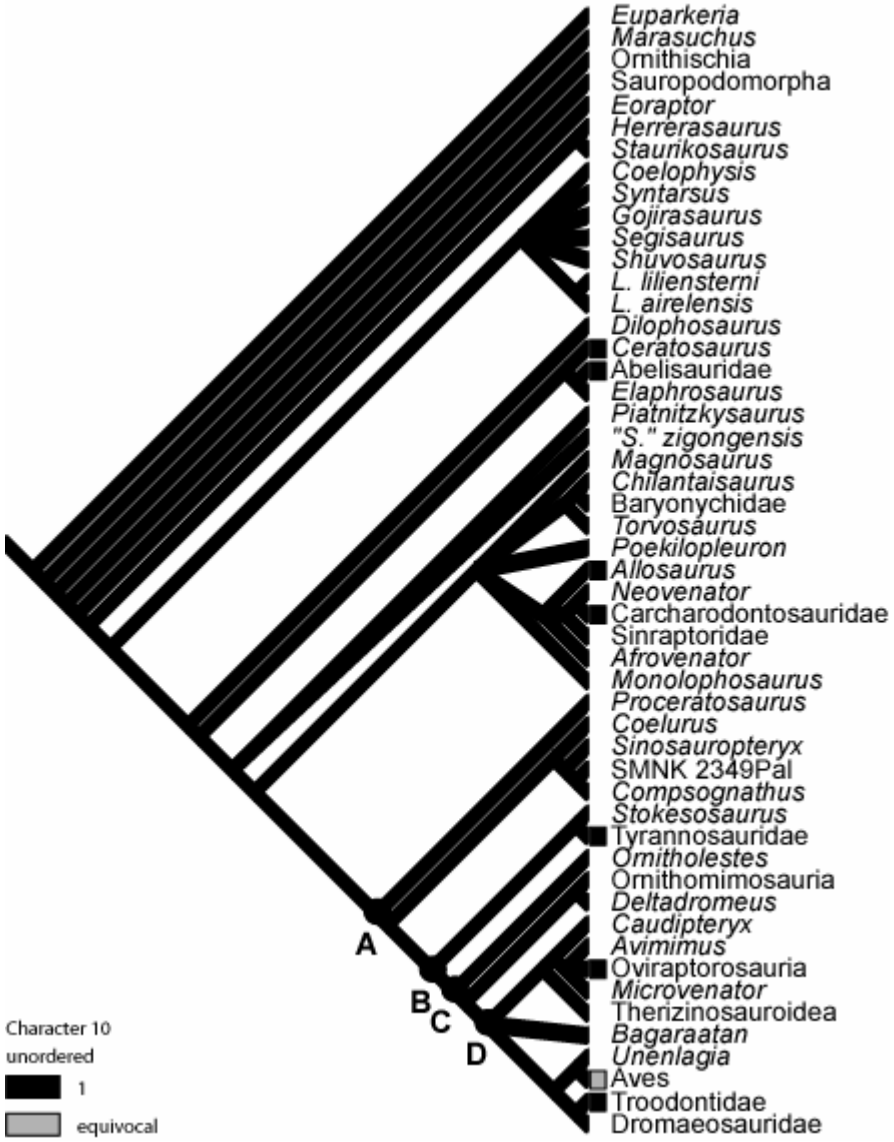

Figure 83. Resolution of character 10 on Rauhut's data + my data strict consensus tree.

A, **B**, **C**, and **D** serve to distinguish nodes mentioned in the accompanying text.

Rauhut's Data + My Data- Floccular Lobe Shape (Character 11) Resolution

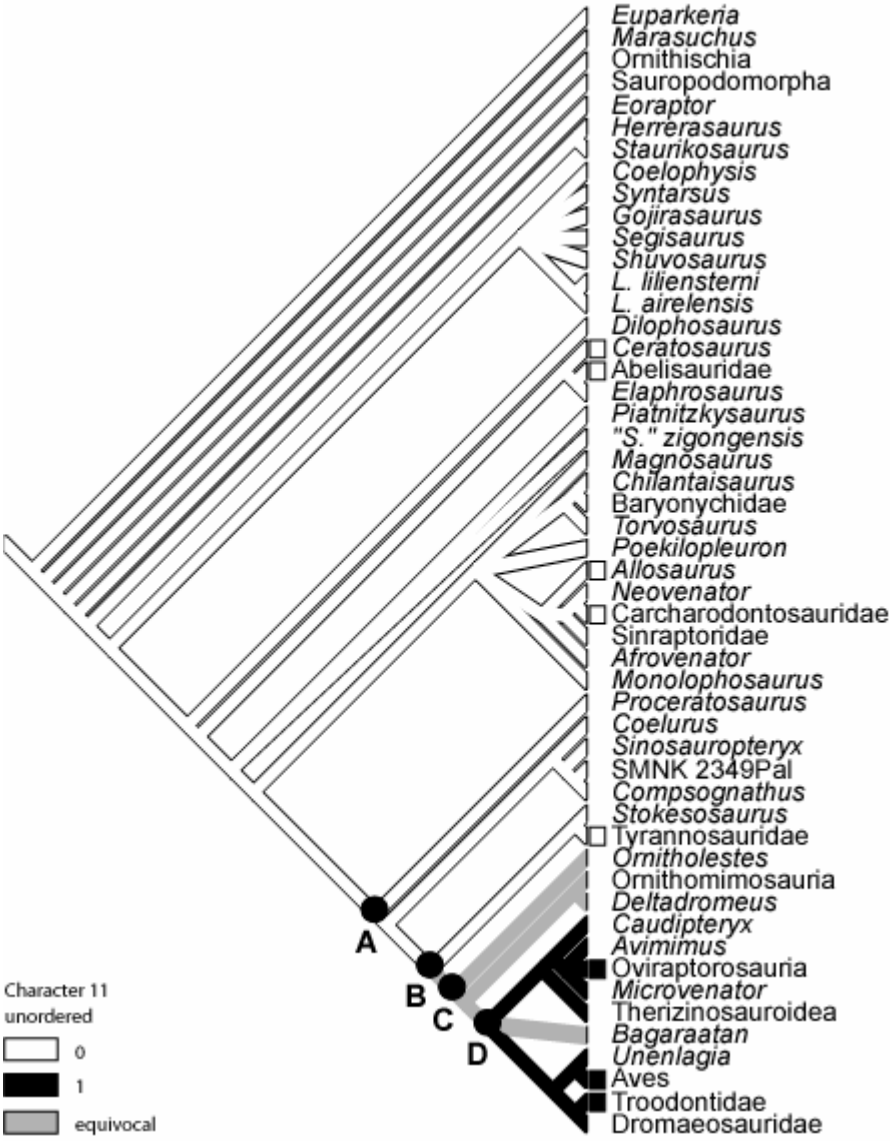

Figure 84. Resolution of character 11 on Rauhut's data + my data strict consensus tree.

A, **B**, **C**, and **D** serve to distinguish nodes mentioned in the accompanying text.

Rauhut's Data + My Data- Posterior Semicircular Canal Orientation (Character 12) Resolution

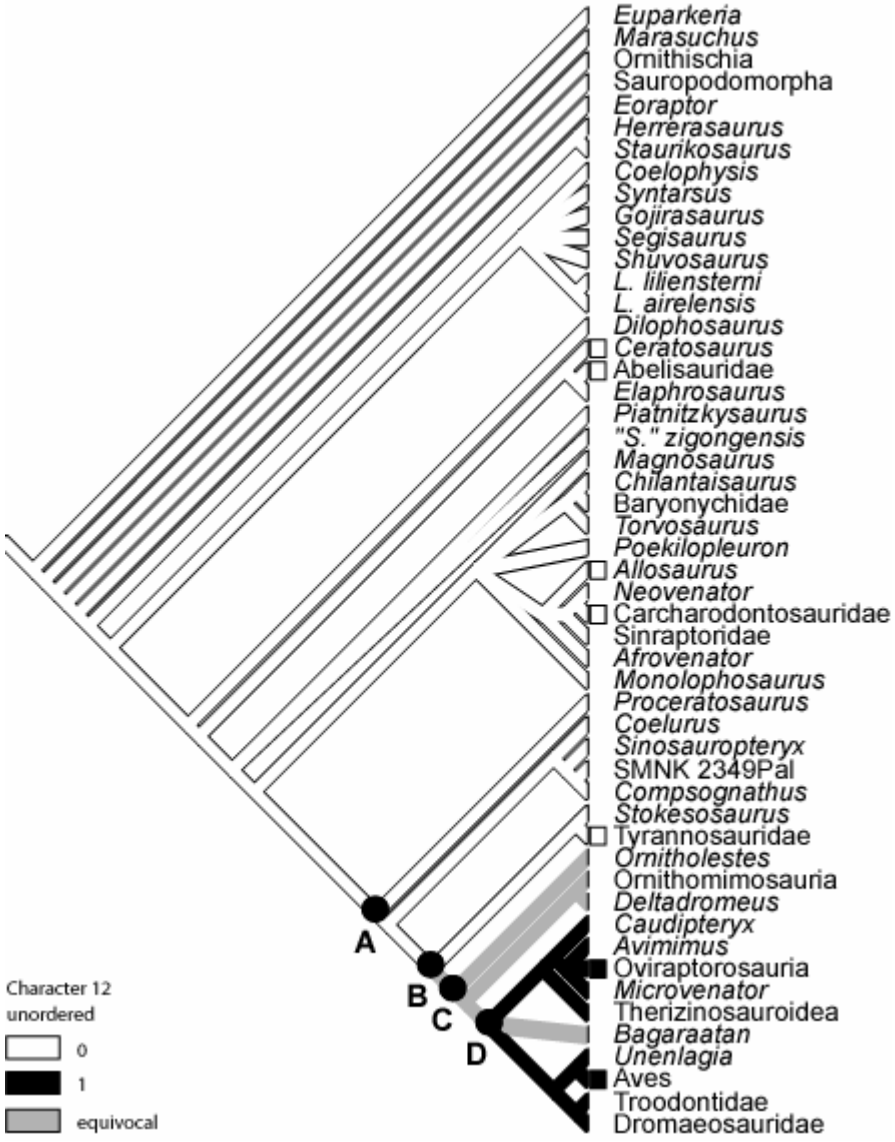

Figure 85. Resolution of character 12 on Rauhut's data + my data strict consensus tree.

A, **B**, **C**, and **D** serve to distinguish nodes mentioned in the accompanying text.

Rauhut's Data + My Data- Number of Hypoglossal Nerve Foramina (Character 13) Resolution

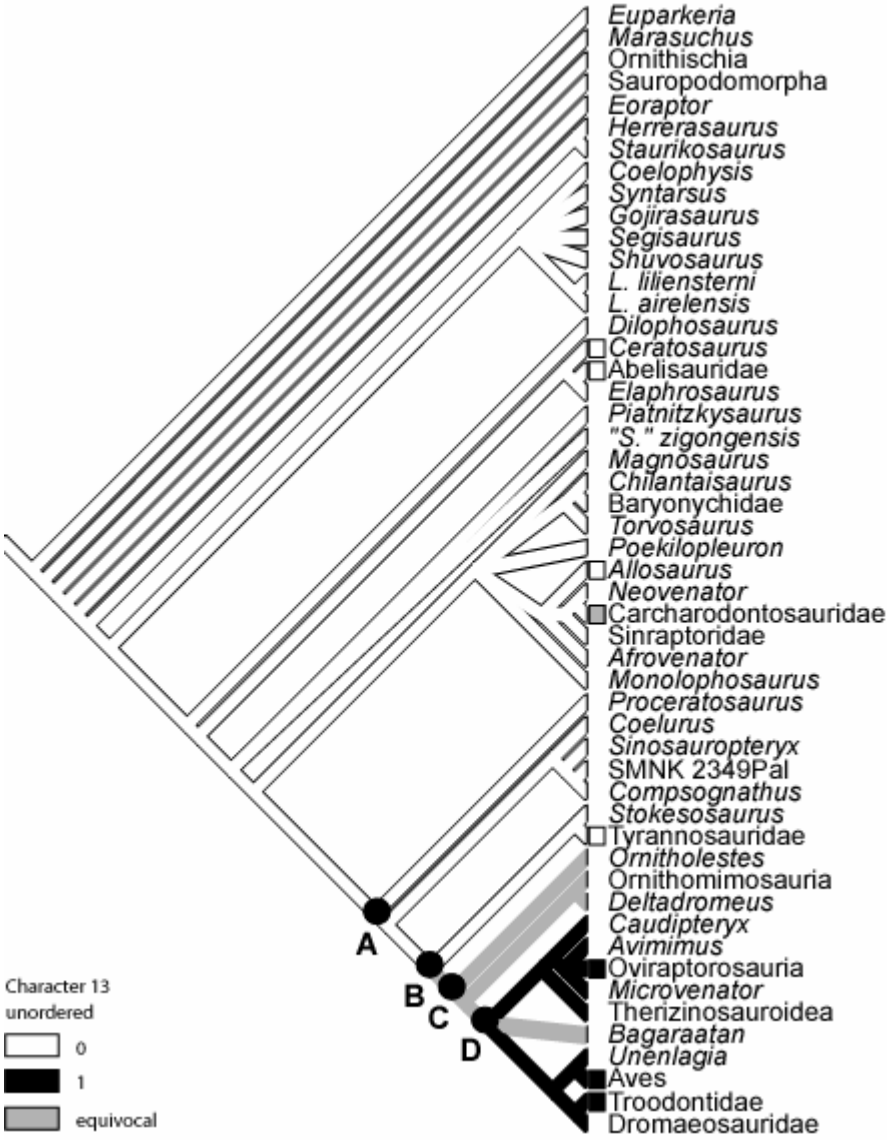

Figure 86. Resolution of character 13 on Rauhut's data + my data strict consensus tree.

A, **B**, **C**, and **D** serve to distinguish nodes mentioned in the accompanying text.

Rauhut's Data + My Data- Reptile Encephalization Quotient (Character 14) Resolution

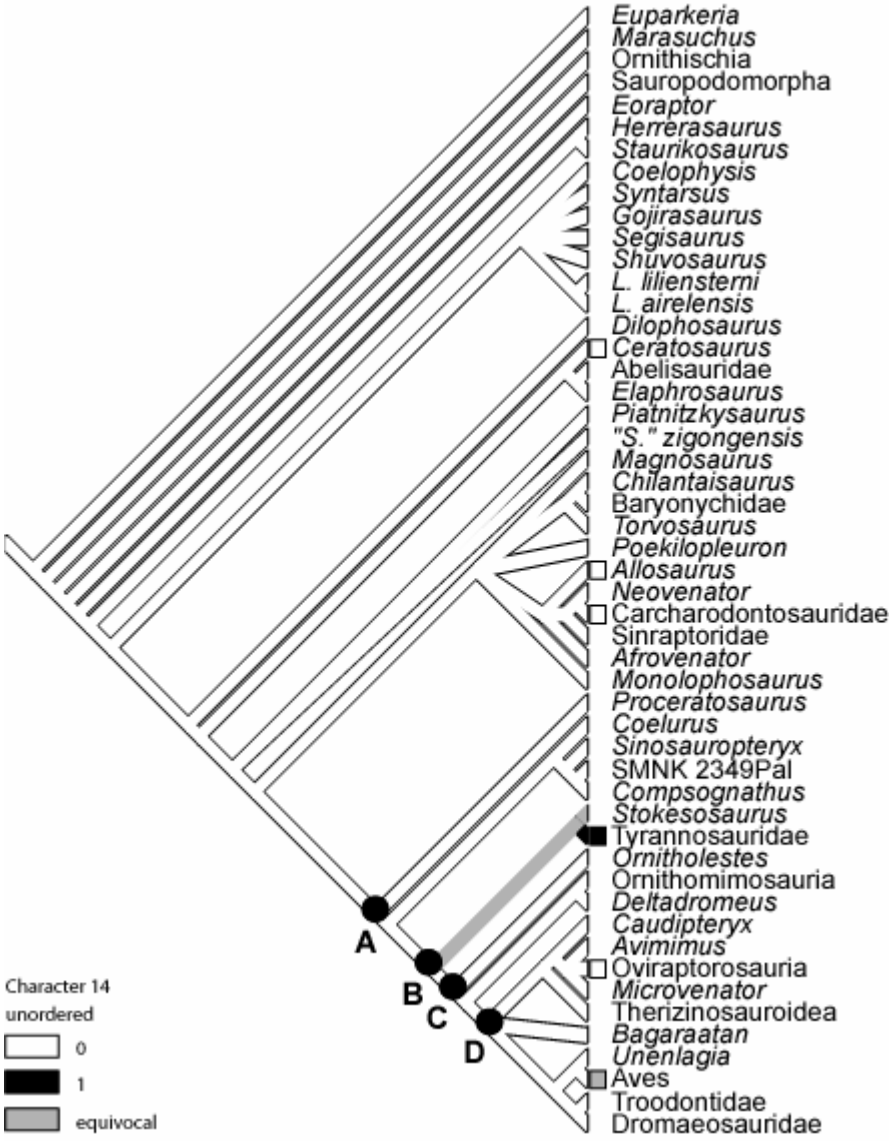

Figure 87. Resolution of character 14 on Rauhut's data + my data strict consensus tree.

A, **B**, **C**, and **D** serve to distinguish nodes mentioned in the accompanying text.

contains taxa that have the primitive character state and the derived character state.

Sereno's Data + My Data

The final analysis that I ran with the endocranial data used the phylogeny proposed by Sereno (1999). This phylogeny was analyzed by Sereno as several separate clades, and the clade that I used in this analysis was the tetanuran clade, which consisted of 17 ingroup taxa and 204 characters. As with the previous analyses, I reran Sereno's data to determine whether or not his results could be replicated. The analysis, run under the same conditions as the previous analyses in this study, yielded 6 equally most parsimonious trees of 391 steps. I obtained a strict consensus tree and opened it in MacClade. A C.I. of 0.66, an R.I. of 0.82, and an R.C. of 0.54 were calculated. This tree was verified as the same one obtained by Sereno's analysis (Figure 88).

I then added the endocranial data to Sereno's data matrix, with alterations. First, I used two ceratosaurian taxa, *Ceratosaurus* and *Majungatholus*, in my analysis. Further up the tree, *Allosaurus* was placed under Allosauridae, but *Acrocanthosaurus* and *Carcharodontosaurus* had to be cut from the analysis because Sereno did not include them. *Tyrannosaurus* was placed in Tyrannosauroidea, and *Citipati* within Oviraptoridae. *Mongolodon, Byronosaurus*, and the Zos Canyon troodontid were combined as Troodontidae. Lastly, Aves contained all my extant taxa, *Dinornis*, and *Archaeopteryx*.

Sereno's Data + My Data- Strict Consensus Tree

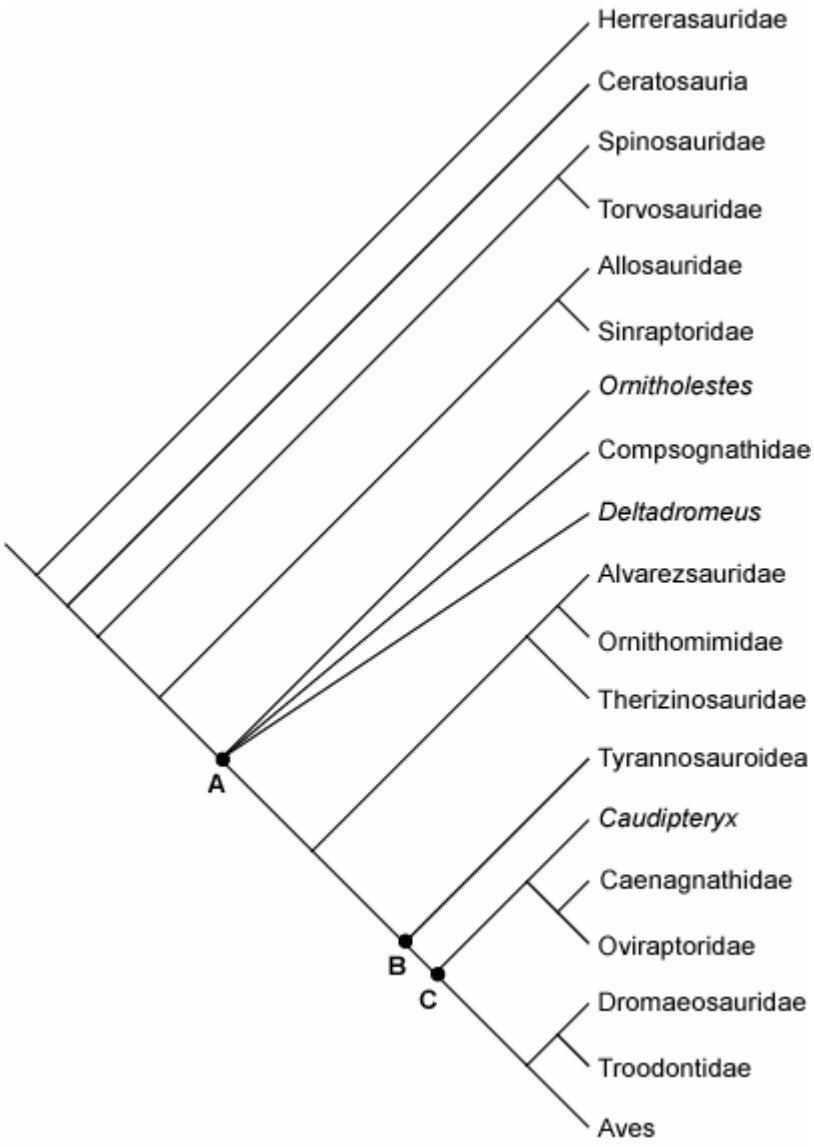

Figure 88. Strict consensus tree of Sereno's taxa and characters + taxa and characters used in my study.

A, **B**, and **C** serve to distinguish nodes mentioned in the accompanying text.

After these modifications were made, I added the characters and reran the analysis in PAUP. Six equally parsimonious trees of 338 steps were obtained, and a strict consensus tree constructed. This tree was the same as that recovered by Sereno. The tree was analyzed in MacClade, and a C.I. of 0.67, an R.I. of 0.82, and an R.C. of 0.55 were obtained. The C.I. and R.C. were each 0.01 higher than found with the Sereno data alone, while the R.I. remained the same.

Character Tracing and Optimization

After I opened the tree in MacClade, the character tracing function was activated, and the distribution of the characters studied. As with the previous analyses, ACCTRAN and DELTRAN were unavailable through MacClade owing to the polytomy present in the tree.

The distribution of the character states for the median septum of the sphenethmoid dividing the sphenethmoidal fossa (character 1) is fairly consistent throughout most of the tree, with all taxa up to and including Tyrannosauroidea showing the primitive character state (Figure 89). Equivocation is found in taxa stemming from node C. This is caused by the occurrence of the derived character state in Oviraptoridae. As was previously discussed for this character, the lack of its presence anywhere else on the tree is more likely because of the small taxon sample size rather than the possibility that it is an autapomorphy of Oviraptoridae.

The olfactory bulb position (character 2) is nearly completely unequivocal on the tree, with all taxa showing the primitive character state except for Aves.

Sereno's Data + My Data- Sphenethmoidal Septum Dividing Sphenethmoidal Fossa (Character 1) Resolution

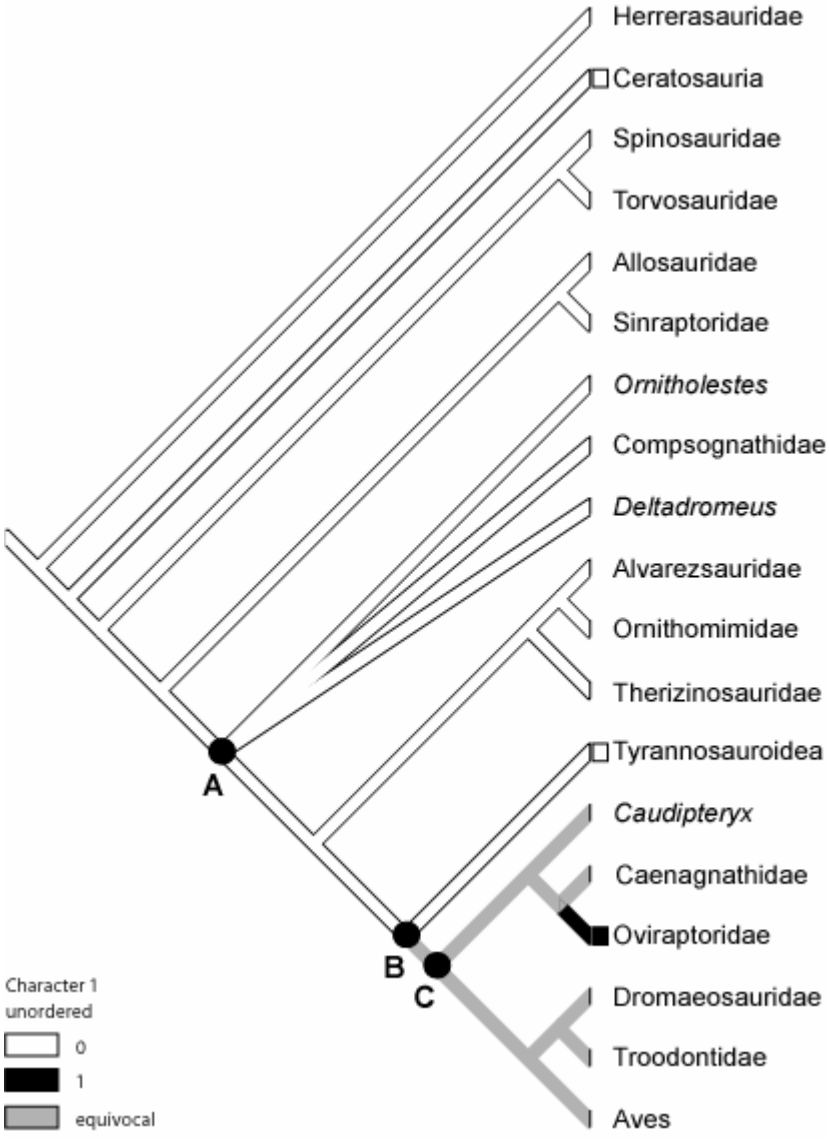

Figure 89. Resolution of character 1 on Sereno's data + my data strict consensus tree.

A, **B**, and **C** serve to distinguish nodes mentioned in the accompanying text.

This terminal taxon shows equivocation because it contains taxa exhibiting both the primitive and the derived character states (Figure 90).

The shape of the cerebral hemispheres (character 3) (Figure 91), the volume of the cerebral hemispheres (character 4) (Figure 92), width of the endocast (character 5) (Figure 93), and optic lobe position (character 6) (Figure 94) characters show the same distribution of character states. In all cases the primitive character state is present in all taxa up to and including Tyrannosauroidea, and the derived character state is present in the taxa stemming from node C.

The distribution of the character states for the number of trigeminal nerve foramina (character 7) is more complex than shown (Figure 95). Most of the tree shows the derived character state, with some equivocation near the base of the tree, because the primitive state is seen in Ceratosauria, and also near Oviraptoridae for the same reason. The character distribution becomes more complicated when the excluded taxa are considered. On the cladogram, Allosauridae is shown as exhibiting the derived character state, but the excluded *Acrocanthosaurus* and *Carcharodontosaurus* have the primitive character state. The addition of these taxa would lead to a different distribution of the character states.

The abducens nerve canal (character 8) shows a lot of equivocation. The equivocation seen is lost in taxa stemming from node B, which exhibit the derived character state. Most of the rest of the tree is equivocal, with the exception of

Sereno's Data + My Data- Olfactory Bulb Position (Character 2) Resolution

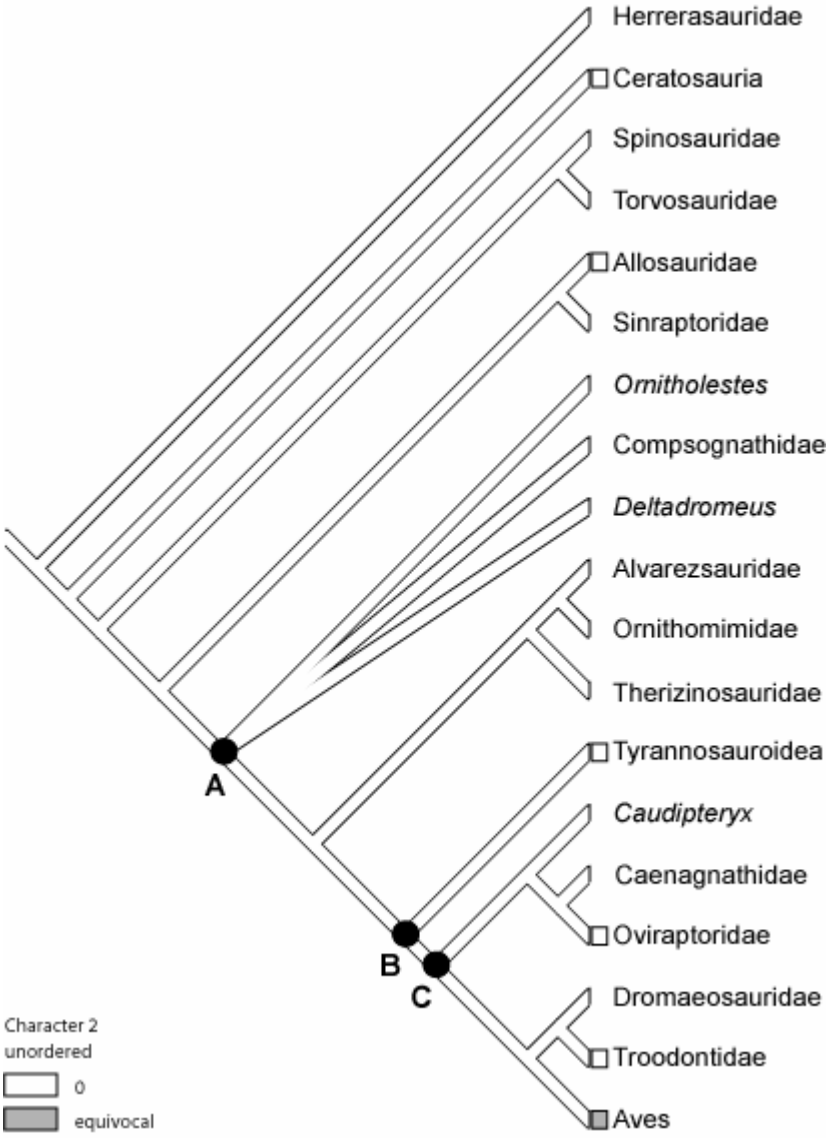

Figure 90. Resolution of character 2 on Sereno's data + my data strict consensus tree.

A, **B**, and **C** serve to distinguish nodes mentioned in the accompanying text.

Sereno's Data + My Data- Cerebral Hemisphere Shape (Character 3) Resolution

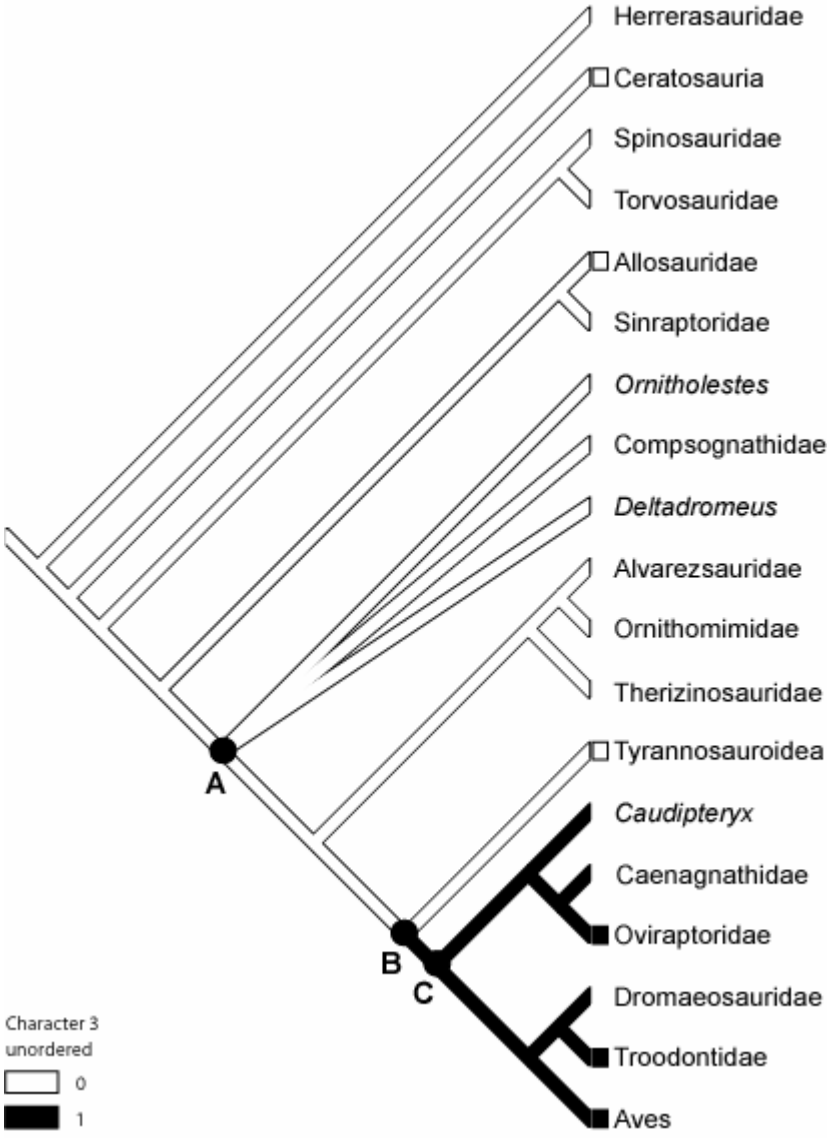

Figure 91. Resolution of character 3 on Sereno's data + my data strict consensus tree.

A, **B**, and **C** serve to distinguish nodes mentioned in the accompanying text.

Sereno's Data + My Data- Volume of the Cerebral Hemispheres (Character 4) Resolution

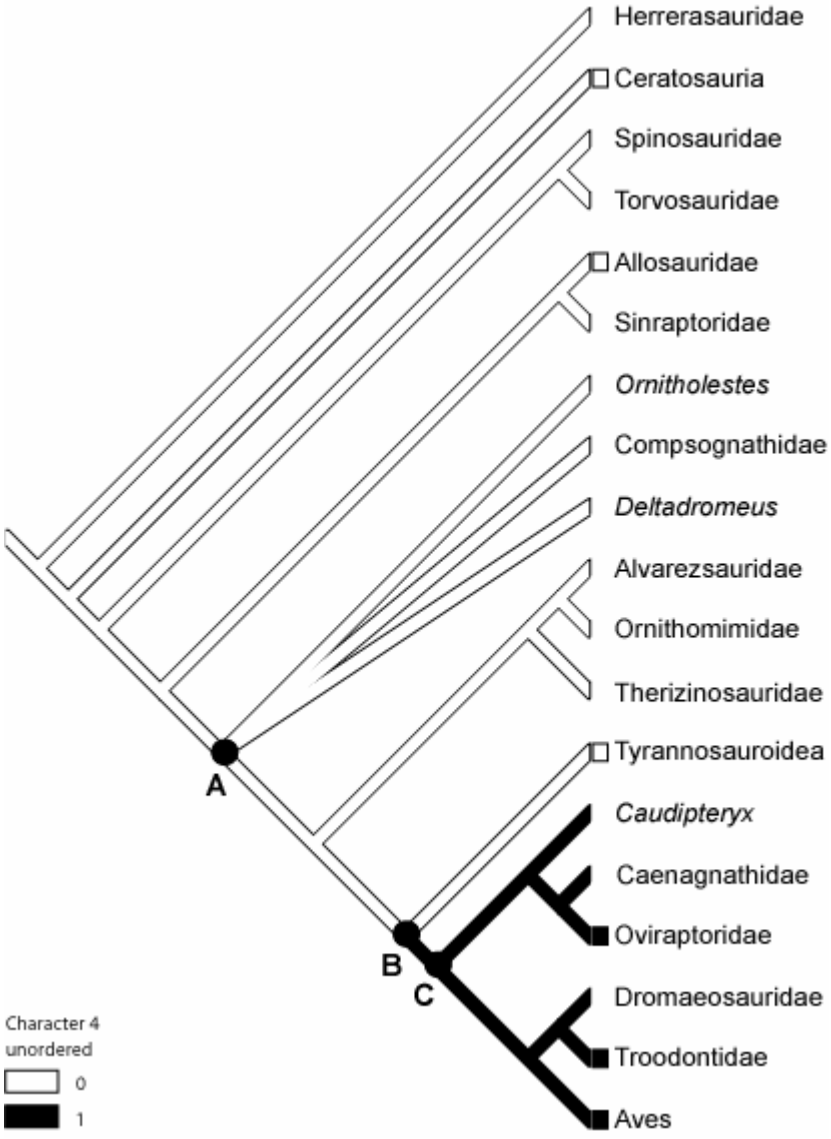

Figure 92. Resolution of character 4 on Sereno's data + my data strict consensus tree.

A, **B**, and **C** serve to distinguish nodes mentioned in the accompanying text.

Sereno's Data + My Data- Width of Endocast (Character 5) Resolution

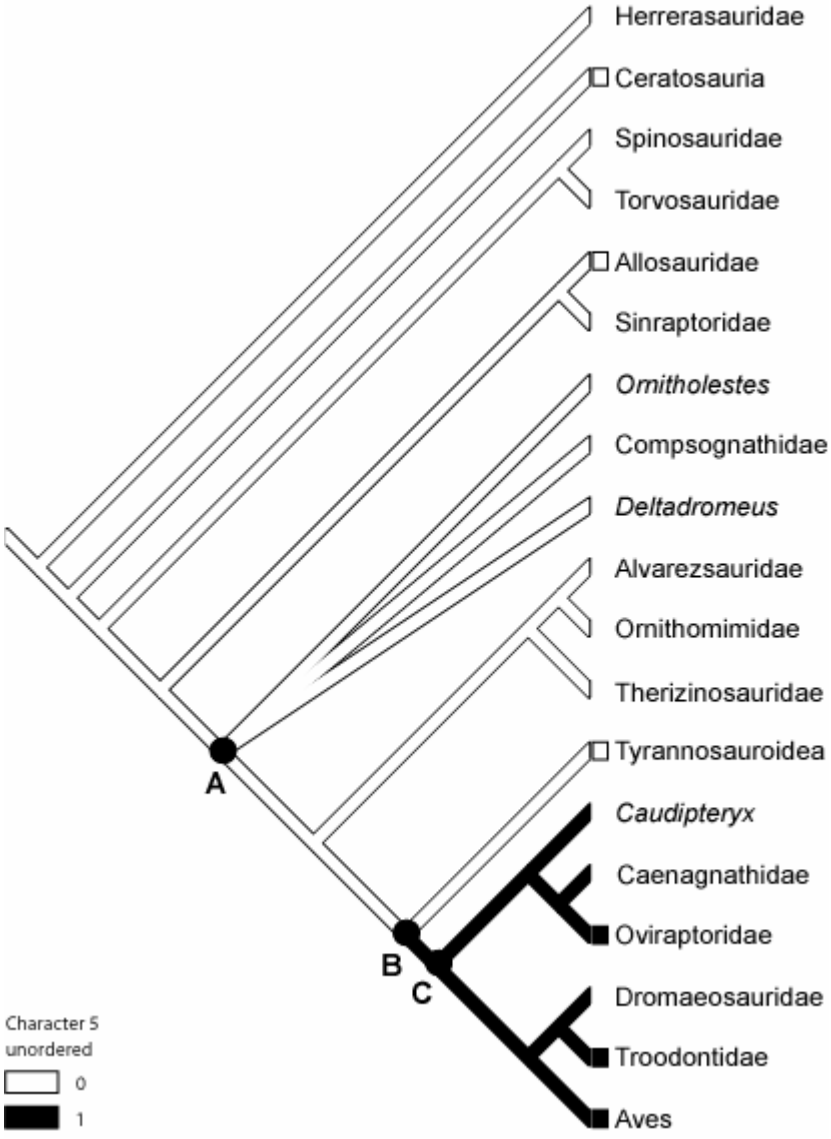

Figure 93. Resolution of character 5 on Sereno's data + my data strict consensus tree.

A, **B**, and **C** serve to distinguish nodes mentioned in the accompanying text.

Sereno's Data + My Data- Optic Lobe Position (Character 6) Resolution

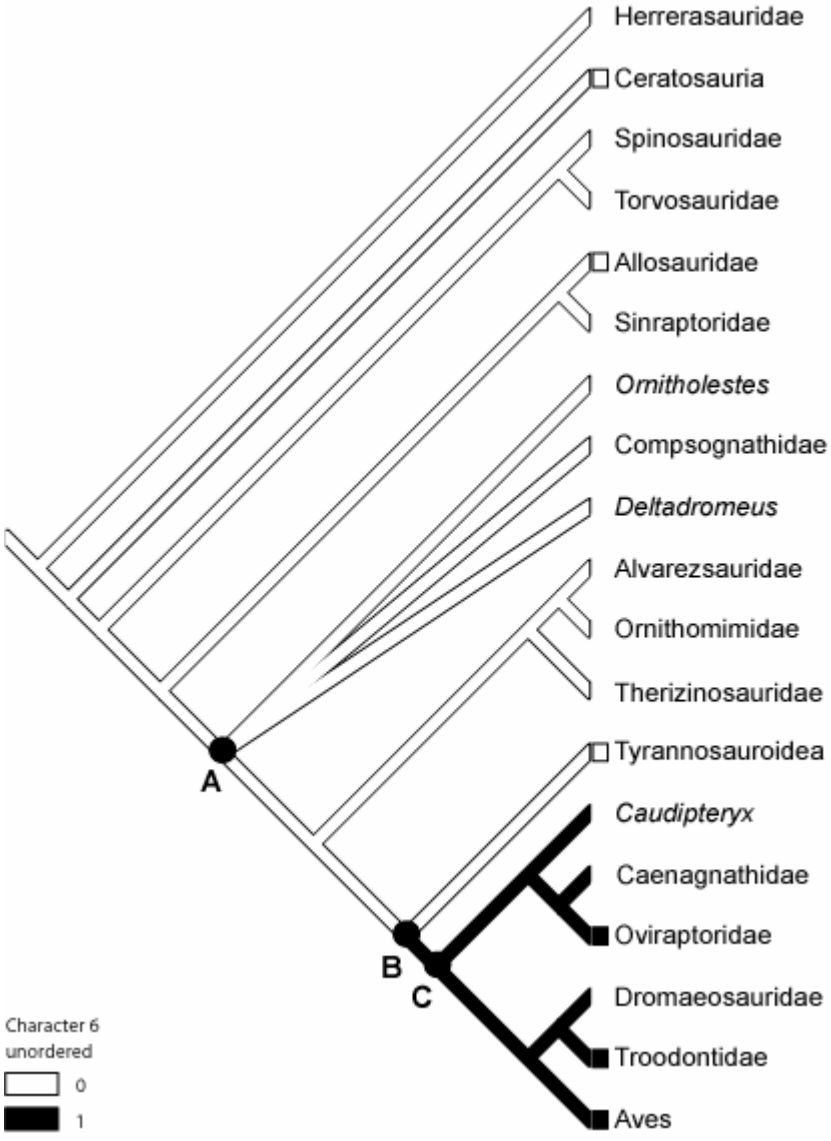

Figure 94. Resolution of character 6 on Sereno's data + my data strict consensus tree.

A, **B**, and **C** serve to distinguish nodes mentioned in the accompanying text.

Sereno's Data + My Data- Number of Trigeminal Nerve Foramina (Character 7) Resolution

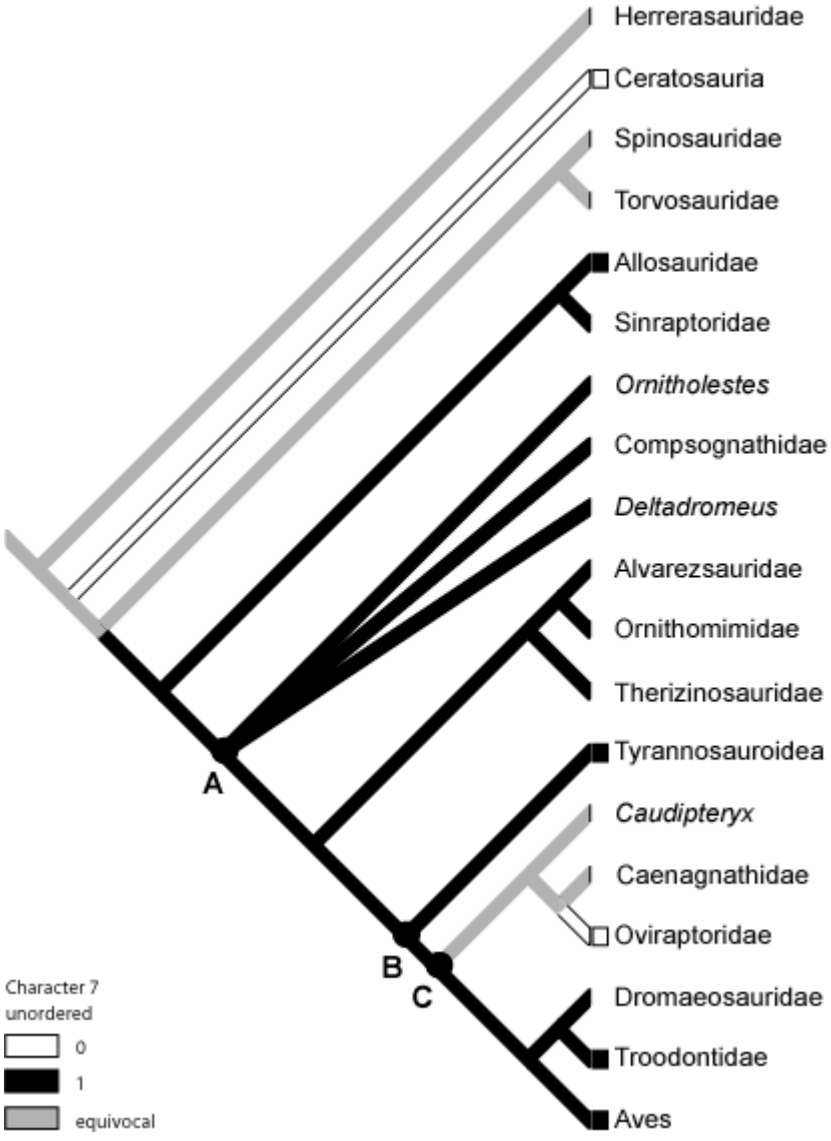

Figure 95. Resolution of character 7 on Sereno's data + my data strict consensus tree.

A, **B**, and **C** serve to distinguish nodes mentioned in the accompanying text.

Allosauridae, which exhibits the primitive state. Ceratosauria is equivocal because it contains taxa exhibiting both the primitive and the derived character states (Figure 96).

The distribution of the character states for the internal carotid canals (character 9) is fairly straightforward (Figure 97). The portion of the tree basal to node A is completely unequivocal, showing only the primitive character state. The taxa stemming from node B are almost completely unequivocal, only the derived character state exhibited in all taxa but Aves, which contains taxa showing the primitive character state. The central portion of the tree, taxa stemming from node A but before taxa stemming from node B, is equivocal.

The floccular fossa (character 10) is almost completely unequivocal on the cladogram (Figure 98). The only taxon where some equivocation is found is in Aves, which contains some taxa with the primitive character state and others with the derived character state.

The floccular lobe shape (character 11) (Figure 99), posterior semicircular canal (character 12) (Figure 100), and number of hypoglossal nerve foramina (character 13) (Figure 101) show the same distribution as that in characters 3, 4, 5, and 6. Those characters show the primitive character state in taxa up to and including Tyrannosauroidea, and the derived character state in the taxa stemming from node C.

The REQ (character 14) is completely unequivocal in taxa up to node B. In taxa stemming from node B, Tyrannosauroidea exhibits the derived character

Sereno's Data + My Data- Abducens Nerve Canal (Character 8) Resolution

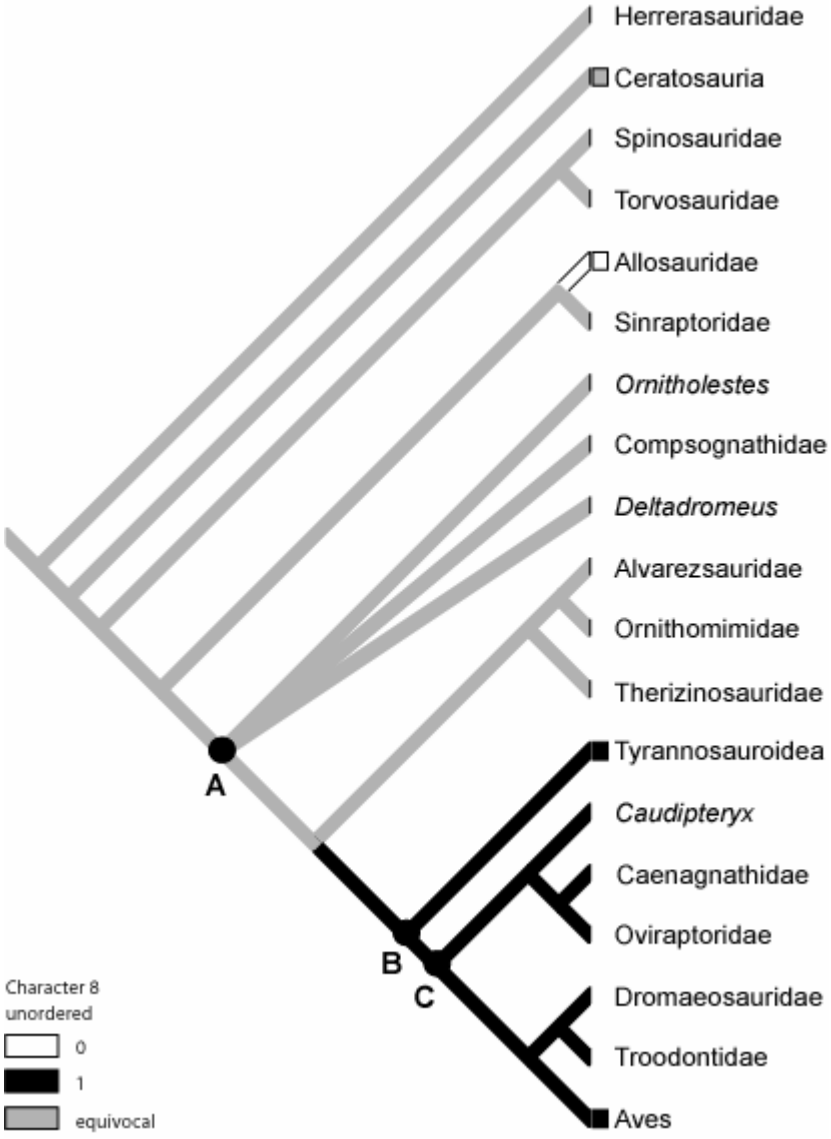

Figure 96. Resolution of character 8 on Sereno's data + my data strict consensus tree.

A, **B**, and **C** serve to distinguish nodes mentioned in the accompanying text.

Sereno's Data + My Data- Internal Carotid Canals (Character 9) Resolution

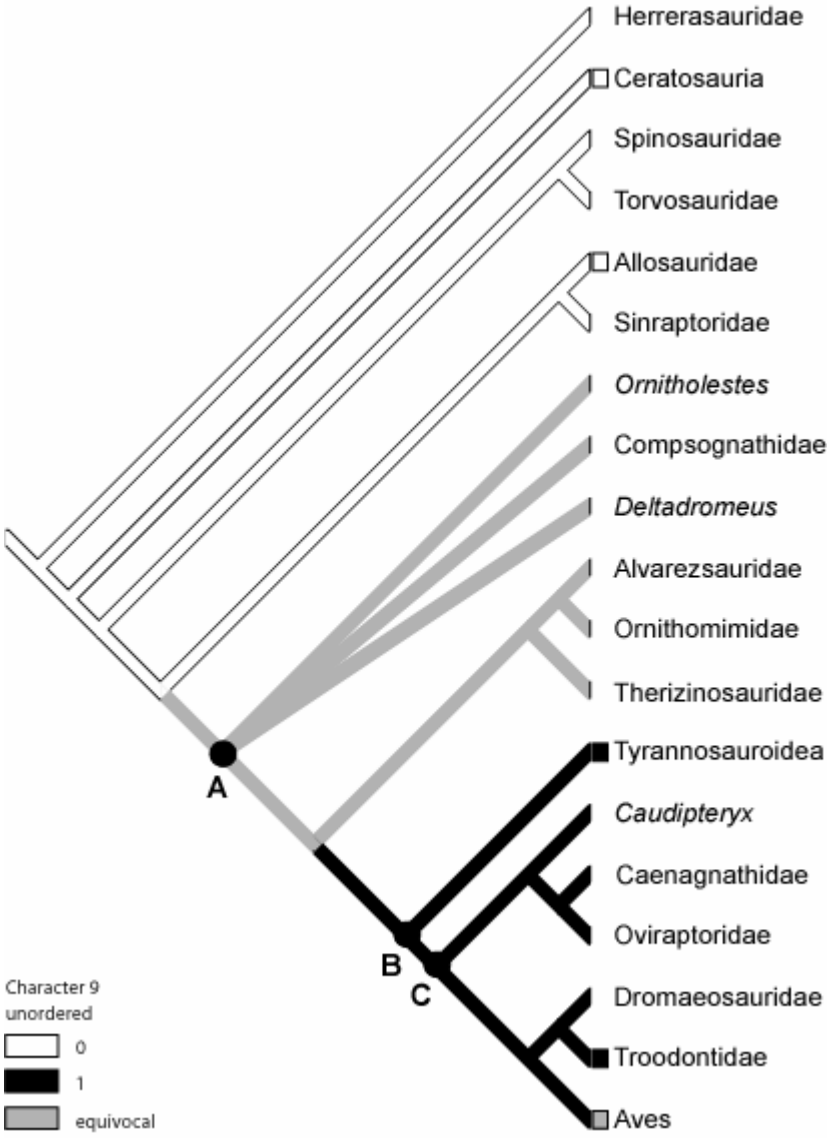

Figure 97. Resolution of character 9 on Sereno's data + my data strict consensus tree.

A, **B**, and **C** serve to distinguish nodes mentioned in the accompanying text.

Sereno's Data + My Data- Floccular Fossa (Character 10) Resolution

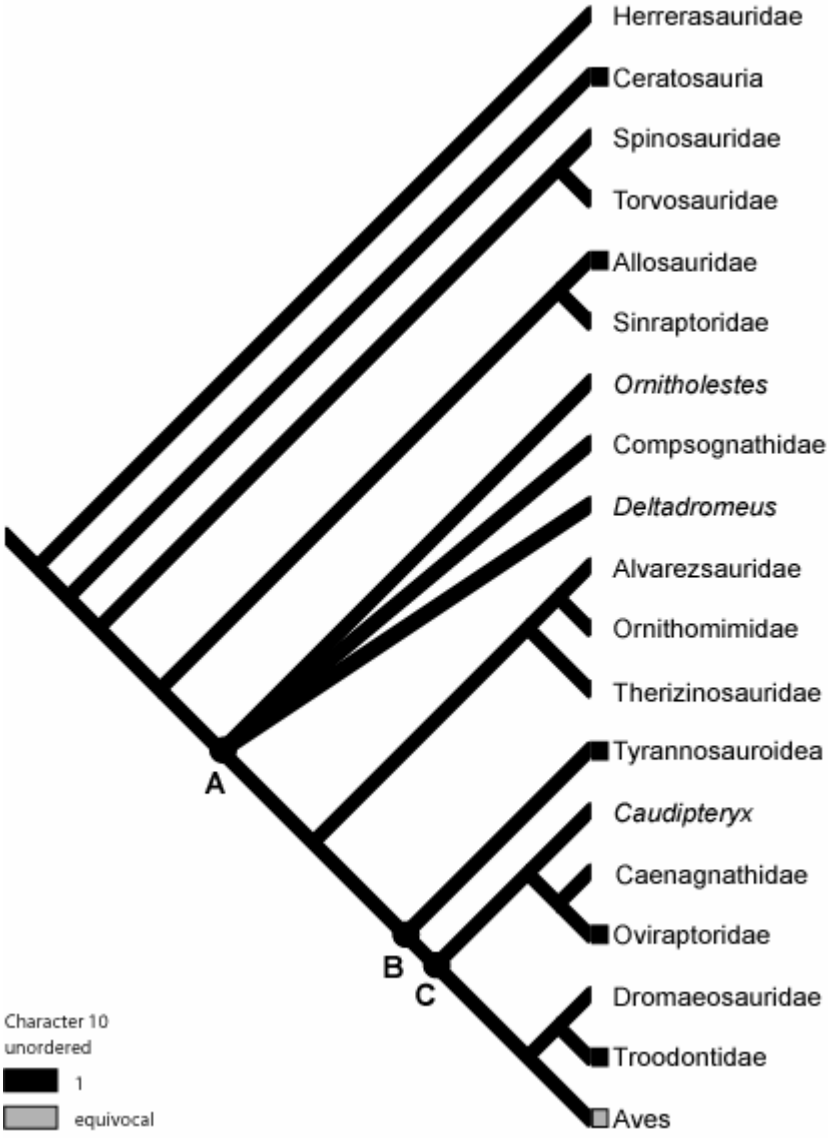

Figure 98. Resolution of character 10 on Sereno's data + my data strict consensus tree.

A, **B**, and **C** serve to distinguish nodes mentioned in the accompanying text.

Sereno's Data + My Data- Floccular Lobe Shape (Character 11) Resolution

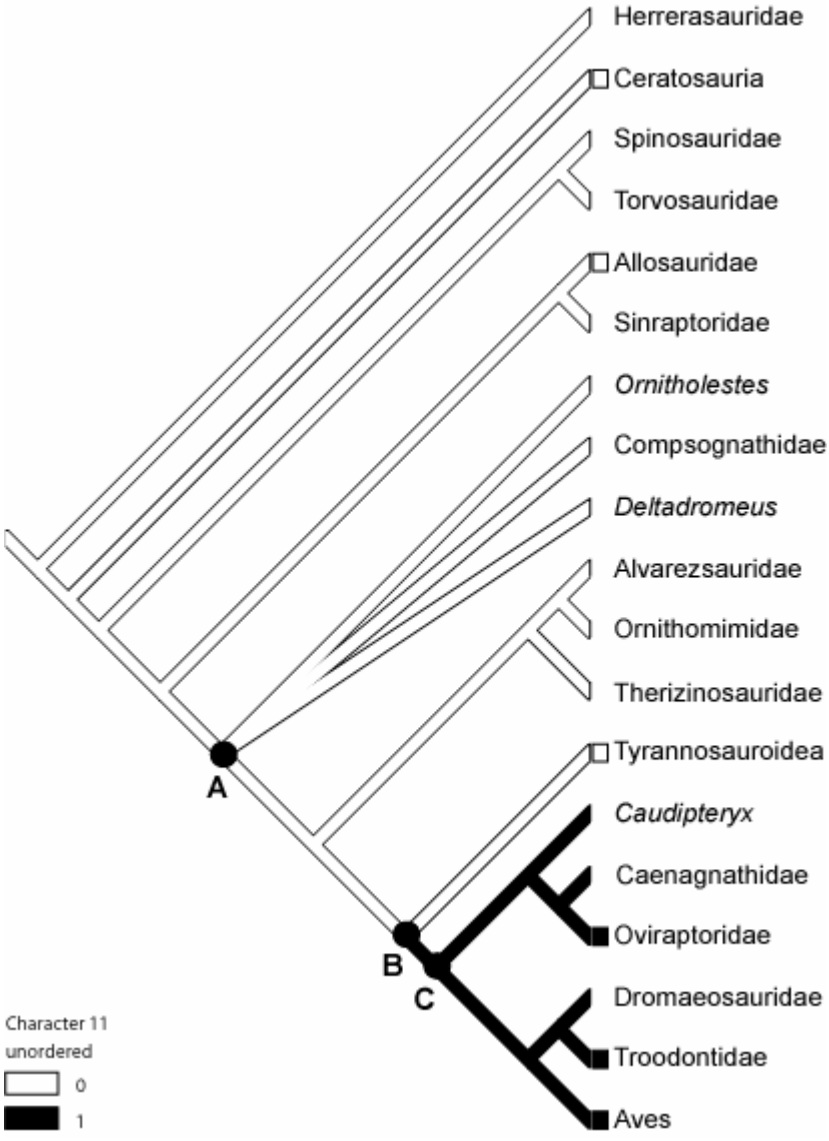

Figure 99. Resolution of character 11 on Sereno's data + my data strict consensus tree.

A, **B**, and **C** serve to distinguish nodes mentioned in the accompanying text.

Sereno's Data + My Data- Posterior Semicircular Canal Orientation (Character 12) Resolution

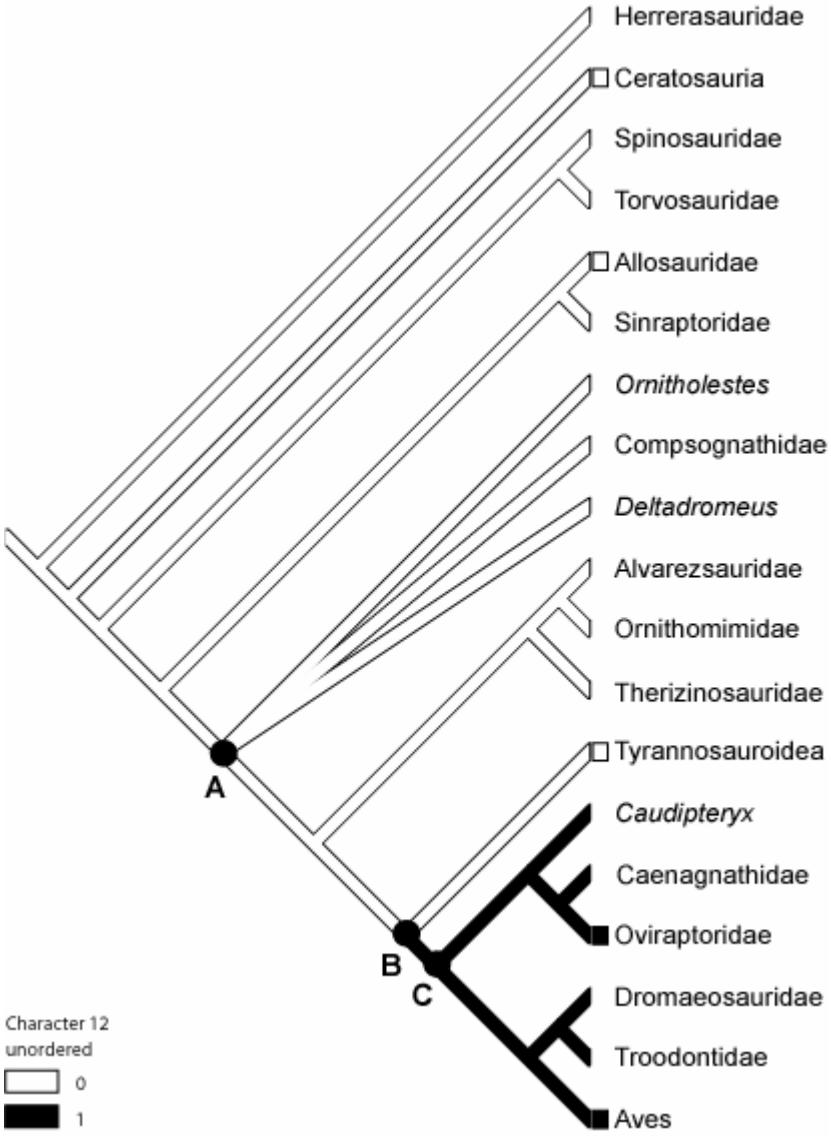

Figure 100. Resolution of character 12 on Sereno's data + my data strict consensus tree.

A, **B**, and **C** serve to distinguish nodes mentioned in the accompanying text.

Sereno's Data + My Data- Number of Hypoglossal Nerve Foramina (Character 13) Resolution

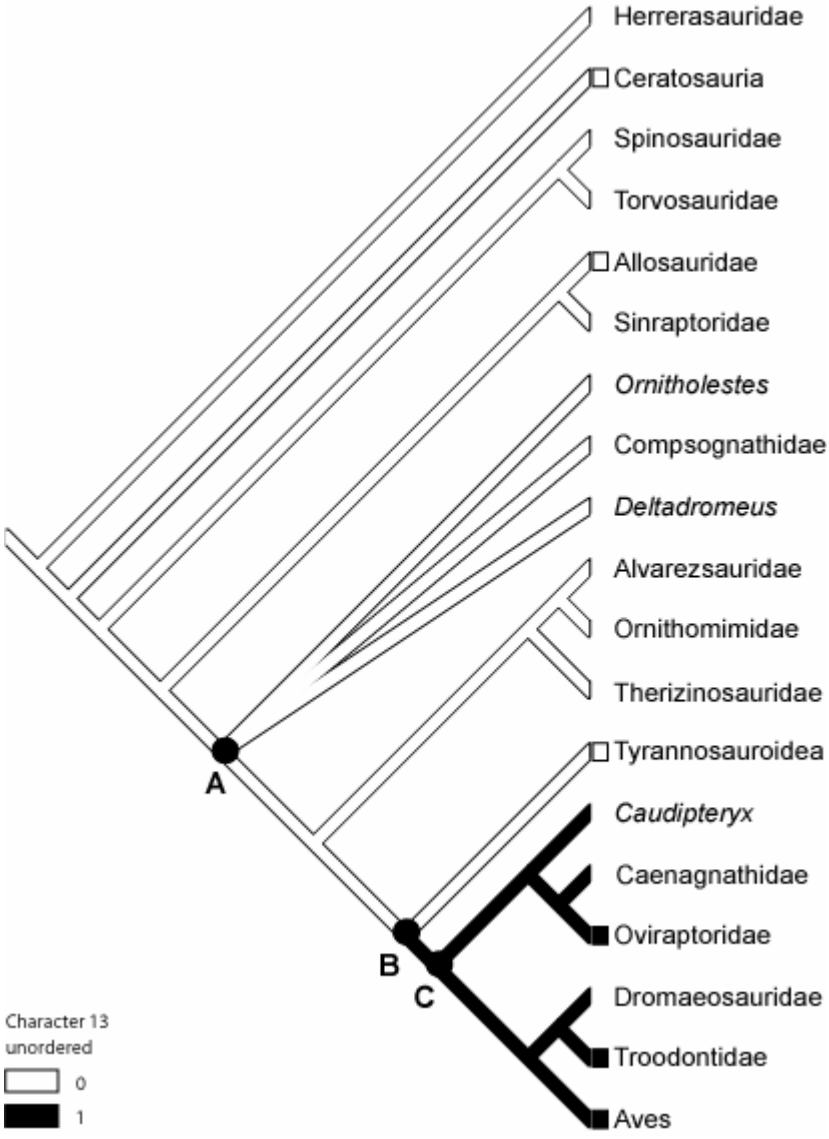

Figure 101. Resolution of character 13 on Sereno's data + my data strict consensus tree.

A, **B**, and **C** serve to distinguish nodes mentioned in the accompanying text.

state, Aves has taxa showing both character states, and the rest of the taxa stemming from node B show the primitive character state (Figure 102). Although not shown in this tree or data, several other taxa have REQs that are known, and they would have an effect on the distribution seen. Ornithomimidae and Troodontidae, two taxa that have no data for this character on the tree, are both known to have endocasts with REQs that would be considered the derived character state (Hurlburt, 1996). The addition of these taxa would lead to a much different character distribution than what is currently seen.

Sereno's Data + My Data- Reptile Encephalization Quotient (Character 14) Resolution

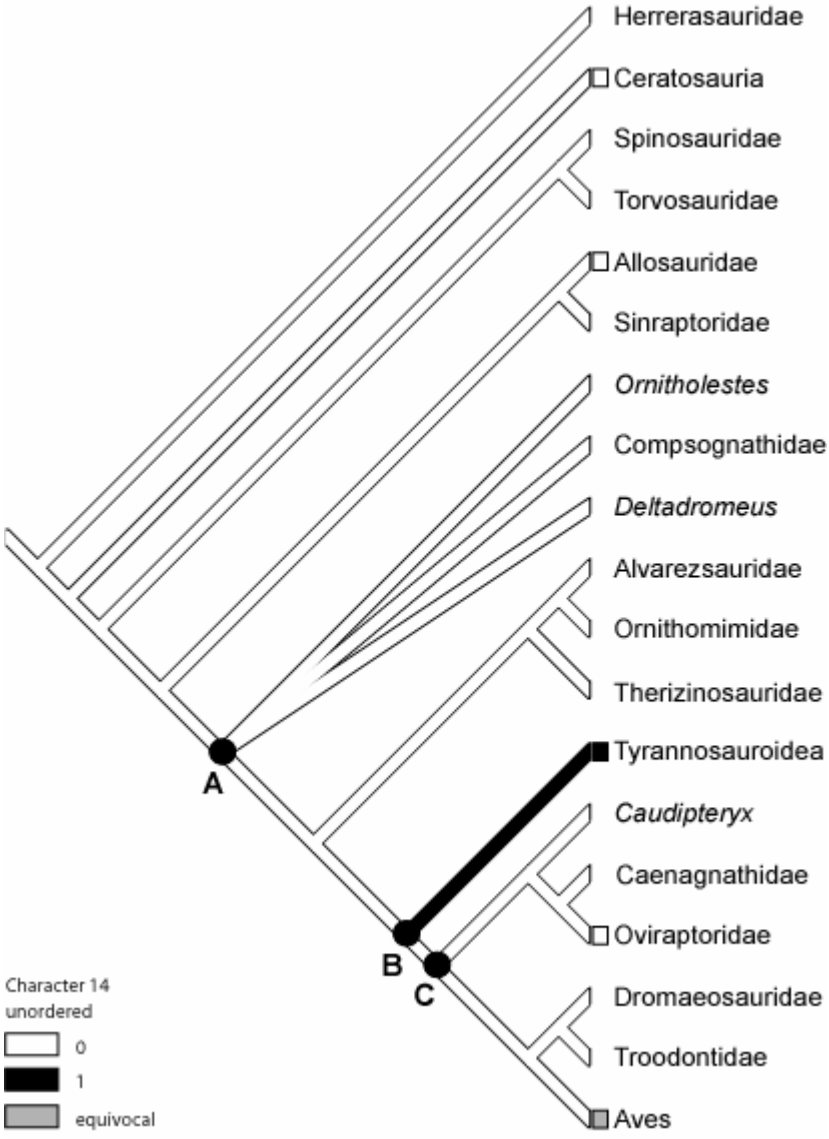

Figure 102. Resolution of character 14 on Sereno's data + my data strict consensus tree.

A, **B**, and **C** serve to distinguish nodes mentioned in the accompanying text.

Chapter 4: Discussion of Results and Their Meaning

TRANSITION OF CHARACTER STATES

In chapter 3, I traced and optimized my 14 endocranial characters on trees consisting of dozens of taxa. This tracing and optimization of the characters was very informative. I did not have access to endocasts for most of the taxa in the analyses however. This led to a lot of equivocation in the 14 characters studied. To get a better idea of how the appearance and acquisition of the character states occurred, I constructed a tree consisting of only the taxa that I scored (Figure 103). The relationships shown on this tree are those found for the taxa in Holtz's (1998), Rauhut's (2003), and Sereno's (1999) trees.

The three troodontid taxa that I scored, *Mongolodon, Byronosaurus,* and the Zos Canyon troodontid, have no conflicting character states, so they were combined under Troodontidae, and those characters that were scored in at least one taxon were used to represent this clade. The exception to this is character 14, in which all three troodontids show a question mark. Because another troodontid endocast (*Troodon formosus*) is known and its REQ is greater than 6 (Hurlburt, 1996), a 1 was scored for this character for troodontids in the data matrix. The modern avian taxa included in the study were also placed on the tree according to their hypothetical relationships to each other (Cracraft, 1974; van Tuinen et al., 2000). The new tree was constructed in MacClade, and the characters were traced on the tree and optimized using ACCTRAN and DELTRAN when necessary.

Taxa Used in My Study on a Consensus Tree from the Three Established Phylogenies

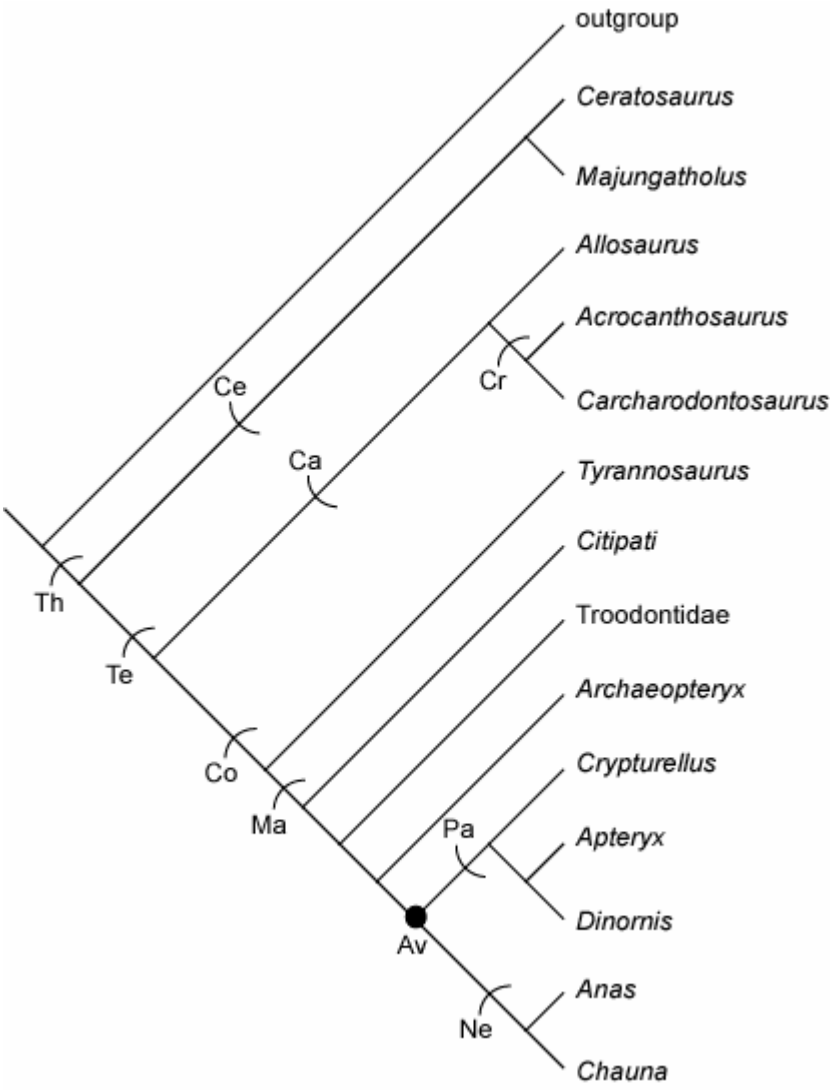

Figure 103. Taxa used in my study on a consensus tree taken from Holtz's (1998), Rauhut's (2003), and Sereno's (1999) trees.

Av- Aves, Ca- Carnosauria, Ce- Ceratosauria, Co- Coelurosauria, Cr- Carcharodontosauridae, Ma- Maniraptora, Ne- Neognathae, Pa- Paleognathae, Te- Tetanurae, Th- Theropoda. Definitions and sources for the stem and node names can be found in chapter 2.

Character 1 (the median septum of the sphenethmoid dividing the sphenethmoidal fossa) is found in the derived state in only one taxon, *Citipati* (Figure 104). Because no taxa more derived than *Citipati* show the character or can be scored for it, they are shown as being equivocal. This equivocation can be resolved using ACCTRAN and DELTRAN optimizations. ACCTRAN optimization assigns the derived character state to all the taxa within Maniraptora (Figure 105), while DELTRAN optimization assigns all the Maniraptora except *Citipati* as having the primitive character state (Figure 106). Although all avian taxa are shown on the cladogram with the derived or primitive character state, this character is not found in these taxa, so they really don't exhibit any character state.

Character 2 (the distribution of the character states for the olfactory bulb position) is completely unequivocal (Figure 107). The derived character state appears on the stem below the node for Aves.

Character 3 (shape of the cerebral hemispheres; Figure 108), character 4 (volume of the cerebral hemispheres; Figure 109), character 5 (width of the endocast) (Figure 110), and character 6 (optic lobe position; Figure 111) all show the same distribution of character states, with the derived state found in Maniraptora.

The distribution of the character states for character 7 (the number of trigeminal nerve foramina) is equivocal in the central portion of the tree (Figure 112). The derived condition either evolved in Tetanurae and was subsequently

Sphenethmoidal Septum Dividing Sphenethmoidal Fossa (Character 1) Resolution on Consensus Tree

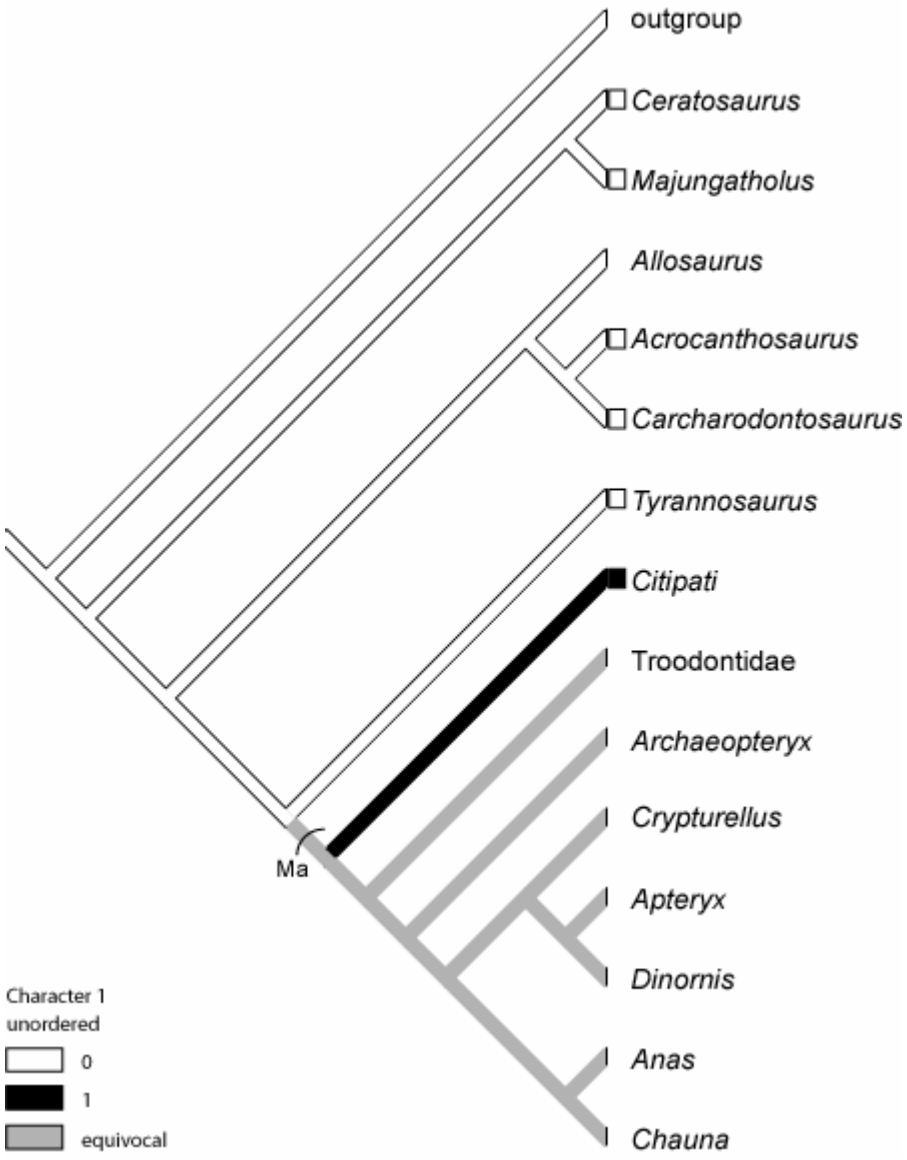

Figure 104. Resolution of character 1 on consensus tree.

For stem and node names and locations see figure 103. Character C.I.= 1.0.

Sphenethmoidal Septum Dividing Sphenethmoidal Fossa (Character 1) Resolution on Consensus Tree- ACCTRAN Optimization

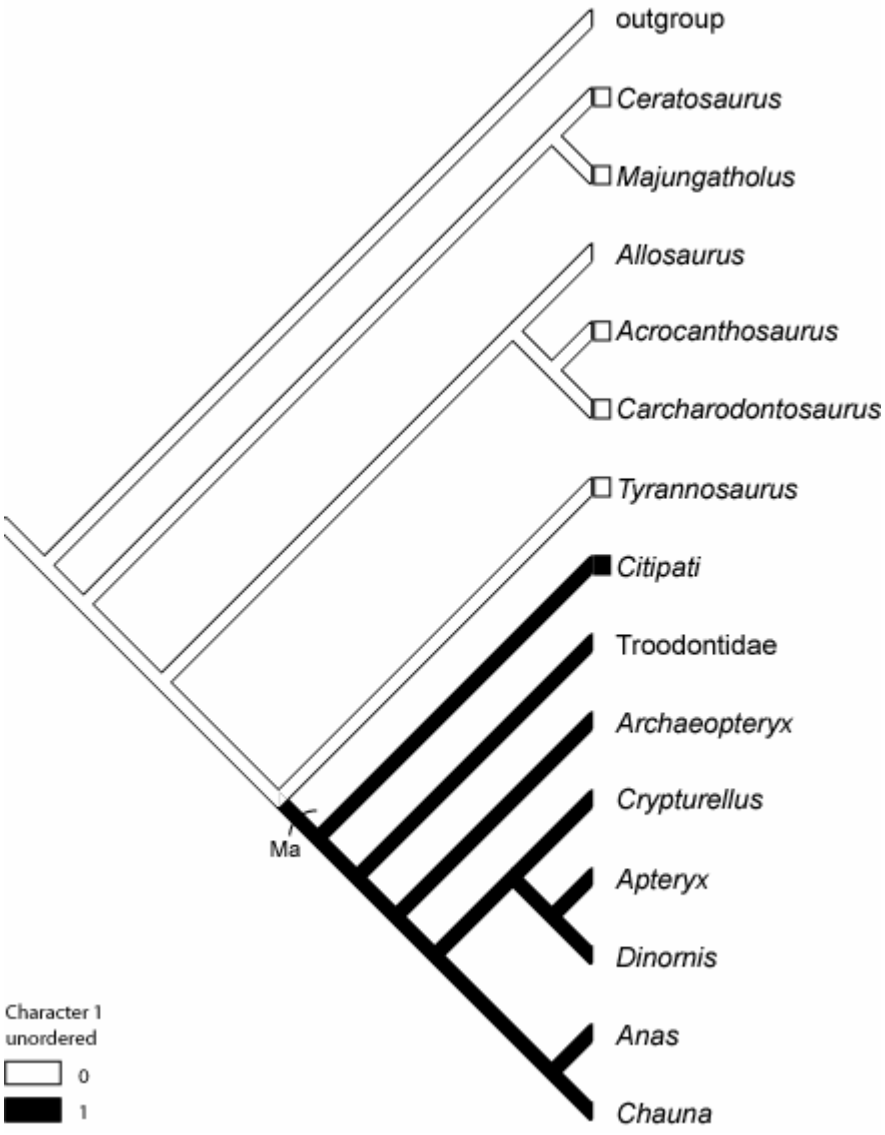

Figure 105. Resolution of character 1 on consensus tree using ACCTRAN optimization.

For stem and node names and locations see figure 103.

Sphenethmoidal Septum Dividing Sphenethmoidal Fossa (Character 1) Resolution on Consensus Tree- DELTRAN Optimization

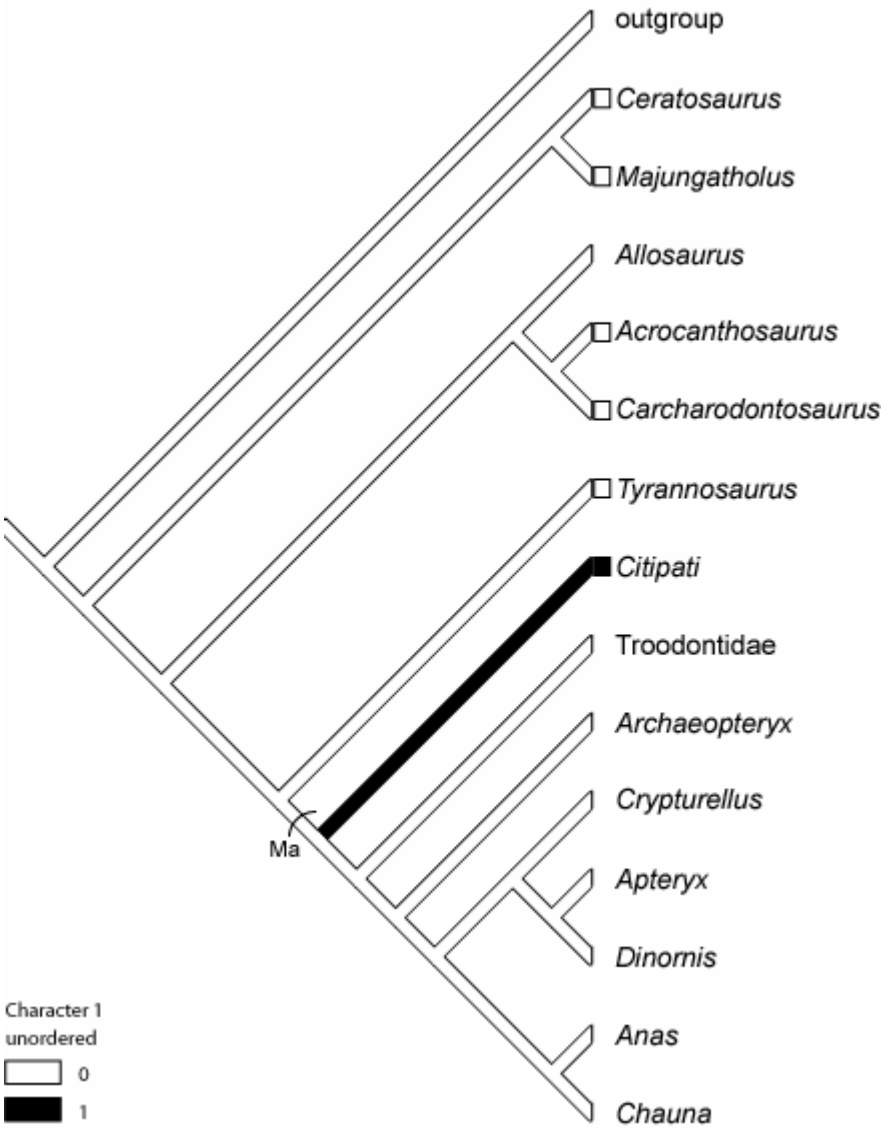

Figure 106. Resolution of character 1 on consensus tree using DELTRAN optimization.

For stem and node names and locations see figure 103.

Olfactory Bulb Position (Character 2) Resolution on Consensus Tree

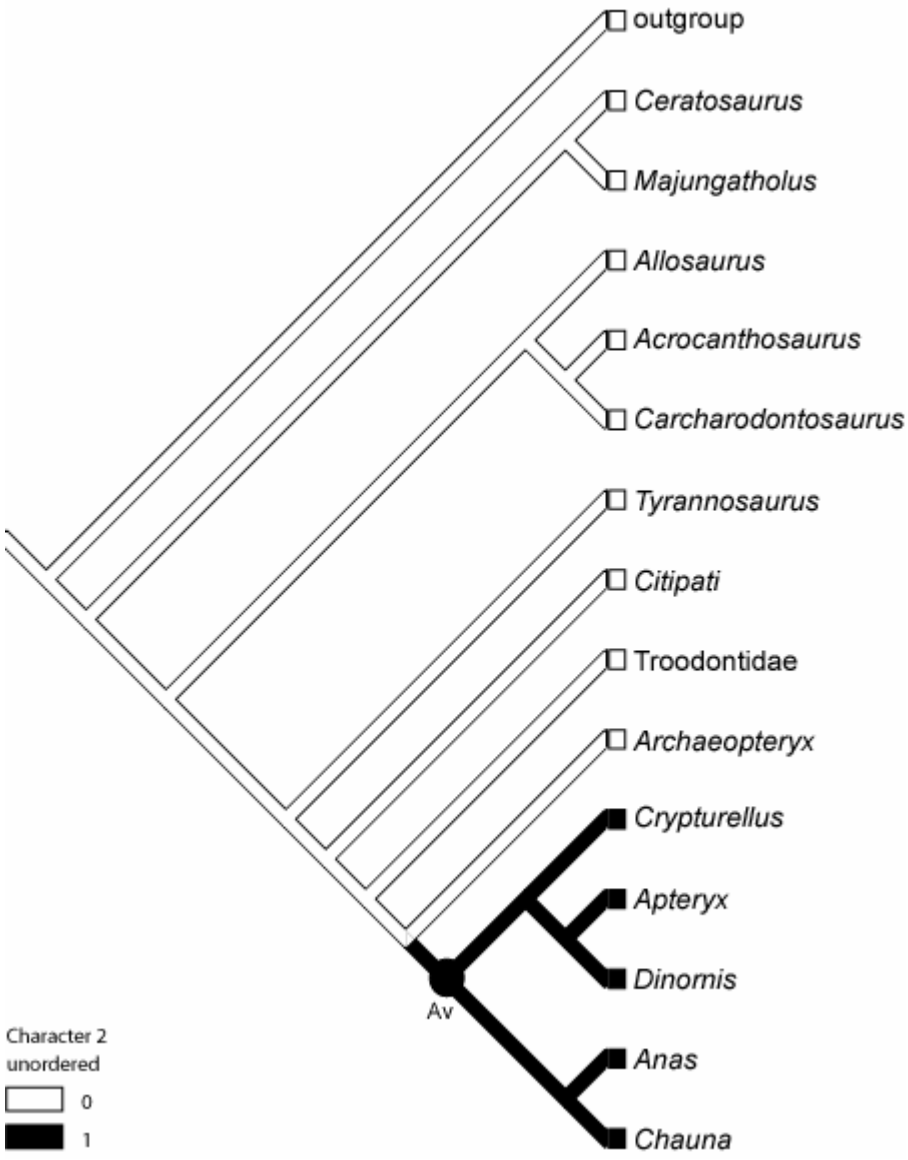

Figure 107. Resolution of character 2 on consensus tree.

For stem and node names and locations see figure 103. Character C.I.= 1.0.

Cerebral Hemisphere Shape
(Character 3) Resolution on Consensus Tree

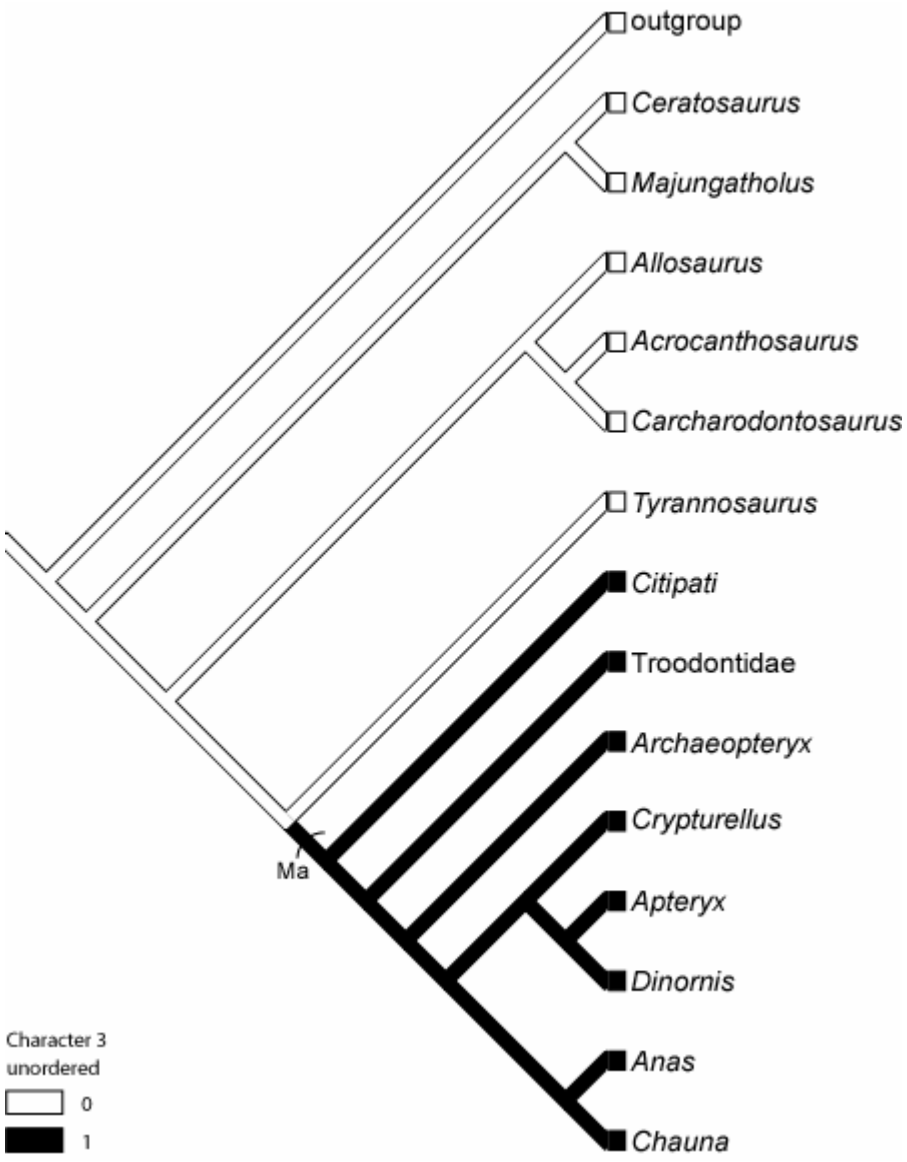

Figure 108. Resolution of character 3 on consensus tree.

For stem and node names and locations see figure 103. Character C.I.= 1.0.

Volume of the Cerebral Hemispheres (Character 4) Resolution on Consensus Tree

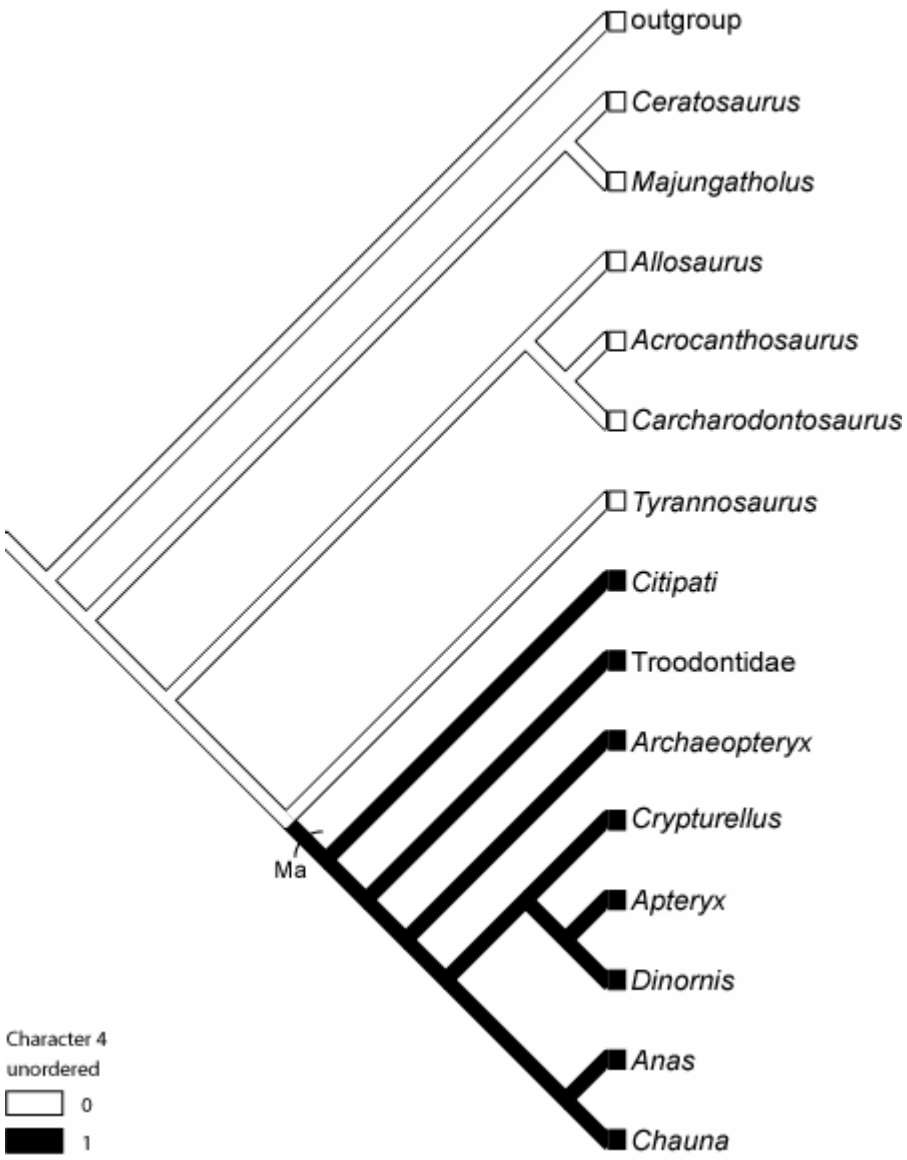

Figure 109. Resolution of character 4 on consensus tree.

For stem and node names and locations see figure 103. Character C.I.= 1.0.

Width of Endocast (Character 5) Resolution on Consensus Tree

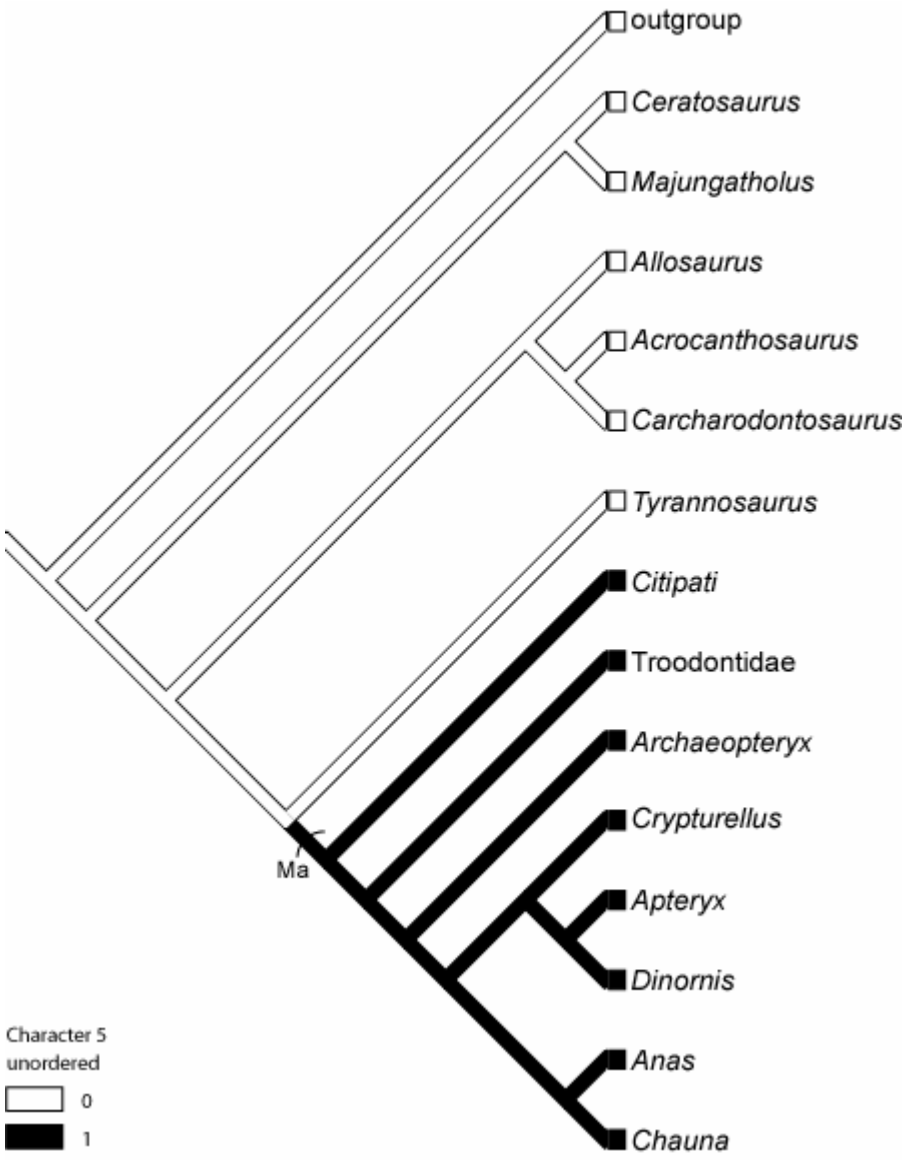

Figure 110. Resolution of character 5 on consensus tree.

For stem and node names and locations see figure 103. Character C.I.= 1.0.

Optic Lobe Position (Character 6) Resolution on Consensus Tree

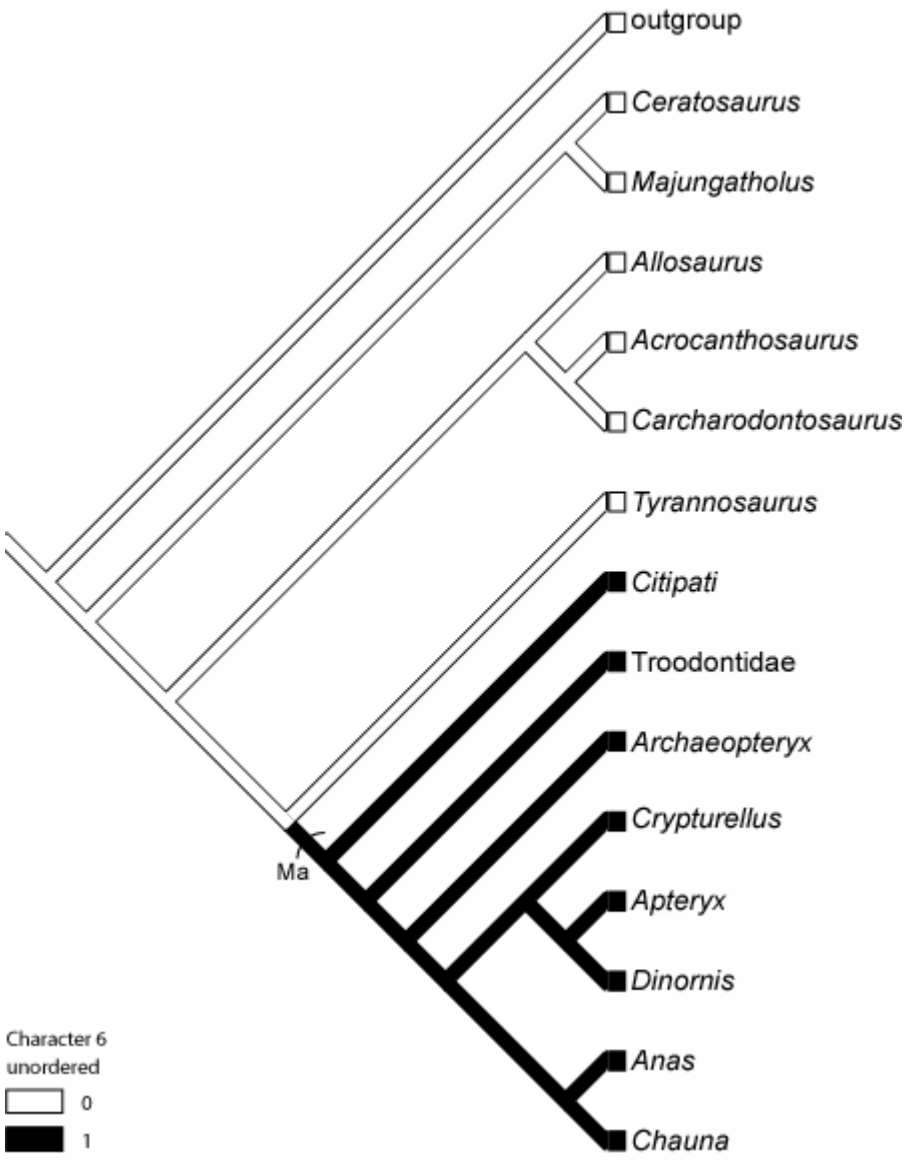

Figure 111. Resolution of character 6 on consensus tree.

For stem and node names and locations see figure 103. Character C.I.= 1.0.

Number of Trigeminal Nerve Foramina (Character 7) Resolution on Consensus Tree

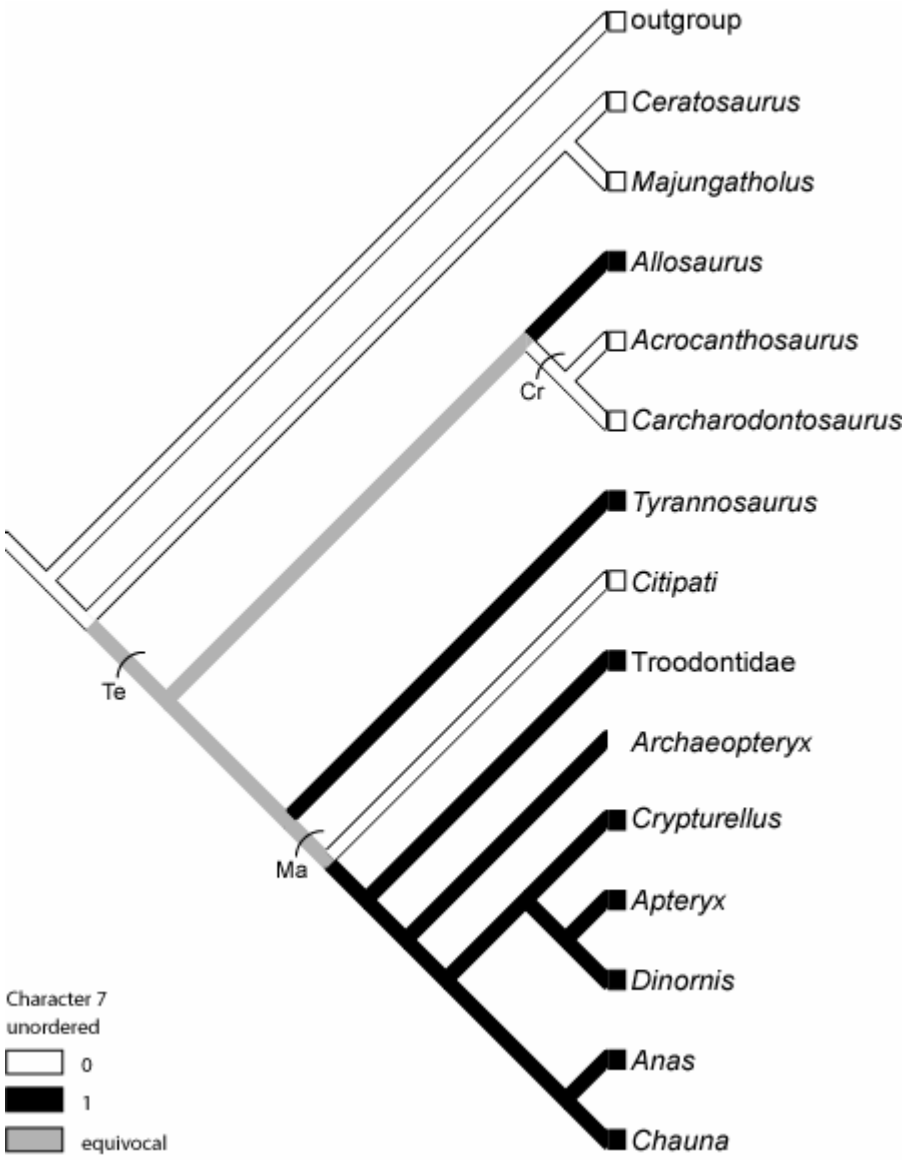

Figure 112. Resolution of character 7 on consensus tree.

For stem and node names and locations see figure 103. Character C.I.= 0.33.

lost in Carcharodontosauridae and *Citipati* (ACCTRAN; Figure 113), or was acquired independently in *Allosaurus, Tyrannosaurus*, and Maniraptora excluding *Citipati* (DELTRAN; Figure 114).

The derived character state for character 8 (the abducens nerve canal passing lateral to the pituitary fossa) is optimized as being independently obtained in *Ceratosaurus*, *Acrocanthosaurus*, and Coelurosauria (Figure 115). Character 9 (the internal carotid canals) shows the derived state evolving in Coelurosauria, and subsequently being independently lost in *Dinornis* and *Chauna* (Figure 116).

The derived condition of character 10 (the floccular fossa present and noticeable) appears at Theropoda (Figure 117). It was subsequently lost in Paleognathae, and then reacquired in *Apteryx* (ACCTRAN; Figure 118), or independently lost in *Crypturellus* and *Dinornis* (DELTRAN; Figure 119).

Character 11 (floccular lobe shape; Figure 120) and character 12 (posterior semicircular canal orientation; Figure 121) show the same distribution of the character states as characters 3, 4, 5, and 6. For these characters the derived state is found in Maniraptora. Although character 11 is shown on the cladogram to be in the derived state for *Crypturellus* and *Dinornis*, the character does not apply to these two taxa since they do not show any evidence of floccular lobes on the endocasts.

The derived state for character 13 (number of hypoglossal nerve foramina 2 to 3) is optimized as independently evolving in Maniraptora and *Carcharodontosaurus* (Figure 122). Character 14 (REQ) shows a complex

Number of Trigeminal Nerve Foramina (Character 7) Resolution on Consensus Tree- ACCTRAN Optimization

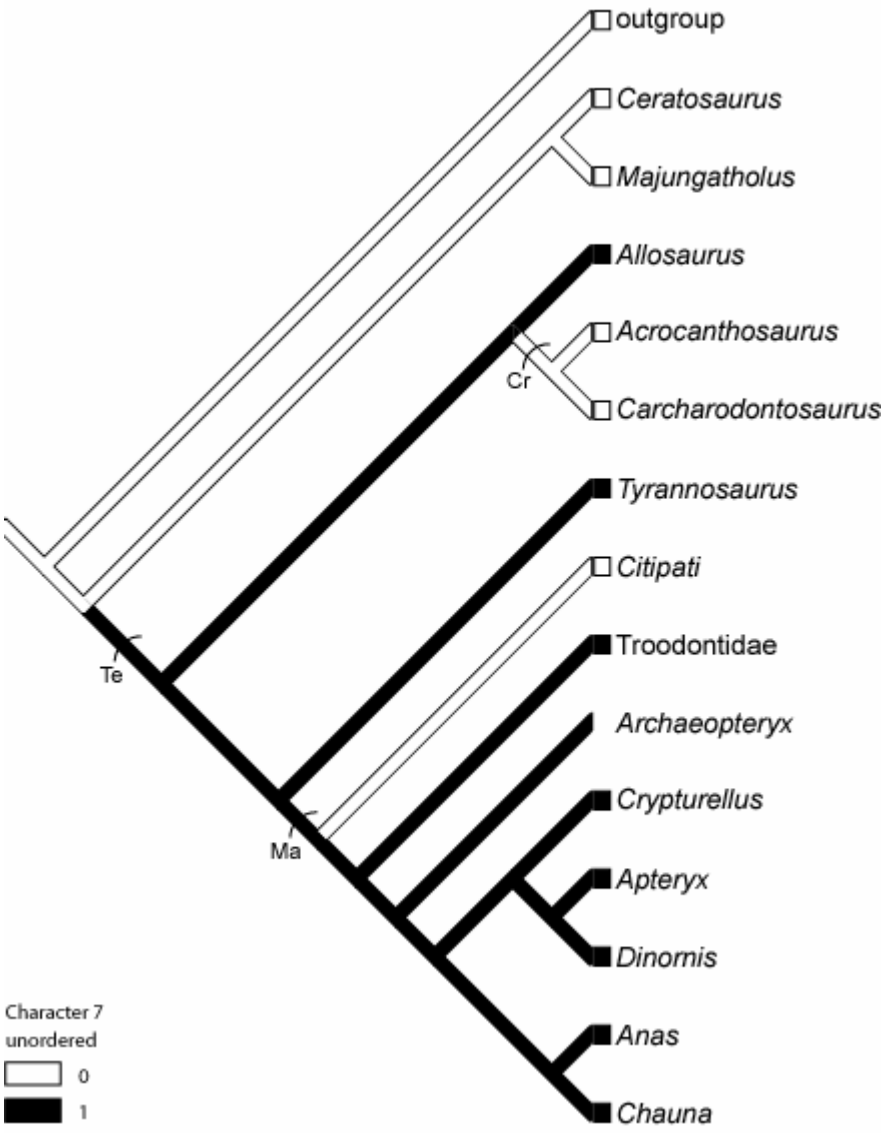

Figure 113. Resolution of character 7 on consensus tree using ACCTRAN optimization.

For stem and node names and locations see figure 103.

Number of Trigeminal Nerve Foramina (Character 7) Resolution on Consensus Tree- DELTRAN Optimization

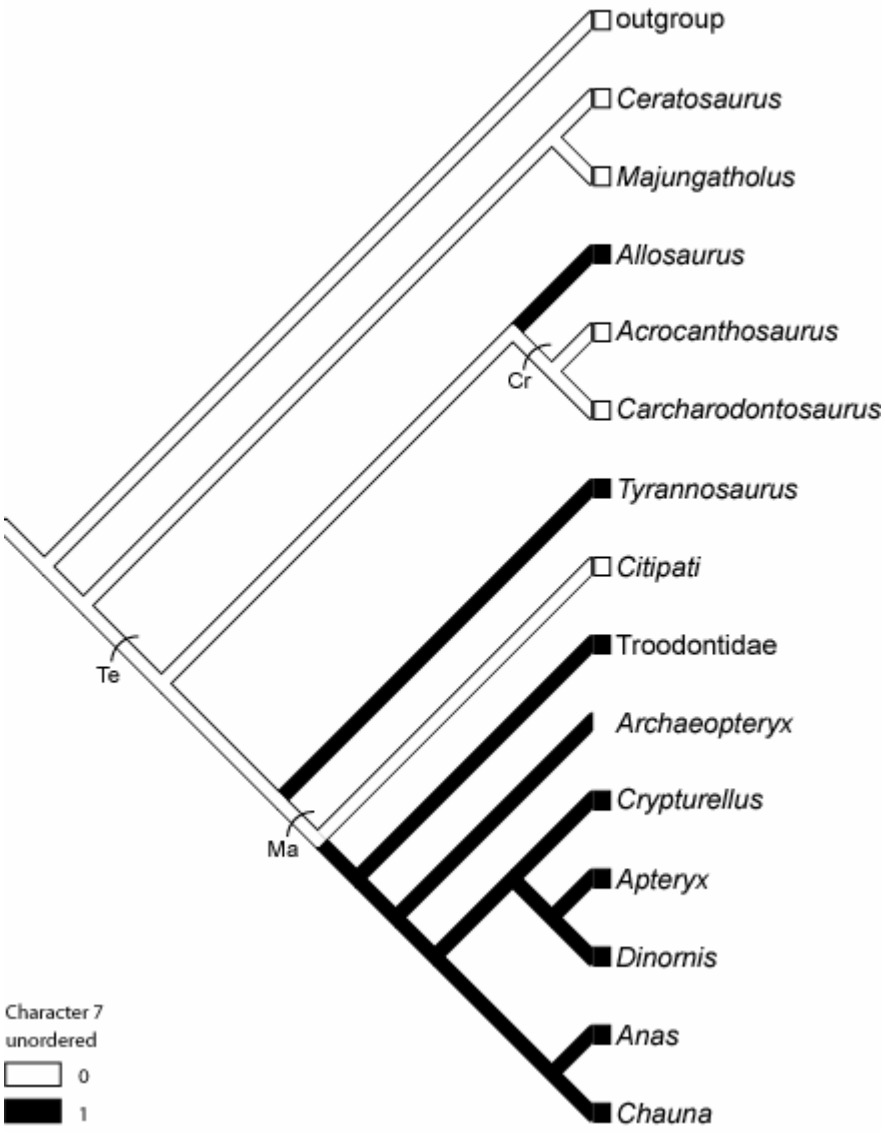

Figure 114. Resolution of character 7 on consensus tree using DELTRAN optimization.

For stem and node names and locations see figure 103.

Abducens Nerve Canal (Character 8) Resolution on Consensus Tree

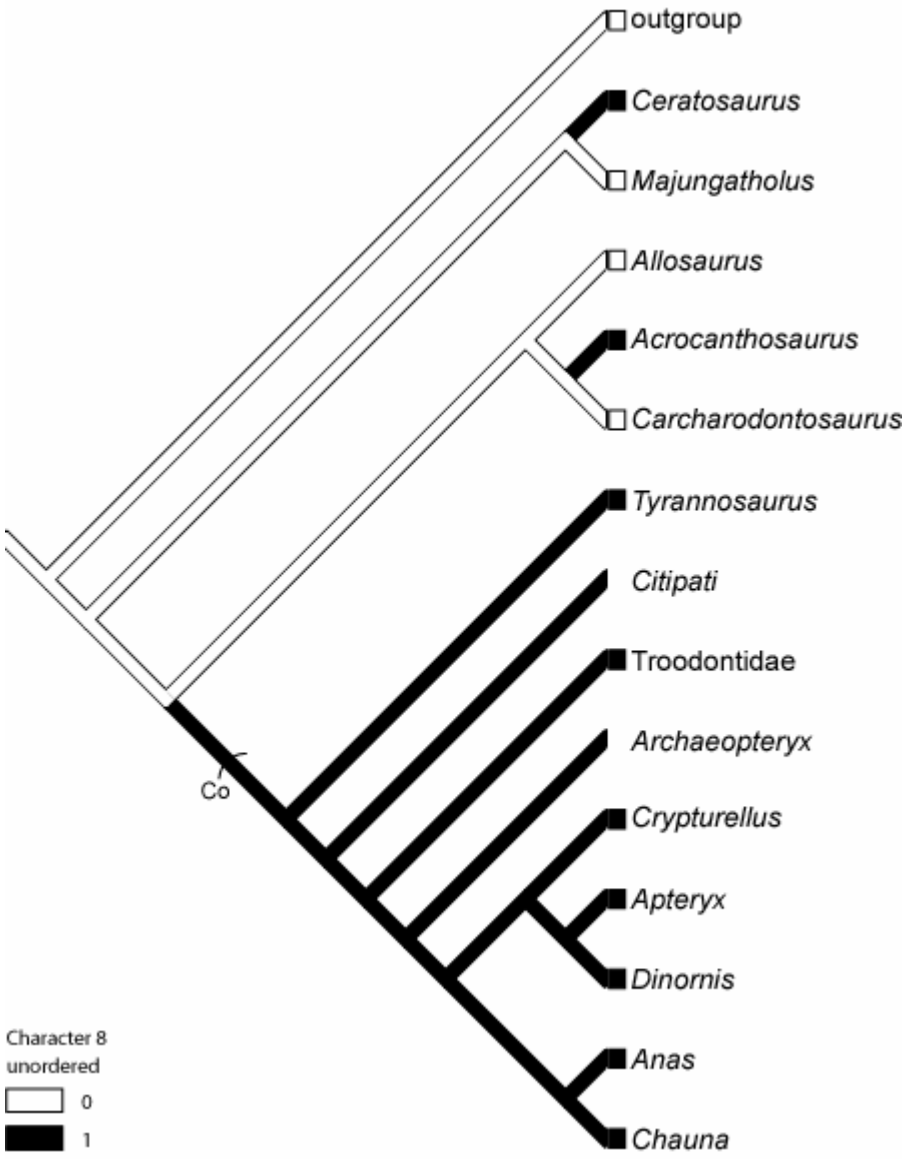

Figure 115. Resolution of character 8 on consensus tree.

For stem and node names and locations see figure 103. Character C.I.= 0.33.

Internal Carotid Canals (Character 9) Resolution on Consensus Tree

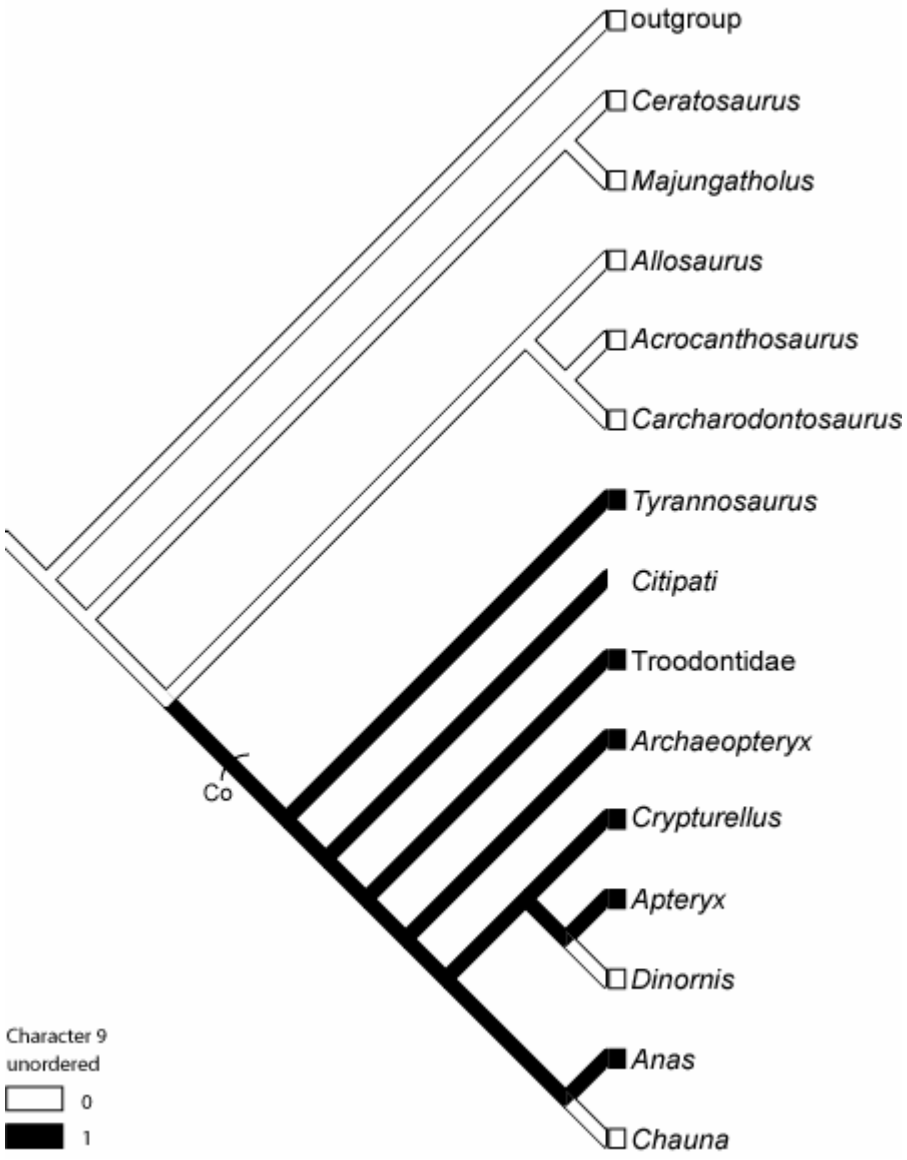

Figure 116. Resolution of character 9 on consensus tree.

For stem and node names and locations see figure 103. Character C.I.= 0.33.

Floccular Fossa (Character 10) Resolution on Consensus Tree

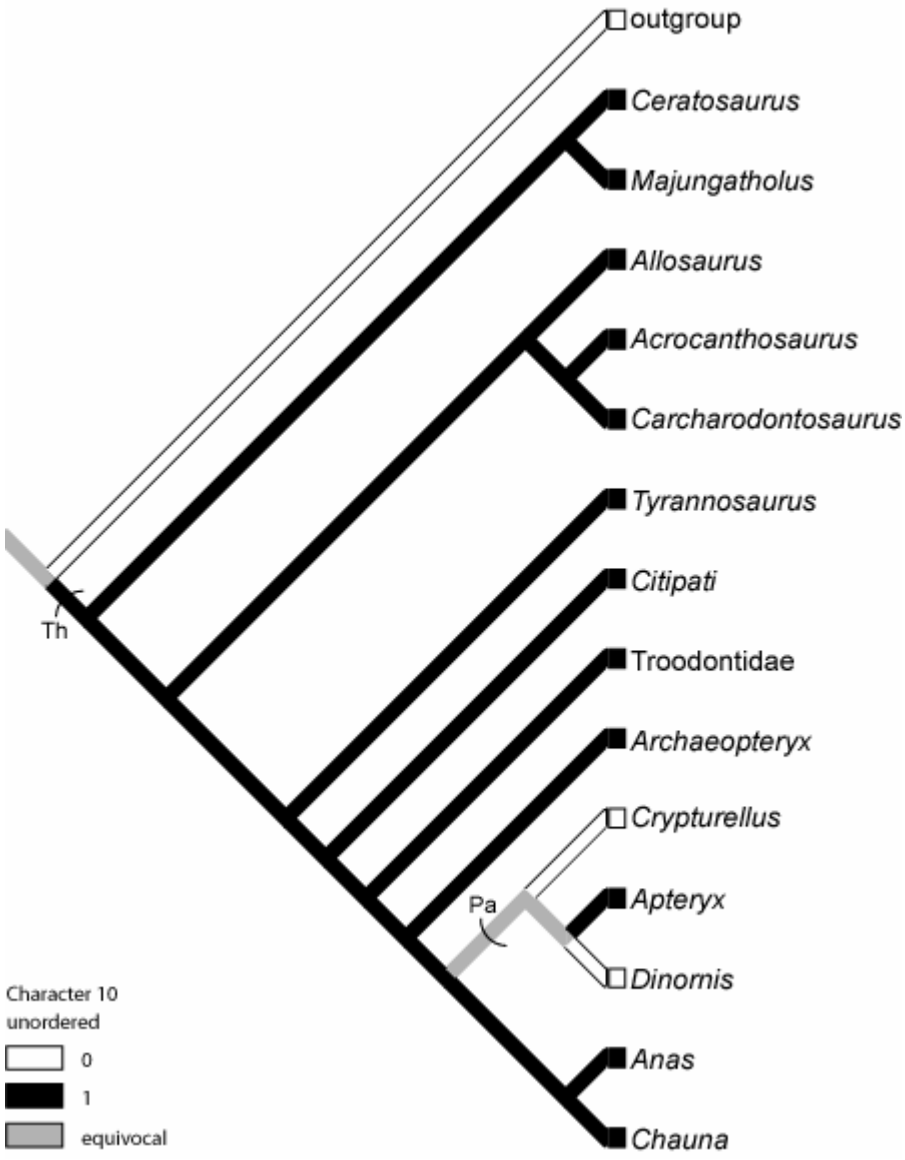

Figure 117. Resolution of character 10 on consensus tree.

For stem and node names and locations see figure 103. Character C.I.= 0.33.

Floccular Fossa (Character 10) Resolution on Consensus Tree- ACCTRAN Optimization

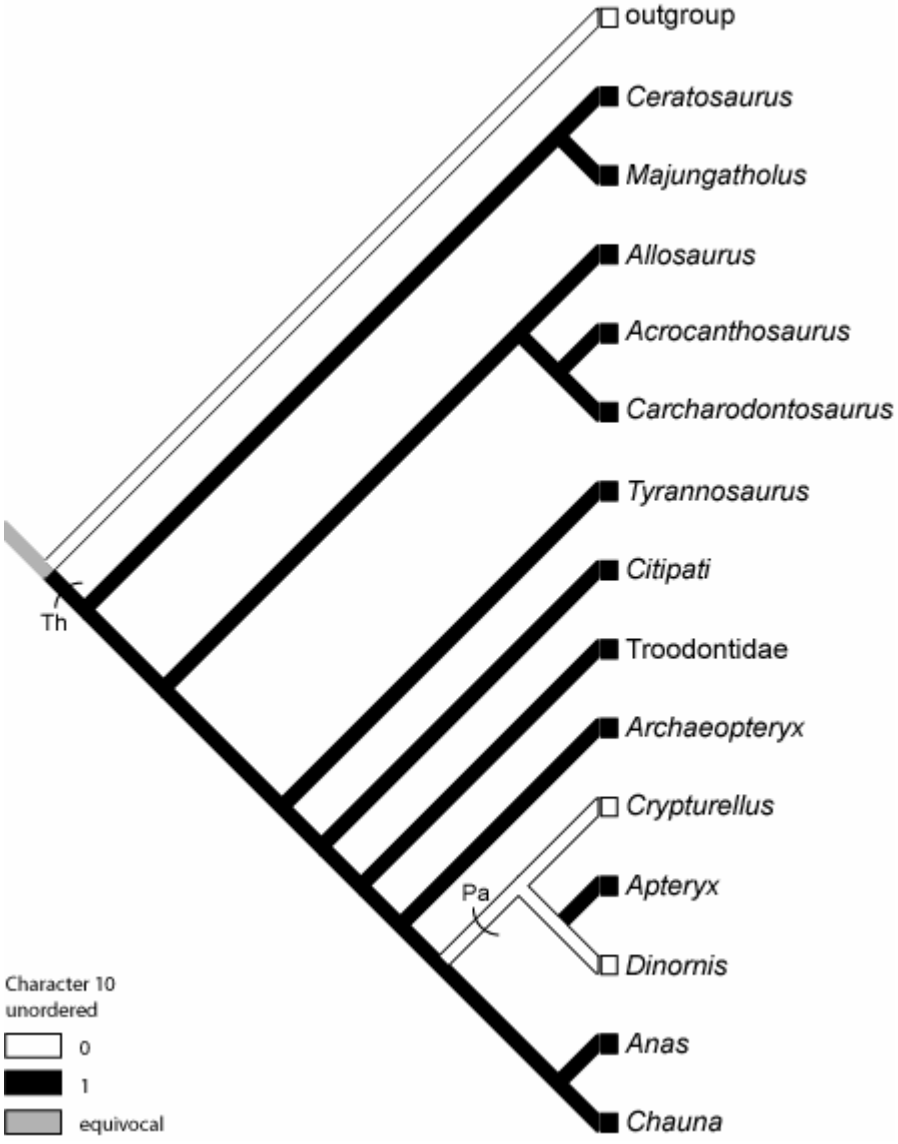

Figure 118. Resolution of character 10 on consensus tree using ACCTRAN optimization.

For stem and node names and locations see figure 103.

Floccular Fossa (Character 10) Resolution on Consensus Tree- DELTRAN Optimization

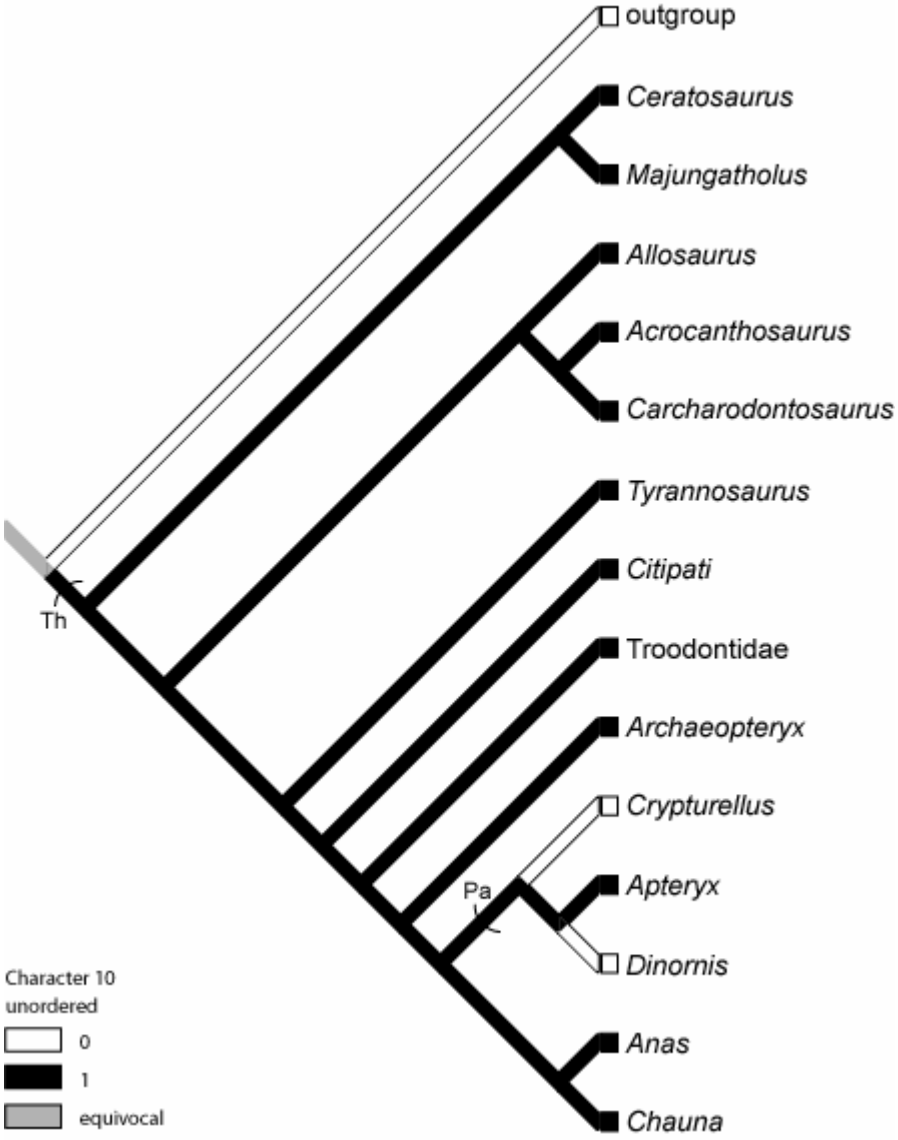

Figure 119. Resolution of character 10 on consensus tree using DELTRAN optimization.

For stem and node names and locations see figure 103.

Floccular Lobe Shape (Character 11) Resolution on Consensus Tree

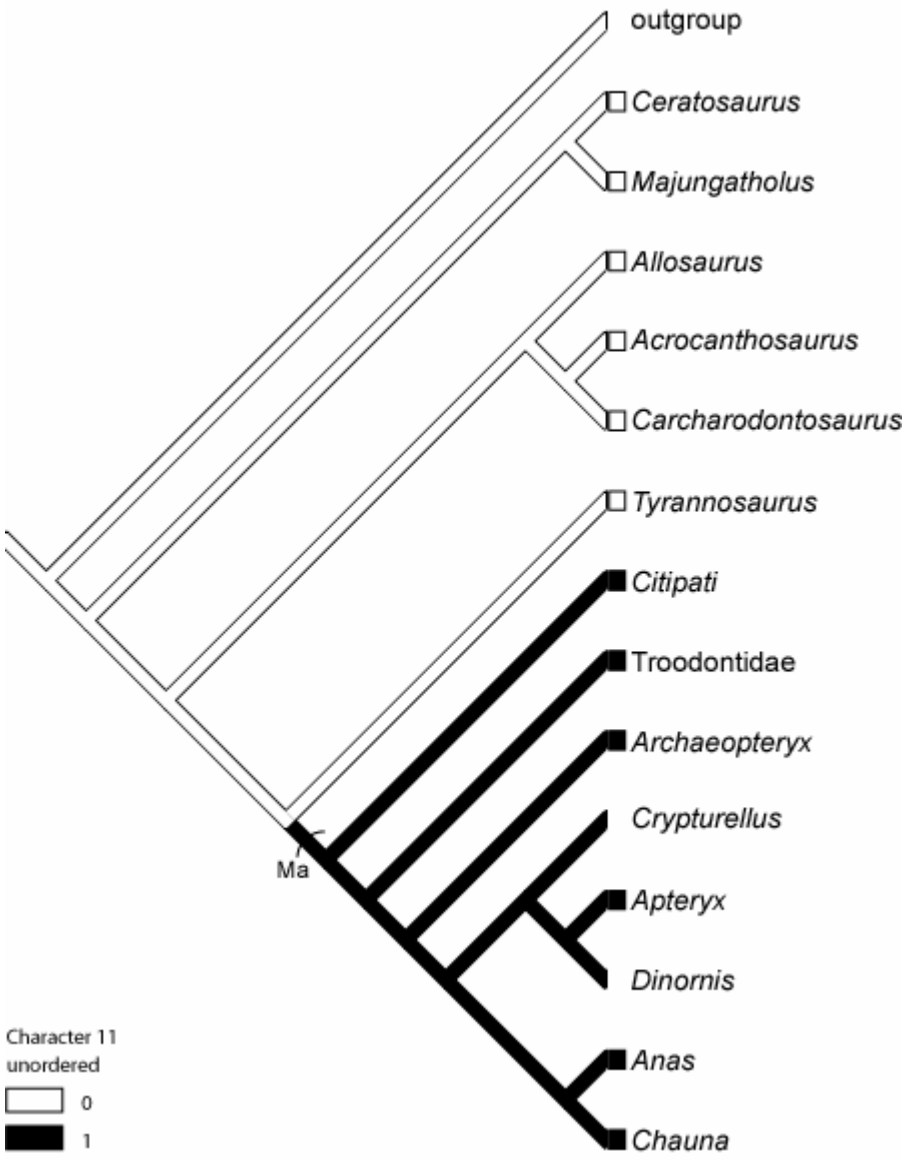

Figure 120. Resolution of character 11 on consensus tree.

For stem and node names and locations see figure 103. Character C.I.= 1.0.

Posterior Semicircular Canal Orientation (Character 12) Resolution on Consensus Tree

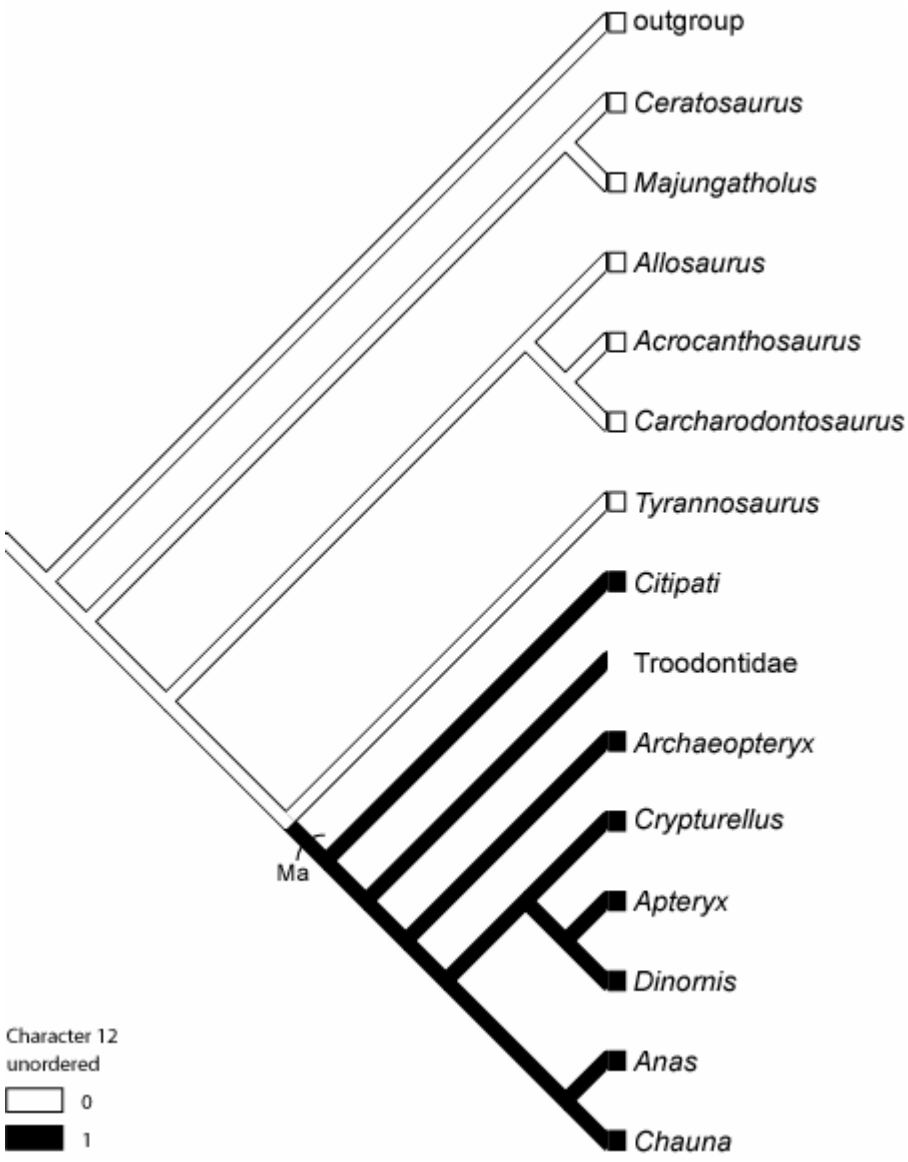

Figure 121. Resolution of character 12 on consensus tree.

For stem and node names and locations see figure 103. Character C.I.= 1.0.

Number of Hypoglossal Nerve Foramina (Character 13) Resolution on Consensus Tree

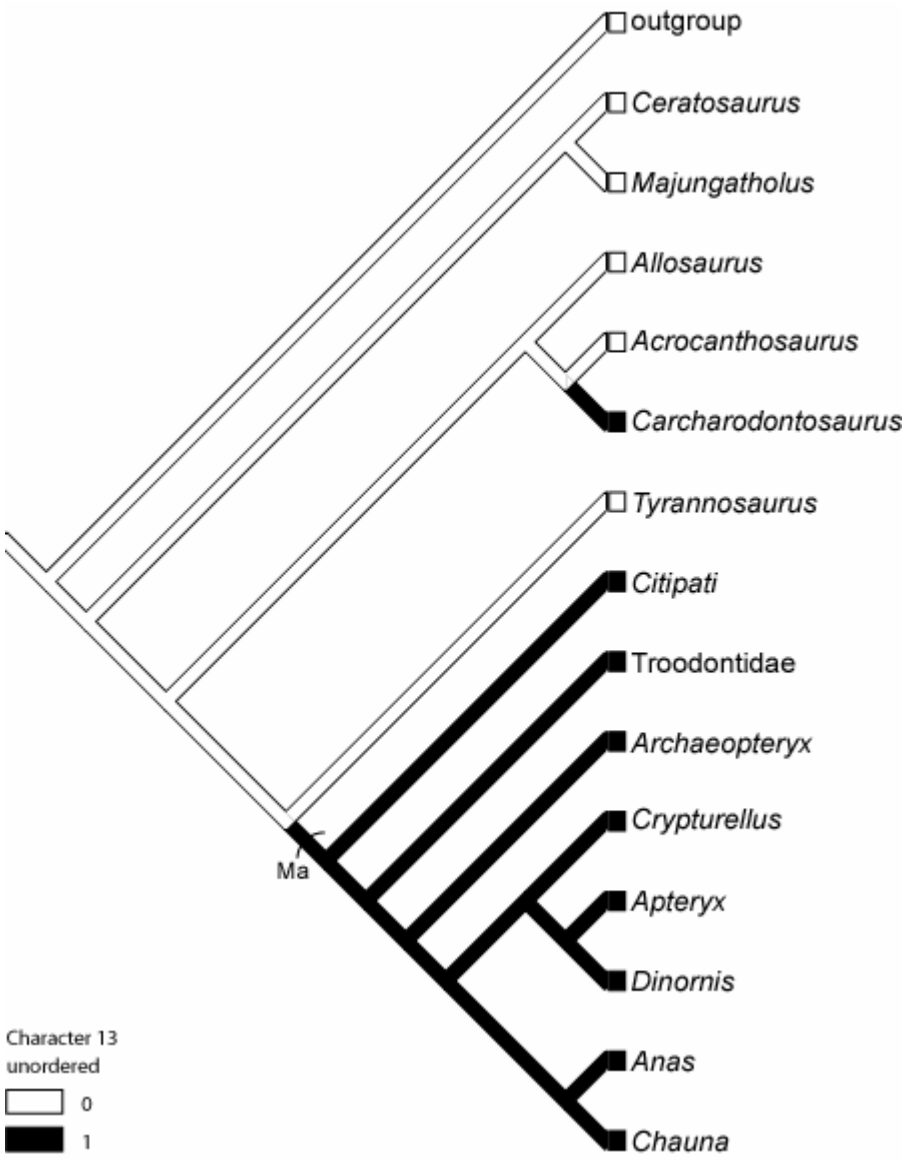

Figure 122. Resolution of character 13 on consensus tree.

For stem and node names and locations see figure 103. Character C.I.= 0.5.

distribution of states (Figure 123). The derived state is shown as being independently attained in *Tyrannosaurus,* Troodontidae, *Apteryx*, and Neognathae.

Even though the character is unequivocally optimized, there are some REQ data available for taxa that are not included in this tree. One of the more important of these is the ornithomimid *Dromiceiomimus*. The phylogenetic relationships of ornithomimids are debatable, and vary depending on whose phylogeny is used. *Dromiceiomimus* has an REQ greater than 6 (Hurlburt, 1996), representing the derived character state. To determine the influence that this taxon would have on character optimizations for character 14, it was added onto the tree in the various positions that have been applied to it in the phylogenies already examined.

The consensus tree generated from my data + Holtz's data has Ornithomimidae as a sister taxon to *Tyrannosaurus*. This placement of Ornithomimidae has no effect on the equivocation of character 14, because it is constrained to a branch that already has the derived character state (Figure 124).

In the consensus tree generated from my data + Rauhut's data, the Ornithomimidae are placed between *Tyrannosaurus* and *Citipati*. This placement causes an equivocation on the tree that begins in Coelurosauria (Figure 125). Resolving this equivocation with ACCTRAN optimization results in a small portion of the main tree showing the derived character state, this portion being from Coelurosauria to Maniraptora (Figure 126). After this segment, the main tree

Reptile Encephalization Quotient
(Character 14) Resolution on Consensus Tree

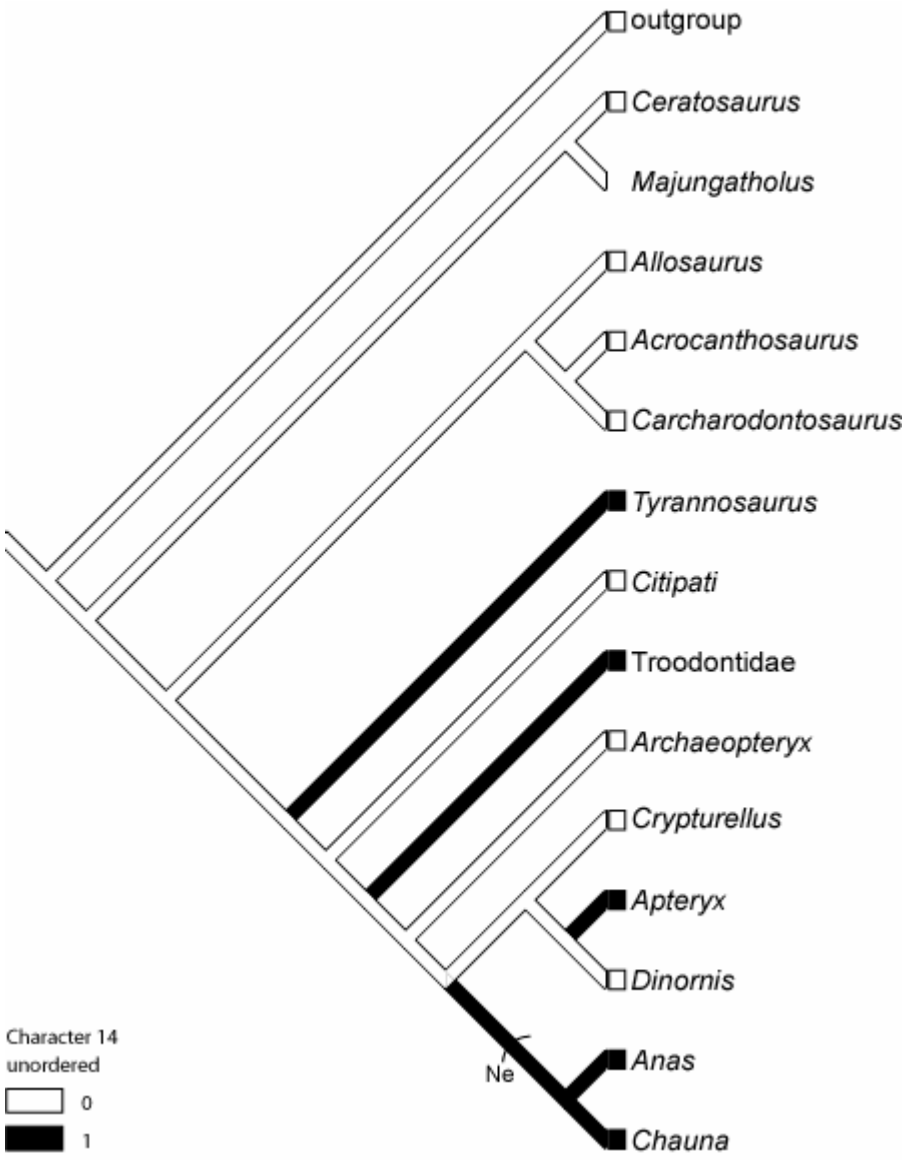

Figure 123. Resolution of character 14 on consensus tree.

For stem and node names and locations see figure 103. Character C.I.= 0.25.

Reptile Encephalization Quotient (Character 14) Resolution on Consensus Tree with Holtz's Placement of Ornithomimidae

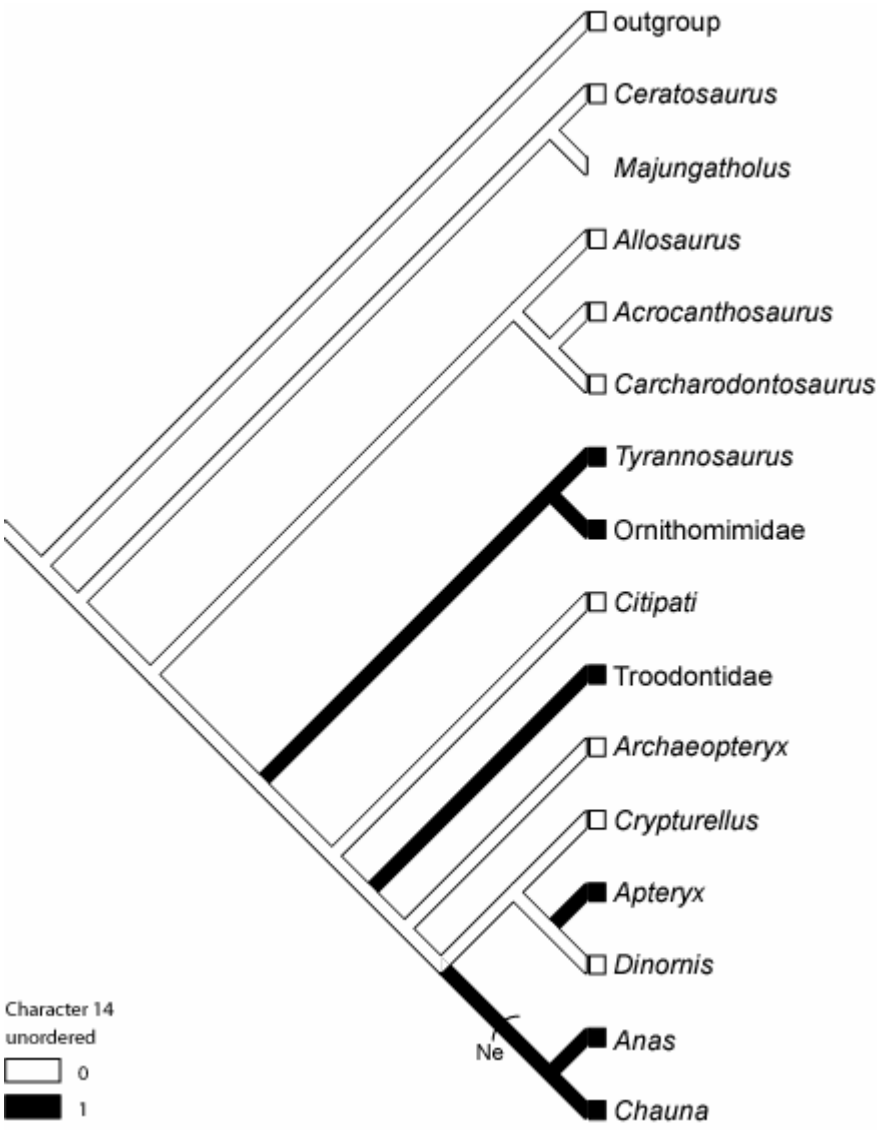

Figure 124. Resolution of character 14 on consensus tree containing Holtz's placement of Ornithomimidae.

For stem and node names and locations see figure 103. Character C.I.= 0.25.

Reptile Encephalization Quotient (Character 14) Resolution on Consensus Tree with Rauhut's Placement of Ornithomimidae

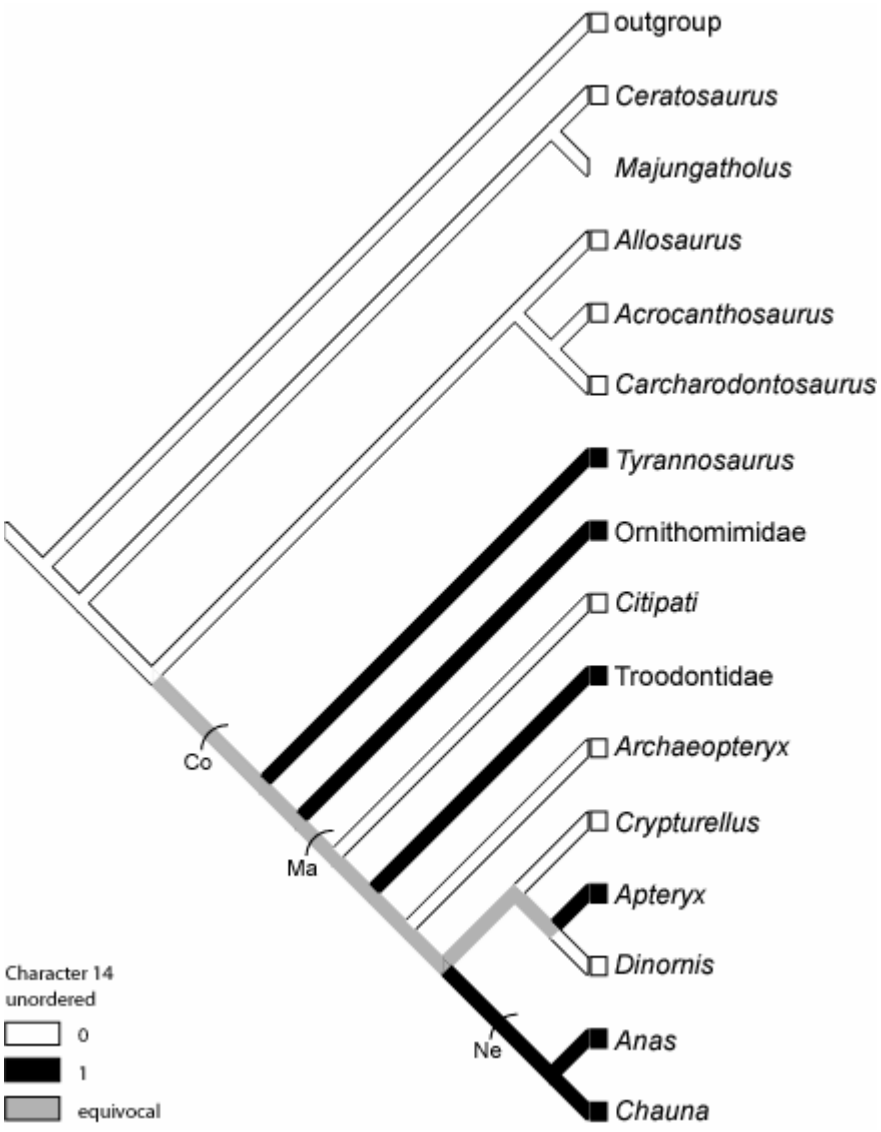

Figure 125. Resolution of character 14 on consensus tree containing Rauhut's placement of Ornithomimidae.

For stem and node names and locations see figure 103. Character C.I.= 0.2.

Reptile Encephalization Quotient (Character 14) Resolution on Consensus Tree with Rauhut's Placement of Ornithomimidae- ACCTRAN Optimization

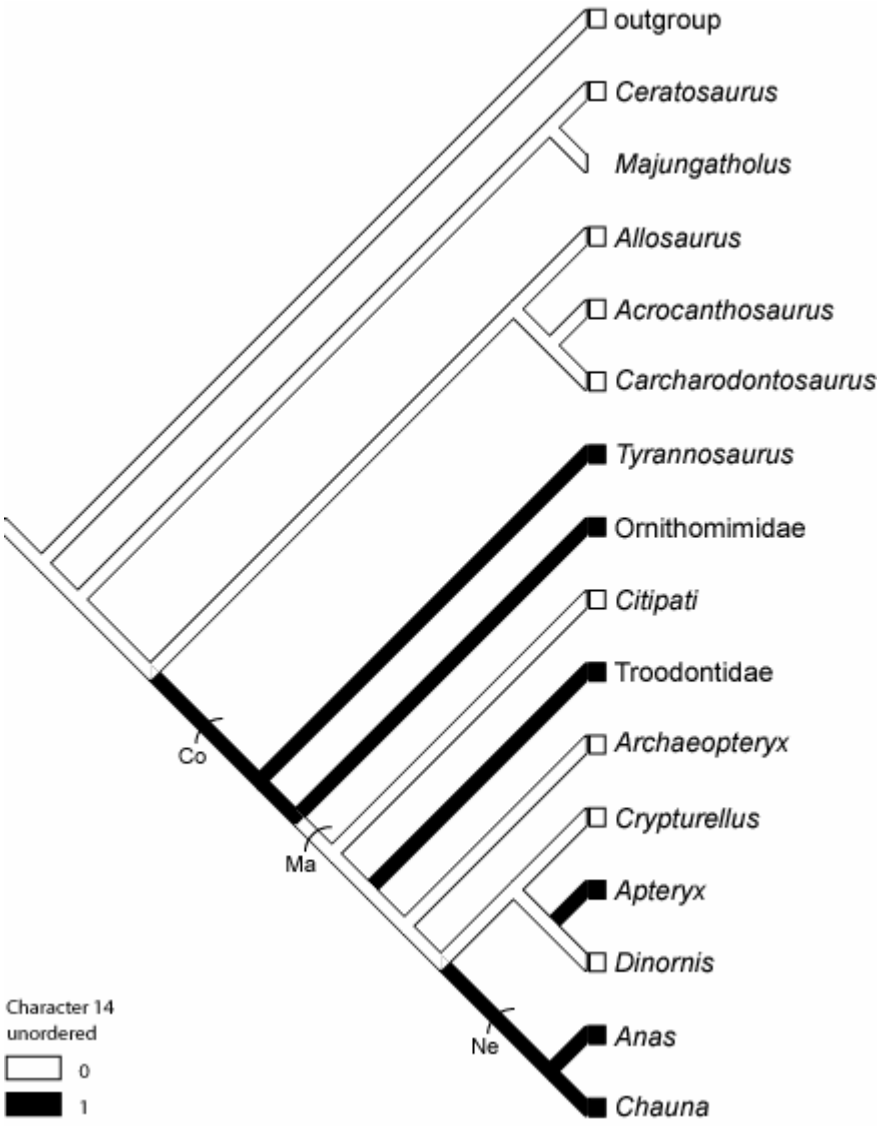

Figure 126. Resolution of character 14 on consensus tree containing Rauhut's placement of Ornithomimidae, using ACCTRAN optimization.

For stem and node names and locations see figure 103.

reverts back to the primitive character state before its final change to the derived character state in Neognathae. Resolving this equivocation with DELTRAN optimization results in a tree similar to the original tree for character 14, with the exception that Ornithomimidae joins the list of taxa that independently attain the derived character state (Figure 127).

The consensus tree generated from my data + Sereno's data shows the third position that the Ornithomimidae might occupy, that position being just basal to the *Tyrannosaurus* branch. This leads to the same equivocation just noted (Figure 128). The solutions to this equivocation using ACCTRAN and DELTRAN optimization are also the same (Figures 129, 130), the only difference being that Ornithomimidae is more basal than *Tyrannosaurus* instead of more derived. Although these analyses give some possibilities for the resolution of character 14, more data on theropod REQs is required before a strongly supported resolution can be attained.

The previous discussion of where character state transitions occur can be summarized on a single tree (Figure 131). Those transition points are shown using ACCTRAN optimization. By having those transitions shown together, rather than discussed separately character by character, it can be seen that although some of the derived states of the characters were acquired in a stepwise fashion throughout the cladogram, a large number evolved at Maniraptora, between *Tyrannosaurus* and *Citipati*. It may be tempting to say that this shows a lot of support for this step in the tree. However, it is possible that some of these characters are correlated and

Reptile Encephalization Quotient (Character 14) Resolution on Consensus Tree with Rauhut's Placement of Ornithomimidae- DELTRAN Optimization

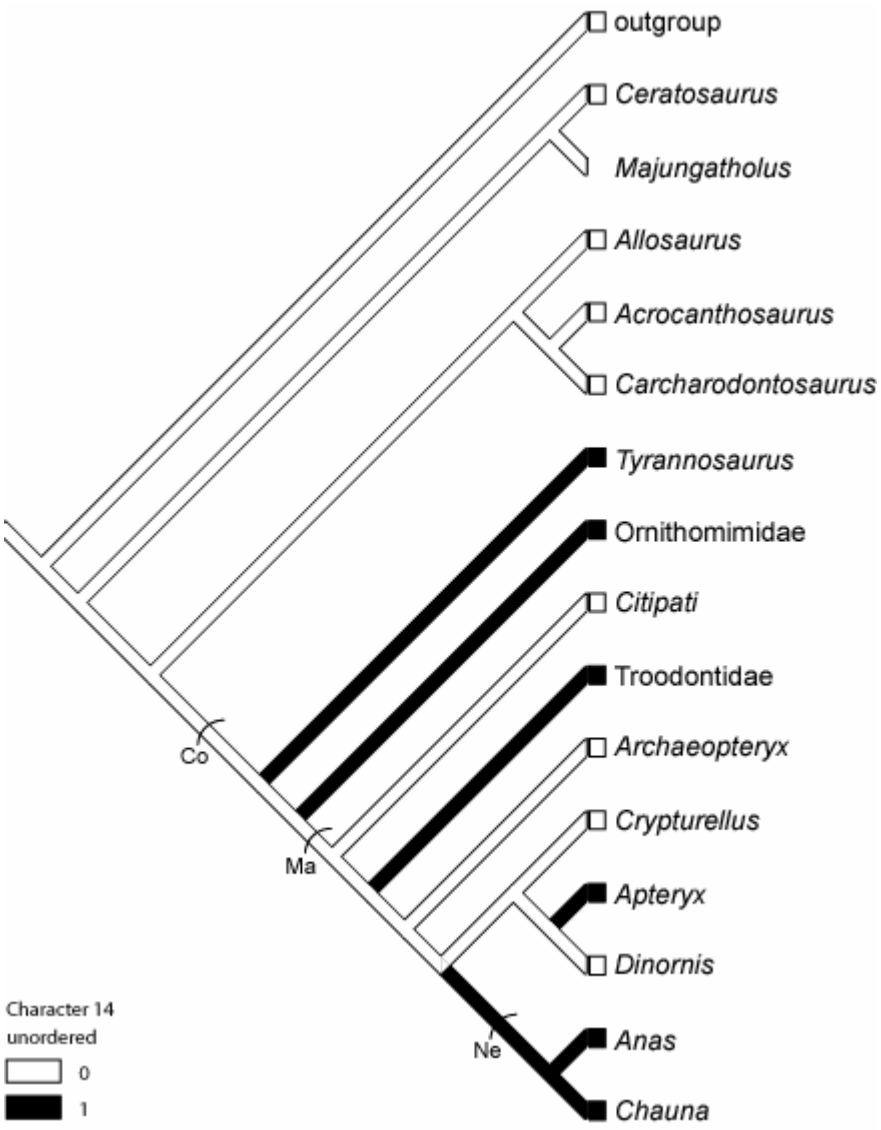

Figure 127. Resolution of character 14 on consensus tree containing Rauhut's placement of Ornithomimidae, using DELTRAN optimization.

For stem and node names and locations see figure 103.

Reptile Encephalization Quotient (Character 14) Resolution on Consensus Tree with Sereno's Placement of Ornithomimidae

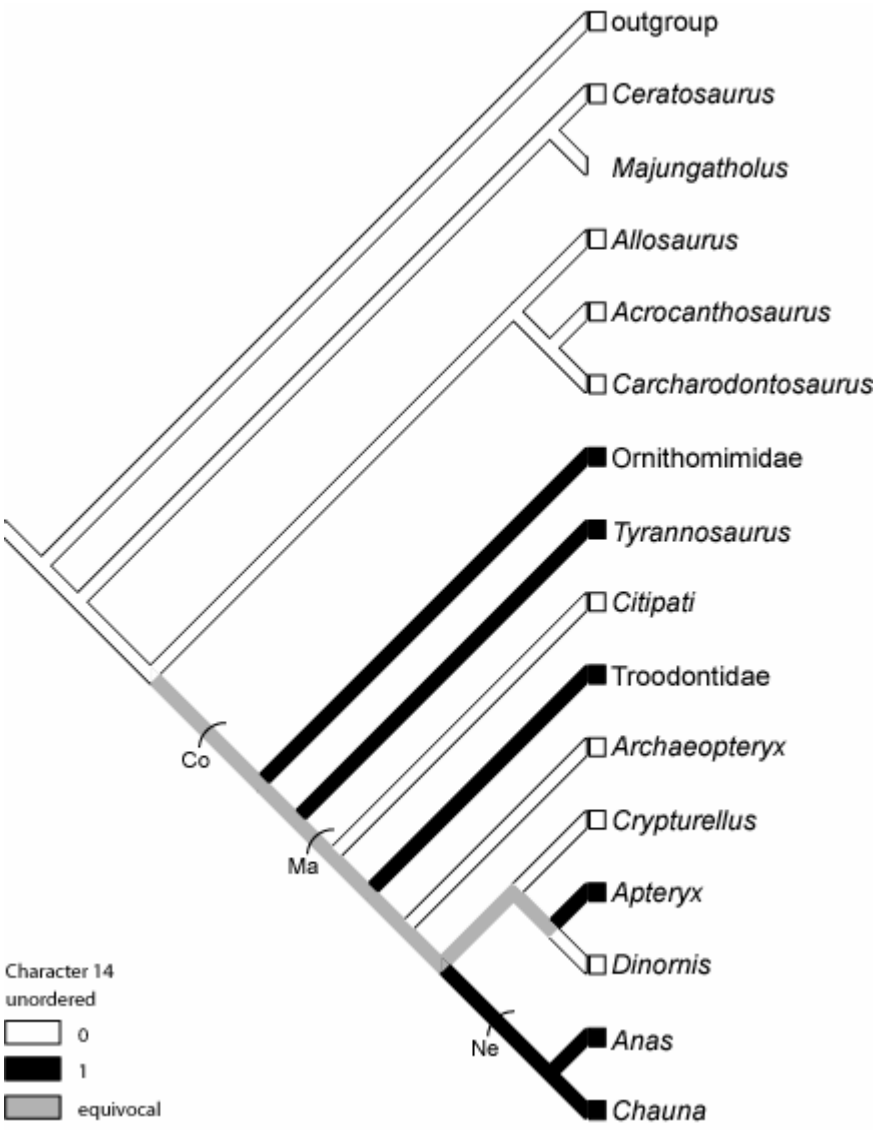

Figure 128. Resolution of character 14 on consensus tree containing Sereno's placement of Ornithomimidae.

For stem and node names and locations see figure 103. Character C.I.= 0.2.

Reptile Encephalization Quotient (Character 14) Resolution on Consensus Tree with Sereno's Placement of Ornithomimidae- ACCTRAN Optimization

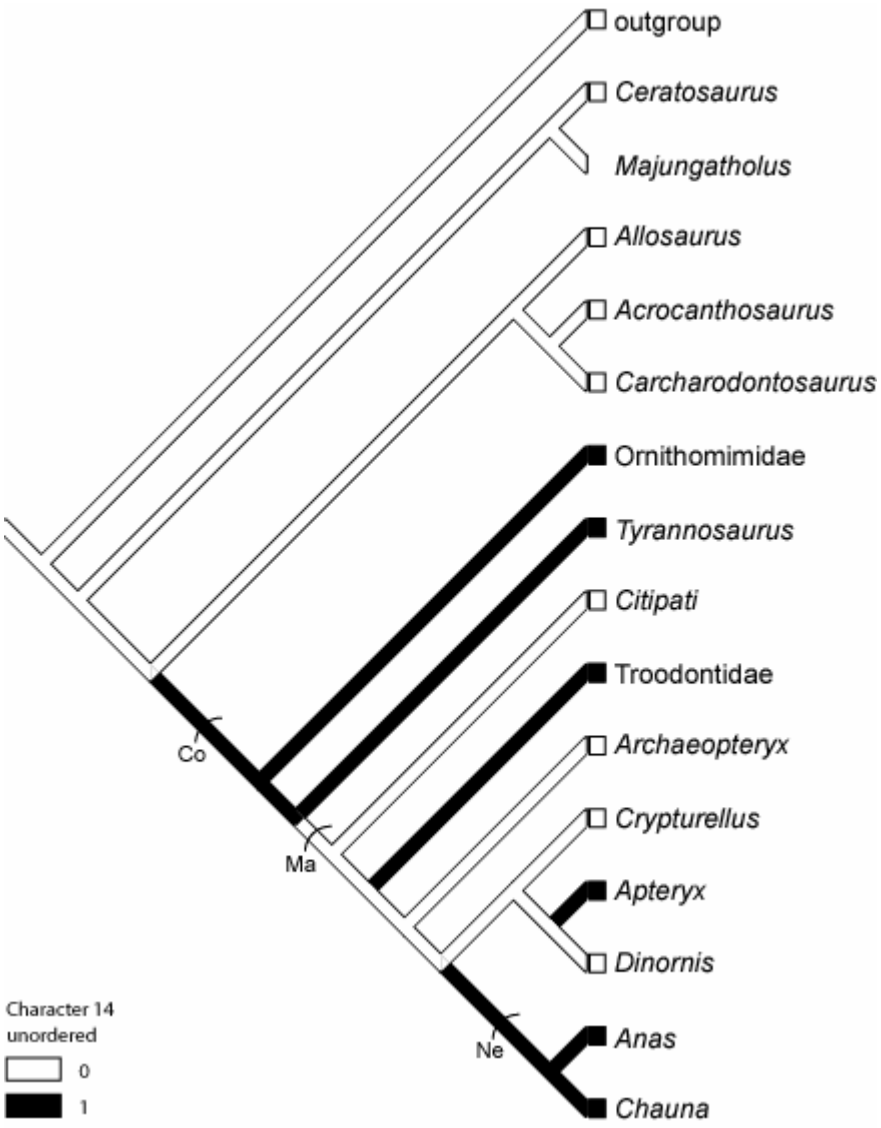

Figure 129. Resolution of character 14 on consensus tree containing Sereno's placement of Ornithomimidae, using ACCTRAN optimization.

For stem and node names and locations see figure 103.

Reptile Encephalization Quotient (Character 14) Resolution on Consensus Tree with Sereno's Placement of Ornithomimidae- DELTRAN Optimization

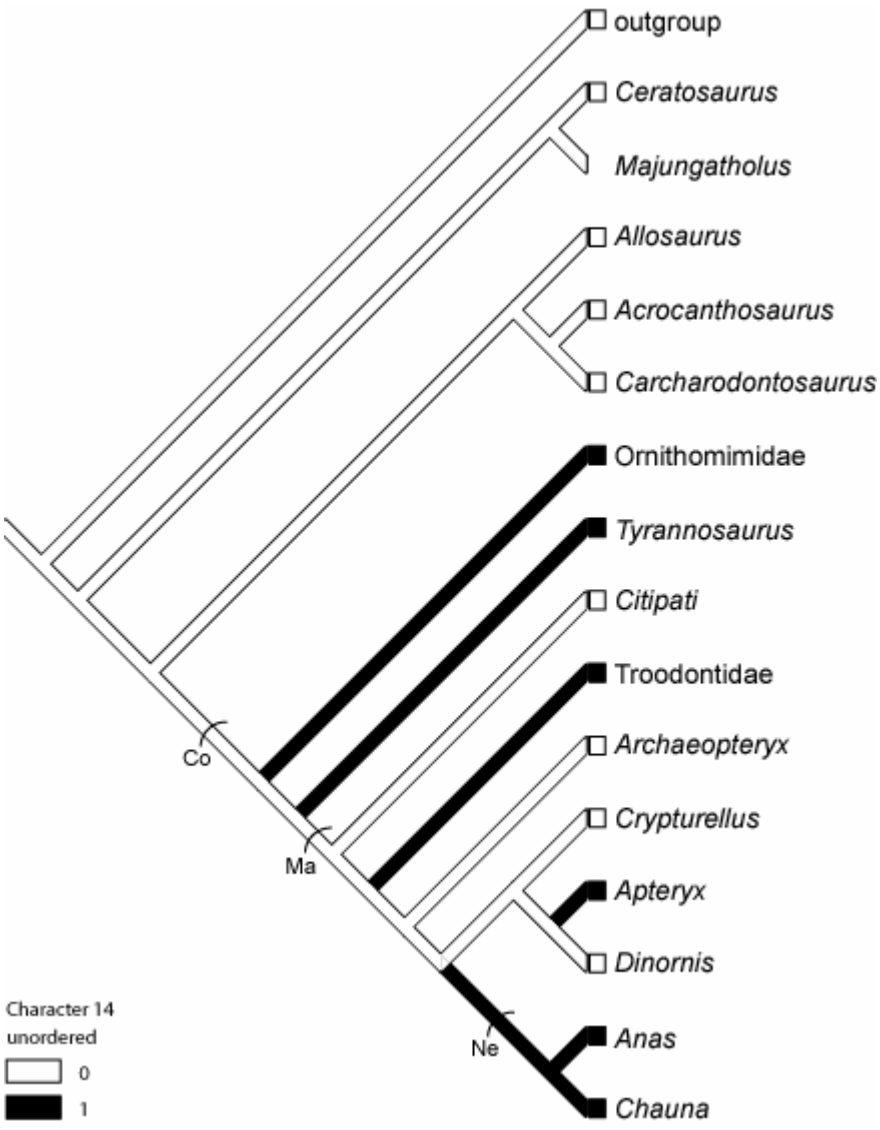

Figure 130. Resolution of character 14 on consensus tree containing Sereno's placement of Ornithomimidae, using DELTRAN optimization.

For stem and node names and locations see figure 103.

Character Acquisition on Consensus Tree with ACCTRAN Optimization

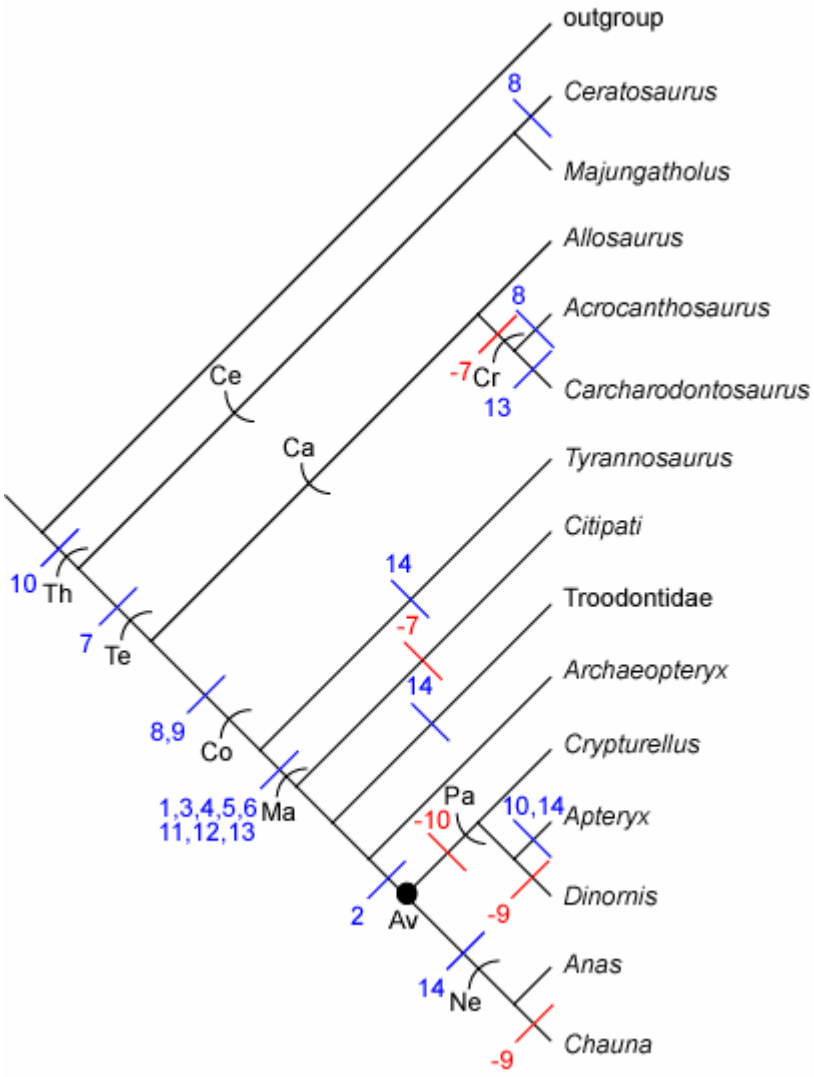

Figure 131. Consensus tree showing the sequence of character acquisition using ACCTRAN optimization.

Those characters in blue represent a transition from the primitive state to the derived state, while those characters in red represent a transition back to the primitive state from the derived state. For meaning of abbreviations, see figure 103.

not truly independent (Emerson and Hastings, 1998), leading to a false sense of security. It is also possible that there are intervening taxa that have not been found, and that once those taxa (if they exist) are discovered and scored for the characters, those characters may be divided between various nodes. Regardless of these possibilities, the gradual evolution of the theropod brain throughout the theropod clade can be seen in this summary cladogram.

Being able to plot character transitions on a cladogram is very useful, but it is also indispensable to look at the endocasts themselves, in a phylogenetic sequence, to get a general idea of what changes occur through the lineage, and this is done in the following figures (Figures 132, 133, 134). In these figures, I have divided the theropods into three artificial groups. The first group consists of basal theropods; those figured are *Ceratosaurus, Majungatholus, Allosaurus,* and *Acrocanthosaurus*. The second group is more derived non-avian theropods; those in the figure are *Citipati, Mongolodon,* and the Zos Canyon troodontid. The final group contains avian theropods. The two given in the figure are *Dinornis* and *Chauna*. Several changes can be seen moving through the three figures. A couple of the most noticeable changes are in the casts of the cerebral hemispheres and optic lobes. In the first figure, the casts of the cerebral hemispheres are partially obscured by the casts of the dorsal sagittal sinus and occipital sinus. All that can be seen of the cerebral hemisphere casts are the lateral portions showing an oval outline. In the derived non-avian theropods the casts of the cerebral hemispheres

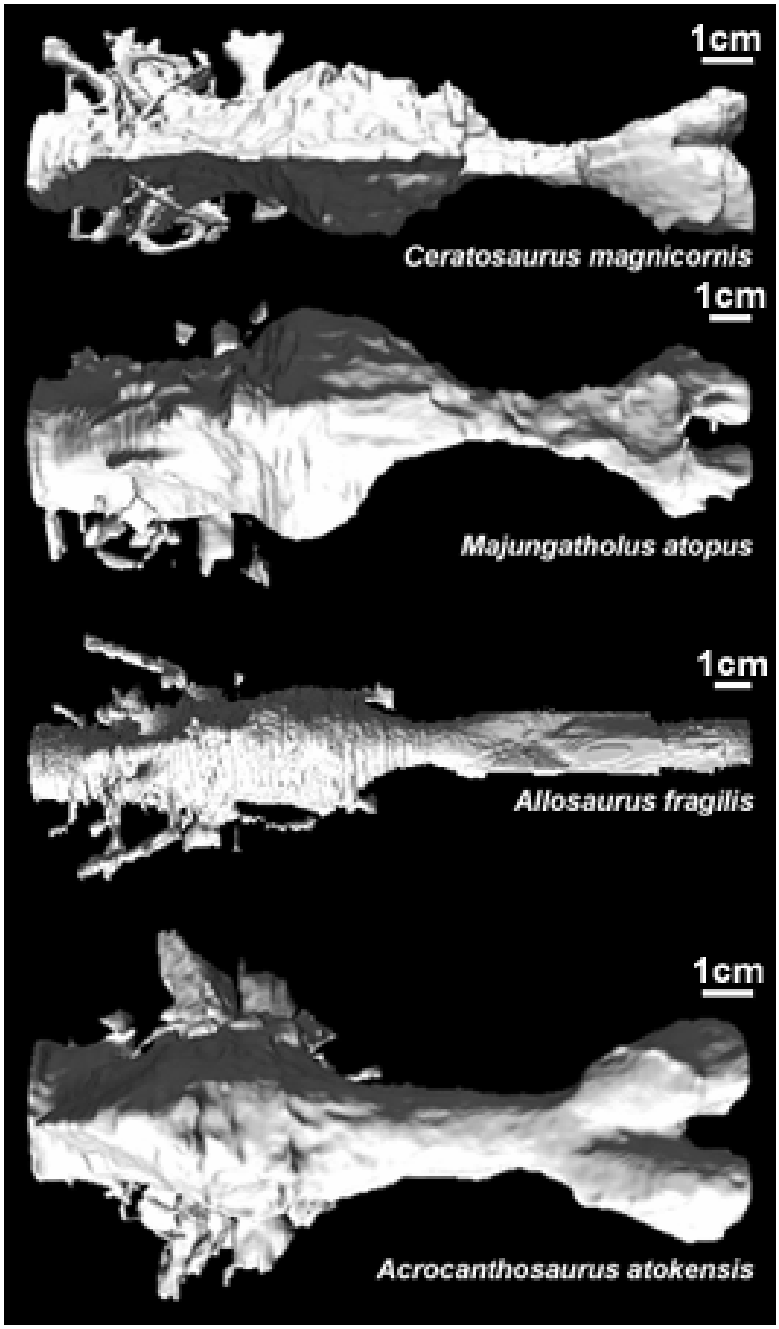

Figure 132. Dorsal view of four basal non-avian theropod endocasts.

The phylogenetic position of the four endocasts above goes from the most basal at the top to the most recent at the bottom.

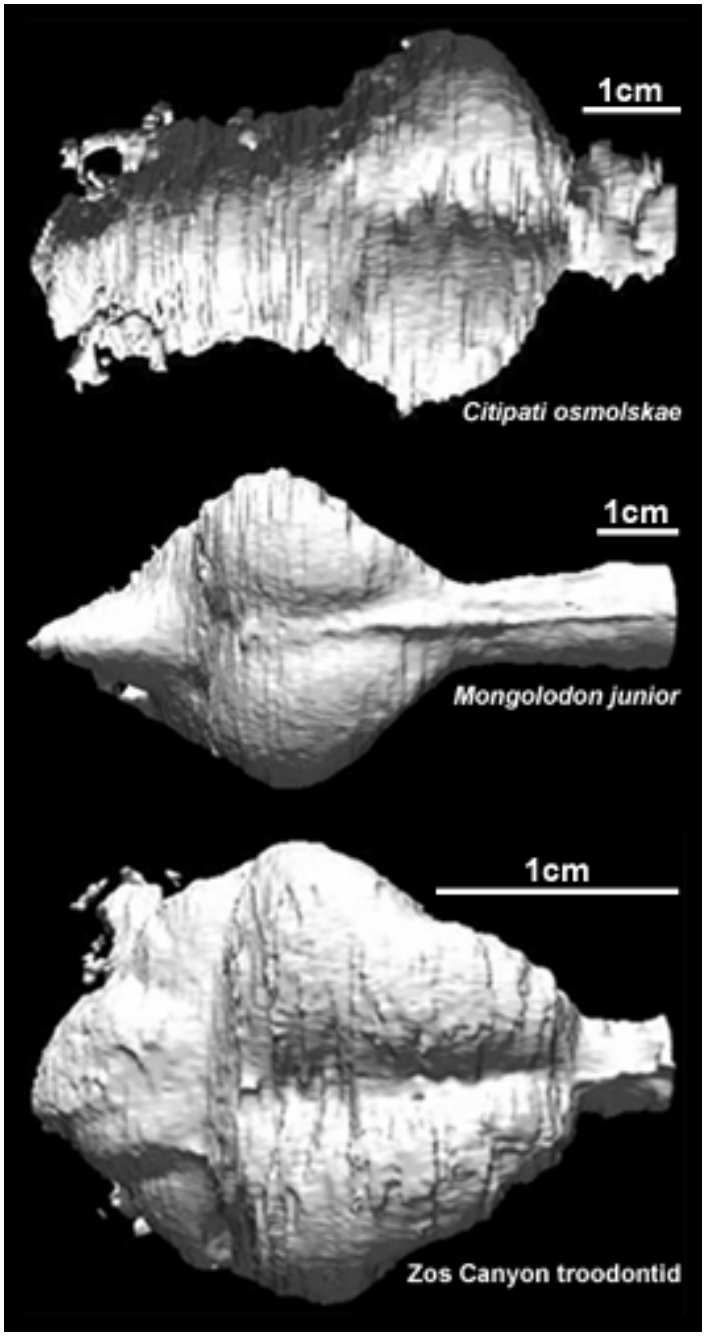

Figure 133. Dorsal view of three derived non-avian theropod endocasts.

The phylogenetic position of the three endocasts above goes from the most basal at the top to the most recent at the bottom.

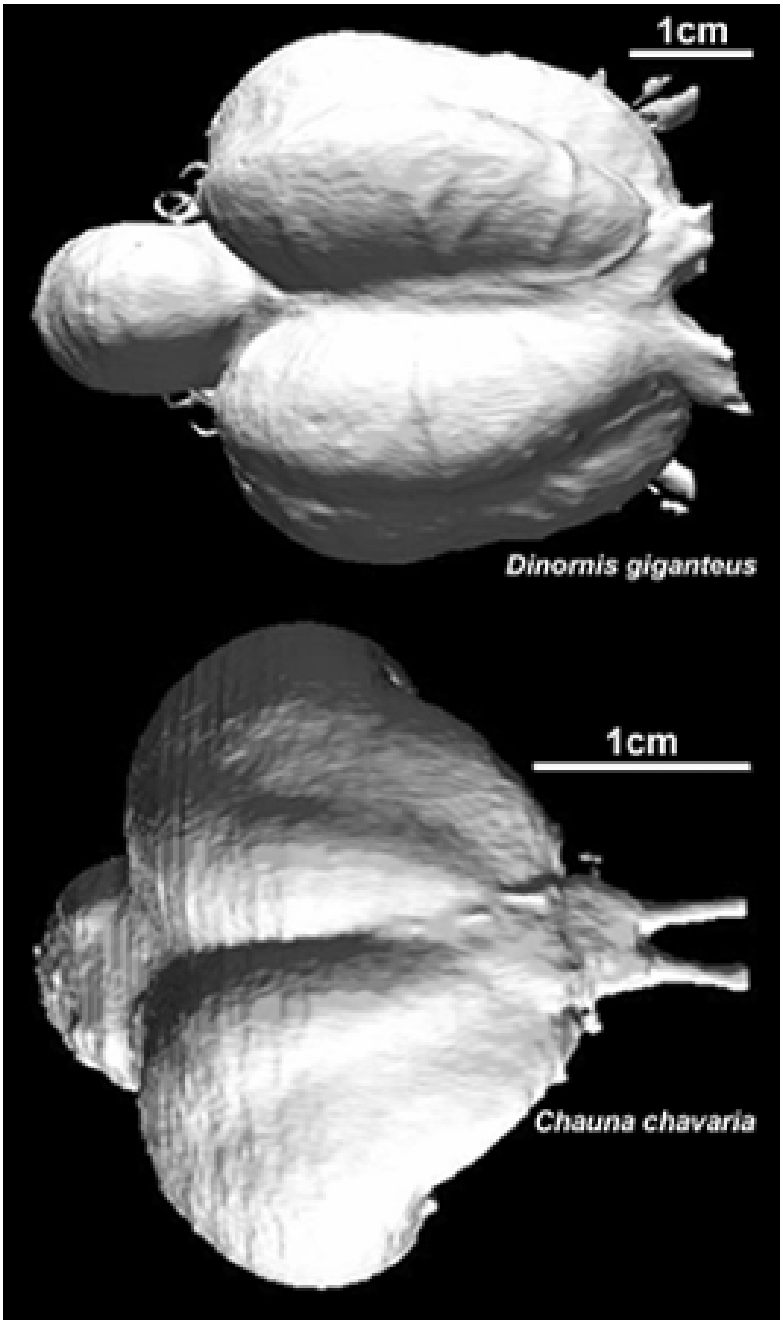

Figure 134. Dorsal view of two avian theropod endocasts.

The phylogenetic position of the two endocasts above goes from the most basal at the top to the most recent at the bottom.

are larger and more distinct, and they have started to expand in a posteroventral direction due to the posterior orbital wall. In avian theropods, the casts of the cerebral hemispheres are larger, more distinct, and the sagittal eminence is visible. The casts of the optic lobes also change through the figures. In the basal theropods, the optic lobes are in a dorsomedial position, and they are not even partially visible in the endocasts due to the overlying casts of the dorsal sagittal sinus and occipital sinus. Moving into the derived non-avian theropods, the casts of the optic lobes are somewhat visible in *Citipati*, and they have started to move from their dorsomedial position. In *Mongolodon* and the Zos Canyon troodontid, the casts of the optic lobes are large, and they have rotated into a ventrolateral position. In the avian theropods, the casts of the optic lobes have fully attained their ventrolateral position, and they are no longer visible in the dorsal view due to the expansion of the casts of the cerebral hemispheres. These changes are only two of the various changes that can be seen by looking at the endocasts themselves in a phylogenetic sequence.

BIOLOGY AND BEHAVIOR

The descriptions and phylogenetic analyses of the endocasts of various theropod taxa permit me to speculate about the evolution of theropod behavior and biology. It also permits the comparison of theropod endocasts with the endocasts of taxa from other clades.

Olfactory Bulbs and Optic Lobes

Several hypotheses involving the actual size and shape of the brain and its various structures have been proposed for the theropod lineage. I can test these hypotheses with the endocast character data compiled in this dissertation. One of the suggested hypotheses states that there was a decrease in theropod dependence on smell, with an accompanying increase in dependence on sight, moving through the theropod lineage (Wharton, 2002). This hypothesis can be supported or disputed by looking at the olfactory bulb and optic lobe data available in the endocasts.

Olfactory Bulbs

The first part of this hypothesis can be tested by looking at olfactory bulb size. Initially, theropods had large olfactory bulbs, and, like crocodilians, they were found at the end of long olfactory tracts. As discussed in chapter one, animals with large olfactory bulbs are hypothesized to have a well-refined sense of smell, while those with smaller bulbs are less reliant on smell (Bang, 1964; Bang and Cobb, 1968; Russell, 1969; Pearson, 1972; Jerison, 1973; Starck, 1979; Wall and Galton, 1979; Giffin, 1989; Butler and Hodos, 1996). This implies that basal theropods had a good sense of smell, and probably relied on this to a large degree in finding food. This large olfactory bulb cast size relative to the overall size of the endocasts can be seen in the basal theropod endocasts studied, and as far up the tree as *Tyrannosaurus*, although the overly large size suggested by Brochu (2000) for this taxon is most likely incorrect owing to misinterpretation of

the CT scan data. As theropod evolution continued, the olfactory bulb decreased in relative size, and began to move posteriorly, eventually becoming appressed against the front of the cerebral hemispheres in Aves. This reduction in relative size suggests that smell became less important in later theropods. This means that the first part of the hypothesized trend is supported. There is a decrease in olfactory bulb size, and hence a decrease in dependence on smell moving through the theropod lineage. The next segment of the hypothesis states that there is an increase in dependence on sight.

Optic Lobes

The second segment of the trend statement can be tested the same way as the first segment. Similar to what was hypothesized with the olfactory bulbs, the larger the optic lobe size, the larger the role that sight is hypothesized to play in the behavior and lifestyle of an animal (Pearson, 1972; Jerison, 1973; Butler and Hodos 1996). Basal theropods had relatively small optic lobes located in a dorsomedial position in the brain. These optic lobes could not be seen in the endocasts owing to the overlying venous sinuses. The fact that these lobes could not be seen even in this narrow region of the endocasts lends further evidence to the very small size they had relative to the overall size of the endocast. With such small optic lobes, sight was probably not as important to these basal theropods as smell. As relative olfactory bulb size decreased throughout the lineage, the relative optic lobe size increased. This correlation can be seen in *Citipati* and *Mongolodon*. These taxa have relatively small olfactory bulbs, and from *Citipati*

to *Mongolodon*, the increase in the relative size of the optic lobes to the overall size of the endocast can be seen. Along with this increase, the cerebral hemispheres and cerebellum also increased in relative size. These increases, and possibly midbrain expansion, led to the optic lobes being displaced from a dorsomedial position to a ventrolateral position in the brain. The increase in relative optic lobe size suggests that more derived theropods had a well-developed sense of vision that was more important than their sense of smell. Thus, the endocast data support a decrease in theropod dependence on smell, and an accompanying increase in dependence on sight moving through the theropod lineage.

Hunting

Does the shift from large olfactory bulbs to large optic lobes tell us something about the hunting behavior of theropods? All of the basal theropods have large olfactory bulbs, implying that smell was a more important sense than sight. Modern theropod scavengers, such as turkey vultures, also have enormous olfactory bulbs (Bang, 1964). It has been hypothesized that large olfactory bulbs imply an animal may have been primarily a scavenger (Horner and Lessem, 1993), using their sense of smell to locate rotting carcasses from great distances. Although the idea of *Tyrannosaurus* and other large theropods as only scavengers has largely been dismissed, it is still likely that they used their sense of smell to locate dead animals (Farlow, 1994), as even active predators are not likely to pass up a free meal.

As olfactory bulbs decreased in relative size and optic lobes increased in relative size, a decrease in overall animal size was also seen. One possible cause of this is a decrease in prey size. To effectively hunt and track small prey, good eyesight would be much more important than a good sense of smell, hence the larger optic lobes and smaller olfactory bulbs. This change in tactics still applies today, because many birds, such as owls and raptors, rely upon their eyesight to find and catch prey rather than relying on smell.

Sizes of the Cerebral Hemispheres, Cerebellum, and Floccular Lobes

Along with the increase in relative optic lobe size, the cerebral hemispheres and cerebellum also increased in relative size. Why would a shift from olfactory-based behavior to vision-based behavior occur in parallel with an increase in cerebrum and cerebellum size? Hopson (1980) hypothesized that this also had to do with prey size and acquisition. As mentioned above, the average size of theropods decreased through the lineage. This reduction in size suggests a reduction in prey size. Smaller prey, in general, are quicker and more agile than larger prey. In order to successfully catch these smaller animals, the theropods would also have to become more agile and quick, as well as show better hand-eye coordination, orientation, and balance. This idea can be tested by evaluation of the information available in the digital endocasts used in this study.

To achieve greater agility and hand-eye coordination, larger optic lobes and cerebral hemispheres are expected (Russell, 1969). The attainment of larger optic lobes was discussed in the previous section, and even a cursory glance at the

cerebral hemispheres in the digital endocasts shows an increase in relative cerebral hemisphere size to overall endocast size. In Maniraptora, the cerebral hemispheres occupy greater than 35% of the total volume of the endocranial cavity/endocast (character 4 of my characters). So why does this increase in cerebral hemisphere size suggest greater agility and hand-eye coordination?

The reason is the dorsal ventricular ridge (DVR) (Ulinski, 1983). The DVR is a structure found in the forebrains of reptiles and birds that can be broken down into two major divisions. The first division is the anterior dorsal ventricular ridge (ADVR). The ADVR receives input from the visual, auditory, and somatosensory systems. This input is then sent to the striatum, which is involved with animal movement through motorneuron modulation. This means that some motion and agility has its basis in the cerebral hemispheres. The second division is the basal dorsal ventricular ridge (BDVR). The BDVR receives input from the olfactory lobes, as well as some input from the ADVR. This input is then sent to the hypothalamus (Ulinski, 1983).

The number of sensory regions within the ADVR varies between crocodilians and birds. In crocodiles, there is one sensory area for auditory input, one for visual input, and one for somatosensory input. The majority of expansion as the ADVR develops is into the lateral ventricles. In modern birds, there are three sensory areas for auditory input, two for visual input, and two for somatosensory input. In birds, the ontogenetic expansion of the ADVR is seen on the lateral surfaces of the telencephalon/cerebral hemispheres (Ulinski, 1983). By looking at the endocasts of crocodilians and then theropods, a gradual increase in

the size of the cerebral hemispheres is seen. *Citipati* is one of the first taxa showing a large increase in relative cerebral hemisphere size. Several things may account for the increase. First, there is a change in the orientation of the posterior semicircular canal. This may be correlated to the addition of one of the extra auditory sensory regions in the ADVR. Second, taxa closely related to *Citipati* have feathers (Padian et al., 2001b), suggesting their possible presence in *Citipati* as well. This may have led to the addition of the second somatosensory region found in the ADVR of birds. Another increase in relative cerebral hemisphere size is seen in *Mongolodon*, and then the largest increase of all with the attainment of modern birds, in which all the increased sensory regions are found. The addition of visual and somatosensory regions not only leads to an increase in the relative size of the cerebral hemispheres, but also to the attainment of greater hand-eye coordination.

Concomitant with an increase in relative cerebral hemisphere size, an increase in relative cerebellar and floccular lobe size should also be seen if there is an increase in balance and orientation ability, because of the involvement of these regions as orientation and balance centers (Pearson, 1972). Relative floccular lobe size does increase through the theropod lineage, with a notable increase occurring in Maniraptora (character 11 of my characters), suggesting improved orientation and balance abilities.

Therefore, theropods are not only hypothesized to have evolved great vision and hand-eye coordination, but also great balance and agility, a necessary combination for capturing smaller, faster, and more agile prey. The features seen

in the digital endocasts support Hopson's hypothesis (1980) regarding the increase in relative cerebral hemisphere and cerebellum sizes.

Although a decrease in predator size may lead to a decrease in prey size, this is not necessarily always the case, as illustrated by *Deinonychus*. *Deinonychus* was a small, Early Cretaceous theropod known from the western United States (Ostrom, 1969) that is hypothesized to have routinely killed prey, usually *Tenontosaurus*, much larger than itself. Evidence for this includes dozens of sites where *Tenontosaurus* skeletons are found with isolated *Deinonychus* teeth (Ostrom, 1969; Maxwell and Ostrom, 1995), and one remarkable site where the remains of three to five *Deinonychus* were found with a single *Tenontosaurus*, suggesting that the predator was engaged in pack hunting. This type of coordinated activity, which would involve leaping and slashing attacks, would also require the balance and coordination gained by an enlarged cerebellum and floccular lobes.

Endothermy

Increase in brain size has also been used in the debate over whether theropods were ectothermic or endothermic. Hopson (1980) hypothesized that endothermy requires a large brain size. His reasons for this hypothesis were:

> (1) the much greater maintenance energy requirements of living endotherms require more intense activity over more extended periods of time than is necessary for ectotherms; and (2) increased levels of activity have led to selection for more complex perceptual abilities and precise sensorimotor control mechanisms, requiring larger brains (Hopson, 1980:304).

Based on this reasoning he argued that most theropods had a metabolic rate that was intermediate between living "reptiles" and mammals/birds, with the exception of coelurosaurs, which may have had a metabolic rate more like endothermy.

Even though Hopson used brain size in this discussion, a large range of topics, from predator/prey ratios (Bakker, 1972) to a fully erect gait (Bakker, 1971), have been used to argue for total endothermy in theropods. One of the more telling areas of investigation is histology. Several authors studied histological sections of dinosaur bones (de Ricqlès, 1980; Varricchio, 1993; Chinsamy et al., 1994; Padian et al., 2001a), and most came to the conclusion that dinosaurs had a metabolic rate that was intermediate between modern day ectotherms and endotherms. Although intermediate, the presence of fibro-lamellar bone, dense Haversian bone (de Ricqlès, 1980; Varricchio, 1993), and lack of well-developed bone growth rings suggests that dinosaurs had rapid growth rates initially, only slowing in maturity (de Ricqlès, 1980). These are all features seen in endothermic animals, suggesting that although intermediate, non-avian dinosaurs were closer to endotherms than ectotherms. Where the change to complete endothermy occurred is debatable, because Mesozoic birds still are not thought to exhibit complete endothermy (Chinsamy et al., 1994).

Comparisons between Birds and Pterosaurs

Optic lobe, and Overall Brain Size, Comparisons

Birds and pterosaurs are not only similar to each other in their ability to fly, but they also show a great deal of similarity in their endocasts, and this has

been noted for a long time (Edinger, 1941). Both have endocasts in which the brain nearly completely filled the endocranial cavity. Jerison (1973) hypothesized that this evolved in pterosaurs to reduce weight through the removal of cranial bones and having very thin braincase bones. Birds and pterosaurs are not only similar in their brains filling the entire endocranial cavity, but the architecture of their brains is also similar (Edinger, 1941; Jerison, 1973; Hopson, 1979). They have very small olfactory bulbs that are appressed against the anterior surface of the cerebral hemispheres, their optic lobes are in a ventrolateral position, the cerebellum touches the posterior border of the cerebral hemispheres, and they have large floccular lobes. These similarities suggest that, as in birds, sight was the most important sense in pterosaurs, based on the small relative size of the olfactory bulbs compared to the optic lobes. The relatively large size of the floccular lobes, which are important for orientation and balance, also suggests that they were adept fliers.

Although bird and pterosaur endocasts are similar in many respects, there are some differences, particularly regarding the sizes of their optic and floccular lobes. Birds tend to have relatively larger optic lobes than pterosaurs (Jerison, 1973). The opposite is true with regards to the floccular lobes, pterosaurs' being much larger than birds' (Edinger, 1927). Pterosaurs and birds also show some differences in their Reptile Encephalization Quotients (REQs) and Bird Encephalization Quotients (BEQs). Pterosaurs have values for both quotients that are at a level very close to that of *Crypturellus*, which, along with *Dinornis*, has the lowest values among those birds that are shown on the chart (figured and

discussed later). Although these pterosaur values are higher than other reptiles, they are not as high as what is seen in most modern birds. This discrepancy in values may seem surprising, but the answer for it is found in the closest relatives of the two groups. Theropods and pterosaurs are both descendants of archosaurian ancestors that had brains much more similar to what is seen in crocodiles than in birds. Pterosaurs, as a group of flying reptiles, are derived immediately from this ancestor, so they had a small "reptilian" brain as a starting point. Even with this, they evolved the necessary attributes to become proficient fliers. Birds, on the other hand, did not evolve straight from this ancestral archosaur, but rather are nested deep within theropods. The theropods, as has been shown by the endocasts in this study, began to gain a larger brain well before the advent of avian flight. So when flight was first achieved by birds, they had a much larger brain as a starting point.

Semicircular Canal Orientation

The semicircular canals also can be compared in theropods and pterosaurs. The semicircular canals of basal archosaurs and early theropods outline an area that in lateral view has a subtriangular appearance, with the posterior semicircular canal moving more posteriorly than laterally. In more derived theropods such as *Citipati, Archaeopteryx,* and modern birds, the posterior semicircular canal moves more laterally than posteriorly (Figure 135). This change in posterior semicircular canal orientation is not as pronounced in pterosaurs as in birds, but the canal is

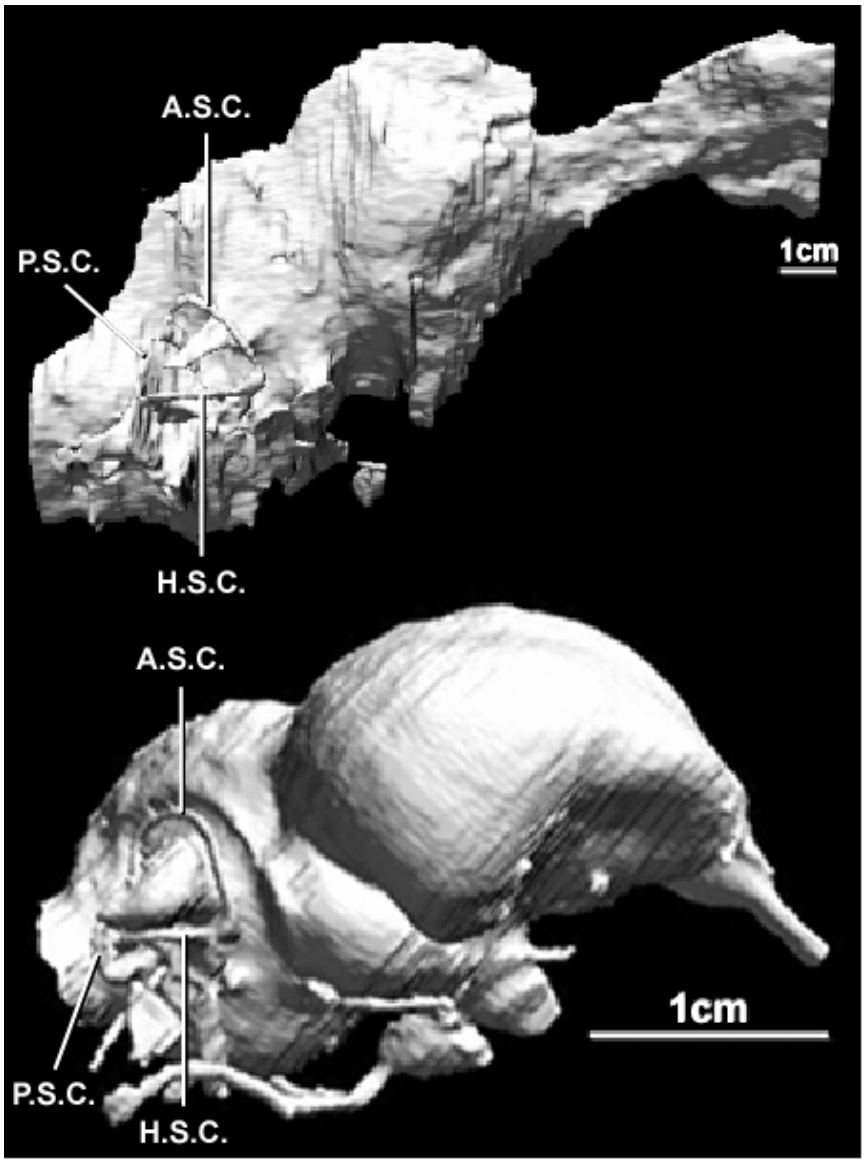

Figure 135. Semicircular canal orientation in basal versus derived theropods.

The above figure shows the difference in semicircular canal orientation, mainly the difference in posterior semicircular canal orientation, in basal versus derived theropods. The basal theropod shown at the top of the figure is *Ceratosaurus magnicornis*, and the derived theropod at the bottom of the figure is *Chauna chavaria*. See Appendix A for explanation of abbreviations.

slightly more laterally projecting in *Anhanguera* than what is seen in other basal archosaurs and non-avian theropods.

Semicircular canals can also be used to estimate head posture. According to several studies (Blanks et al., 1972; Erichsen et al., 1989; Spoor and Zonneveld, 1998; Witmer et al., 2003), the preferred orientation of the head for an animal can be determined by looking at the orientation of the horizontal semicircular canal. As the name suggests, the normal orientation of this canal is horizontal, so the common, or 'alert', posture for an animal has this canal at an angle between 0-5° (de Beer, 1947; Blanks et al., 1972; Erichsen et al., 1989; Spoor and Zonneveld, 1998; Witmer et al., 2003).

For many animals, this orientation involves a posture where the jawline is horizontal, but this is not always the case. A good example of this is the two pterosaurs described in this dissertation, *Rhamphorhynchus* and *Anhanguera*. In *Rhamphorhynchus*, the horizontal semicircular canal suggests that the head is held such that the jawline is horizontal. For *Anhanguera* though, making the horizontal semicircular canal horizontal results in a sharply downturned skull. The reasons for this orientation are not known for sure, but it has been suggested that it may be behaviorally related to feeding, allowing the animal to scan for food while in flight, or may be related to locomotion, pertaining to a more upright posture when walking on the ground (Witmer et al., 2003).

These differences in head orientation can also be seen in non-avian theropods. Some, such as *Allosaurus*, have a horizontal semicircular canal that suggests a head orientation with the jawline horizontal, while others, such as

Acrocanthosaurus, have a horizontal semicircular canal that suggests a sharply downturned head. For non-avian theropods, this difference in head posture is interesting, and more studies addressing its significance are needed.

REQs, BEQs, and 'Intelligence'

REQs and 'Intelligence'

One of the more interesting characters analyzed above is REQ, or Reptile Encephalization Quotient. Since the studies of Jerison (1969, 1973), encephalization quotients have been calculated for a variety of dinosaurs, and its relationship to 'intelligence' has been debated. Through studies conducted for his dissertation in 1996, Grant Hurlburt showed that a single EQ for "lower" vertebrates was inadequate, and an EQ for "reptiles" alone, REQ (see character description above), needed to be established. This EQ, likes those of Jerison, gives data as to whether or not an animal has an expected brain size relative to other "reptiles." Using this information and the calculations performed on the digital endocasts for character 14, I constructed a chart for REQs (Figure 136).

The most striking thing about the REQs is that all the theropod taxa have REQs that put them well above the expected REQs for "reptiles" of their size, and also above the REQ of most extant "reptiles" (Hurlburt, 1996). The lowest REQ exhibited by theropods is 2.30 for *Carcharodontosaurus saharicus*. This REQ may be underestimated because the endocast did not include the cast of the olfactory bulbs and a portion of the cast of the olfactory tract. The lowest values

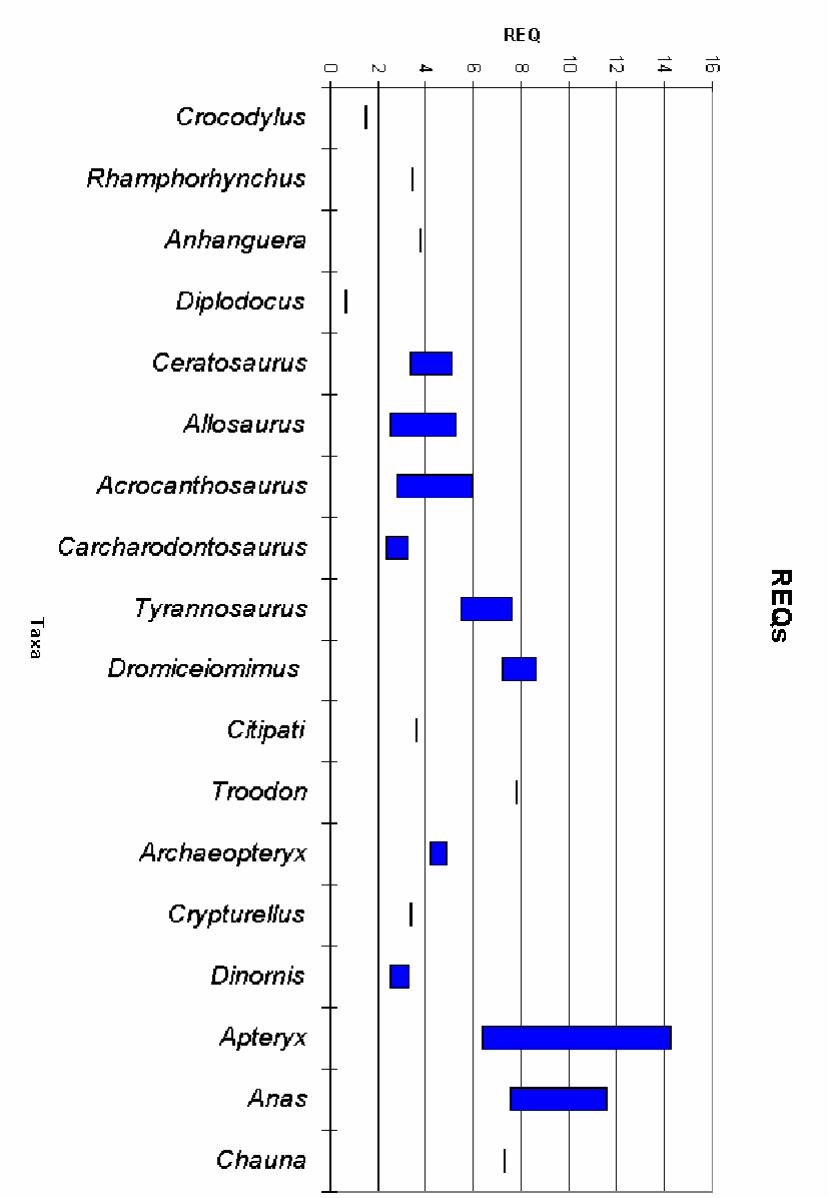

Figure 136. Chart showing the Reptile Encephalization Quotients (REQs) of the specified taxa.

The upper end of each bar represents the REQ of the taxon with the lower weight estimate of the taxon, and the lower end of the bar represents the REQ of the taxon with the higher weight estimate of the taxon.

given for the taxa also represent the maximum weights estimated for these taxa, and this will also make the values a little lower than they probably should be. Only those taxa with one measurement represent the weight of the particular specimen examined. The exception to this are the pterosaurs, which only have one value, although the weights are estimates for each taxon as a whole, and not the particular animal whose endocast was measured (Witmer et al., 2003). This was done owing to the lack of associated postcranial material for those specimens. The upper end of the chart gives the REQs with the lowest weights estimated for the taxa. Similar to the highest weights depressing the REQs, these lowest weights will inflate the REQs. The chart is organized phylogenetically, with the most basal taxa to the left, and the more derived taxa to the right. Looking at the chart, an overall upward trend of the REQs within theropods can be seen. Beginning with *Ceratosaurus*, which has a range of 3.31-5.07, to *Anas*, which has a range of 7.49 to 11.57, the REQs tend to increase. There are exceptions to this trend however.

First, *Carcharodontosaurus* appears to have a much lower value than its closest relatives *Allosaurus* and *Acrocanthosaurus*. Part of this apparent difference reflects the low endocast volume available for *Carcharodontosaurus*, which excludes the cast of the olfactory bulbs and part of the cast of the olfactory tract. It is also possible that the apparent low value reflects differences in size between *Carcharodontosaurus* and *Acrocanthosaurus/Allosaurus* (size issues will be discussed later in this chapter).

Second, *Citipati* has an REQ well below that of the surrounding taxa, with a value similar to the median values of *Ceratosaurus, Acrocanthosaurus,* and *Allosaurus*. As with *Carcharodontosaurus*, the complete extent of the casts of the olfactory tract and bulbs is not represented, leading to a slight lowering of the REQ. A bigger problem though is determining the size of *Citipati*. A complete skeleton of *Citipati* was recovered, and this allowed a size to be estimated using the equation proposed by Anderson et al. (1985). This equation has several critics though, and Dr. Mark Norell tested the equation on several living taxa, only to get many values that were off by a factor of two or three (pers. comm.). This means that the value used for the weight of *Citipati* in the REQ equation may be wrong, and this would then lead to an incorrect REQ. Even using drastically different values for its weight, it is unlikely that the REQ of *Citipati* would end up anywhere near that of *Dromiceiomimus* or *Troodon*.

Third, *Archaeopteryx* also has a value well below what would be expected for its location on the chart. Similar to *Citipati*, it has a value close to that of *Ceratosaurus, Acrocanthosaurus,* and *Allosaurus*. As with *Carcharodontosaurus* and *Citipati*, the *Archaeopteryx* endocast is missing the casts of the olfactory tract and bulbs, lowering its REQ somewhat. Another problem is an accurate weight for *Archaeopteryx*. This is difficult to obtain because all the specimens are flattened in limestone slabs. Again, though, whether these discrepancies would be enough to elevate its REQ to a position equivalent to *Dromiceiomimus* and *Troodon* is doubtful.

Lastly, *Crypturellus* and *Dinornis* both have surprisingly low REQs. The REQs of these birds are below those of some basal theropod taxa. The possible explanations postulated for the other low REQ taxa do not apply here, because both taxa have complete skulls, and well-known weights. One possible reason for the low values is the loss of the ability to fly in these taxa, because many of the lowest modern bird REQs belong to the paleognaths (Hurlburt, 1996). However, *Apteryx*, which has a large REQ, is also flightless.

So what does a gradual increase in REQ mean? According to Jerison, as relative brain size of a species increases, its ability to process information increases (1969, 1973, 1985), and the species is therefore more 'intelligent.' So, using this standard, *Troodon* is more 'intelligent' than *Ceratosaurus*. This explanation for what REQs mean may be viable if an increase was seen through the entire theropod lineage, but the large trend of decreasing REQs in the middle of the chart is cause for concern. This discrepancy, for me, is enough to suggest that a brain/body weight ratio may not be the best way to evaluate 'intelligence.' Other types of problems with these ratios were discussed by Felsenstein (1985).

BEQs and 'Intelligence'

Non-avian theropods may be more 'intelligent' than other "reptiles," but how 'intelligent' are they compared to avian theropods? Not only did Grant Hurlburt develop an equation for calculating "reptile" encephalization quotients, he also developed an equation for measuring Bird Encephalization Quotients, or BEQs (Hurlburt, 1996). That equation is: $BEQ=M_{Br}/(0.117 \times M_{Bd}^{0.590})$. M_{Br} is the

mass of the brain (or endocast) in grams, and M_{Bd} is the mass of the body in grams. This equation was used to calculate the BEQs of those taxa present in the REQ chart, and the results are shown in Figure 137.

The relative values of the taxa to each other has not changed much, except that *Archaeopteryx* is much closer to the values of *Dromiceiomimus* and *Troodon*, and it is now higher than most of the values seen for *Ceratosaurus, Acrocanthosaurus,* and *Allosaurus*. *Dinornis*, being the avian taxon on the chart with the lowest BEQ, gives a baseline for the comparison of non-avian taxa. Two of the taxa, *Crocodylus* and *Diplodocus*, fall below the BEQ level found in Aves. This finding is not unexpected. What is surprising is the fact that all of the non-avian theropod taxa fall within the range of Aves. Most of them are in the lower portion of this range, but within it nonetheless.

Archaeopteryx, being in the middle of the range, is above the BEQ of most non-volant modern bird taxa (Hurlburt, 1996). *Tyrannosaurus* is found within this same range. Two non-avian theropods, *Dromiceiomimus* and *Troodon*, actually have BEQs within the range seen in modern flying birds. These last two charts, if nothing else, show that, unlike Jerison's claim (1969, 1973), theropods have EQs that are above the level expected for "reptiles," and they broadly overlap with the range seen in modern birds. Does this mean that non-avian theropods were as 'intelligent' as modern avian taxa? Most of these taxa are in the lower end of this range, but based on the chart, several were just as 'intelligent' as some modern volant taxa.

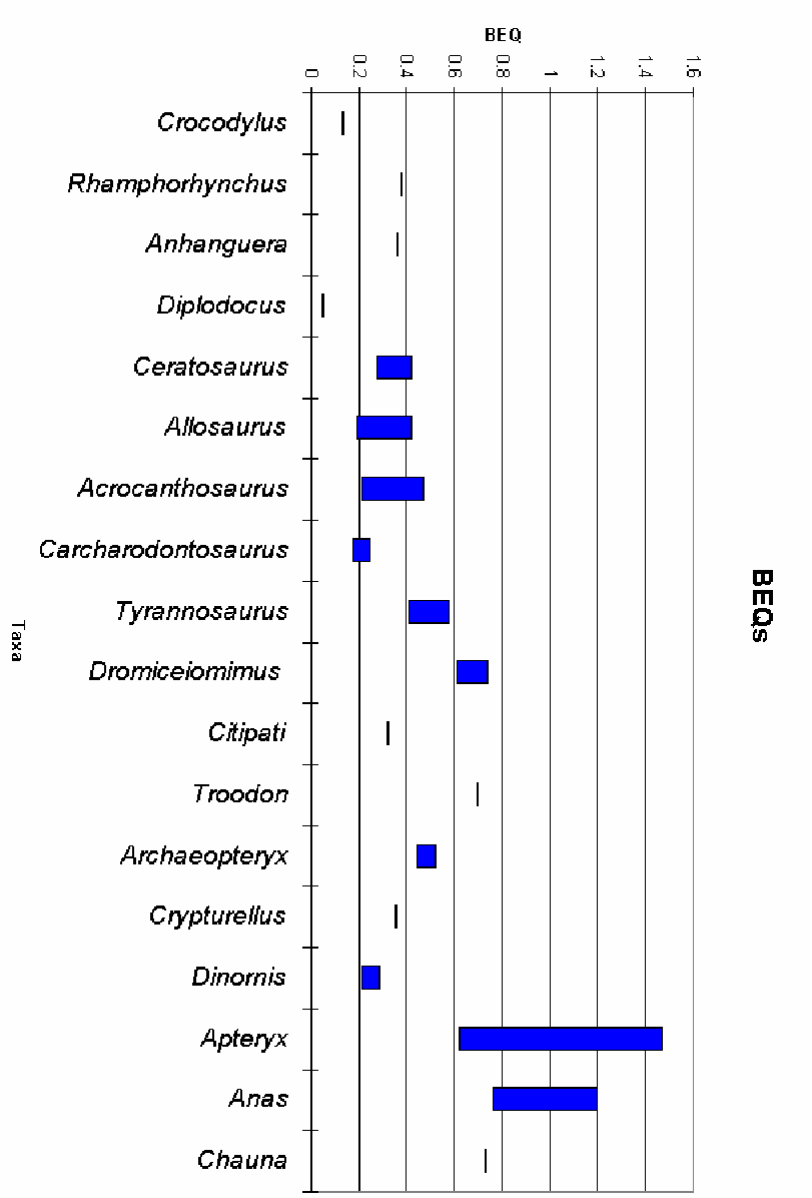

Figure 137. Chart showing the Bird Encephalization Quotients (BEQs) of the specified taxa.

The upper end of each bar represents the BEQ of the taxon with the lower weight estimate of the taxon, and the lower end of the bar represents the BEQ of the taxon with the higher weight estimate of the taxon.

Even though the REQ and BEQ of Hurlburt are an improvement over Jerison's equations, they are still fundamentally flawed because Hurlburt's equations use the same basic structure as Jerison's equations (Jerison, 1973; Hurlburt, 1996). That structure involves the use of body weight in the denominator of the equation. As we have seen, the calculation of body weight for taxa is an inexact science at best (Peczkis, 1994). The use of inexact weights leads to inexact results. This means that the overlapping seen between the REQs and BEQs for basal non-avian theropods and avian theropods may be an artifact of calculation errors. With such a large error margin, the calculations are only good for relative comparisons in which there are large value differences. Owing to the errors in weight calculation, an equation that does not include this measurement is necessary. Radinsky used an equation that compared endocranial volume to the area of the foramen magnum (Radinsky, 1967). He obtained promising results in his calculations with mammals, but I don't know whether a similar equation has been tested on reptiles and/or birds. Other equations using solely endocranial data have been proposed (Larsson et al., 2000). The testing of these types of alternative equations should be a priority since the current equations are of little value.

Size

One question that may be asked, especially upon seeing the cladogram with character state distributions, is what affect, if any, does size have on these features? Is it possible that the character distributions reflect size-related allometry? It is true that most of the derived theropods are smaller than the basal

theropods. In fact, if we consider Maniraptora a dividing point in the theropod phylogeny, all theropods in this study within Maniraptora are smaller than those basal to Maniraptora. Could the same brain complexity seen in the derived theropods be hidden in the larger braincases of the basal theropods? Although this is a possibility, it is rather unlikely.

One reason this is unlikely is that *Diplodocus hayi*, which is within the outgroup, does not support the hidden derived brain possibility. Unlike large theropods, the brain of *Diplodocus* is hypothesized to have filled the entire endocranial cavity (Hopson, 1977; 1980). Even though this is the same case as the derived theropod taxa, the casts of the olfactory bulbs are not found in the derived ventrolateral position, but still in the primitive dorsomedial position. Also, the endocast of *Herrerasaurus*, a small basal theropod, shows none of the derived features that would be expected if the features were purely size related. Of course, the best way to prove this would be to find a 1+ ton maniraptoran with an intact braincase showing derived character states, but this has yet to happen. The testing and answering of these questions are other priorities in endocast studies, and I plan to address these questions as part of my future research.

Chapter 5: Summary and Future Areas of Research

SUMMARY

I used high-resolution X-ray computed tomography (CT) scan data to generate 13 theropod endocasts. Some of these endocasts confirmed features that were described previously based on natural or artificial endocasts, while a large number provided the first look at an endocast for a given taxon. Most of these endocasts were complete enough to allow a full description of not only the main regions of the brain, but also of the passages of cranial nerves and various associated arterial and venous features and vessels.

I studied the endocasts for characters that could be used in phylogenetic analyses. My study resulted in 14 characters, which were analyzed by themselves, and added to the published data matrices of Holtz (1998), Sereno (1999), and Rauhut (2003).

Using the simple parsimony heuristic mode in PAUP 4.0b10(Altivec), I resolved three nodes on a strict consensus tree of all the most parsimonious trees for the 14 characters and 16 theropod taxa. The recovered nodes included Coelurosauria, Maniraptora, and a node consisting of *Crypturellus* and *Dinornis*. Although this is not a huge amount of resolution, its clear distinction between the basal and derived taxa, with *Tyrannosaurus* in between, suggests that the characters obtained from the endocasts contain valuable phylogenetic information. A 50% majority rule analysis in PAUP resulted in even more resolution, grouping all of the modern bird taxa, plus *Dinornis*, within a single

clade. Character tracing and optimizations were investigated using MacClade 4.04PPC.

I also added the characters to the existing data matrices of Holtz (1998), Rauhut (2003), and Sereno (1999), to see if they affected the tree topologies. This resulted in some clarification of a polytomy in the upper area of Holtz's tree, but the topologies of the Rauhut and Sereno trees did not change. Strict consensus trees based on these three analyses were then opened in MacClade for character tracing and optimization.

Finally, I created a preferred tree containing only endocast data. This tree, which was conformable with those of the other authors, was used for character tracing and optimization, giving a clearer picture of where the transitions of the character states occurred.

The majority of these transitions occurred between the branches containing *Tyrannosaurus* and *Citipati*. Whether this represented correlated character changes or not could not be determined based on this sample.

After the character tracing and optimization were completed, I observed several trends in the data, including a decrease in relative olfactory bulb size and a concurrent increase in relative optic lobe size. This transition represented a change from olfactory dependence to a greater reliance on sight as a dominant sense. An increase in relative cerebral hemisphere, cerebellum, and floccular lobe size was also seen, and may have been tied to a decrease in body size, necessitating an increase in hand-eye coordination, and balance and orientation for the acquisition of smaller, more agile prey.

In conjunction with a smaller body size, and increased brain size and agility, I discussed the issue of theropod endothermy. The increase in brain size necessitated an increase in food intake and metabolism, something suggested by the attainment of features needed for speed and agility. Previous studies of bone histology support a metabolism that was closer to that of modern endothermic animals than ectothermic ones, although it is still hypothesized that the metabolism of non-avian theropods was intermediate between the two.

I also addressed the transition from non-avian theropods to modern birds. All of the changes that were seen in the transition from basal to derived non-avian theropod taxa were useful as flight adaptations, and these changes were even more apparent in modern birds. The majority of these changes (large optic lobes, large cerebellum and floccular lobes, and posterior semicircular canal orientation) were also found in pterosaurs, the closest flying relatives of birds. This similarity of features suggests a convergence towards features adapted for flight.

Another feature that was expected to be similar in both birds and pterosaurs is an increase in overall brain size. Although pterosaur EQs (REQ or BEQ) were large in comparison to most other archosaurs, they were nowhere near the range of values found in most modern birds. In fact, pterosaurian EQ ranges were similar to those in basal non-avian theropods. The reason modern birds have higher EQs is the elevated EQ of the ancestor of Aves, which was a non-avian theropod like *Troodon*, versus the lower EQ that basal archosaurs had, which was the starting point for pterosaurs.

One EQ value I found interesting was the low value of *Archaeopteryx* compared to non-avian theropods such as *Troodon* and *Dromiceiomimus*. More studies are necessary to fully explain this difference, because even though the value of *Archaeopteryx* was within the range of some modern volant birds, such as *Crypturellus*, this type of divergent value shows an inherent problem with using a brain/body weight ratio.

FUTURE AREAS OF RESEARCH

Although significant data were obtained and examined in this dissertation, there are still large amounts of work in several areas where I will center my future work.

Clearly, more theropod taxa need to be investigated. Although the selection used in this dissertation was a good starting point, ideally, I would like to have digital endocasts created for all available theropod braincases. Several areas of uncertainty in the evolution of characters could be resolved by having a larger sample of taxa. While this is not possible for all taxa, due to a lack of endocranial material, those taxa that do have complete braincases, such as *Sinraptor dongi* (Currie and Zhao, 1993a), and *Giganotosaurus carolinii* (Coria and Currie, 2002), need to be scanned and examined so that their endocast characters can be added to my data matrix.

Although there are available braincases that can be scanned to fill some of the gaps, there are other gaps that can only be filled by the discovery of new specimens and taxa with complete braincases. One area in which more taxa would

be useful is after *Archaeopteryx* and before modern birds. Some taxa are available, but more are necessary to elucidate the changes in the brain that occur in this time frame.

Not only do I plan on obtaining more taxa, but I am also examining more characters for addition to the data matrix. The 14 characters I used in this study cover the entire endocast, but I am obtaining more quantitative data and measurements from them. Some of the characters I am in the process of examining and measuring are relative volume of the olfactory bulbs to the volume of the entire endocast, relative volume of the floccular lobes to the volume of the entire endocast, relative volume of the optic lobes to the volume of the entire endocast, and several linear measurements taken from homologous points amongst the endocasts, such as cerebellar breadth. Another area that I am examining for the possibility of new characters is the pneumaticity of the braincase bones. Depending on the taxon, several bones in the braincase are hollow. From the paroccipital processes, to the basioccipital processes of the basisphenoid, pneumaticity is found in most groups (Currie and Zhao, 1993b; Makovicky and Norell, 1998). Dr. Lawrence Witmer studied pneumaticity in the area of the snout (Witmer, 1990; 1997), and other pneumatic chambers can be readily studied with CT data. An analysis of these pneumatic passages may prove to be a valuable source of characters that can be used to help elucidate theropod relationships.

I will also examine ontogenetic stages as a source of characters. Determining the age of specimens is important in any comparison and character

analysis, and unfortunately, little data of this type are available for fossil species. By looking at the ontogenetic sequences of the non-avian theropods closest extant relatives, crocodiles and birds, I will obtain an ontogenetic sequence of endocasts and braincases bracketing non-avian theropods. With this completed, any opportunities seen in the fossil record for this kind of ontogenetic work will have a set of data for comparisons, and a better idea of the ontogenetic changes that non-avian theropod groups underwent can be determined. I will employ the information gained in these studies in the choosing of characters for more phylogenetic analyses.

One final area of available research is similar studies of other groups. With this technology, any group can be examined in a similar way, be it ornithischian dinosaurs, pterosaurs, lizards, and even smaller clades. Currently, a similar study focusing on mammals is under way (Thomas Macrini, pers. comm.). The completion of that study will be a great resource for comparisons of the pathways taken to modern mammals and birds.

Theropod dinosaurs, while being a good starting point, are just that, a starting point. More complicated groups can be studied and analyzed within the framework laid out above, whether or not their brain completely filled the endocranial cavity.

Appendices

APPENDIX A

Abbreviations Used in the Figures

A.C.V.- Anterior cerebral vein

A.S.C.- Anterior semicircular canal

Cart.- Cartilage area

Cb.- Cerebellum

C.H.- Cerebral hemisphere

D.H.V.- Dorsal head vein

D.S.S.- Dorsal sagittal sinus

F.L.- Floccular lobe

F.O.- Fenestra ovalis

F.P.- Fenestra pseudorotunda

H.S.C.- Horizontal semicircular canal

I.C.- Internal carotid artery

I.E.- Inner ear

I.F.- Interhemispherical fissure

L.- Lagena

M.C.V.- Middle cerebral vein

O.B.- Olfactory bulb

O.F.- Olfactory filaments

O.L.- Optic lobe

O.T.- Olfactory tract

Pit.- Pituitary

P.S.C.- Posterior semicircular canal

S.- Sacculus

S.E.- Sagittal eminence

T.S.- Transverse sinus

T.V.- Telencephalic vallecula

V.B.- Vascular branch

II- Optic nerve

III- Oculomotor nerve

IV- Trochlear nerve

V- Trigeminal nerve

V_1- Ophthalmic branch of the trigeminal nerve

V_2- Maxillary branch of the trigeminal nerve

V_3- Mandibular branch of the trigeminal nerve

VI- Abducens nerve

VII- Facial nerve

VII_H- Hyomandibular branch of the facial nerve

VII_P- Palatine branch of the facial nerve

VIII- Vestibulocochlear nerve

IX- Glossopharyngeal nerve

X- Vagus nerve

XI- Accessory nerve

XII- Hypoglossal nerve

APPENDIX B

Institution and Collection Abbreviations

AMNH- American Museum of Natural History

CM- Carnegie Museum of Natural History

FMNH- Field Museum of Natural History

IGM- Institute of Geology, Mongolian Academy of Sciences

KU- Kansas University

MUO- Museum of the University of Oklahoma

MPM- Milwaukee Public Museum

MWC- Museum of Western Colorado

OMNH- Oklahoma Museum of Natural History

PVSJ- Division of Vertebrate Paleontology of the Museo de Ciencias Naturales de la Universidad Nacional de San Juan

SGM- Ministère de l'Energie et des Mines

TMM- Texas Memorial Museum

TMP- Tyrrell Museum of Paleontology

USNM- National Museum of Natural History

UUVP- University of Utah Vertebrate Paleontology Collection

APPENDIX C

The following chart shows the REQs, BEQs, body masses (M_{Bd}), and endocast masses (M_{Br}) for the listed taxa. Some taxa do not have calculated REQs and BEQs due to a lack of body mass values. The REQs and BEQs were calculated using Hurlburt's equations (1996). REQ= $M_{Br}/(0.0155 \times M_{Bd}^{0.553})$, and BEQ= $M_{Br}/(0.117 \times M_{Bd}^{0.590})$. Those taxa that have an empty block beneath them have REQs and BEQs calculated for two weights. The first row is using the lighter of the two weights. Those values followed by parenthesized letters or letters and numbers were obtained from the denoted sources. The abbreviations refer to: **(A8)**= Alexander, 1985; **(A9)**= Alexander, 1991; **(B)**= BBC website, www.bbc.co.uk/nature/wildfacts/factfiles/3047.shtml; **(C,Z)**= Currie and Zhao, 1993b; **(D)**= Dunning, Jr., 2000; **(H)**= Hopson, 1977; **(Hu)**= Hurlburt, 1996; **(L)**= Larsson, 2001; **(M,W:A)**= Madsen and Welles, 2000, femoral diameter used in Anderson et al.'s 1985 equation for calculating dinosaur masses, Weight(in g)= 0.16 X femoral circumference(in mm)$^{2.73}$; **(N p.c.:A)**= Mark Norell, personal communication of femur diameter, used in Anderson et al.'s dinosaur mass equation; **(O)**= Osborn, 1912; **(P)**= Peczkis, 1994; **(R p.c.)**= Mark Robbins from the Kansas University Museum, personal communication; **(R p.c.:A)**= Mark Robbins, personal communication of femoral diameter used in Anderson et al.'s equation for calculating bird masses, W= 1.08 X femoral circumference$^{2.28}$; and **(W)**= Witmer et al., 2003.

TAXA	REQ	BEQ	MBd (g)	MBr (g)
Acrocanthosaurus atokensis	5.92	0.47	1000000 (P)	190.810986
	2.75	0.208	4000000 (P)	190.810986
Allosaurus fragilis	5.24	0.417	1000000 (P)	169 (L)
	2.44	0.184	4000000 (P)	169 (L)
Anas platyrhynchos	11.57	1.2	720 (D)	6.821396
	7.49	0.756	1580 (D)	6.821396
Anhanguera santanae	3.76	0.358	7600 (W)	8.158766
Apteryx sp.	14.24	1.47	880 (D)	9.380806
	6.3	0.615	3850 (D)	9.380806
Archaeopteryx lithographica	4.85	0.52	300 (H)	1.76 (H)
	4.13	0.439	400 (H)	1.76 (H)
Byronosaurus jaffei	-	-	-	4.559172
Carcharodontosaurus saharicus	3.23	0.244	4000000 (Based on *T. rex*)	224.4 (L)
	2.3	0.17	7400000 (Based on *T. rex*)	224.4 (L)
Ceratosaurus magnicornis	5.07	0.42	324000 (M,W:A)	87.696125
	3.31	0.267	700000 (P)	87.696125
Chauna chavaria	7.29	0.727	2201 (R p.c.:A)	7.974891
Citipati osmolskae	3.6	0.317	62153 (N p.c.:A)	24.988768
Crocodylus acutus	1.47	0.126	134000 (Hu)	15.6 (Hu)
Crocodylus moreleti	-	-	-	15.847958
Crypturellus cinnamomeus	3.35	0.354	440 (R p.c.)	1.50295
Dinornis giganteus	3.29	0.283	117000 (B)	32.381157
	2.45	0.206	200000 (B)	32.381157
Diplodocus hayi	0.689	0.0499	12000000 (A9)	87.784823
	0.534	0.0381	19000000 (A9)	87.784823
Dromiceiomimus brevitertius	8.61	0.739	125000 (Hu)	87.85 (Hu)
	7.15	0.606	175000 (Hu)	87.85 (Hu)
Majungatholus atopus	-	-	-	168.27198
Mongolodon junior	-	-	-	26.479269
Rhamphorhynchus muensteri	3.39	0.374	136 (W)	0.794479
Saurosuchus galilei	-	-	-	60.899867
Troodon formosus	7.76	0.691	45000 (C,Z)	45 (C,Z)
Tyrannosaurus rex	7.63	0.577	4000000 (P)	530 (O)
	5.44	0.401	7400000 (A8)	530 (O)
Zos Canyon troodontid	-	-	-	3.104171

APPENDIX D

Information for Specimens Scanned at The University of Texas at Austin

Acrocanthosaurus atokensis:

Scan of the braincase of *Acrocanthosaurus atokensis*, OMNH 10146 (formerly MOU or UOM 8-0-S9), Stovall and Langston (1950), Antlers Formation, Lower Cretaceous (Aptian-Albian), Cochran Farm Locality, Atoka County, Oklahoma. Part of incomplete skeleton, holotype of *A. atokensis*, collected in 1940-41 by Works Projects Administration (WPA) crews under direction of Professor John Willis Stovall (University of Oklahoma Department of Geology, Norman, Oklahoma). Scanning done for Dr. Wann Langston and Dr. Timothy Rowe, The University of Texas Department of Geological Sciences. Scanning done by Richard Ketcham and Matt Colbert on 1/12/1999.

Allosaurus fragilis:

Scan of the braincase of *Allosaurus fragilis*, UUVP 5961, done for Sankar Chatterjee of Texas Tech University. Scanning done by Richard Ketcham on 6/25/1999.

Anas platyrhynchos:

Scan of the skull of *Anas platyrhynchos*, unnumbered TMM specimen, for David Dufeau and Timothy Rowe of The University of Texas Department of Geological Sciences. Scanning done by Richard Ketcham on 5/12/1998.

Anhanguera santanae:

Scan of the skull of *Anhanguera santanae*, AMNH 25555, for Dr. Sankar Chatterjee of Texas Tech University. All scanning done by Richard Ketcham and Matthew Colbert on 5/26/1999.

Apteryx sp.:

Scan of the skull and lower jaw of *Apteryx sp.*, ANMH 18456, for Timothy Rowe, Department of Geological Sciences, The University of Texas at Austin. Scanned by Matthew Colbert on 12/21/2001.

Byronosaurus jaffei:

Scan of the braincase of *Byronosaurus jaffei*, IGM 100/983, done in 5/1997 for the American Museum of Natural History. Samples delivered by Jim Clark. All scanning done by Rich Ketcham with the assistance of Tim Rowe.

Ceratosaurus magnicornis:

Scan of the braincase of *Ceratosaurus magnicornis*, MWC 1, Fruita Paleontological Area (FPA) near Fruita, in the SW 1/4 Sec. 24, T1N, R3W, Ute Meridian, Mesa County, Colorado; lower part of the Brushy Basin Member of the Morrison Formation; Late Jurassic) for Jon Franzosa of the Department of Geological Sciences, The University of Texas at Austin, and Dr. Timothy Rowe of the Department of Geological Sciences, The University of Texas at Austin. Specimen scanned by Matthew Colbert 9/10/2003.

Chauna chavaria:

Scan of the skull of *Chauna chavaria*, KU 81969, obtained from the University of Kansas Museum of Natural History. Collected by R.M. Chandler at the Henry Doorly Zoo, Omaha, NE, early 1982. Scanned for David Dufeau of The University of Texas Department of Geological Sciences. Scanning done by Cambria Denison and Richard Ketcham on 2/25/1998.

Citipati osmolskae:

Scan of the skull of *Citipati osmolskae*, IGM 100/978, from American Museum of Natural History, found in Mongolia, done for Jim Clark and Mark Norell of the American Museum of Natural History, from 11/3/1997 to 11/5/1997. All scanning done by Rich Ketcham and Cambria Denison.

Crocodylus moreleti:

Scan of the skull and mandibles of *Crocodylus moreleti*, TMM M-4980, adult female, HZG #I-56; died 12/1/79 at Houston Zoological Gardens while on loan from the Gladys Porter Zoo, Brownsville, TX, on permanent loan (until revoked) from the U.S. Fish and Wildlife Service [see loan permit 2-LA-192]), for Jon Franzosa of the Department of Geological Sciences, The University of Texas at Austin and Dr. Timothy Rowe of the Department of Geological Sciences, The University of Texas at Austin. Specimen scanned by Matthew Colbert on 8/21/2003.

Crypturellus cinnamomeus:

Scan of the skull of *Crypturellus cinnamomeus*, KU 34658, collected from El Astillero, Guatemala, on 2 February 1955, belonging to the collections of the University of Kansas Museum of Natural History. Scanned for David Dufeau.

Dinornis giganteus:

Scan of the skull of *Dinornis giganteus*, AMNH FR1000001, for Jackson Dodd and Timothy Rowe of the Department of Geological Sciences, The University of Texas at Austin. Scanned by Richard Ketcham on 1/11/2002. Corrective processing done by Matthew Colbert and Jessie Maisano.

Diplodocus hayi:

Scan of the braincase of *Diplodocus hayi*, CM 662, for Tim Rowe of The University of Texas Department of Geological Sciences. All scanning done by Richard Ketcham on 10/23/1998.

Mongolodon junior:

Scan and image processing of the skull of *Mongolodon junior*, IGM 100/1. Scanned for Dr. Mark Norell of the American Museum of Natural History in collaboration with Dr. Timothy Rowe, Department of Geological Sciences, The University of Texas at Austin. Skull delivered in two pieces by Dr. Gene Gaffney of the AMNH, reassembled by Bob Rainey of the TMM. Skull scanned by

Richard Ketcham and Matthew Colbert on 10/31/2000. Image processing done by Farrah Welch.

Rhamphorhynchus muensteri:

Scan of the skull of *Rhamphorhynchus muensteri*, CM 11434, from the Late Jurassic Solnhofen limestone in the Altmuhl River Valley in Germany, Carnegie Museum, Pittsburgh.

Saurosuchus galilei:

Scan of the braincase of *Saurosuchus galilei*, PVSJ 32, from the Upper Triassic (228 m.y.) aged lower part of the Ischigualasto Fm., Ischigualasto Basin, San Juan, Argentina, done for Dr. Timothy Rowe of The University of Texas at Austin. Specimen from the University Museum of San Juan, Argentina. Scanning done by Richard Ketcham and Matthew Colbert on 12/18/1998.

Zos canyon troodontid:

Scan of the skull of the Zos Canyon troodontid, IGM 100/1005, from Ukhaa Tolgod, Mongolia, collected in 1997. Scanning done by Richard Ketcham and Cambria Denison on 4/29/1998.

APPENDIX E

Parameters for Specimens Scanned at UTCT

Definitions for the parameters in the following chart.

Detector- three detector systems were used for scanning the specimens at UTCT, the P250D and RLS for larger specimens, and the image intensifier (II) for smaller specimens.

Slice thickness- the thickness of each slice in the dataset.

Interslice spacing- the distance between slices; this may be less than the slice thickness. This oversampling will sometimes improve image quality.

Field of reconstruction- the dimensions of the CT slices.

File size- 512 X 512 pixel slice, or 1024 X 1024 pixel slice. This, together with the field of reconstruction, determines the in-plane resolution of the image (i.e., interpixel spacing equals the field of recon/512 or 1024).

Taxa	Detector	Slice thickness	Interslice spacing	Field of reconstruction	File size	Scanned for
Acrocanthosaurus atokensis	P250D	1.0 mm	0.8 mm	255 mm	512 X 512	Dr. Langston, Dr. Rowe
Allosaurus fragilis	P250D	1.0 mm	0.8 mm	233 mm	512 X 512	Dr. Chatterjee
Anas platyrhynchos	II	0.5 mm	0.4 mm	62.5 mm	512 X 512	David Dufeau
Anhanguera santanae	P250D	0.5 mm	0.45 mm	182 mm	1024 X 1024	Dr. Chatterjee
Apteryx sp.	II	0.1644 mm	0.1644 mm	43 mm	512 X 512	Dr. Rowe
Byronosaurus jaffei	II	0.20 mm	0.20 mm	36.3 mm	1024 X 1024	Dr. Clark
Ceratosaurus magnicornis	P250D	1.0 mm	0.9 mm	194 mm	1024 X 1024	Jonathan Franzosa, Dr. Rowe
Chauna chavaria	II	0.295 mm	0.25 mm	52 mm	512 X 512	David Dufeau
Citipati osmolskae	P250D	0.5 mm	0.5 mm	200 mm	1024 X 1024	Dr. Clark, Dr. Norell
Crocodylus moreleti	P250D	0.5 mm	0.5 mm	195 mm	1024 X 1024	Jonathan Franzosa
Crypturellus cinnamomeus	II	0.15 mm	0.1 mm	61 mm	512 X 512	David Dufeau
Dinornis giganteus	P250D	0.5 mm	0.4 mm	146 mm	1024 X 1024	Dr. Rowe, Jackson Dodd
Diplodocus hayi	P250D	1.0 mm	0.8 mm	232 mm	512 X 512	Dr. Rowe
Mongolodon junior	RLS	0.5 mm	0.45 mm	117 mm	512 X 512	Dr. Norell, Dr. Rowe
Rhamphorhynchus muensteri	II	0.25 mm	0.2 mm	35.5 mm	512 X 512	Dr. Chatterjee
Saurosuchus galilei	P250D	1.0 mm	0.8 mm	215 mm	512 X 512	Dr. Rowe
Zos Canyon troodontid	II	0.24 mm	0.2 mm	46 mm	512 X 512	Dr. Clark, Dr. Norell

References

Alcober, O. 2000. Redescription of the skull of *Saurosuchus galilei* (Archosauria: Rauisuchidae). Journal of Vertebrate Paleontology 20:302-316.

Alexander, R. M. 1985. Mechanics of posture and gait of some large dinosaurs. Zoological Journal of the Linnean Society 83:1-25.

Alexander, R. M. 1991. How dinosaurs ran. Scientific American 264(4):130-136.

Allman, J. M. 1999. Evolving Brains. Scientific American Library, New York, New York, 224 pp.

Anderson, J. F., A. Hall-Martin, and D. A. Russell. 1985. Long-bone circumference and weight in mammals, birds and dinosaurs. Journal of Zoology, London (A) 207:53-61.

Bakker, R. T. 1971. Dinosaur physiology and the origin of mammals. Evolution 25:636-658.

Bakker, R. T. 1972. Anatomical and ecological evidence of endothermy in dinosaurs. Nature 238:81-85.

Bang, B. G. 1964. The nasal organs of the Black and Turkey Vultures; a comparative study of the cathartid species *Coragyps atratus atratus* and *Cathartes aura septentrionalis* (with notes on *Cathartes aura falklandica,*

Pseudogyps bengalensis, and *Neophron percnopterus*). Journal of Morphology 115:153-184.

Bang, B. G., and S. Cobb. 1968. The size of the olfactory bulb in 108 species of birds. Auk 85:55-61.

Barsbold, R. 1974. Saurornithoididae, a new family of small theropod dinosaurs from Central Asia and North America. Palaeontologia Polonica 30:5-22.

Bauchot, R. 1978. Encephalization in vertebrates: a new mode of calculation for allometry coefficients and isoponderal indices. Brain, Behavior, and Evolution 15:1-18.

Bauchot, R., and H. Stephan. 1969. Encéphalisation et niveau évolutif chez les simiens. Mammalia 33:225-275.

Baumel, J. J., A. S. King, J. E. Breazile, H. E. Evans, and J. C. Vanden Berge (eds.). 1993. Handbook of Avian Anatomy: Nomina Anatomica Avium. Second Edition. Publications of the Nuttall Ornithological Club Number 23. Nuttall Ornithological Club, Cambridge, Massachusetts, 779 pp.

Blanks, R. H. I., I. S. Curthoys, and C. H. Markham. 1972. Planar relationships of semicircular canals in the cat. American Journal of Physiology 223:55-62.

Breazile, J. E., and H.-G. Hartwig. 1989. Central nervous system; pp. 485-566 *in* A. S. King, and J. McLelland (eds.), Form and Function in Birds, Volume 4. Academic Press Inc., New York, New York.

Brochu, C. A. 2000. A digitally-rendered endocast for *Tyrannosaurus rex*. Journal of Vertebrate Paleontology 20:1-6.

Brochu, C. A. 2003. Osteology of *Tyrannosaurus rex*: insights from a nearly complete skeleton and high-resolution computed tomographic analysis of the skull. Society of Vertebrate Paleontology Memoir 7:1-138.

Bubień-Waluszewska, A. 1981. The cranial nerves; pp. 385-438 *in* A. S. King, and J. McLelland (eds.), Form and Function in Birds, Volume 2. Academic Press Inc., New York, New York.

Buchholtz, E. A., and E.-A. Seyfarth. 1999. History of neuroscience. The gospel of the fossil brain: Tilly Edinger and the science of paleoneurology. Brain Research Bulletin 48:351-361.

Butler, A. B., and W. Hodos. 1996. Comparative Vertebrate Neuroanatomy: Evolution and Adaptation. Wiley-Liss Inc., New York, New York, 514 pp.

Carlson, W. D., T. Rowe, R. A. Ketcham, and M. W. Colbert. 2003. Applications of high-resolution X-ray computed tomography in petrology, meteoritics and palaeontology; pp. 7-22 *in* F. Mees, R. Swennen, M. van Geet, and P. Jacobs (eds.), Applications of X-ray Computed Tomography in the Geosciences. The Geological Society Special Publication Number 215. The Geological Society, London, England.

Chinsamy, A., L. M. Chiappe, and P. Dodson. 1994. Growth rings in Mesozoic birds. Nature 368:196-197.

Chure, D. J., and J. H. Madsen. 1998. An unusual braincase (?*Stokesosaurus clevelandi*) from the Cleveland-Lloyd Dinosaur Quarry, Utah (Morrison Formation; Late Jurassic). Journal of Vertebrate Paleontology 18:115-125.

Clark, J. M., M. A. Norell, and R. Barsbold. 2001. Two new oviraptorids (Theropoda: Oviraptorosauria), Upper Cretaceous Djadokhta Formation, Ukhaa Tolgod, Mongolia. Journal of Vertebrate Paleontology 21:209-213.

Clark, J. M., M. A. Norell, and T. Rowe. 2002. Cranial anatomy of *Citipati osmolskae* (Theropoda, Oviraptorosauria), and a reinterpretation of the holotype of *Oviraptor philoceratops*. American Museum Novitates 3364:1-24.

Colbert, E. H. 1962. The weights of dinosaurs. American Museum Novitates 2076:1-16.

Coria, R. A., and P. J. Currie. 2002. The braincase of *Giganotosaurus carolinii* (Dinosauria: Theropoda) from the Upper Cretaceous of Argentina. Journal of Vertebrate Paleontology 22:802-811.

Cracraft, J. 1974. Phylogeny and evolution of the ratite birds. Ibis 116:494-521.

Cracraft, J. 1986. The origin and early diversification of birds. Paleobiology 12:383-399.

Cracraft, J. 1988. The major clades of birds; pp. 339-361 *in* M. J. Benton (ed.), The Phylogeny and Classification of the Tetrapods, Volume 1:

Amphibians, Reptiles, Birds. The Systematics Association Special Volume Number 35A. Clarendon Press, Oxford, England.

Currie, P. J. 1985. Cranial anatomy of *Stenonychosaurus inequalis* (Saurischia, Theropoda) and its bearing on the origin of birds. Canadian Journal of Earth Sciences 22:1643-1658.

Currie, P. J. 1995. New information on the anatomy and relationships of *Dromaeosaurus albertensis* (Dinosauria: Theropoda). Journal of Vertebrate Paleontology 15:576-591.

Currie, P. J. 1997. Braincase anatomy; pp. 81-85 *in* P. J. Currie, and K. Padian (eds.), Encyclopedia of Dinosaurs. Academic Press Inc., San Diego, California.

Currie, P. J., and J.-H. Peng. 1993. A juvenile specimen of *Saurornithoides mongoliensis* from the Upper Cretaceous of Northern China. Canadian Journal of Earth Sciences 30:2224-2230.

Currie, P. J., and X.-J. Zhao. 1993a. A new carnosaur (Dinosauria, Theropoda) from the Jurassic of Xinjiang, People's Republic of China. Canadian Journal of Earth Sciences 30:2037-2081.

Currie, P. J., and X.-J. Zhao. 1993b. A new troodontid (Dinosauria, Theropoda) braincase from the Dinosaur Park Formation (Campanian) of Alberta. Canadian Journal of Earth Sciences 30:2231-2247.

de Beer, G. R. 1947. How animals hold their heads. Proceedings of the Linnean Society of London 159:125-139.

de Ricqlès, A. J. 1980. Tissue structures of dinosaur bone: functional significance and possible relation to dinosaur physiology; pp. 103-139 *in* R. D. K. Thomas, and E. C. Olson (eds.), A Cold Look at the Warm-Blooded Dinosaurs. Westview Press Inc., Boulder, Colorado.

Domínguez-Alonso, P., A. C. Milner, M. J. Cookson, and T. B. Rowe. In review. The avian nature of the brain and inner ear of *Archaeopteryx*. Nature.

Dunning, J. B., Jr. 2000. CRC Handbook of Avian Body Masses. CRC Press, Boca Raton, Florida, 371 pp.

Edinger, T. 1921. Über *Nothosaurus*. I. Ein Steinkern der Schädelhöhle. Senckenbergiana 3:121-129.

Edinger, T. 1925. Die *Archaeopteryx*. Natur und Museum 55:491-496.

Edinger, T. 1926a. Fossile Fledermausgehirne. Senckenbergiana 8:1-6.

Edinger, T. 1926b. The brain of *Archaeopteryx*. Annals and Magazine of Natural History, Series 9 18:151-156.

Edinger, T. 1927. Das Gehirn der Pterosaurier. Zeitschrift für Anatomie und Entwicklungsgeschichte 83:105-112.

Edinger, T. 1928. Über einige fossile Gehirne. Paläontologische Zeitschrift 9:379-402.

Edinger, T. 1929. Die fossilen Gehirne. Ergebnisse der Anatomie und Entwicklungsgeschichte 28:1-249.

Edinger, T. 1934. Anton Fritsch's "Grosshirn von *Polyptychodon*" ist der Steinkern eines Schildkrötenschädels. Psychiatrische en Neurologische Bladen 38:396-404.

Edinger, T. 1937. Paläoneurologie. Fortschritte der Paläontologie 1:235-251.

Edinger, T. 1938. Über Steinkerne von Hirn- und Ohr-Höhlen der Mesosuchier *Goniopholis* und *Pholidosaurus* aus dem Bückeburger Wealdon. Acta Zoologica 19:467-505.

Edinger, T. 1941. The brain of *Pterodactylus*. American Journal of Science 239:665-682.

Edinger, T. 1948. Evolution of the horse brain. Geological Society of America Memoir 25:1-177.

Edinger, T. 1951. The brains of the Odontognathae. Evolution 5:6-24.

Edinger, T. 1956. Objets et résultats de la paléoneurologie. Annales de Paléontologie 42:97-116.

Edinger, T. 1962. Anthropocentric misconceptions in paleoneurology. Proceedings of the Rudolf Virchow Medical Society in the City of New York 19:56-107.

Edinger, T. 1975. Paleoneurology 1804-1966: an annotated bibliography. Advances in Anatomy, Embryology, and Cell Biology 49:1-258.

Emerson, S. B., and P. A. Hastings. 1998. Morphological correlations in evolution: consequences for phylogenetic analysis. Quarterly Review of Biology 73:141-162.

Erichsen, J. T., W. Hodos, C. Evinger, B. B. Bessette, and S. J. Phillips. 1989. Head orientation in pigeons: postural, locomotor and visual determinants. Brain, Behavior, and Evolution 33:268-278.

Farlow, J. O. 1994. Speculations about the carrion-locating ability of tyrannosaurs. Historical Biology 7:159-165.

Felsenstein, J. 1985. Phylogenies and the comparative method. American Naturalist 125:1-15.

Fenton, C. L., and M. A. Fenton. 1958. The Fossil Book: A Record of Prehistoric Life. Doubleday & Company Inc., Garden City, New York, 482 pp.

Forster, C. A., S. D. Sampson, L. M. Chiappe, and D. W. Krause. 1998. The theropod ancestry of birds: new evidence from the Late Cretaceous of Madagascar. Science 279:1915-1919.

Franzosa, J. W. 2001. Constructing digital endocasts of theropods using a high-resolution X-ray computed tomography scanner. Journal of Vertebrate Paleontology 21(Supplement to 3):51A.

Franzosa, J. W. 2002. A description of the anatomy of a digitally constructed *Acrocanthosaurus atokensis* (Theropoda: Allosauroidea) endocast, and its uses. Journal of Vertebrate Paleontology 22(Supplement to 3):55A.

Galton, P. M. 1985. Cranial anatomy of the prosauropod dinosaur *Plateosaurus* from the Knollenmergel (Middle Keuper, Upper Triassic) of Germany. II. All the cranial material and details of soft-part anatomy. Geologica et Palaeontologica 19:119-159.

Gauthier, J. 1986. Saurischian monophyly and the origin of birds; pp. 1-55 *in* K. Padian (ed.), The Origin of Birds and the Evolution of Flight. Memoirs of the California Academy of Sciences Number 8. California Academy of Sciences, San Francisco, California.

Giffin, E. B. 1989. Pachycephalosaur paleoneurology (Archosauria: Ornithischia). Journal of Vertebrate Paleontology 9:67-77.

Gower, D. J., and A. G. Sennikov. 1996. Morphology and phylogenetic informativeness of early archosaur braincases. Palaeontology 39:883-906.

Holtz, T. R., Jr. 1998. A new phylogeny of the carnivorous dinosaurs. Gaia 15:5-61.

Hopson, J. A. 1977. Relative brain size and behavior in archosaurian reptiles. Annual Review of Ecology and Systematics 8:429-448.

Hopson, J. A. 1979. Paleoneurology; pp. 39-146 *in* C. Gans, R. C. Northcutt, and P. Ulinski (eds.), Biology of the Reptilia, Volume 9, Neurology A. Academic Press Inc., New York, New York.

Hopson, J. A. 1980. Relative brain size in dinosaurs: implications for dinosaurian endothermy; pp. 287-310 *in* R. D. K. Thomas, and E. C. Olson (eds.), A Cold Look at the Warm-Blooded Dinosaurs. Westview Press Inc., Boulder, Colorado.

Horner, J. R., and D. Lessem. 1993. The Complete *T. rex*. Simon & Schuster Inc., New York, New York, 239 pp.

Horner, J. R., and R. Makela. 1979. Nest of juveniles provides evidence of family structure among dinosaurs. Nature 282:296-298.

Hurlburt, G. R. 1996. Relative brain size in recent and fossil amniotes: determination and interpretation. Ph.D. dissertation, University of Toronto, Toronto, Canada, 250 pp.

Hurlburt, G. R. 1999. Comparison of body mass estimation techniques, using Recent reptiles and the pelycosaur *Edaphosaurus boanerges*. Journal of Vertebrate Paleontology 19:338-350.

Janensch, W. 1935. Die Schädel der Sauropoden *Brachiosaurus, Barosaurus* und *Dicraeosaurus* aus den Tendaguru-Schichten Deutsch-Ostafrikas. Palaeontographica Supplement 7, Reihe 1, Teil 2:145-297.

Jerison, H. J. 1969. Brain evolution and dinosaur brains. American Naturalist 103:575-588.

Jerison, H. J. 1970. Brain evolution: new light on old principles. Science 170:1224-1225.

Jerison, H. J. 1973. Evolution of the Brain and Intelligence. Academic Press Inc., New York, New York, 482 pp.

Jerison, H. J. 1985. Animal intelligence as encephalization. Philosophical Transactions of the Royal Society of London. Series B, Biological Sciences 308:21-34.

Knoll, F., E. Buffetaut, and M. Bülow. 1999. A theropod braincase from the Jurassic of the Vaches Noires cliffs (Normandy, France): osteology and palaeoneurology. Bulletin de la Société Géologique de France 170:103-109.

Larsson, H. C. E. 2001. Endocranial anatomy of *Carcharodontosaurus saharicus* (Theropoda: Allosauroidea) and its implications for theropod brain evolution; pp. 19-33 *in* D. H. Tanke, and K. Carpenter (eds.), Mesozoic Vertebrate Life. New Research Inspired by the Paleontology of Philip J. Currie. Indiana University Press, Bloomington, Indiana.

Larsson, H. C. E., P. C. Sereno, and J. A. Wilson. 2000. Forebrain enlargement among nonavian theropod dinosaurs. Journal of Vertebrate Paleontology 20:615-618.

Maddison, W. P., and D. R. Maddison. 1992. MacClade: analysis of phylogeny and character evolution. Version 4.04PPC. Sinauer Associates, Sunderland, Massachusetts.

Maddison, W. P., M. J. Donoghue, and D. R. Maddison. 1984. Outgroup analysis and parsimony. Systematic Zoology 33:83-103.

Madsen, J. H., Jr. 1976. *Allosaurus fragilis*: a revised osteology. Utah Geological Survey Bulletin 109:1-163.

Madsen, J. H., Jr., and S. P. Welles. 2000. *Ceratosaurus* (Dinosauria, Theropoda): a revised osteology. Utah Geological Survey Miscellaneous Publication 00-2:1-80.

Makovicky, P. J., and M. A. Norell. 1998. A partial ornithomimid braincase from Ukhaa Tolgod (Upper Cretaceous, Mongolia). American Museum Novitates 3247:1-16.

Makovicky, P. J., M. A. Norell, J. M. Clark, and T. Rowe. 2003. Osteology and relationships of *Byronosaurus jaffei* (Theropoda: Troodontidae). American Museum Novitates 3402:1-32.

Malthus, T. 1798. An essay on the principle of population, as it affects the future improvement of society with remarks on the speculations of Mr. Godwin, M. Condorcet, and other writers. Printed for J. Johnson, in St. Paul's Church-Yard, London, England.

Marsh, O. C. 1874. Small size of the brain in Tertiary mammals. American Journal of Science and Arts, Series 3 8(whole volume 108):66-67.

Marsh, O. C. 1880a. Odontornithes: a monograph on the extinct toothed birds of North America. Memoirs of the Peabody Museum of Yale College 1:1-201.

Marsh, O. C. 1880b. Principal characters of American Jurassic dinosaurs. III. American Journal of Science, Series 3 19(whole volume 119):253-259.

Marsh, O. C. 1881. Principal characters of American Jurassic dinosaurs. IV. Spinal cord, pelvis, and limbs of *Stegosaurus*. American Journal of Science, Series 3 21(whole volume 121):167-170.

Marsh, O. C. 1883. Birds with teeth. Annual Report of the United States Geological Survey 3:45-88.

Marsh, O. C. 1884a. Principal characters of American Jurassic dinosaurs. VII. On the Diplodocidae, a new family of the Sauropoda. American Journal of Science, Series 3 27(whole volume 127):161-168.

Marsh, O. C. 1884b. Principal characters of American Jurassic dinosaurs. VIII. The order Theropoda. American Journal of Science, Series 3 27(whole volume 127):329-340.

Marsh, O. C. 1886. Dinocerata: a monograph of an extinct order of gigantic mammals. United States Geological Survey Monograph 10:1-243.

Marsh, O. C. 1889. Notice of new American Dinosauria. American Journal of Science, Series 3 37(whole volume 137):331-336.

Marsh, O. C. 1890. Additional characters of the Ceratopsidae, with notice of new Cretaceous dinosaurs. American Journal of Science, Series 3 39(whole volume 139):418-426.

Marsh, O. C. 1891. The gigantic Ceratopsidae, or horned dinosaurs, of North America. American Journal of Science, Series 3 41(whole volume 141):167-178.

Marsh, O. C. 1895. The dinosaurs of North America. Annual Report of the United States Geological Survey 16:133-414.

Maxwell, W. D., and J. H. Ostrom. 1995. Taphonomy and paleobiological implications of *Tenontosaurus-Deinonychus* associations. Journal of Vertebrate Paleontology 15:707-712.

Newton, E. T. 1888. On the skull, brain, and auditory organ of a new species of pterosaurian (*Scaphognathus purdoni*), from the Upper Lias near Whitby, Yorkshire. Philosophical Transactions of the Royal Society of London. B 179:503-537.

Nilsson, G. E. 2000. The cost of a brain. Natural History 108:66-73.

Norell, M. A., P. J. Makovicky, and J. M. Clark. 2000. A new troodontid theropod from Ukhaa Tolgod, Mongolia. Journal of Vertebrate Paleontology 20:7-11.

Osborn, H. F. 1912. Crania of *Tyrannosaurus* and *Allosaurus*. Memoirs of the American Museum of Natural History 1:1-30.

Ostrom, J. H. 1969. Osteology of *Deinonychus antirrhopus*, an unusual theropod from the Lower Cretaceous of Montana. Peabody Museum of Natural History Bulletin 30:1-165.

Padian, K., and L. M. Chiappe. 1998. The origin and early evolution of birds. Biological Reviews 73:1-42.

Padian, K., A. J. de Ricqlès, and J. R. Horner. 2001a. Dinosaurian growth rates and bird origins. Nature 412:405-408.

Padian, K., J. R. Hutchinson, and T. R. Holtz, Jr. 1999. Phylogenetic definitions and nomenclature of the major taxonomic categories of the carnivorous Dinosauria (Theropoda). Journal of Vertebrate Paleontology 19:69-80.

Padian, K., J. Qiang, and S.-a. Ji. 2001b. Feathered dinosaurs and the origin of flight; pp. 117-135 *in* D. H. Tanke, and K. Carpenter (eds.), Mesozoic Vertebrate Life. New Research Inspired by the Paleontology of Philip J. Currie. Indiana University Press, Bloomington, Indiana.

Parkes, K. C. 1995. Tinamou; *in* Microsoft Encarta CD-ROM (1995 Edition). Microsoft Corporation, Redmond, Washington.

Pearson, R. 1972. The Avian Brain. Academic Press Inc., New York, New York, 658 pp.

Peczkis, J. 1994. Implications of body-mass estimates for dinosaurs. Journal of Vertebrate Paleontology 14:520-533.

Portmann, A., and W. Stingelin. 1961. The central nervous system; pp. 1-36 *in* A. J. Marshall (ed.), Biology and Comparative Physiology of Birds, Volume 2. Academic Press Inc., New York, New York.

Radinsky, L. 1967. Relative brain size: a new measure. Science 155:836-838.

Radinsky, L. 1973. Evolution of the canid brain. Brain, Behavior, and Evolution 7:169-202.

Radinsky, L. 1976. The brain of *Mesonyx*, a middle Eocene mesonychid condylarth. Fieldiana: Geology 33:323-337.

Radinsky, L. 1977. Brains of early carnivores. Paleobiology 3:333-349.

Radinsky, L. 1978. Evolution of brain size in carnivores and ungulates. American Naturalist 112:815-831.

Radinsky, L. 1981. Brain evolution in extinct South American ungulates. Brain, Behavior, and Evolution 18:169-187.

Rauhut, O. W. M. 2003. The interrelationships and evolution of basal theropod dinosaurs. Special Papers in Palaeontology 69:1-213.

Romer, A. S. 1966. Vertebrate Paleontology, Third Edition. The University of Chicago Press, Chicago, Illinois, 468 pp.

Rowe, T. 1989. A new species of the theropod dinosaur *Syntarsus* from the Early Jurassic Kayenta Formation of Arizona. Journal of Vertebrate Paleontology 9:125-136.

Rowe, T., W. D. Carlson, and W. Bottorff. 1993. *Thrinaxodon*: digital atlas of the skull. CD-ROM. University of Texas Press, Austin, Texas, 623 megabytes.

Rowe, T., W. D. Carlson, and W. Bottorff. 1995. *Thrinaxodon*: digital atlas of the skull. CD-ROM (Second Edition). University of Texas Press, Austin, Texas, 547 megabytes.

Rowe, T., J. Kappelman, W. D. Carlson, R. A. Ketcham, and C. Denison. 1997. High-resolution computed tomography: a breakthrough technology for Earth scientists. Geotimes 42(9):23-27.

Rowe, T., C. A. Brochu, M. Colbert, J. W. Merck, Jr., K. Kishi, E. Saglamer, and S. Warren. 1999. Introduction to *Alligator*: digital atlas of the skull; pp. 1-8 *in* T. Rowe, C. A. Brochu, and K. Kishi (eds.), Cranial Morphology of *Alligator mississippiensis* and Phylogeny of Alligatoroidea. Society of Vertebrate Paleontology Memoir 6. Society of Vertebrate Paleontology, Northbrook, Illinois.

Russell, D. A. 1969. A new specimen of *Stenonychosaurus* from the Oldman Formation (Cretaceous) of Alberta. Canadian Journal of Earth Sciences 6:595-612.

Russell, D. A., and Z.-M. Dong. 1993. The affinities of a new theropod from the Alxa Desert, Inner Mongolia, People's Republic of China. Canadian Journal of Earth Sciences 30:2107-2127.

Sereno, P. C. 1991. Basal archosaurs: phylogenetic relationships and functional implications. Society of Vertebrate Paleontology Memoir 2:1-53.

Sereno, P. C. 1999. The evolution of dinosaurs. Science 284:2137-2147.

Sereno, P. C., D. B. Dutheil, M. Iarochene, H. C. E. Larsson, G. H. Lyon, P. M. Magwene, C. A. Sidor, D. J. Varricchio, and J. A. Wilson. 1996. Predatory dinosaurs from the Sahara and Late Cretaceous faunal differentiation. Science 272:986-991.

Snell, O. 1892. Die Abhängigkeit des Hirngewichtes von dem Körpergewicht und den geistigen Fähigkeiten. Archiv für Psychiatrie und Nervenkrankheiten 23:436-446.

Spoor, F., and F. Zonneveld. 1998. Comparative review of the human bony labyrinth. Yearbook of Physical Anthropology 41:211-251.

Starck, D. 1979. Cranio-cerebral relations in recent reptiles; pp. 1-38 *in* C. Gans, R. C. Northcutt, and P. Ulinski (eds.), Biology of the Reptilia, Volume 9, Neurology A. Academic Press Inc., New York, New York.

Stovall, J. W., and W. Langston, Jr. 1950. *Acrocanthosaurus atokensis*, a new genus and species of Lower Cretaceous Theropoda from Oklahoma. American Midland Naturalist 43:696-728.

Stresemann, E. 1928-1929. Fünfte Klasse der Craniota. Zweite und zugleich letzte Klasse der Sauropsida. Aves=Vögel; pp. 1-544 *in* W. Kükenthal, and T. Krumbach (eds.), Handbuch der Zoologie. Volume 7(2). Walter de Gruyter and Co., Berlin, Germany.

Swofford, D. 1993. PAUP: Phylogenetic Analysis Using Parsimony. Version 4.0b10 (Altivec). The Illinois Natural History Survey, Champaign, Illinois.

Tykoski, R. S., T. B. Rowe, R. A. Ketcham, and M. W. Colbert. 2002. *Calsoyasuchus valliceps*, a new crocodyliform from the Early Jurassic Kayenta Formation of Arizona. Journal of Vertebrate Paleontology 22:593-611.

Ulinski, P. S. 1983. Dorsal Ventricular Ridge: a Treatise on Forebrain Organization in Reptiles and Birds. John Wiley & Sons Inc., New York, New York, 284 pp.

van Tuinen, M., C. G. Sibley, and S. B. Hedges. 2000. The early history of modern birds inferred from DNA sequences of nuclear and mitochondrial ribosomal genes. Molecular Biology and Evolution 17:451-457.

Varricchio, D. J. 1993. Bone microstructure of the Upper Cretaceous theropod dinosaur *Troodon formosus*. Journal of Vertebrate Paleontology 13:99-104.

Wall, W. P., and P. M. Galton. 1979. Notes on pachycephalosaurid dinosaurs (Reptilia: Ornithischia) from North America, with comments on their status as ornithopods. Canadian Journal of Earth Sciences 16:1176-1186.

Wharton, D. S. 2002. The evolution of the avian brain. Ph.D. dissertation, University of Bristol, Bristol, England, 340 pp.

Wiman, C., and T. Edinger. 1941. Sur les crânes et les encéphales d'*Aepyornis* et de *Mullerornis*. Bulletin de L'Académie Malgache, Nouvelle Série 14:1-48.

Witmer, L. M. 1990. The craniofacial air sac system of Mesozoic birds (Aves). Zoological Journal of the Linnean Society 100:327-378.

Witmer, L. M. 1995. The Extant Phylogenetic Bracket and the importance of reconstructing soft tissues in fossils; pp. 19-33 *in* J. J. Thomason (ed.), Functional Morphology in Vertebrate Paleontology. Cambridge University Press, New York, New York.

Witmer, L. M. 1997. The evolution of the antorbital cavity of archosaurs: a study in soft-tissue reconstruction in the fossil record with an analysis of the function of pneumaticity. Society of Vertebrate Paleontology Memoir 3:1-73.

Witmer, L. M., S. Chatterjee, J. Franzosa, and T. Rowe. 2003. Neuroanatomy of flying reptiles and implications for flight, posture and behaviour. Nature 425:950-953.

Witmer, L. M., S. Chatterjee, T. Rowe, and J. Franzosa. 2002. Anatomy of the brain and vestibular apparatus in two pterosaurs: implications for flight, head posture, and behavior. Journal of Vertebrate Paleontology 22(Supplement to 3):120A-121A.

Xu, X., M. A. Norell, X.-L. Wang, P. J. Makovicky, and X.-C. Wu. 2002. A basal troodontid from the Early Cretaceous of China. Nature 415:780-784.

Zhao, X.-J., and P. J. Currie. 1993. A large crested theropod from the Jurassic of Xinjiang, People's Republic of China. Canadian Journal of Earth Sciences 30:2027-2036.

Vita

Jonathan William Franzosa was born to William and Carol Franzosa on December 26th, 1975, in Cincinnati, Ohio. After graduating from Cincinnati's Saint Xavier High School in 1994, he went on to Louisiana State University in Baton Rouge, where he obtained a Bachelor of Science in Geology in 1998. Jonathan then continued his studies at The University of Texas at Austin, completing a Ph.D. in Vertebrate Paleontology in 2004.

While attaining this degree, Jonathan spent most semesters working as a Teaching Assistant, teaching labs for: Earth, Wind, and Fire; Introduction to Physical Geology; Age of Dinosaurs; Paleobiology; and Comparative Vertebrate Anatomy. During the summers, he worked as a Research Assistant for the Vertebrate Paleontology Laboratory, for the Department of Geological Sciences, and as a volunteer for field seasons in the Kayenta and Chinle Formations of Arizona.

During his stay at The University of Texas, Jonathan was third author on a paper published in Nature, fourth author on a paper in review for publication in American Museum Novitates, and lead author on a paper being reviewed for publication in Journal of Vertebrate Paleontology.

Permanent address: 1800 East Stassney Lane, Apt. #201, Austin, TX 78744

This dissertation was typed by the author.